A Model for Microcirculatory Fluid and Solute Exchange in the Heart

by

Michael R. Kellen

A dissertation submitted in partial fulfillment

of the requirements for the degree of

Doctor of Philosophy

University of Washington

2002

Program Authorized to Offer Degree: Bioengineering

UMI Number: 3053518

ProQuest Information and Learning Company
300 North Zeeb Road
P.O. Box 1346
Ann Arbor, MI 48106-1346

University of Washington

Graduate School

This is to certify that I have examined this copy of a doctoral dissertation by

Michael Robert Kellen

and have found that it is complete and satisfactory in all respects,
and that any and all revisions required by the final
examining committee have been made.

Chair of Supervisory Committee:

James B. Bassingthwaighte

Reading Committee:

James B. Bassingthwaighte

Thomas L. Daniel

Eric O. Feigl

Zheng Li

Pedro J. Verdugo

Date: May 30, 2002

Doctoral Dissertation

In presenting this dissertation in partial fulfillment of the requirements for the Doctoral degree at the University of Washington, I agree that the Library shall make its copies freely available for inspection. I further agree that extensive copying of the dissertation is allowable only for scholarly purposes, consistent with "fair use" as prescribed in the U.S. Copyright Law. Requests for copying or reproduction of this dissertation may be referred to Bell and Howell Information and Learning, 300 North Zeeb Road, P.O. Box 1346, Ann Arbor, MI 48106-1346, to whom the author has granted "the right to reproduce and sell (a) copies of the manuscript in microform and/or (b) printed copies of the manuscript made from microform."

Signature: 

Date: May 30, 2002

University of Washington

Abstract

A Model for Microcirculatory Fluid and Solute Exchange in the Heart

by Michael Kellen

Chairperson of the Supervisory Committee:
Professor James B. Bassingthwaighte
Department of Bioengineering

The exchange of fluids and solutes across the capillary wall is necessary to sustain multicellular life. Although the basic physiology of these processes is understood qualitatively, predicting the detailed kinetics of processes remains a challenge. An quantitatively precise understanding of the exchange process would benefit several practical application areas, including the optimization of drug delivery, engineering of new tissues, and understanding mechanisms of diseases including diabetes and cardiac edema.

I have developed a quantitative model of microvascular exchange which includes a detailed description of the physical processes and anatomical structures involved in this process. Three features advance the model beyond previous work. First, my description of the transcapillary exchange process contains separate descriptions of coupled water and solute exchange through the endothelial junction, as well as a pathway for water exchange only across the endothelial cells. Treating each of these pathways individually provides a more accurate representation of the exchange process than models that lump different pathways into a single set of parameters. Second, an axially-distributed blood-tissue exchange region accounts for axial concentration gradients in the exchange region, and provides more accurate parameters estimates. Finally, the presence of a lymphatic drain in the interstitium permits net filtration across the capillary wall at steady-state, which is necessary to set the correct interstitial concentrations of chemical species.

I have validated the model by comparison to osmotic weight transient experiments conducted in an isolated heart preparation. These experiments consist of the measurement

of water fluxes across the capillary wall caused by changes in the solute concentration of the perfusate. Additionally, I have applied the model to two additional sets of experimental data: multiple indicator dilution curves, and lymph sampling methods. These methods provide independent and complementary information to my own data. The fact that a single model can be matched all of these diverse sets of data is powerful evidence that is the model is an accurate representation of the underlying physiology. The model therefore provides an integrative framework for understanding the microvascular exchange process.

Table of Contents

List of Figures

List of Tables

1 Introduction

1.1 Integrative physiology

Since Watson and Crick discovered the structure of DNA in 1953, the biological sciences have become increasingly dominated by work on the molecular scale as scientists unraveled the structure and function of the key biological molecules: nucleic acids and proteins. Scientists ability to understand the properties of these molecules has led to staggering progress in biology and medicine over the last half-century because the behavior of living organisms ultimately depends on the properties of their molecular components. Biological systems are organized hierarchically, with functioning of higher level systems like cells, organs, and whole organisms dependent on the properties of lower-level components. Changes at the most basic genetic level can have a profound effect on an organism's phenotype as they propagate upward through hierarchy. For example, sickle cell anemia is caused by a single base-pair substitution in one gene that changes one amino acid on the surface of hemoglobin. The resulting charge pattern on the molecule's surface causes these altered proteins to stick to each other, distorting the shape of the red blood cell and ultimately impairing circulation.

However, this sort of simple and straightforward story has proven to be the exception rather than the rule in biology. The basic premise of reductionist biology, that understanding and manipulating organisms on their genetic level will permit the engineering of whole organisms, is now less certain than ever because the detailed dynamical behaviors of cells, organs, and whole organisms are extremely non-intuitive and difficult to predict, even when their molecular components are known. This is not to say that genetic work is unimportant or irrelevant, but simply that a straightforward relationship between genes and observable physiological behavior is exceedingly rare. Systemic behavior emerges from the complex and non-linear interactions among many components, biological systems typically have redundant components and multiple regulatory mechanisms, and the functioning of individual elements is exquisitely sensitive to a highly heterogeneous environment. The redundancy and complexity built into

biological systems complicates intervention. Unlike sickle cell anemia, diseases like cancer, heart disease, and Parkinson's have many poorly understood risk factors, few straightforward causes, and no obvious cures based on the modification of a single molecule.

Integrative biology is gaining recognition as the "new frontier" in biology as efforts are made to capitalize on the information obtained through the Human Genome Project. In 1990, the long-range planning committee of the American Physiological Society (APS) issued a white paper on the future of physiology in which the authors noted this trend towards integration:

> "Inevitably, however, as with all scientific revolutions, the rate of significant discovery using the tools of molecular biology has declined and the newly recruited legions of workers employing this ever growing armamentarium are generating ever-increasing volumes of factual information. Increasingly, however, attempts are being made to bridge the gap between the discoveries in molecular genetics and the control of cellular processes. Unanswered questions regarding the functioning of complex systems and, indeed, of whole organisms are again coming to the fore as the new frontier in the biological sciences. Unquestionably, the next revolution in biology will be in the integrative or organismic domain." (Giebisch, 1990)

In recent years, even molecular biologists have increasingly begun describing their work as "functional genomics" or "proteomics" as simply cataloging DNA sequences is no longer viewed as working on the scientific frontier. The concluding remarks of one recent conference succinctly summarized the situation, "Clearly, genome technology is now sufficiently powerful to push the biological limits of its own relevance" (Bains, 1998). Proteome technology is not yet at this stage, but there are fundamental limits to the understanding that even complete knowledge of all the expressed proteins in an organism will bring. For example, Kuile and Westerhoff (2001) have shown that much of the metabolic regulation of even simple bacteria occurs without changes in the expression levels of enzymes; there are even more opportunities for higher-level regulation in complex multicellular organisms.

1.2 Computational biology and bioinformatics

Sophisticated tools are needed to help biologists deal with the complexity of living organisms. Non-linearity, redundancy, and heterogeneity have arisen in many different biological contexts because systems that incorporate these traits provide for a faster and more robust response to the wide range of environmental conditions that an organism may encounter during its lifetime (Csete and Doyle, 2002). The reduction of biochemical and biophysical systems to static cartoon-like diagrams identifying qualitative relationships among molecular components is a necessary first step, but insufficient to predict behavior of complex systems. Transforming biology from a descriptive into a predictive science will necessitate the use of mathematical models as a more refined and precisely articulated scientific hypothesis (Kitano, 2002). By providing specific and testable predictions, models guide the design of novel experiments, improve insight into complex behavior, and succinctly communicate sophisticated ideas to the scientific community. Models that ground systemic behavior in well-established facts of molecular biology are becoming increasingly important to diverse fields including cell signaling (Asthagiri and Lauffenburger, 2000), cardiac electrophysiology (Noble, 2002, Winslow et al., 2000) and microcirculatory exchange (Rippe and Haraldsson, 1994, Michel and Curry, 1999).

The scope of the models needed to address full-scale biological complexity will require advancements in software infrastructure including databases of biological information, tools for rapid model construction and data analysis, and languages for precise communication among diverse research groups (Bassingthwaighte, 1995, Kitano, 2002). The higher-level biological disciplines will need to follow the path of the genomics community, which took the lead in large scale online databasing and model analysis. The challenge is now to expand molecular databases to include information on higher levels of physiology. Although significant scientific and technological hurdles remain (Macauley et al., 1998), technologies such as the Biology Workbench are beginning to integrate molecular information that is currently scattered among hundreds of databases with tools for analysis (Subramaniam, 1998). Several XML-based languages including Systems Biology Markup Language (Hucka et al., 2001) and CellML (Hedley and Nelson, 2001)

are beginning to define standards for precisely communicating descriptions of biological systems.

The study of higher level systems will benefit from central sources of information just as the genetics field has, and it is not necessary to wait until the molecular databases are complete before beginning work at higher levels. The Physiome Project is one effort to systematically catalogue physiological behavior from the gene to whole organism, an undertaking similar but many orders of magnitude more complex than the genome project that inspired it (Bassingthwaighte, 1995). The project has already begun to organize around organ systems; the Cardiome Project, for example is an attempt to catalog anatomical measurements, functional data, and mathematical models relating to cardiac physiology (Bassingthwaighte et al., 1997, 1998). Another independent effort is the Human Brain Project (Shepherd, 1998), which originated in the 1980s as an effort to provide a comprehensive source of neurophysiological data online. The project encompasses diverse types of data including DNA and protein sequences, molecular structures for important molecules, ion-channel currents, neural firing patterns, neural circuit behavior, and large-scale functional maps of brain regions.

1.3 Microcirculatory solute and solvent exchange

Another subdivision of the Physiome Project is the Microcirculation Physiome Project, an attempt to catalogue the structures and functions relevant to the exchange of materials between capillaries and surrounding tissues (Popel et al., 1998). The delivery of nutrients to, and removal of wastes from the cells of the body is an engineering problem that all multicellular organisms must solve. Vertebrates break this task into two major components. The first is the macro-scale circulation of blood through the arteries and veins of the body, responsible for transporting large quantities of substances among the various organ systems. Oxygen from the lungs and food from the gut are delivered to the rest of the body, and wastes are brought to the liver and kidneys. This process is purely convective. The second step is the micro-scale exchange of substances between the capillaries and living cells of the surrounding tissue. Although convection is important in

the microcirculation, the spatial scales are small enough that molecular diffusion is also a critical process. While the basic physical principles underlying mass transport in the microcirculation are well understood, the application of these principles to practical problems is difficult because of the complexity of the biology. Microvascular exchange occurs through several coupled processes: axial convection through the capillaries, radial exchange across the capillary wall, convective and diffusive transport within the interstitium, drainage by the lymphatics, and uptake by parenchymal cells.

An improved understanding of the microcirculation can be expected to have many positive impacts on medicine and engineering practice. Changes in these components play an important role in the development and progression of several diseases. Abnormally high capillary permeabilities develop with advanced diabetes and cardiac edema induced by heart failure (Plante, 1996), and the loss of proteoglycans and glycosaminoglycans from the extracellular matrix leads to the development of osteoarthritis (Eisenberg and Grodzinsky, 1988). Changes in vascular permeability and interstitial matrix characteristics play a dominant role in the physiological response to a burn injury (Kinsky, 1998). Microcirculatory phenomena also affect the delivery of drugs to a disease site, as Baxter and Jain (1989) demonstrated with a model of monoclonal antibody distribution in a tumor. Without a circulatory system, tissue engineering products will be limited to thin two dimensional sheets so no cells are far from a boundary.

1.3.1 Summary of the field

Modern ideas about the nature of exchange between the circulatory and extravascular bodily fluids date to Starling's (1896) hypothesis that opposing hydrostatic and osmotic pressures drive the flux of water across the capillary wall. According to Starling's hypothesis, the capillary wall is a passive barrier to fluid exchange; equilibrium occurs when the hydrostatic pressure difference between capillary and interstitium is balanced by an opposing osmotic pressure difference. The theoretical foundation for transcapillary exchange was expanded greatly when Kedem and Katchalsky (1958) applied the ideas of non-equilibrium thermodynamics to biological membranes, and quantitatively described

coupled solute and water fluxes using three phenomenological coefficients: the hydraulic conductivity, L_p, the permeability, P, and the reflection coefficient, σ. These parameters are still widely used to describe the kinetic exchange properties of microvessels.

Microcirculatory transport rates are ultimately determined by the anatomical structure of the capillary wall and interstitial matrix. Ultimately, mechanistic models can provide a deeper explanation of microcirculatory phenomena than phenomenological descriptions. The observed phenomenological coefficients should be explainable in terms of the underlying tissue anatomy and chemical composition. For example, a number of models of the interendothelial cleft have been proposed that attempt to predict the observed solute permeabilities and reflection coefficients based on the structure of the interendothelial clefts and surface glycocalyx. Other phenomenological parameters like volumes of distribution should likewise be derived from the interstitial matrix structure and the physical characteristics of the solute. The ultimate reductionist goal would be to relate these mechanistic molecular models to the organism's genetics, but such an extension is presently not feasible.

Quantitative information about microcirculatory exchange has been gathered from complete vascular networks in whole organs, single vessels, and cultured endothelial cell layers. Of these preparations, whole organs provide access to the most complete and natural microvascular networks. In addition to transcapillary exchange, transport through the interstitium, drainage by the lymphatics, and interactions with parenchymal cells may be important *in vivo*. These processes also can be described by phenomenological parameters such as tissue compliance and fractional volumes of distribution. Since so many processes may contribute to microcirculatory function, it is necessary either to develop sophisticated models of the blood-tissue exchange region, or to design experiments in such a way that only a few phenomena dominate the experimental results. Three major techniques provide information on microcirculatory exchange in whole organs: osmotic transient, tracer-transient, and lymph analysis. A model of transcapillary exchange needs to explain data from all three of these methods using a single set of phenomenological parameters to be considered complete.

1.3.2 Starling's hypothesis

The cornerstone of modern ideas of fluid exchange between the circulation and the interstitial fluid is Starling's hypothesis. By 1896, Starling was already convinced that interstitial fluid was formed from plasma filtered across the capillary wall because of the hydrostatic pressure difference between capillaries and interstitium. In a classic paper, Starling (1896) observed that an isotonic salt solution injected into the interstitial space of a dog hind limb was absorbed into the plasma. After discounting the role of changes in tissue pressure in this process, Starling measured the osmotic pressure of plasma proteins and found them to be of the same order of magnitude as the capillary pressure. He realized that while small molecules like salt would rapidly equilibrate across the capillary wall and exert no osmotic driving force, even small concentration differences of an impermeable solute could be significant because they would require bulk fluid exchange to dissipate. A difference in impermeable protein concentration across the capillary wall would cause the absorption of isotonic salt solution into the plasma, until the dilution of plasma and concentration of interstitial protein restored osmotic balance. Starling concluded that water flux across the capillary membrane was determined by a combination of hydrostatic pressure, p, which normally drives filtration from the plasma into the interstitium, and the osmotic pressure of proteins, Π, which acts to absorb interstitial fluid back into the vasculature. Although Starling never expressed these ideas in quantitative terms himself, his hypothesis can be expressed by the equation:

$$J_v = L_p((p_{cap} - p_{isf}) - (\Pi_{cap} - \Pi_{isf})) \qquad (1.1)$$

where J_v is the flux of water from capillary to interstitium, and L_p is the hydraulic conductivity. A more detailed discussion of the development of Starling's hypothesis can be found in Michel's (1984) review.

1.3.3 Theory of coupled solute-solvent exchange

Starling's ideas were developed more fully when Kedem and Katchalsky (1958) used the theory of nonequilibrium thermodynamics to derive equations for mass transport

across membranes (See Appendix A). The transport of solute and water across a membrane was now understood to be a coupled process, with volume and solute fluxes given by

$$J_V = L_p(\Delta p - \sigma\Delta\Pi) \tag{1.2}$$

$$J_s = P\Delta C + J_V(1-\sigma)\overline{C} \tag{1.3}$$

The first equation is identical to the Starling equation, with the addition of the solute reflection coefficient, σ. This parameter varies between 0 for a freely permeable solute and 1 for a impermeable solute, and is a measure of the relative selectivity of the membrane for the solute as compared to the bulk solution. The more solute transport is restricted by the membrane, the more of the solute's full osmotic pressure difference will exerted across the membrane.

The solute flux is also dependent on σ as well as the third phenomenological transport coefficient, the permeability, *P*. Solute flux is comprised of two components, the diffusive component given by the first term of Equation 1.3, and the solvent drag component given by the second term. The solvent drag is the amount of solute carried across the membrane by the water flux. $\overline{C}$ is the logarithmic mean of solute concentration on either side of the membrane

$$\overline{C} = \frac{(C_1 - C_2)}{\ln(C_1/C_2)} \tag{1.4}$$

These equations assume that the volume fraction of solute is negligible, the partial molar volume of the solute is constant, and the membrane is of negligible thickness.

Patlak et al. (1963) later introduced a more correct non-linear solute flux equation by integrating the Kedem and Katchalsky expressions (See Appendix B) across a membrane of finite thickness

$$J_s = P\Delta C\left(\frac{Pe}{e^{Pe}-1}\right) + J_V(1-\sigma)C_1 \qquad (1.5)$$

In this equation, the solute diffusive term is multiplied by a term involving the Péclet number, Pe, the ratio of convective to diffusive solute transport across the membrane

$$Pe = \frac{J_V(1-\sigma)}{P} \qquad (1.6)$$

The term $Pe/(e^{Pe}-1)$ corrects for changes in the diffusive rate of mass transfer in the presence of simultaneous convection, which changes the steady-state concentration profile in the membrane. The term approaches 1 for pure diffusion ($Pe \ll 1$) and 0 for pure convection ($Pe \to \infty$). Historically, the Kedem and Katchalsky equation has enjoyed more widespread use, often with the further approximation of replacing the logarithmic mean with the arithmetic mean, reasonable when concentration differences across the membrane are small. However, with modern computing power and numerical solution techniques, implementing the Patlak equation is not significantly more difficult than using the original Kedem and Katchalsky solute flux equation.

1.3.4 Isolated capillary microperfusion

Quantitative support for Starling's hypothesis did not begin to accumulate until Landis (1927) measured the rate at which water entered or left single micro-perfused vessels of frog mesentery. He found that an increase in capillary pressure correlated with an increase in fluid filtration and that no fluid flux occurred when the capillary pressure was approximately the same as the protein osmotic pressure of the capillary perfusate, in agreement with Equation 1.1. The slope of the best fit line to a plot of filtration vs. capillary pressure (Figure 1-1) is the capillary filtration coefficient, which Landis estimated as 6×10^{-7} cm sec^{-1} cmH_2O^{-1}.

A widely taught corollary of Starling's hypothesis, derived from the linear relationship between J_v and p_{cap}, is that filtration occurs at the arteriolar end of the

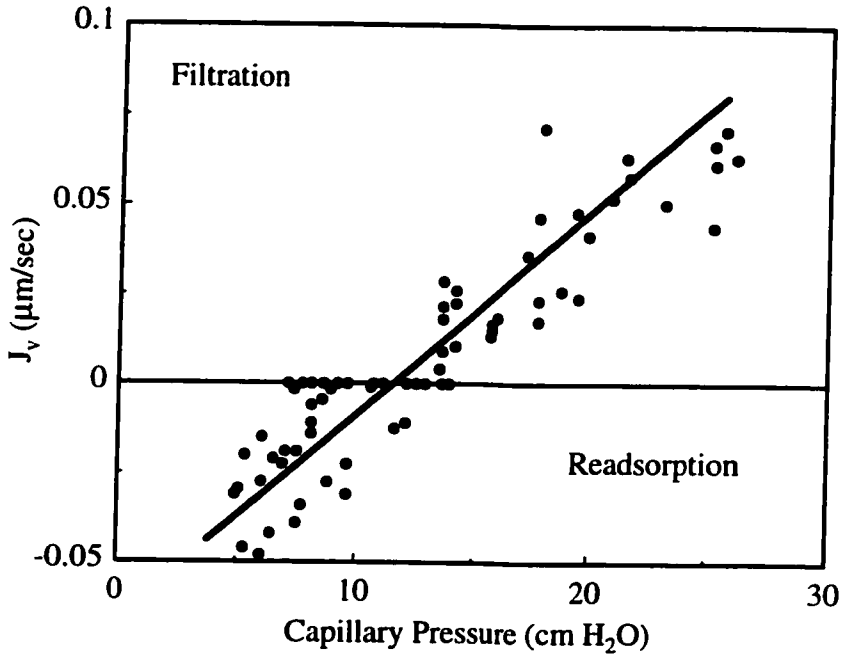

Figure 1-1 Filtration rate in isolated capillaries as a function of capillary hydrostatic pressure was measured by Landis (1927) in the isolated capillaries of frog mesentery.

capillary bed, while readsorption occurs at the venous end because the capillary hydrostatic pressure declines towards the venous end of the microvasculature, while capillary oncotic pressure remains nearly constant. Consequently, the net filtration, equal to the lymph flow in an isovolumetric tissue, is much less than the unidirectional fluxes into and out of the vascular bed. This interpretation has been challenged by the experiments of Michel and Phillips (1987). In a variation of the Landis technique, a protein-free Ringer's superfusate continually bathed a microperfused vessel that was kept at a high lumenal pressure. When the pressure was rapidly dropped, the initial filtration rate (within 20 seconds of a pressure change) was a linear function of capillary pressure, in agreement with the Landis study. However, after about 2 minutes, readsorption into the capillary ceased, and the steady-state plot of J_v vs. capillary pressure was no longer linear (see Figure 1-2).

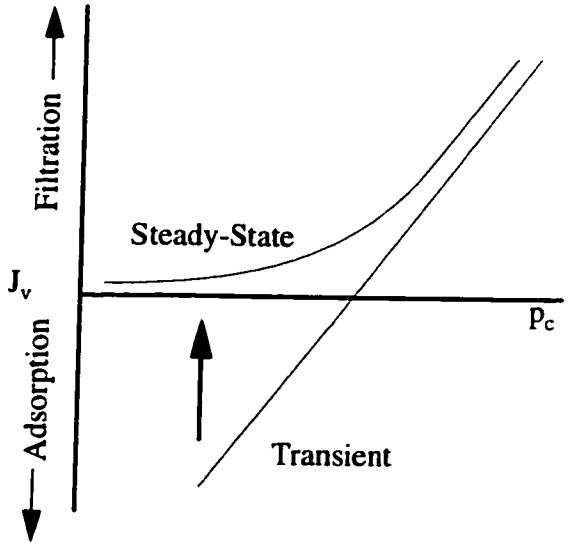

Figure 1-2 Steady state and transient water fluxes in a single isolated capillary.

The steady-state filtration rate in an isolated capillary is not a linear function of capillary pressure because other Starling forces are altered by sustained fluid movements across the capillary wall. At high filtration rates, a substantial protein oncotic pressure gradient is maintained across the capillary wall because the capillary superfusate concentration (C_{out}) is set by the concentration of capillary filtrate: $C_{out}=(1-\sigma)C_{in}$. With low transcapillary filtration rates, diffusion reduces the steady-state concentration difference, so the decrease in capillary pressure is partially offset by an increased C_{out}. With readsorption, the capillary oncotic pressure is reduced by the influx of protein-free superfusate, until a steady-state is reached where the lowered capillary pressure is balanced by a lowered capillary oncotic pressure. Michel and Phillips derived a simple equation that predicted the steady-state oncotic pressure at different capillary pressures, thus explaining their results.

However, extending their analysis to the whole-organ case is not straightforward. Unlike Michel's isolated capillary preparation where the superfusate was open to the atmosphere, interstitial fluid in an intact organ is enclosed by a compliant compartment, and interstitial hydrostatic pressure changes as interstitial volume changes. Furthermore, unlike an isolated capillary, capillaries in perfused organs contain axial gradients in

hydrostatic pressure, and can not be treated as single well-mixed compartments, as Michel's analysis assumes. Guyton and Lindsey (1959) and Perl et al. (1975) found that lung weight varies linearly with atrial pressure above 25 mmHg, but is constant below that value. Hu and Weinbaum (1999) have argued on this basis for the extension of Michel's model to the whole organ case, but a more detailed analysis is needed to justify this assertion. These observations do not mean that Equation 1.1 is incorrect; at any point in time filtration is dependent on the current driving forces for exchange. However, it must be remembered that sustained fluxes of water or solute can alter the driving forces, and a more detailed analysis than simple application of Starling's hypothesis is necessary to predict the dynamic response to a perturbation.

While single capillary experiments provide specific information on a given vessel's permeability characteristics, no information is obtained about how these properties interact with rest of the system. Isolating a vessel from its natural environment has the potential to change its transport properties, and experiments are usually restricted to a small number of convenient vessel types. Cultured endothelial cell monolayers are even farther removed from the natural state and usually do not have normal permeability properties, but have proven convenient for studying intracellular signaling mechanisms (Michel and Curry, 1999). In contrast, whole organ experiments probe complete and usually undisturbed networks of vessels, but the whole blood-tissue exchange process must be considered in the experimental analysis.

1.3.5 Early whole organ experiments

Krogh et al. (1932) began testing Starling's hypothesis in intact human tissues by measuring the volume of a human forearm subjected to various degrees of venous congestion, and found that the rate of fluid accumulation in the forearm tissue was proportional to the increase in venous pressure. Since capillary pressure would rise along with the venous pressure, the increased filtration rate was consistent with Starling's hypothesis. Additionally, an increase in blood osmolarity induced by having the subject

stand resulted in a uniformly lower rate of fluid transfer compared to a supine control at the same hydrostatic pressure.

The evidence that cemented support for the Starling hypothesis was obtained by Pappenheimer and Soto-Rivera (1948), who controlled the venous and arterial pressures of isolated cat limbs while continuously measuring the limb's weight. Changes in limb weight provided a measurement of the rate of water flux into or out of the limb, which closely approximates transcapillary fluid exchange (J_v). Pappenheimer and Soto-Rivera were able to estimate the capillary pressure using the model shown in Figure 1-3. If the limb is maintained in the isogravimetric condition (at constant weight), J_v=0 and flow through the system can be described by the expressions

$$F_{isog} = \frac{1}{R_a}(p_a - p_c) = \frac{1}{R_v}(p_c - p_v) \tag{1.7}$$

By simultaneously increasing p_v and decreasing p_a, the authors could create a number of isogravimetric states at any given capillary pressure. It can be seen from these equations that if either R_a or R_v is independent of flow, the plot of F vs. p_a or p_v in the isogravimetric state will be linear. Pappenheimer and Soto-Rivera found that this was indeed the case for F vs. p_v, which allowed them to estimate p_c. Flow is not a linear function of p_a because of the numerous autoregulatory mechanisms that exist in arterioles. By applying this technique to estimate capillary pressures at various perfusate osmolarities, Pappenheimer

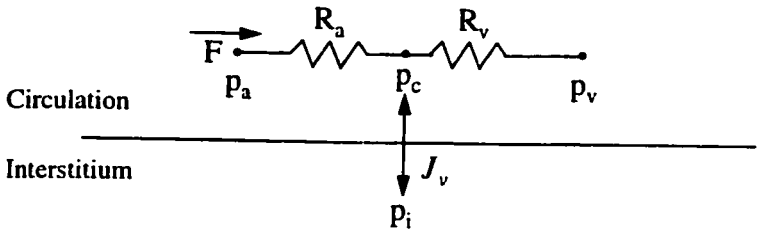

Figure 1-3 Pappenheimer and Soto-Rivera's model of circulation and exchange in a whole organ. p_a, p_v, p_c, p_i indicate the arterial, venous, capillary, and interstitial hydrostatic pressures respectively. R_a and R_v are the arterial and venous hydraulic resistances, F is the flow into the vascular system, and J_v is the transcapillary water flux.

and Soto-Rivera determined that p_c was typically 1-2 mmHg less than Π_c at steady state over a wide range of capillary protein concentrations. Since p_i was negligible, and Π_i was a few mmHg, the Starling forces in their preparation were in equilibrium.

Since R_v was independent of flow, the authors could also estimate L_p. Following a change in either arterial or venous pressure, the new capillary pressure could be calculated from

$$p_c = FR_v + p_v \tag{1.8}$$

and the capillary filtration coefficient from

$$L_p = \frac{J_v}{p_c - p_{c,\,isog}} \tag{1.9}$$

Since fluid transfer to or from the interstitial compartment will result in changes in p_i and Π_i, it is necessary that the initial rate of fluid exchange be used in this analysis.

Pappenheimer et al. (1951) also used the isogravimetric technique to measure diffusive transcapillary solute exchange by continually adjusting the arterial and venous pressures to maintain constant limb weight following injection of a test solute. This provided a time course of the osmotic pressure exerted by the solute, typically approximated by an exponential decay. The authors found that the time constants of this process were inversely related to the free diffusion coefficients of the test substances. This means that the permeabilities of the solutes were not a function of molecular size beyond the reduction in molecular mobility for larger solutes. Thus, the exchange of small hydrophilic solutes across the capillary wall was seen as a simple passive diffusive process with little steric hindrance. These measurements of filtration and diffusion rates in the microcirculation also led to the first models which attempted to explain the phenomenological behavior of the capillary wall in terms of a specific anatomical structure (see Chapter 3).

Thus, in the first half of the twentieth century it was well established that the equilibrium distribution of solutes and water across the capillary wall was passively determined by a combination of protein osmotic and hydrostatic pressures. However, it was already beginning to be recognized that the human body did not always exist in a state of equilibrium, and that other factors could influence the transient behavior of capillary exchange. One of the first workers to recognize this fact was Ancel Keys (1937) who noted:

> "... the capillaries do not actively influence the exchanges across their membranes and the final equilibrium is the result of purely passive exchanges of both water and crystalloids... It does not follow, however, that the different crystalloids penetrate the capillary membrane at equal rates or that, in normal life, equilibrium or 'steady state' conditions are invariably established."

Keys went on to argue that under certain conditions, such as those induced by exercise or drinking, the transient rate of trans-capillary water exchange is affected not only by the distribution of the relatively impermeable proteins, but also by "permeable" electrolytes which cross the capillary wall rapidly and are normally at equilibrium. However, even the fastest moving solutes diffuse more slowly than water and can exert transient osmotic effects.

By the late 1950s it was understood that transcapillary exchange of water and solutes was governed by the differences in two driving forces on either side of the capillary wall, hydrostatic pressure and concentration difference. The functional transport characteristics of the capillary wall could be described by three phenomenological parameters: the hydraulic conductivity, L_p, the solute permeability, P, and the reflection coefficient, σ. With this understanding, the focus of blood-tissue exchange research turned to ways of estimating the phenomenological transport parameters in various vessels.

1.4 Morphology of the capillary wall

The phenomenological description of transcapillary exchange based on hydraulic conductivity, permeability, and reflection coefficients must ultimately depend on the micro-scale anatomical structure of the capillaries and tissues, and the physical-chemical

properties of the solutes. A mechanistic description of transcapillary exchange not only provides more insight into the actual physical process, but constrains the possible values of the phenomenological parameters. Developing a relationship between structure and function is difficult because there are many possible pathways for transcapillary exchange, and their significance varies for different solutes, and among different organs within the same animal. Capillary walls (Figure 1-4) are comprised of endothelial cells anchored to a basement layer of intertwined collagen fibers forming a basal lamina. The endothelial lumenal surface is also coated with a glycoprotein layer called the glycocalyx, which may extend into the caveolae on the endothelial surface, and the intercellular junctions. Large gaps between or within endothelial cells known as fenestrae are present only in certain very permeable capillary beds where rapid exchange of even the largest molecules is essential to the organ's function, such as in the liver and kidney glomerulus (Taylor and Granger, 1984). Fenestrae are not present in the heart or other muscles, and the focus of the remainder of this section is on continuous capillaries where these structures are not present.

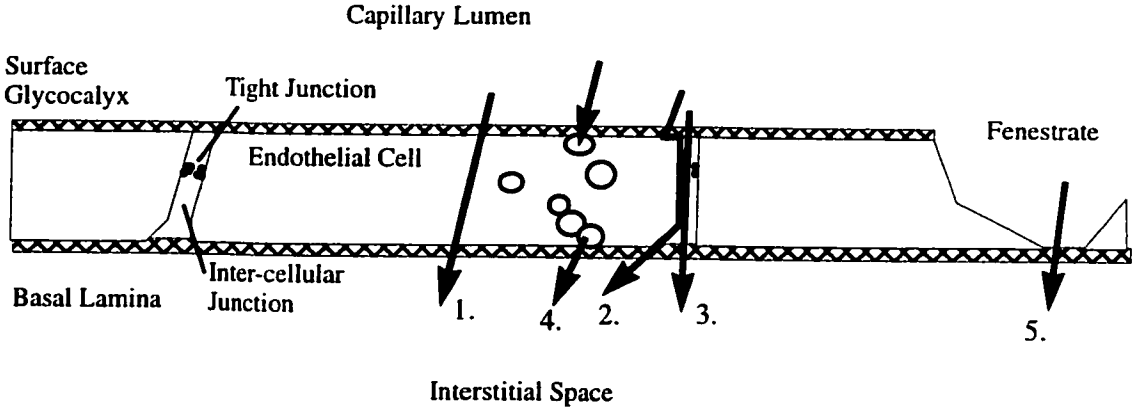

Figure 1-4 Transport pathways across the capillary wall 1. Diffusion through endothelial cells. 2. Diffusion through the plasma membrane. 3. Convection and diffusion through the intercellular junction. 4. Active transport by endothelial cell vesicles. 5. Flow through endothelial cell fenestrate.

Small lipid-soluble molecules like O_2 and CO_2 can readily diffuse across the endothelial cell membrane, and cross the capillary predominately by diffusing through the

endothelial cells or plasma membranes. Because their surface areas for exchange and permeabilities are extremely high, the movement of these solutes is not limited by the capillary wall, and their transport is not coupled to water fluxes (Renkin, 1952). Blood-tissue exchange rates for these solutes are dominated by factors such as the solubility of the gas in solution and binding to carrier molecules.

For small hydrophilic solutes, which cannot cross the endothelial cell membrane, the predominant pathway for solute transfer across the capillary wall is likely through the clefts between adjacent endothelial cells, an idea that originated with Chambers and Zwiefach (1947). These investigators noted that the very high permeability of capillaries to water and solutes compared to cellular membranes, and the lack of selectivity on any basis other than molecular size argued against bulk transport through the endothelial cells. They also argued that it would be metabolically expensive for bulk transport of all solutes to occur through endothelial vesicles. For these solutes, the permeability of the solute across the capillary wall is often the rate limiting step in transport. Water also crosses the capillary barrier through the interendothelial clefts, but water flux through the endothelial cells may also be significant for some organs.

1.4.1 The endothelial cell junction

A complete model of the capillary wall structure must explain solute permeabilities and reflection coefficients for a large range of solute sizes, as well as capillary hydraulic conductivity. A number of different models have been developed that relate phenomenological transport coefficients to a model of the physical structure of the capillary wall and the solutes that cross it. These models can be grouped into two major types. Pore theory, originated by Pappenheimer et al. (1951), is the idea that the channel between endothelial cells forms a narrow passageway through the capillary which act as a molecular filter through frictional interactions with the passing solution. Hydrodynamic models of the transport of idealized spherical solutes through right cylindrical pores or parallel-walled rectangular slits (Bean, 1972, Curry, 1974, 1984, Lightfoot et al., 1976) can be used to derive estimates of L_p, P, and σ from channel and solute dimensions (See

Appendix C). While Pappenheimer's original proposal of a single capillary pore for all solute and solvent exchange is no longer tenable, transcapillary exchange can be described in terms of multiple populations of pores (Pappenheimer, 1969, Wolf, 1994).

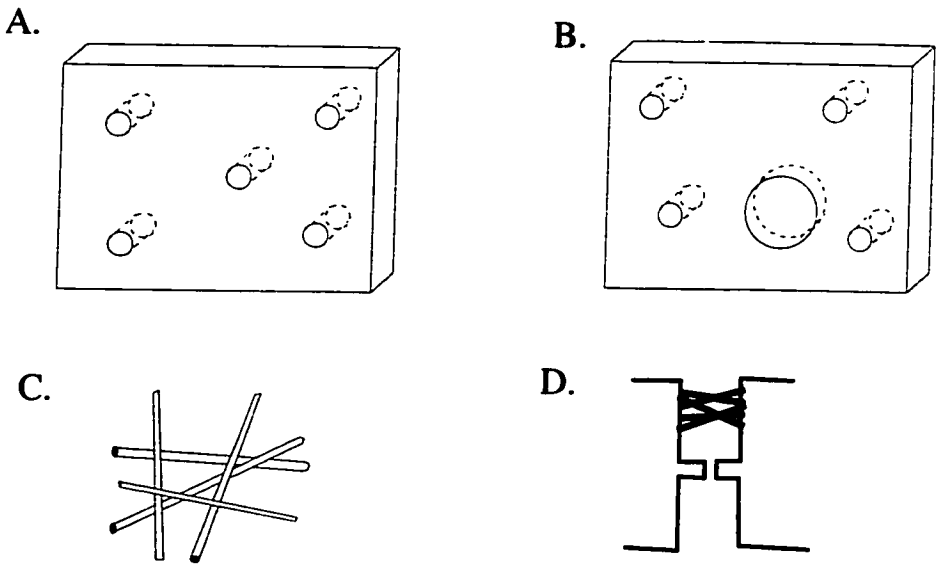

Figure 1-5 Models of the interendothelial cleft. A: Capillary wall penetrated by cylindrical pores. B: Small and large pore cylindrical pathways. C: Fiber matrix. D: Three dimension model of cleft with fiber matrix and tight junction.

Fiber matrix theory (Curry and Michel, 1980) hypothesizes that a fibrous network of proteins, such as the glycocalyx, is involved in determining transport parameters, particularly the membrane selectivity. Recently, these models have evolved into three-dimensional cleft models which include both the surface glycocalyx as a significant determinant of the transport characteristics, as well as a description of fluid flow through the endothelial junction (Weinbaum, 1992, Fu et al., 1994, Hu and Weinbaum, 1999). These models of the endothelial junction have been used to predict phenomenological coefficients without resorting to a water-exclusive pathway through the endothelial cells. In the following sections a number of quantitative models based on these two basic ideas are introduced.

1.4.2 Pathways for large solutes

The appearance of even the largest plasma proteins in the interstitial fluid, which would be predicted to be excluded from the glycocalyx and interendothelial cleft has long been taken as evidence for an additional non-selective "leak" across the capillary wall. Indeed, it is almost impossible to explain observed lymph to plasma concentration ratios for large solutes without postulating a large pore system (Taylor and Granger, 1984).

For proteins, transport through chains of fused vesicles crossing endothelial cells, or the diffusion of free vesicles between the lumenal and basal endothelial cell membranes, have been suggested to play a significant role in exchange in addition to penetration through the interendothelial junction (reviewed by Simionescu, 1984). This suggestion has arisen largely from electron microscopic observations that particles introduced into the vessel lumen are later observed in the interstitium, and in vesicles in the endothelial cells. However, much current evidence suggests that this observation may be a secondary effect, quantitatively unimportant for bulk mass transfer. This evidence (reviewed in Rippe and Haraldsson, 1994) is: 1. Bulk transport of plasma proteins follows first-order kinetics, and not Michaelis-Menton kinetics, as would be expected if proteins were binding to receptors in the vesicles. 2. The temperature dependence of the rate of protein transport is similar to that of other passive processes, and inconsistent with metabolically active process like vesicular transport. 3. Transcapillary protein transport is dependent on the capillary pressure and net water filtration, suggesting that water and proteins share a pathway across the cell. While transendothelial transport by receptor-mediated transcytosis may be significant for signaling molecules such as hormones which are present in extremely low concentrations in the plasma, it now seems unlikely to provide much capacity for bulk transport. However, it is possible that vesicles could provide a pathway for transcellular convective transport if vesicles transiently fused to create continuous fluid channels through endothelial cells, and vesicular transport is still supported by some investigators (See review by Michel and Curry, 1999).

Regardless of the exact nature of this pathway, the fact that it is not size-selective means that a simple non-selective pore model should provide an adequate description. The

cylindrical pore model presented in Appendix C will be used as a description of the large pore pathway.

1.4.3 Water-exclusive pathway

Water has only a limited solubility in the lipid bilayers of cell membranes, and most cell types with high water permeabilities have been found to express aquaporin water channel proteins (reviewed in Verkman et al., 1996, Agre et al., 1993). Although some small molecules including urea and glycerol have been shown to pass through some aquaporins, most small solutes including ions are excluded from the channels. Although the actual transcellular pathway for water consists of transport through aquaporin channels on both the lumenal and basolateral membranes, and diffusion through the endothelial cytoplasm, this path is functionally equivalent to a pure hydraulic conductance, with a permeability of 0 and reflection coefficient of 1 for all solutes. The single-channel aquaporin-1 (AQP-1) water permeability of 10^{-13} cm^3/s and density of $1.4x10^{12}$ AQP-1 monomers/cm^2 of pulmonary endothelial cell plasma membrane predict a trans-endothelial cell water permeability of 0.035 cm/s or an L_p of 3.3×10^{-8} cm $mmHg^{-1}$ s^{-1}, in good agreement with the measured value (Carter et al., 1998). Thus, in tissues with high trans-membrane hydraulic conductivity, aquaporins likely account for the majority of this capacity.

Aquaporins have predominately been localized where rapid and controlled water transport is key to the function of the organ, such as the renal proximal tubule, and pulmonary endothelium, but AQP-1 is also expressed in heart tissue (Ma et al., 1997). L_p for cardiac myocytes has been measured as $3.2x10^{-9}$ cm s^{-1} $mmHg^{-1}$ at 37 °C, which is in the range observed for protein-free lipid bilayers (Suleymanian and Baumgarten, 1996), so most transcellular water fluxes in myocytes probably occur via diffusion through the lipid bilayer. However, cardiac myocytes do express AQP-1, which is localized to the sarcolemmal caveolae under normal conditions. AQP-1 is reversibly internalized when cardiac myocytes are exposed to hypertonic solutions, so the protein may have a role in myocyte cell volume regulation (Page et al., 1998). Cardiac endothelial cells also express

AQP-1 (Hasegawa et al., 1994) and have a relatively high L_p of $1x10^{-7}$ cm s^{-1} $mmHg^{-1}$ (estimated by Vargas and Johnson, 1964). While the hydraulic conductivity through cardiac endothelial cells is too high to be explained solely by diffusion though the lipid bilayer, it is unclear whether AQP-1 is the predominant pathway, or only one of several water-specific channels expressed by these cells.

Mercurials have been shown to reversibly inhibit water transport through most aquaporins including AQP-1. $HgCl_2$ does not affect small solute transport across lung endothelium and renal *vasa recta*, but does greatly reduce osmotically-driven water fluxes when small solutes like NaCl and sucrose are the osmotic agent (Schnitzer and Oh, 1996, Carter et al., 1998, Pallone et al., 1997) .In contrast, water fluxes driven by hydrostatic pressure differences or the osmotic pressure of large solutes (e.g. albumin) persisted in the presence of $HgCl_2$. The likely explanation of these observations is that, with the aquaporin pathway blocked by $HgCl_2$, there is no remaining pathway for small solutes which has a non-negligible σ, and therefore no net volume flux across the endothelial barrier. Hydrostatic pressure and albumin concentration changes, however, are able to induce net volume flux through the endothelial cell junctions. This interpretation is complicated by the fact that mercury is extremely toxic, and the preparations required pre-fixation with glutaraldehyde. Tetraethylammonium (TEA), a blocker of K^+ channels, has also been reported to inhibit water transport by AQP-1 expressed in xenopus oocytes (Brooks et al., 2000), but has not be widely used in this role.

A pathway for solute-free water exchange appears to be a general feature of most vascular beds. The high osmotically-driven fluid movements observed during osmotic weight transient experiments in heart are strong evidence that this organ is no exception. Although there has not yet been any direct evidence that aquaporin channels play a functionally significant role in the heart, their ubiquitous expression in membranes with elevated transcellular flows suggests that they are the likely molecular basis for the solute-free water pathway.

1.5 Whole organ methods for assessing microvascular function

1.5.1 Osmotic transient methods

The isogravimetric experiments of Pappenheimer et al. (1951), designed before Staverman's (1951) introduction of the reflection coefficient, were the first experiments to track fluid movements induced by osmolarity changes. A measurement of the capillary hydrostatic pressure necessary to balance an increase in capillary osmotic pressure theoretically constitutes a measurement of $\sigma\Delta\Pi$ and permits an estimation of σ if the transcapillary concentration gradient is known. However, the isogravimetric method requires a long gradual increase of capillary concentration while the arterial and venous pressures are adjusted to maintain the isogravimetric state. Consequently, measurements of the transcapillary osmotic pressure do not begin until the transient is already well underway, and the test solute concentration in the interstitium has begun to change.

1.5.1.1 The experimental method

The osmotic weight transient approach developed by Vargas and Johnson (1964), was designed to bypass the difficulties associated with the isogravimetric approach and provide an estimate of solute reflection coefficient. In this technique, an isolated organ is continuously weighed while perfused with a Ringer's solution. When a sudden switch in perfusate osmolarity is made, the organ responds by gaining or losing fluid from the interstitial and cellular spaces. Vargas and Blackshear (1981a) demonstrated that finite post capillary volumes and compliances cause negligible delay and smoothing of the weight response by comparing osmotic weight measurements to effluent concentrations of an impermeable dye. The time course of weight change is thus nearly identical to the time course of transcapillary fluid exchange (J_v).

1.5.1.2 Analysis techniques

Analysis of osmotic weight transient time courses depends on a model of the exchange process to provide estimates of solute and solvent phenomenological transport parameters. The starting point for Vargas and Johnson's (1964) original analysis was the Kedem and Katchalsky equation for volume flow across a membrane

$$J_v = L_p\left(\Delta p - RT\sum_i \sigma_i \Delta C_i\right) \tag{1.10}$$

The volume flux across the capillary wall is given by the sum of the hydrostatic pressure difference and effective osmotic pressure differences of each solute species present. If the concentration of a test solute is increased while all other concentrations and pressures are held steady, the reflection coefficient can be estimated by

$$\sigma = \frac{J_v}{L_p RTC_{cap}} \tag{1.11}$$

Using this equation, the authors estimated σ for a series of solutes by measuring the initial rate of water loss (J_v) from isolated hearts in response to a known driving force (ΔC=C_{cap} very early in the transient before solute begins entering the interstitium).

Vargas and Johnson (1967) later expanded their analysis to include estimates of capillary permeability. The authors derived the equation

$$J_V = \sigma L_p RT e^{-\left(\frac{PS}{V_{ISF}}\right)t} \tag{1.12}$$

to estimate the time course of the weight transient, and fit this expression to the time course of weight loss to determine *PS*.

Although these simple analysis techniques continue to be used, particularly to estimate solute reflection coefficients, there have been a few attempts to apply more complete models to the osmotic transient condition. Grabowski and Bassingthwaighte (1976) developed a more detailed model that included an axially distributed blood-tissue exchange region, mechanical buffering by a compliant interstitium, fluid exchange among capillaries, interstitium, and parenchymal cells, and transcapillary fluxes of both test and resident solutes. They found this last point to be crucial in obtaining accurate estimates of

P and σ, since fluid flux out of the interstitium would sieve resident solutes previously at equilibrium and result in a concentration gradient opposing that of the test solute.

Bloom and Johnson (1981) also developed a model that incorporated separate interstitial and parenchymal volumes, convective transcapillary solute exchange, interstitial compliance, buffering by resident solutes, and drainage by the lymphatics. Simulation results showed osmolarity changes that induced a reduction in parenchymal cell volume caused a reduction in interstitial fluid concentration, because of the entry of solute-free water from the cells. This change is in the opposite direction of the buffering caused by sieving at the capillary wall. Consequently, Bloom and Johnson found a limited role for solute buffering of osmotic transients (see Section 2.4.3). The addition of other factors like the interstitial compliance to the model led to more accurate estimations of P (Johnson and Bloom, 1981). However, estimates of σ remained the same as the simple original expression.

1.5.1.3 Summary of results

Measurements of solute permeability and reflection coefficients for a range of solutes have been made in skeletal or cardiac muscle by a number of investigators including Vargas and Johnson (1964, 1967), Diana et al. (1972, 1974), Grabowski and Bassingthwaighte (1976), Bloom and Johnson (1981), Rippe and Haraldsson (1986), and Wolf and Watson (1989). These results are summarized in Figure 1-6. Due to differences in the tissue used and experimental protocol, exact comparisons among the various data sets are difficult. In particular, Wolf noted that experiments at low flow would cause a systematic under-estimation of σ, and found that he could produce estimates of σ consistent with those of previous studies in skeletal muscle by using the low flows that those authors used. While Bloom and Johnson used high flows, their experimental protocol relied on a protein-free perfusate, which may have resulted in hearts with abnormally high permeabilities (Mann, 1981, Huxley and Curry, 1991). The results most consistent with those of Wolf were Grabowski and Bassingthwaighte who used a model that accounted for flow limitation to exchange and perfused their hearts with a Ringer

solution containing albumin (although at a concentration substantially reduced from that found *in vivo*). Thus, there is considerable scatter in the estimates of σ.

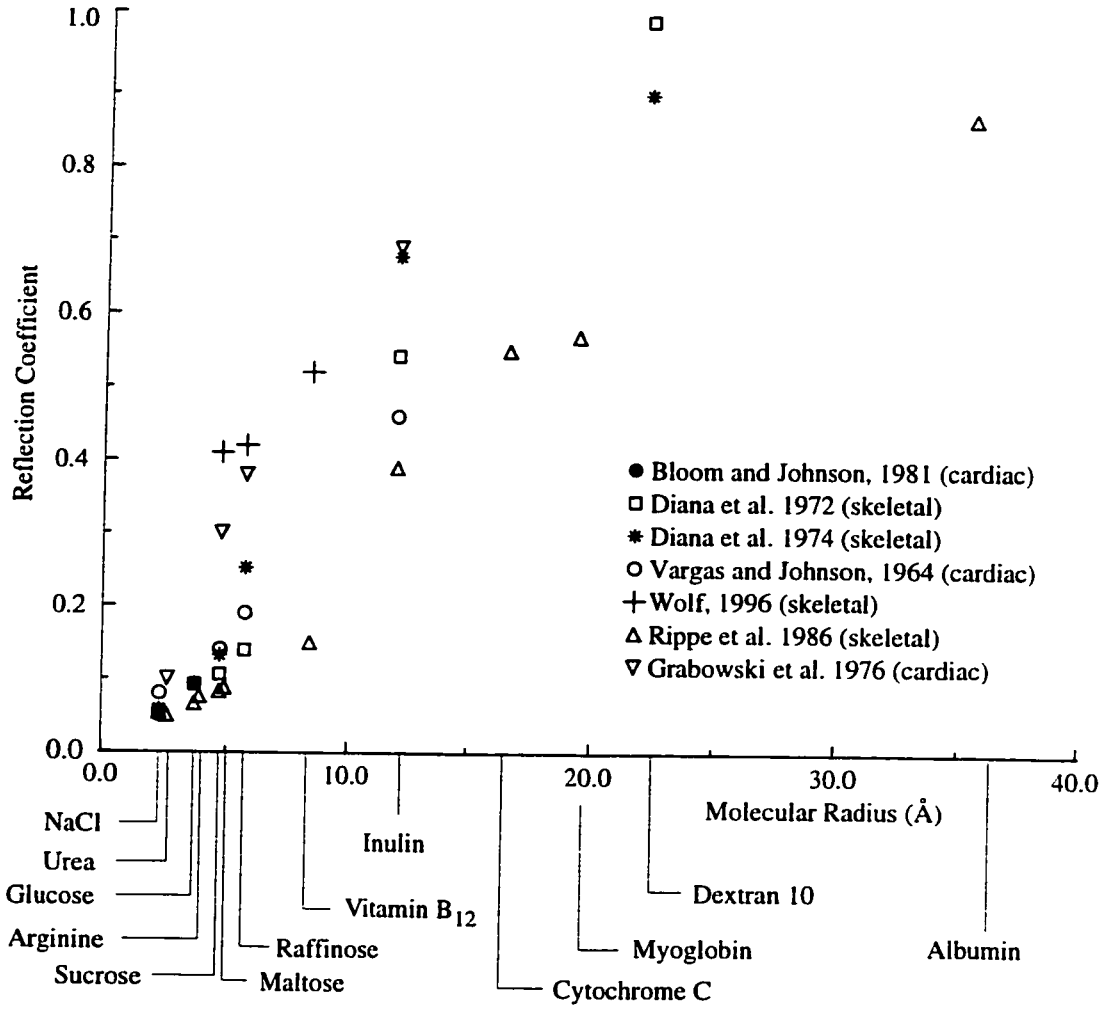

Figure 1-6 Reflection coefficient data obtained by the osmotic transient method. Data are taken from both skeletal and cardiac muscle.

In spite of these differences, some general trends are apparent from the experimental data. The reflection coefficients for even the smallest hydrophilic solutes are non-zero and increase as a function of solute size. For solutes as large as albumin, the reflection coefficient approaches but is significantly less than 1 when measurements of capillary

filtration coefficient are obtained by independent methods (such as responses to changes in hydrostatic pressure). These results imply that there is some size-selective structure to the pathway that these solutes are moving through of the same order of size as the molecules themselves and some restriction of all solutes relative to water. The walls of the endothelial cell junction, surface glycocalyx, or tight junction strand are possible structural interpretations of these results.

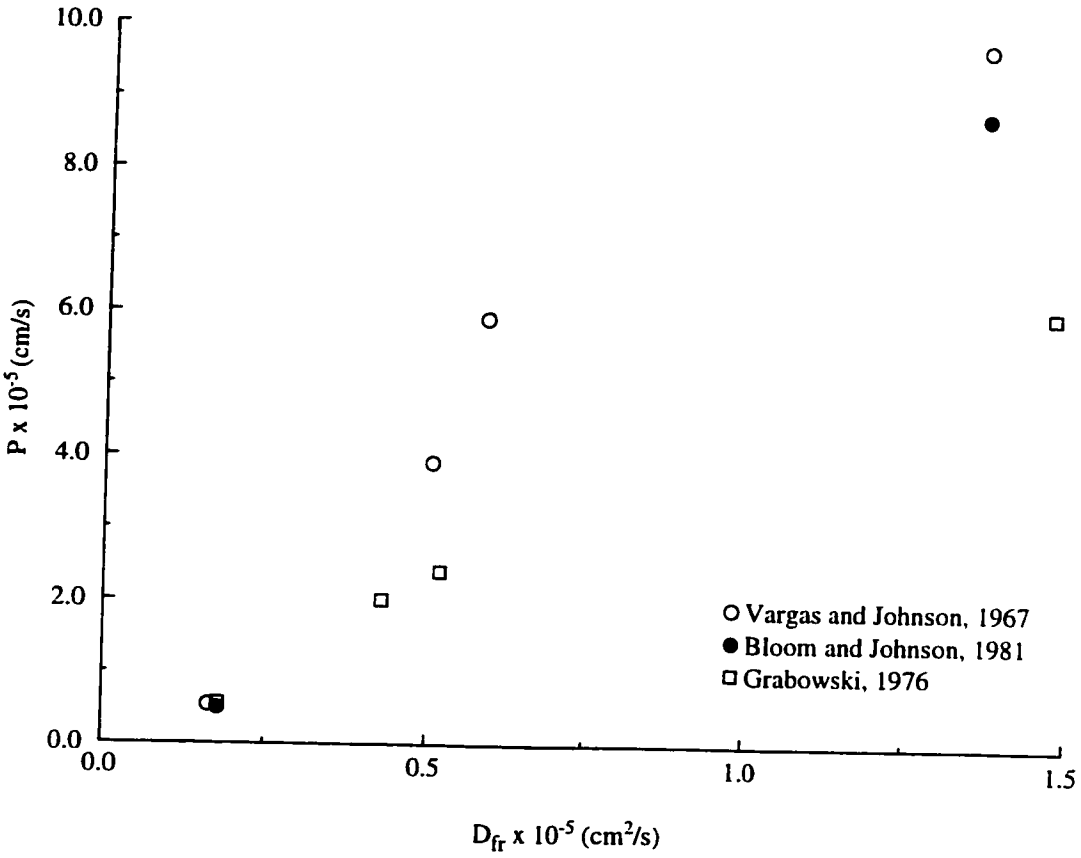

Figure 1-7 Permeabilities measured by osmotic transient in the isolated rabbit heart. Solutes used for these experiments were urea, sucrose, raffinose, and inulin for Vargas and Johnson, NaCl and inulin for Bloom and Johnson, and NaCl, sucrose, raffinose, and inulin for Grabowski and Bassingthwaighte. Some of the solutes are plotted at slightly different locations on the x-axis for different authors because the experiments were done at different temperatures and solvent viscosities, which affect D_{fr}.

The use of osmotic transient methods to estimate permeabilities has been less common for two reasons. First, accurate estimates of permeabilities depend on an accurate model of the entire time course of the weight transient, not just the initial rate of transcapillary fluid exchange. This makes osmotic-based permeability estimates much more subject to errors than estimates of reflection coefficients (Bloom and Johnson, 1981, Grabowski and Bassingthwaighte, 1976). Secondly, indicator dilution methods are commonly used to estimate solute permeability, so there is less of a need for an osmotic approach. Attempts to measure permeabilities of test molecules in the rabbit heart are shown in Figure 1-7. Grabowski and Bassingthwaighte reported uniformly lower permeabilities than Vargas and Johnson, but the origin of this discrepancy is not clear. Although Grabowski and Bassingthwaighte utilized a theoretically improved model, recent work has shown that a coding error caused them to incorrectly calculate the transcapillary solute fluxes. Additionally, the use of albumin reduced small solute permeabilities and stabilized isolated organ preparations for Grabowski and Bassingthwaighte, but not Vargas and Johnson or Bloom and Johnson.

Other osmotic transient based approaches have been developed recently and applied to lung tissue. Seale and Harris (2000) developed a novel technique for measuring the outflow concentrations of NaCl by monitoring changes in ultrasonic conduction velocity following the injection of a bolus of hypertonic saline. They were able to estimate the lumped parameter σL_p using a simple model of transcapillary exchange, but did not determine actual reflection coefficients. Responses to osmolarity changes have also been measured by using a surface fluorescence method (Carter et al., 1998, Verkman, 1998). Quantitative transport parameters for solutes were not determined from these experiments, but the authors were able to show that a significant fraction of transcapillary water flux could be blocked using the aquaporin-specific blocker $HgCl_2$.

1.5.1.4 Limitations of the method

A problem with the Vargas and Johnson analysis is that changing the volume of the interstitial region will cause other changes in the system, such as the concentration of the other resident solutes in the interstitium, and the interstitial hydrostatic pressure. This

error can be minimized by measuring the rate of weight change immediately after the test solute is introduced, before any of these errors can become significant. The technique also assumes that the concentration of test solute in the capillaries is maintained at a constant level, and that the switch from one osmolarity to another occurs quickly. For these reasons, it was essential that the flow be much higher than the permeability-surface area product of the solute to ensure a sharp change to a new constant capillary osmolarity. To achieve this condition, the authors used high flows in all their experiments, but this required perfusing the hearts with a protein-free Ringer's solution to lower perfusate viscosity. Removal of albumin from the perfusate increases capillary permeability and hydraulic conductivity, likely a result of the degradation of the endothelial glycocalyx (Mann, 1981, Huxley and Meyer, 1990, Huxley and Curry, 1991). The same treatment would therefore also presumably lower reflection coefficients.

Another source of error is that this method requires an independent estimation of the hydraulic conductivity, L_p, which must be known to determine σ. Vargas and Johnson measured this parameter by inducing osmotic transients with albumin and assumed that the reflection coefficient of this solute was 1; since $\sigma_{albumin}$ must actually be less that one L_p is overestimated and other solute reflection coefficients are underestimated. Finally, the analysis does not apply to situations in which multiple pathways for solute and water exchange occur in parallel. Errors resulting from applying single pathway methodology to a multiple path system will be examined in more detail in Section 3.4.2.

Five potential sources of error were noted by Vargas and Johnson (1967) in the derivation of Equation 1.12, and correction factors for each were applied to their final estimates of solute permeability. The first was the assumption of no flow limitation to exchange. If the transfer of material across the capillary wall is limited by the rate at which solute is entering the capillary this method will underestimate the permeability. Second, the authors noted that the solutes would have different volumes of distribution in the interstitium, with inulin experiencing a smaller volume because of steric restriction, and urea partially distributing into the cellular compartment. Third, the interstitial volume would change during the transient, but the authors did not derive any quantitative

predictions of the effect this would have on either interstitial pressure or osmolarity. Fourth, they also neglected any loss of interstitial fluid through the lymphatic system. Finally, they assumed that the contribution of solvent drag to transcapillary solute exchange would be negligible. Subsequent modeling efforts by other investigators have focused on quantitatively accounting for some of these potential sources of error by developing a more comprehensive description of the processes occurring in blood-tissue exchange, or by experimentally verifying that the effects are truly negligible.

1.5.2 Tracer-transient methods

1.5.2.1 Experimental method

Another method of estimating phenomenological parameters in whole organs was developed by Crone (1963), who developed an analytical method for determining the solute permeability from experimental methods developed by Chinard et al. (1955). In what is now known as the indicator-dilution technique, a single brief injection of a permeable test solute and a non-permeable reference solute is made into the afferent artery of an organ, and the concentration profile as a function of time is measured at the effluent vein. Since the test solute can penetrate the capillary wall and distribute in the interstitial region, its initial outlet concentration will be diluted with respect to the impermeable reference. No transcapillary water fluxes are induced because sub-micromolar quantities of the solutes are used; consequently, no information about σ or L_p is obtained using this method. (Water labeled with $^{[2]}H$ or $^{[3]}H$ as the test solute can provide information about water permeability.)

1.5.2.2 Analysis techniques

Crone's analytical method estimates solute permeability from the measured extraction of the test solute, defined as the fractional reduction of concentration as the solute passes through the organ

$$E = \frac{C_A - C_V}{C_A} \tag{1.13}$$

In the absence of a significant transcapillary water flux (J_v=0), the permeability can be defined from either the Kedem and Katchalsky or Patlak equations

$$P = \frac{J_S}{S\Delta C} \tag{1.14}$$

Early in the experiment there will be a negligible concentration of test solute in the interstitium, so ΔC can be replaced by the average capillary concentration. If the transcapillary exchange is purely passive, the axial concentration along the capillary will decay exponentially. The mean concentration in the capillary is

$$\Delta C = \bar{C}_{cap} = \frac{C_A - C_V}{\ln C_A - \ln C_V} \tag{1.15}$$

J_s, the amount of substance crossing the capillary wall, can also be calculated from the expression

$$J_S = FEC_A \tag{1.16}$$

where F is the total flow. Algebraically manipulating these expressions yields the result

$$P = \frac{F}{S}\ln\frac{1}{1-E} \tag{1.17}$$

Experimentally, E is determined by comparing the test solute outflow curve to that of the reference intravascular tracer at any given time. Many more detailed models have been developed to extend this basic method to additional cases, for example non-negligible back-diffusion of test solute, uptake and metabolism of solutes by the cells, active membrane transport, flow limitation to exchange, and binding to carrier molecules in the plasma (see review in Bassingthwaighte and Goresky, 1984).

1.5.2.3 Summary of results

Early indicator-dilution results by Crone in the dog hind limb and Alvarez and Yudilevich (1969) in the dog heart found relatively constant ratios of solute permeability to free diffusion coefficient (*P/D*) for urea, glycerol, glucose, sucrose, and inulin. Since pores with dimensions comparable to molecules hinder large molecules more than small ones, these results indicated that no restricted diffusion existed. Alvarez and Yudilevich estimated the gap between endothelial cells would need to be at least 8-10 nm for an aqueous pore to show no size-dependent properties for these molecules. Similar results were also found by a number of other workers in various preparations (see review by Crone and Levitt, 1984), and are summarized in Figure 1-8.

Experiments performed on Ringer perfused hearts show substantially higher permeabilities than those perfused with blood, even when albumin is used to augment the basic Ringer's solution. This result is consistent with microperfusion experiments performed on isolated coronary capillaries (Huxley and Curry, 1991, Huxley and Meyer, 1990) which shows that both albumin and additional serum proteins are necessary to maintain normal capillary permeability. It is crucial to note this variation because osmotic transient experiments have been performed exclusively with Ringer's or low albumin Ringer's perfusates, which has led to a historical discrepancy between indicator dilution and osmotic transient estimates of small solute permeability. Compared to estimates of permeability obtained from osmotic transient techniques, multiple indicator studies give results roughly comparable with those obtained by Grabowski and Bassingthwaighte (1976), but noticeably lower than those obtained by the simple exponential fit of Vargas and Johnson (1967).

1.5.2.4 Limitations of the method

The limitations of the indicator dilution method are generally well understood, and have been discussed in detail elsewhere (Bassingthwaighte and Goresky, 1984, Bassingthwaighte et al., 1989a). More detailed models can quantitatively account for the errors present in the Crone-Renkin approach. The uptake and metabolism of tracer solute by the parenchymal and endothelial cells and transmembrane exchange by active or

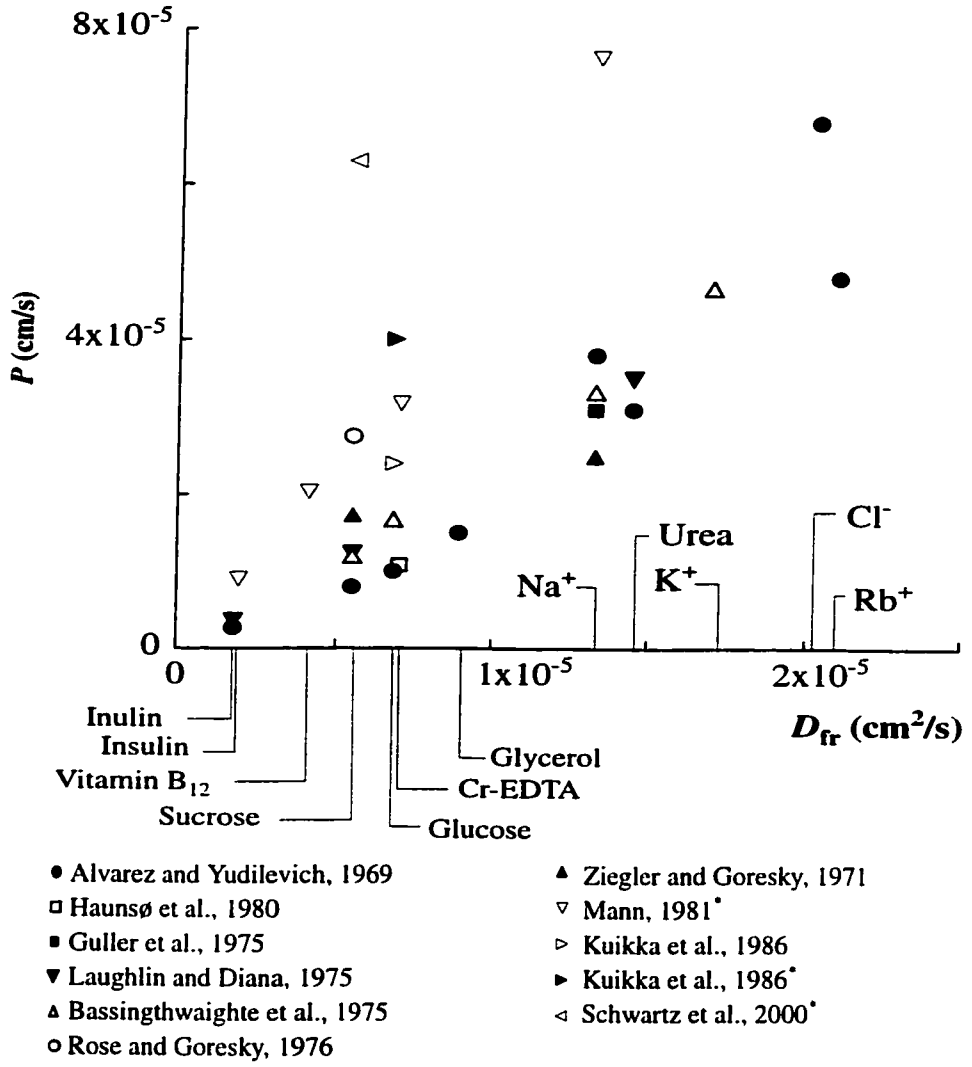

Figure 1-8 Solute permeability measured by multiple indicator dilution in cardiac tissue.
* indicates experiments performed on Ringer perfused hearts, all others are blood perfused.

passive carrier proteins have been modeled in quantitative detail by models specialized for tracer-transient analysis. These analyses permit the extension of the indicator dilution method to metabolic kinetics (Schwartz et al., 1999, 2000). Additionally, coronary perfusion is not uniform, but is distributed through a range of flows in different anatomic regions (Bassingthwaighte et al., 1989b). Flow heterogeneity has been successfully

modeled by splitting the capillary flow among a number of parallel pathways, and has been found to impact parameter estimates for multiple indicator dilution data (King et al., 1996, Kuikka et al., 1986).

1.5.3 Lymph methods

Under steady-state conditions, net flux of solute from capillary to interstitium must balance the quantity drained away by the lymphatics. The transcapillary concentration ratio approaches 1 for solutes with high diffusive permeability compared to convective transport (low Péclet number), and 1-σ for exchange dominated by convection, assuming the capillary wall acts as a single-path semi-permeable barrier to exchange. This fact has been exploited to measure the selectivity of the capillary wall, with lymph to plasma concentration ratio (C_L/C_p) commonly used as an approximation of capillary filtrate to plasma concentration ratio.

1.5.3.1 Experimental method

It has long been assumed that the fluid collected from the lymphatics has the same composition as the interstitial fluid. Extensive evidence (reviewed in Taylor and Granger, 1984) indicates that this is the case under steady-state conditions, when the lymph is sampled prior to entering a node. Thus, the steady-state ratio of lymphatic and plasma solute concentration, C_L/C_p, contains information about the transcapillary exchange process. This was first demonstrated by Grotte (1956), who showed that the C_L/C_p was dependent on molecular weight, and Mayerson et al. (1960) who demonstrated that the equilibrium C_L/C_p and equilibration rate were dependent on the organ sampled.

1.5.3.2 Analysis techniques

Renkin (1964) was the first to develop a quantitative expression for C_L/C_p. By neglecting convective solute flux across the capillary wall (assuming σ=1), Renkin derived the expression

$$PS = \frac{J_v C_L}{C_P - C_L} \tag{1.18}$$

from the Kedem and Katchalsky solute flux equation. However, the neglect of convection limits this equation to small solutes, which diffuse so rapidly across the capillary wall that a steady state concentration difference is not measurable. His analysis was later improved by Granger and Taylor (1980), who used the Patlak equation to derive an equation for the lymph to plasma ratio of solutes which included solvent drag

$$\frac{C_L}{C_P} = \frac{1-\sigma}{1-\sigma e^{-Pe}} \tag{1.19}$$

An important consequence of this equation is that with high *Pe*, C_L/C_p goes to 1-σ. This fact led to attempts to measure reflection coefficients by measuring the filtration-independent concentration ratios of lymph to plasma for various solutes.

1.5.3.3 Summary of results

The ratio of lymph to plasma concentrations typically drops rapidly from near 1 for solutes with a Stokes-radius of less than 4 nm to around 0.1 for solutes of 7 nm radius, and then declines much more slowly (Figure 1-9). The data from Arturson show almost complete size independence above an effective molecular radius of about 7 nm, which is probably because dextrans are an unbranched chain-like polymer. These molecules can reptate head-on through small openings in a movement essentially independent of the length of the molecule. When compared to reflection coefficient estimates from the osmotic transient experiments, estimates of σ from C_L/C_p ratios give lower values for solutes the size of albumin and larger. If diffusion contributes to transcapillary solute exchange, C_L/C_p will be brought closer to 1 and use of the pure convection approximation, $\sigma=1-C_L/C_p$ will overestimate σ. Pilati (1990) was careful to ensure filtration-independence and estimated a reflection coefficient for albumin of 0.59. However, adenosine, known to increase of capillary permeability, was needed in addition to venous congestion to raise filtration rates high enough to achieve filtration rate independence. It is possible that Pilati underestimated the *in vivo* value. Laine and Granger (1985) measured a filtration-rate independent value of C_L/C_p of 0.04, implying a σ of 0.96 for β-lipoprotein (molecular

radius 12.4 nm), while Pilati predicted a value of 0.88 based on a two pore model fit to a number of smaller solutes.

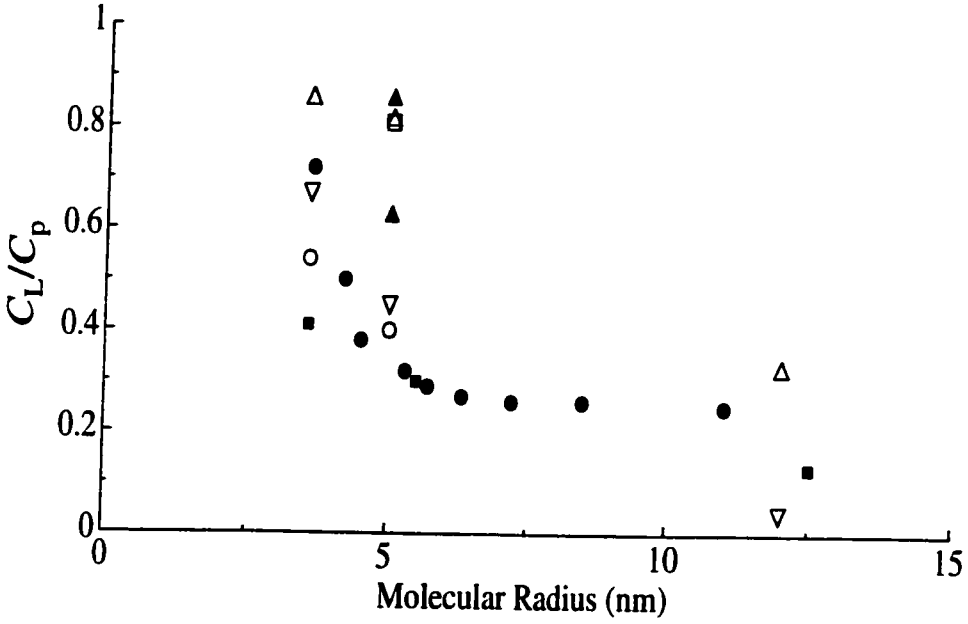

• Arturson et al., 1969 (dextran series)
▵ Laine et al., 1985 (control alb., tot. protein, β-lipoprotein)
▿ Laine et al., 1985 (high lymph flow alb., tot. protein, β-lipoprotein)
▪ Pilati, 1990 (filtration independent alb., IgG, IgM)
o Ullal et al., 1972 (alb., tot. protein)
▫ Feola and Glick, 1975 (total protein)
▴ Harris et al., 1978 (range for tot. protein)

Figure 1-9 Lymph to plasma concentration rations for various sized solutes in cardiac tissue.

1.5.3.4 Limitations of the methods

Some of the earlier measurements of cardiac C_L/C_p are of limited use because filtration rates were not reported along with the lymph composition, making application of even the simple Granger and Taylor expression (Equation 1.19) impossible (Ullal et al., 1972, Feola and Glick, 1975, Harris et al., 1978). Filtration independent measurements of C_L/C_p are particularly difficult to make in the heart because there is no single effluent vein that can be occluded to increase capillary pressure. Occlusion of the coronary sinus is not sufficient to achieve filtration rate independence for any but the largest macromolecules,

e.g. β-lipoprotein (Laine and Granger 1985). Capillary pressures of about 60 mmHg are necessary to achieve filtration rate independence for albumin, which can only be achieved through pharmacological intervention (Pilati, 1990).

1.5.4 Experimental inconsistencies

Three phenomenological transport parameters describe coupled solute-solvent transport across a permeable barrier: the hydraulic conductivity, L_p, the permeability, P, and the reflection coefficient, σ. These parameters are also commonly used to characterize transcapillary exchange, although the capillary wall is far from the infinitely thin idealized membrane presumed by irreversible thermodynamics (Kedem and Katchalsky, 1958). Several experimental techniques were devised specifically to provide estimates of these parameters in the intact vascular systems of whole organs. These included gravimetric measurements of the response to osmotic or pressure changes, the analysis of steady-state or transient concentration ratios of lymph to plasma, and the multiple-tracer indicator dilution technique. Simple analytical methods like the Crone (1965) estimate of capillary permeability and the Vargas and Johnson (1964) estimate of reflection coefficient provided a reasonable fit to the data, and enjoyed widespread use for indicator dilution and osmotic transient data respectively.

However, the various analyses, looked at together, lead to apparent contradictions. Using Crone's method for estimating capillary permeability-surface area products, Alvarez and Yudilevich (1969) observed that the ratios of solute permeability to free diffusion coefficient (P/D) were very nearly the same for urea, glycerol, glucose, sucrose, and inulin. This fact was confirmed by other researchers using the same technique (Bassingthwaighte et al., 1975, Mann, 1981), and refinements of the tracer analysis methods have not changed the result (Bassingthwaighte et al., 1989). The various hydrodynamic theories summarized by Curry (1984) predict that the cleft widths between endothelial cells through which the solutes travel must be at least 10 to 20 nm to show size independent P/D, consistent with cleft dimensions of about 20 nm observed by serial-section electron microscopy (Bundgaard, 1984).

Meanwhile, osmotic transient experiments in both whole organs (Grabowski and Bassingthwaighte, 1976, Vargas and Johnson, 1964, Vargas and Blackshear, 1981) and single capillaries (Curry et al., 1976) showed that even the smallest hydrophilic solutes had reflection coefficients that were non-zero and size-dependent, implying steric hindrance of the same molecules that showed size-independent permeability estimates. The postulation of an additional pathway allowing water exchange but no solute exchange in parallel to the endothelial cleft partly resolved the problem, as it explained non-zero reflection coefficients, but did not explain the size-dependence of σ. An endothelial gap of about 6 nm in width was necessary to make the junction a size-dependent molecular filter (Pappenheimer, 1951).

More advanced three dimensional models of the cleft and surface glycocalyx (Fu et al., 1997, Hu and Weinbaum, 1999) predict much of the separation of solutes and water occurs at the capillary glycocalyx. Although these models are consistent with the actual morphology of the capillary wall and explain large solute exchange, they do not result in a reduction of the number of pathways across the capillary wall. For example, these models do not adequately explain large transient water fluxes driven by solutes as small as urea and NaCl, because the 7 nm spacing of glycocalyx fibers is too wide. Additional evidence, presented in Section 1.4.3, implicates aquaporin water channels expressed by endothelial cells as providing the parallel pathway for solute-free water exchange.

1.6 Project summary

The central theme of this thesis is the importance of a complete theoretical model in understanding coupled fluid and solute flow across the capillary wall. The model that we develop provides the means to analyze all three of the major experimental techniques for investigating microcirculatory phenomena in whole organs (osmotic weight transient, indicator dilution, and lymph sampling). This ability to describe the results of distinct sets experimental data with the same model is an important unifying advance for the field. Chapter 2 presents a description of the model, as well as fits to previously obtained indicator dilution and lymph sampling data in cardiac tissue. Chapter 3 then presents a

detailed analysis of novel osmotic weight transient data in isolated Ringer-perfused hearts. Together, these two studies demonstrate that the model provides a relatively complete and accurate description of the transcapillary exchange process.

2 An Integrative Model of Coupled Solute-Solvent Exchange in Cardiac Tissue

Physiologists have devised many models for interpreting water and solute exchange data in whole organs, but the models have typically neglected key aspects of the underlying physiology to present the simplest possible model for a given experimental situation. We have developed a physiologically realistic model of microcirculatory water and solute exchange and applied it to diverse observations on water and solute exchange in the heart. Model simulations are consistent with the results of osmotic weight transient, tracer indicator dilution, and steady-state lymph sampling experiments. The key model features that permit this unification are the use of an axially-distributed blood–tissue exchange region, inclusion of a lymphatic drain in the interstitium, and the independent computation of transcapillary solute and solvent fluxes through three different pathways.

2.1 Introduction

Physiologists are interested in the exchange of material between capillaries and their surrounding tissues because this process is fundamental to the viability of multicellular life. The kinetics of coupled solute–solvent exchange across capillary walls can be described phenomenologically by three parameters: the hydraulic conductivity, L_p, the permeability, P, and the reflection coefficient, σ (Kedem and Katchalsky, 1958). The values of these parameters can be determined by several experimental methods, including the measurement of the outflow concentration time courses of solutes following a bolus injection of tracers (the multiple-tracer indicator dilution technique), the gravimetric or isogravimetric measurement of the response to perturbations of osmotic or hydrostatic pressures (the osmotic transient method), and the simultaneous measurements of solute concentrations in lymph and plasma (lymph sampling techniques). Reasonable fits to data from these sources have been obtained using relatively simple analytical methods, like the Crone-Renkin estimate of capillary permeability (Crone, 1963), the Vargas and Johnson (1963) estimate of reflection coefficient, and the "pore-stripping" analysis of Renkin et al.

(1977). These analysis methods have enjoyed widespread use in determining transport parameter values from indicator dilution, osmotic transient, and lymph data respectively.

Although mathematically independent, all three phenomenological transport parameters must actually arise from the physical and chemical properties of the exchanging solution, and the anatomical structures that create the pathways for its exchange across capillary walls. This fact has motivated the development of models based on fluid dynamics that relate the phenomenological transport parameters to a mechanistic description of transcapillary exchange. Standard pore theory represents the passages across the capillary wall as idealized cylindrical pores through an otherwise impermeable barrier; the transport parameters then arise from frictional interactions between solution and pore walls, and the steric exclusion of solute from part of the pore (Pappenheimer et al. (1951), Bean, 1972, Curry, 1974 , Lightfoot et al., 1976 , Lewellen, 1982). Even though there is no strict correspondence between the idealized pores and actual capillary morphology, pore models have provided both a functional description of diverse sets of exchange data, and a constraint on the possible values of the transport parameters. More recently, three-dimensional models of the cleft and surface glycocalyx, derived from the actual morphology of the capillary wall, have provided a more detailed description of fluid and solute flows through the endothelial junction. These newer models ascribe at least some of the resistance to exchange to endothelial glycocalyx rather than the cleft walls (Fu et al., 1997, Hu and Weinbaum, 1999).

The results of analyzing different experiments using the standard methods of analysis lead to apparent contradictions when examined together and interpreted by pore theory. Using Crone's method for estimating the product of capillary permeability and surface area (*PS*), Alvarez and Yudilevich (1969) observed that the ratios of solute permeability to free diffusion coefficient (*P/D*) were very nearly the same for urea, glycerol, glucose, sucrose, and inulin. This fact was confirmed by other researchers using the same technique (Bassingthwaighte et al., 1975, Mann, 1981), and refinements of the methods for tracer analysis have not changed the observation (Bassingthwaighte et al., 1989). This result implies that permeation of these solutes is dependent only on the solute diffusion

coefficient, and not on any steric hindrance due to glycocalyx or cell walls; the cleft widths between adjacent endothelial cells must be at least 10 to 20 nm for this to be true. Size independent *P/D* for these solutes is consistent with endothelial junction widths of about 20 nm observed by serial-section electron microscopy (Bundgaard, 1984).

On the other hand, osmotic transient experiments in both whole organs (Grabowski and Bassingthwaighte, 1976, Vargas and Johnson, 1964, Vargas and Blackshear, 1981, Wolf and Watson, 1989) and single capillaries (Curry et al., 1976) showed that even the smallest hydrophilic solutes induced transient transcapillary water exchange, demonstrating that their passage across the capillary wall was hindered relative to water. Small solute reflection coefficients were non-zero and weakly size-dependent, implying relative steric hindrance of the same molecules that showed size-independent permeability estimates. Pappenheimer interpreted similar data from an isogravimetric hindlimb preparation as requiring a cleft with an equivalent pore width of 6 mn to make the junction a size-dependent molecular filter (Pappenheimer, 1953).

This contradiction between indicator dilution and osmotic transients results can be resolved by the postulation of an additional pathway for solute-free water exchange, occurring in parallel to the pathway for coupled water and solute exchange through the endothelial cleft. Non-zero reflection coefficients can then be understood as an averaging between selective and non-selective pathways. The evidence supporting a distinct pathway for water-flux only is not purely circumstantial; Effros (1974) demonstrated that the fluid extracted from lung tissues during an increase in perfusate osmolarity was essentially solute-free, implying the existence of an additional, presumably trans-cellular, pathway across the capillary. The recent identification of the ubiquitous expression of aquaporin water channels in the endothelial cells of most organs (Verkman et al., 1996) and the demonstration that the movement of osmotically-driven water exchange can be inhibited by known inhibitors of aquaporins (Carter et al., 1998, Effros et al., 1997) has precisely identified the molecular basis for solute-free water movements.

It is now understood that capillary walls typically contain at least three pore systems: a small pore system corresponding to the endothelial junction, a large pore system through

vesicles or infrequent breaks in the capillary wall structure, and a pathway for water only pathway interpreted as transport across the endothelial cell membranes. However, although it is understood that the behavior of heterogeneous membranes can not be reproduced by a single-pathway equivalent (Rippe and Haraldsson, 1994), this complexity has typically not been built into models of the microcirculatory exchange process. This is one of the reasons that no single model has been applicable to osmotic transient, indicator dilution, and lymph sampling data. This chapter presents a physiologically realistic model of the transcapillary exchange process that successfully reproduces the key behaviors observed during all three of these experimental methodologies. In doing so, it represents a key conceptual unification of the field.

2.2 The Model

Microcirculatory exchange (Figure 2-1) consists of the coupled transcapillary exchange of fluid (J_{Vc}) and solutes (J_s), lymphatic drainage of interstitial fluid (F_L), and water exchange across the parenchymal cell membrane (J_{Vpc}). These fluxes determine changes in the fluid volumes of interstitium ($V_{f,isf}$) and parenchymal cells ($V_{f,pc}$), perfusate velocities (u) in a constant-volume capillary, and solute quantities of N_s different solutes in all three regions (n_c, n_{isf}, and n_{pc})

$$\frac{\partial u}{\partial x} = \frac{-S_c J_{Vc}}{V_c} \tag{2.1}$$

$$\frac{\partial V_{f,isf}}{\partial t} = S_c J_{Vc} + S_{pc} J_{Vpc} - F_L \tag{2.2}$$

$$\frac{\partial V_{f,pc}}{\partial t} = -S_{pc} J_{Vpc} \tag{2.3}$$

$$\frac{\partial n_{c,j}}{\partial t} = -\frac{\partial}{\partial x}(u \cdot n_{c,j}) - S_c J_{s,j} \text{ for j=1 to } N_s \tag{2.4}$$

$$\frac{\partial n_{isf,j}}{\partial t} = S_c J_{s,j} - F_L C'_{isf,j} \text{ for j=1 to } N_s \tag{2.5}$$

$$\frac{\partial n_{pc,j}}{\partial t} = 0 \text{ for j=1 to } N_s \tag{2.6}$$

where the physiological variables are assumed to be functions of time (t) and one spatial dimension (x). S_c and S_{pc} are the surface areas of capillaries and parenchymal cells respectively, and C'_{isf} is the effective solute concentration in the interstitium. Solute exchange across parenchymal cell membrane is set to zero because transplasmalemmal fluxes of most hydrophilic solutes do not occur; even glucose transport is very small (Kuikka et al., 1986). The following sections expand on this foundation by providing more specific definition of the terms used, and by relating perturbations in organ-level flows, pressures, or perfusate composition to changes in fluid and solute fluxes at the microvascular level.

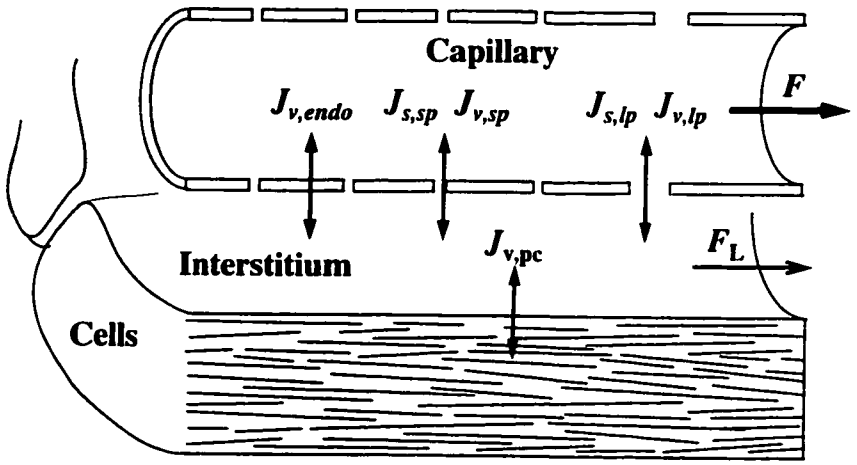

Figure 2-1 Mass transport in a blood-tissue exchange unit consists of axial flow through the capillary (F), transcapillary fluid flux (J_v, calculated in Equation 2.28) and solute flux (J_s, calculated in Equation 2.42) through large and small pore pathways, fluid flux only across endothelial cells ($J_{v,endo}$, calculated in Equation 2.28) and myocardial cells ($J_{v,pc}$, calculated in Equation 2.34), and drainage of interstitial fluid by the lymphatics (F_L, calculated in Equation 2.35).

2.2.1 Pressure-flow relationship in vascular networks

Since capillary hydrostatic pressure can not be measured directly in intact organs, a relationship must be defined between this quantity and observable variables such as flow, arterial pressure, and venous pressure. The organ's vasculature is modeled using lumped hydraulic resistances (Ω) to represent different portions of the vascular network, as shown in Figure 2-2A. The relationship between arterial pressure (p_a), venous pressure (p_v), and flow (F) at any given time is

$$p_a - p_v = F(\Omega_a + \Omega_c + \Omega_v) \tag{2.7}$$

Under many experimental situations p_a, p_v, and F are measurable, allowing calculation of the total vascular resistance from Equation 2.7 (Figure 2-2B). The relative distribution of vascular resistances for the heart (Chilian et al., 1990) and known geometry of the coronary capillary bed (Section 2.2.2) can be used to estimate Ω_c and Ω_v. The capillary inlet (p_{ci}) and outlet pressures (p_{co}) are then

$$p_{ci} = F(\Omega_c + \Omega_v) + p_v \tag{2.8}$$

$$p_{co} = F\Omega_v + p_v \tag{2.9}$$

Equations 2.7-2.9 are good approximations even when the fluid flow in veins is reduced by net filtration (J_v) from capillary to interstitium. The maximal values of J_v, obtained during the initial phase of an osmotic transient experiment, are less than 0.1 mL min^{-1} g^{-1} compared to F of at least 2 mL min^{-1} g^{-1}. These pressures and flows should be understood as mean values averaged over the cardiac cycle; cyclic flows caused by cardiac contraction have a negligible effect on the rate of solute equilibration between perfusate and interstitial fluid (Bassingthwaighte et al., 1970) and occur over a faster time scale than exchange processes. Pressures and flows also vary as hydraulic resistance is modulated by changes in transmural pressure, and neuronal, humoral, and myogenic regulation, but detailed descriptions of these phenomena are beyond the current scope of the model.

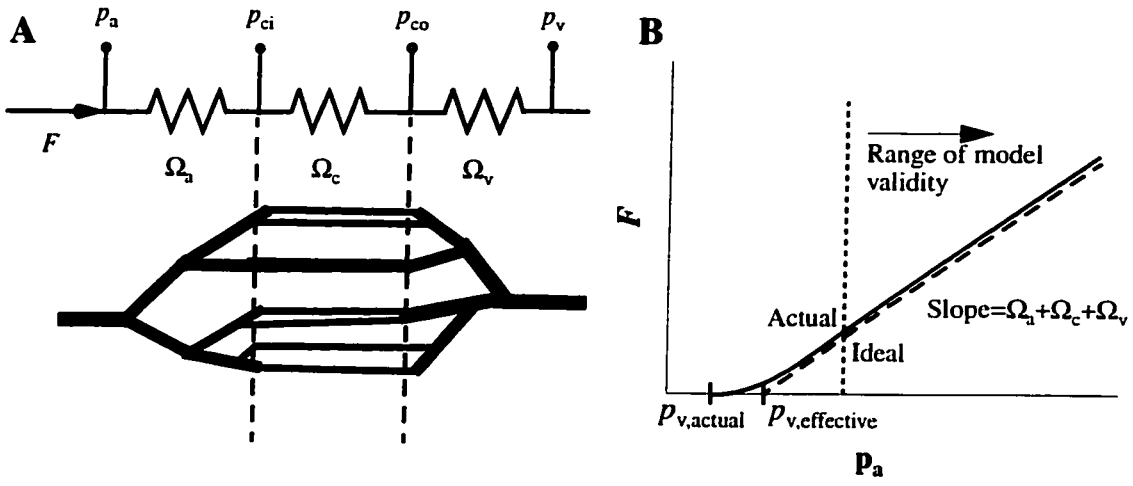

Figure 2-2 Flow through a vascular network (**A**) is modeled as flow through three lumped resistances corresponding to arteries, capillaries, and veins. Electrical analog circuit is shown above. (**B**) At very low flows the observed pressure-flow relationship (solid line) may deviate from the linear relationship of Equation 2.7 (dashed line) due to changing vascular volumes, but the slope is constant in the normal physiological range. Equation 2.7 is valid although the venous pressure does not match the actual zero-flow pressure.

2.2.2 Cardiac tissue organization

The organ volume is taken to consist of large vessels, and a symmetrical array of blood-tissue exchange (BTEX) units comprised of a capillary and surrounding tissue. The relationships between the dimensions of the BTEX unit (see Figure 2-3) and the initial anatomic volumes (v) and surface areas for exchange (S) of the capillary, interstitial and parenchymal cell subregions are

$$v_{btex} = \frac{\sqrt{3}}{2} d_{ic}^2 l_c \tag{2.10}$$

$$v_c = \pi r_c^2 l_c \tag{2.11}$$

$$v_{isf} = \pi[(r_c + d_{im})^2 - r_c^2] l_c + 2[d_{ic} - 2(r_c + d_{im})] d_{im} l_c \tag{2.12}$$

$$v_{pc} = v_{btex} - v_{isf} - v_c \tag{2.13}$$

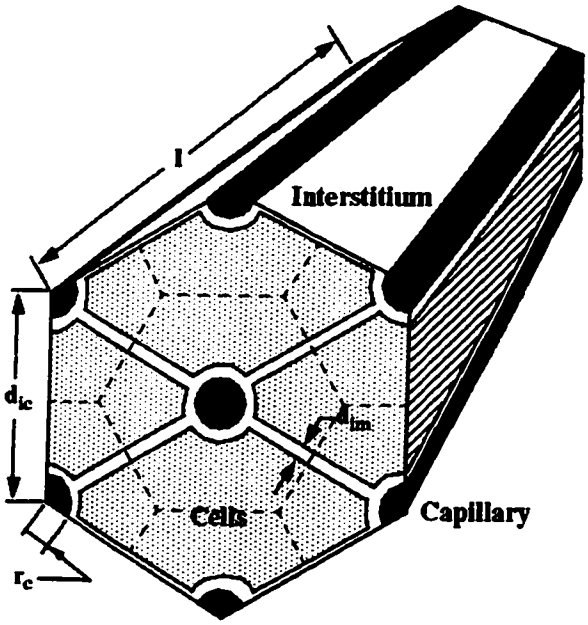

Figure 2-3 Cardiac tissue geometry is modeled using a hexagonal array of Krogh cylinders, with one capillary per blood tissue exchange unit. Intercapillary distance, d_{ic}=19 μm, capillary radius, r_c=2.5 μm, intermyocyte spacing, d_{im}=1.8 μm, capillary length, l_c= 639 μm.

$$S_c = 2\pi r_c l_c \tag{2.14}$$

$$S_{pc} = 2l_c\pi(r_c + d_{im}) - 4l_c d_{im} + 4l_c[d_{ic} - 2(r_c + d_{im})] \tag{2.15}$$

The interstitium and myocardial cells are modeled as a composite of fluid and solid phases uniformly distributed throughout the region. The solids present in cardiac tissue are predominately collagen (col) and other matrix proteins (im) in the interstitium, and myofilaments and other large protein structures in the cells. The fluid volume and solid volumes in each region (V_f and V_s) are

$$V_{f,c} = v_c \tag{2.16}$$

$$V_{s,isf} = v_{isf}\frac{(Q_{im} + Q_{col})}{\rho_s} \tag{2.17}$$

$$V_{f,\,isf} = v_{isf} - V_{s,\,isf} \tag{2.18}$$

$$V_{s,\,pc} = v_{pc}\frac{Q_{pc}}{\rho_s} \tag{2.19}$$

$$V_{f,\,pc} = v_{pc} - V_{s,\,pc} \tag{2.20}$$

where Q_{col} is the quantity of interstitial collagen per unit interstitial volume, Q_{im} is the quantity of other interstitial matrix proteins per unit interstitial volume, Q_{pc} is the cellular quantity of solid protein components per unit cellular volume, and ρ_s is the density of the solid components.

Table 2-1: Typical Geometric Parameter Values

Parameter	Value
ρ_f	1.01 g/mL (Weast, 1979)
ρ_s	1.33 g/mL (Bassingthwaighte, 1991)
d_{ic}	18 μm (Bassingthwaighte, 1991)
d_{im}	1.8 μm (assumed)
l	639 μm (Batra and Rakusan, 1990)
r_c	2.5 μm (Bassingthwaighte, 1991)
$\hat{V}_{cap}$	0.060 mL/g (calculated*)
$\hat{V}_{isf}$	0.22 mL/g (calculated*)
$\hat{V}_{myo}$	0.43 mL/g (calculated*)
$\hat{V}_{lv}$	0.085 mL/g (calculated*)
$\hat{S}_{cap}$	481 cm^2/g (calculated*)
$\hat{S}_{myo}$	1743 cm^2/g (calculated*)
ρ_{org}	1.061 g/mL (calculated*)
$\hat{N}_{caps}$	$4.8 \times 10^6\ g^{-1}$ (calculated)

*Consistent with values in Gonzalez and Bassingthwaighte (1990)
+average density of protein, carbohydrate and fat in cardiac tissue

Changes in volumes at the level of BTEX units are related to more readily observable whole organ quantities (see Table 2-1). On a whole organ basis, if the volume fraction of the large vessels is $\widehat{V}_{lv}$, the fractional volumes ($\widehat{V}_i$) of the capillary, interstitial, and myocyte regions are

$$\widehat{V}_i = (1 - \widehat{V}_{lv})\frac{V_i}{v_{btex}} \quad \text{for } i = \text{cap, isf, or pc fluid or solid volumes.} \tag{2.21}$$

The density of the organ (ρ_{org}) can then be computed from

$$\rho_{org} = \rho_f \widehat{V}_{lv} + \sum_i (\rho_f \widehat{V}_{f,i} + \rho_s \widehat{V}_{s,i}) \tag{2.22}$$

Specific volumes and surface areas ($\hat{V}$) are

$$\hat{V}_i = \frac{\widehat{V}_i}{\rho_{org}} \tag{2.23}$$

$$\hat{S}_i = \frac{S_i}{v_{btex}} \frac{(1 - \widehat{V}_{lv})}{\rho_{org}} \quad \text{for } i = \text{c or pc.} \tag{2.24}$$

and the number of capillaries per unit organ mass ($\hat{N}_c$) is

$$\hat{N}_c = \frac{\hat{V}_c}{v_c} \tag{2.25}$$

The total number of capillaries in the organ (N_c) remains constant as the product of $\hat{N}_{cap}$ and the initial organ weight, W^o; capillary recruitment is not considered. The weight of the organ as a function of time can be found by adding the weights of each region. The weight of the solid components and vascular regions is constant, so any observed weight change of the organ is caused by fluid loss or gain in the interstitium or parenchymal cells

$$W(t) = N_c[(V_{cap} + V_{f,isf} + V_{f,pc})\rho_f + (V_{s,isf} + V_{s,pc})\rho_s] + \hat{V}^o_{vas}\rho_f W^o \tag{2.26}$$

The tissue model can also be used to estimate the hydraulic resistance of the capillary bed, assuming Poiseuille flow through the bed of parallel cylindrical capillaries

$$\Omega_C = \left(\frac{8\eta l_c}{\pi r_c^4}\right)\frac{1}{N_c} \tag{2.27}$$

2.2.3 Fluid Exchange

Transcapillary fluid exchange occurs through multiple parallel pathways which are treated purely phenomenologically in this section. The volume flux through the *k*th pathway from capillary to interstitium, J_{vk}, as a function of axial position in the capillary, is given by

$$J_{vk} = L_{pk}\left\{(p_c - p_{isf}) - \sum_j [\sigma_{j,k}(\Pi_{c,j} - \Pi_{isf,j})] + \Pi_M\right\} \tag{2.28}$$

where L_{pk} is the hydraulic conductivity through the *k*th pathway, $\sigma_{j,k}$ is the reflection coefficient of the *j*th solute in the *k*th pathway, and $\Pi_{c,j}$ and $\Pi_{isf,j}$ are the osmotic pressures of the *j*th solute in capillary and interstitium, and Π_M is the osmotic pressure exerted by interstitial matrix proteins. The total transcapillary flux (J_{vc}) is then the sum of the individual pathways

$$J_{vc} = \sum_k J_{vk} \tag{2.29}$$

The osmotic pressures of the mobile solutes in each region are described empirically by the virial expansion (see Table 2-2)

$$\Pi_j = RT(\phi_{1,j}C'_j + \phi_{2,j}C'^{\,2}_j + \phi_{3,j}C'^{\,3}_j) \tag{2.30}$$

This expression contains no solute-solute interaction terms, although these interactions are implied by non-zero second and third virial coefficients. The virial coefficients for one solute should therefore strictly be considered to be a function of the concentrations of all

other solutes. In practice, only one solute (albumin) has non-zero terms beyond the first virial coefficient so this difficulty is avoided.

The effective concentration (C') is

$$C'_j = \frac{n_j}{\gamma_j V_f} \tag{2.31}$$

which accounts for the exclusion of the solute from a certain fraction (γ) of the interstitial space by the interstitial matrix fibers. This fraction is dependent on the solute radius (r_j), and fiber quantity (Q_{im} or Q_{col}), radius (r_f), and density (ρ) (Cury, 1984)

$$\gamma_j = \exp\left[-\frac{Q_{im}}{\rho_{im}}\left(\frac{2r_j}{r_{f,im}} + \frac{r_j^2}{r_{f,im}^2}\right)\right]\exp\left[-\frac{Q_{col}}{\rho_{col}}\left(\frac{2r_j}{r_{f,col}} + \frac{r_j^2}{r_{f,col}^2}\right)\right] \tag{2.32}$$

Distribution effects are neglected in the parenchymal cells where only total cell osmolarity, not concentrations of individual species are modeled.

In addition to the osmotic pressure of the solutes present in plasma and interstitial fluid, interstitial matrix components, especially hyaluronate, exhibit a significant osmotic pressure, as evidenced by the reduction in tissue water following enzymatic digestion of this molecule (Sunnergren, 1985). The osmotic pressure of the immobile interstitial matrix components (Π_M) is given by the empirical relationship

$$\Pi_M = \psi_1 Q_{im} + \psi_2 Q_{im}^2 + \psi_3 Q_{im}^3 \tag{2.33}$$

Similarly, the water flux across the parenchymal cell membrane from cells to interstitium is given by

$$J_{v,pc} = L_{p,pc}\left((p_{pc} - p_{isf}) - \left(\Pi_{pc} - \Pi_M - \sum_j \Pi_{isf,j}\right)\right) \tag{2.34}$$

High interstitial pressures and low lymphatic outlet pressures promote drainage of the interstitium through the lymphatics, while the presence of valves in the lymphatic vessels

prevents back-flow (Laine and Granger, 1985, Schmid-Schöbein and Ikomi, 1995). These facts lead to an empirical relationship between interstitial pressure and lymph flow (F_L)

$$F_L = K_L(p_{isf} - p_L) \text{ for } p_{isf} > p_L \tag{2.35}$$

$$F_L = 0 \text{ for } p_{isf} \leq p_L \tag{2.36}$$

Capillary hydrostatic pressure is modeled as a linear gradient with end points set by the whole organ pressure-flow relationship. Net transcapillary water exchange is negligible compared to axial convection, so the linear gradient remains a reasonable approximation even during transcapillary fluid movements. Interstitial and parenchymal cell hydrostatic pressures are in general functions of the change in volume of these regions, and are modeled using an empirical formula

$$p_c(x) = p_{co} + (p_{ci} - p_{co})\left(\frac{l_c - x}{l_c}\right) \tag{2.37}$$

$$p_{isf} = p^o_{isf} + \Delta V_{isf}(E_1 + E_2|\Delta V_{isf}| + E_3\Delta V^2_{isf}) \tag{2.38}$$

$$p_{pc} = p^o_{pc} + \Delta V_{pc}(E_1 + E_2|\Delta V_{pc}| + E_3\Delta V^2_{pc}) \tag{2.39}$$

Here ΔV is defined as a fractional change in volume compared to the initial value

$$\Delta V_i = \frac{V_i - V^o_i}{V^o_i} \tag{2.40}$$

As a practical matter, terms beyond E_1 are small enough that one can assume a constant compliance, at least over a relatively small range of volume changes. With marked edema, the interstitium may reach a yield point where compliance rapidly increases, and the linear model is no longer appropriate.

Capillary flows are assumed homogeneous, so the perfusate velocity at the capillary inlet is given by the boundary condition

$$u(t, x = 0) = \frac{F(t)}{N_c \pi r_c^2} \tag{2.41}$$

Table 2-2: Fixed Solute Parameters

Solute	C^o (control)	Radius (Å)	D (cm^2/s)$^+$	ϕ_1	ϕ_2	ϕ_3
Collagen	0.05 g/mL[(1)]	40	0	0	0	0
GAG*	1.3 mg/mL[(1)]	4	0	13.5[(2)]	2320[(2)]	154000[(2)]
Albumin	0.75 mM	36[(3)]	0.068×10^{-5} [(3)]	0.924[(5)]	0.483[(5)]	0.279[(5)]
NaCl	150 mM	2.5[(4)]	1.48×10^{-5} [(4)]	1.87[(4)]	0[(4)]	0[(4)]
Sucrose	0 mM	5.2[(4)]	0.521×10^{-5} [(4)]	1[(4)]	0[(4)]	0[(4)]

(1) Aukland and Reed (1993)
(2) Shaw (1977)
(3) Tanford (1961)
(4) Weast (1979)
(5) Levick (1994)
*Lumped interstitial matrix protein, including GAG and hyaluronate, radius is fiber radius
+At 25 °C

2.2.4 Solute Exchange

Solute fluxes are calculated from the non-linear solute flux equation developed by Patlak et al. (1963). This equation correctly accounts for the coupling between convective and diffusive flux that occurs when convection alters the quasi steady-state concentration profile within the membrane. The total flux of a solute from capillary to interstitium, $J_{s,j}$, is given by the sum of diffusive and convective transport for each path

$$J_{s,j} = \sum_k \left[J_{Vk}(1 - \sigma_{j,k}) C_{c,j} + P_{j,k}(C_{c,j} - C'_{isf,j}) \left(\frac{Pe_{j,k}}{e^{Pe_{j,k}} - 1} \right) \right] \tag{2.42}$$

$Pe_{j,k}$ is the Péclet number for the jth solute traveling through the kth pathway, defined by

$$Pe_{j,k} = \frac{J_{Vk}(1-\sigma_{j,k})}{P_{j,k}} \tag{2.43}$$

The boundary conditions at the capillary inlet for solute are

$$\frac{d}{dt}n_{c,j}(t, x=0) = C_{ci,j}(t)F(t) \tag{2.44}$$

2.2.5 Pore models for transcapillary exchange

While transcapillary exchange can be calculated if a complete set of phenomenological coefficients is given, the number of parameters that must be specified soon becomes unwieldy for physiologically realistic conditions. A mechanistic model of each pathway for exchange provides a constraint which limits the values that these parameters can take. Two pathways for solute and water exchange are modeled as cylindrical pores that permit the passage of spherical solutes following the equations derived by Bean (1972) to relate L_p, P, and σ to pore and solute geometry

$$L_p = \left(\frac{A_p}{S_c \Delta r}\right)\frac{r_p^2}{8\eta} \tag{2.45}$$

$$P = \left(\frac{A_p}{S_c \Delta r}\right)(1-\alpha)F(\alpha)D \tag{2.46}$$

$$\sigma = 1-[1-(1-(1-\alpha)^2)^2]G(\alpha) + \frac{16}{9}\alpha^2(1-\alpha)^2F(\alpha) \tag{2.47}$$

with r_s the solute radius, D the solute diffusion coefficient, η the solvent viscosity, r_p the pore radius, A_p the total pore surface area, and $\alpha = r_s/r_p$. Values of the hydrodynamic functions $F(\alpha)$ and $G(\alpha)$ are given in Appendix C, and more completely derived in Curry's (1984) review. An additional pathway exclusive to water ($P = 0$, $\sigma = 1$ for all solutes) representing transport across the endothelial cell plasmalemma is defined by a single value of $L_{p,endo}$. Thus, exchange of fluid and solutes across the capillary wall can be described by

five parameters, assuming r_s, D, and η are assumed known: r_{sp}, $A_{sp}/S\Delta r$, r_{lp}, $A_{lp}/S\Delta r$, and $L_{p,endo}$.

2.2.6 Numerical solution

The numerical solution to the system of the partial differential equations was obtained by discretizing the blood–tissue exchange unit in space, and separating axial convection from radial exchange (Figure 2-4). The model time step was defined as the time for convection to move the capillary fluid exactly one axial segment down stream in the absence of transcapillary fluid exchange (Bassingthwaighte, 1974, Bassingthwaighte et al., 1989)

$$\Delta t = \frac{N_c V_c}{F N_{seg}} \tag{2.48}$$

Radial transfers among the cellular, interstitial, and capillary regions were computed for each axial segment using a numerical ODE solver, either DOPRI5, a 5th order Runge-Kutta method with adaptive step size, or RADAU, a stiff ODE solver (Hairer et al., 1993, Hairer and Wanner, 1996). The model was developed using XSIM, a modeling environment developed by the National Simulation Resource for Circulatory Mass Transport (http://nsr.bioeng.washington.edu).

The accuracy of the numerical method was validated by comparing representative simulations under different numerical conditions. The computation of the exchange step by the Runge-Kutta method was validated by comparison to the results provided by stiff ODE solver RADAU; solutions computed by Runge-Kutta and RADAU were identical within 0.1%. Increasing the number of axial segments provides tighter coupling between the exchange and convective steps, and reduces the artificial axial mixing introduced by the last step of the algorithm (Figure 2-4D). The number of axial segments needed to produce accurate results depended on the type of data to be fit. A single segment model was sufficient to accurately predict lymph to plasma ratios, while osmotic transient and indicator dilution studies required accounting for axial concentration gradients in the

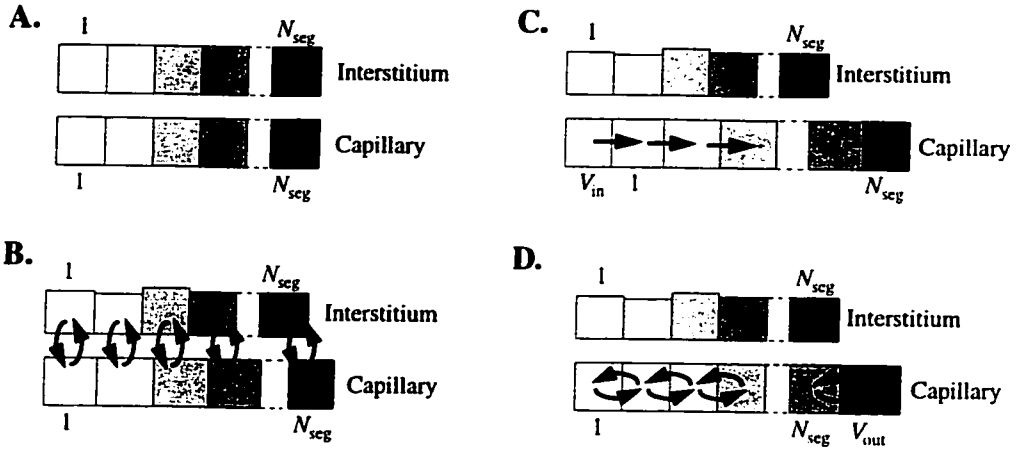

Figure 2-4 Outline of steps for numerical computation of model solutions at N_{seg} axial segments in capillary and interstitium. The cellular region is segmented in the same manner as the interstitial region, but is omitted from the figures for clarity. **A:** Regions are initially divided into N_{seg} axial segments. **B:** Fluid and solute exchange occurs among regions. Because the capillary is modeled as a constant volume, net volume flux into the regions causes fluid to move downstream. **C:** Axial convection occurs with a time step chosen to match the time needed for fluid to move exactly one segment downstream. **D:** Fluid exchange between adjacent capillary segments restores the original spatial grid for the next time step.

capillaries. However, only relatively coarse segmentation is necessary for osmotic transient simulations; seven axial segments provide solutions for osmotic transients accurate to within 0.005% compared to 20 segments. Because doubling the number of axial segments doubles the number of radial transfers and halves the model time step, computational time is approximately proportional to N_{seg}^2.

2.3 Results

2.3.1 Model parameter values

Model simulations were used to predict the steady-state distribution of fluid exchange across the capillary wall, and were compared to experimental data from multiple indicator dilution and lymph sampling experiments in whole hearts. Parameter values were taken to match the specific experimental conditions where possible, but typical values (listed in the Glossary) obtained from other sources were used when specific information was not

available. The transport parameters r_{sp}, $A_{sp}/S\Delta r$, r_{lp}, $A_{lp}/S\Delta r$, and $L_{p,endo}$ were obtained by fitting the model to osmotic weight transient data collected in the Ringer-perfused rabbit heart (described in detail in Chapter 3).

2.3.2 Steady-state fluid exchange

Since our model conserves volume, steady-state net filtration from capillaries to interstitium is equal to the rate of lymph formation. About 90% of the total steady-state filtration occurs through the large pore system despite its relatively low hydraulic conductivity because the low reflection coefficient of plasma proteins through the large pores prevents the development of a capillary osmotic pressure that can counter-balance high capillary hydrostatic pressures. In the steady-state, the model's lower capillary hydrostatic pressures at the venous end of the exchange unit are partially balanced by decreased interstitial fluid pressures and increased interstitial osmotic pressures exerted by components of the interstitial matrix. Net filtration therefore declines towards the venous end, but occurs at all positions in the exchange unit because lymph formation is distributed throughout the interstitial space (Figure 2-5). The remainder of the trans-capillary filtration occurs through the small pores, while flux across the endothelial cells is near zero, and varies between filtration at upstream regions and readsorption at downstream capillary regions.

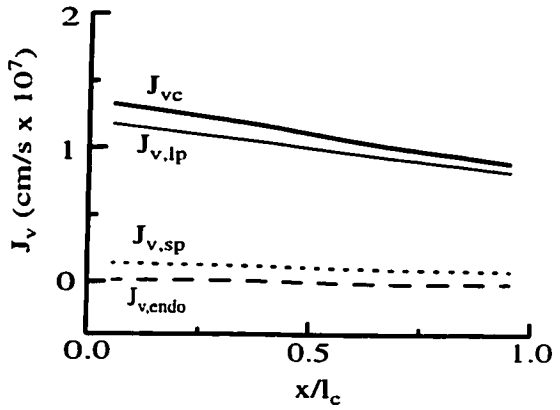

Figure 2-5 Steady-state volume flux across the capillary wall for each pathway as a function of axial position within the BTEX unit.

2.3.3 Lymph studies

Net flux of solute from capillary to interstitium must also balance the quantity drained away by the lymphatics in steady-state. The transcapillary concentration ratio approaches 1 for solutes with high diffusive permeability compared to convective transport (low Péclet number), and falls to 1-σ for exchange dominated by convection, assuming the capillary wall acts as a single-path semi-permeable barrier to exchange. This fact has been exploited to measure the selectivity of the capillary wall, with lymph-to-plasma concentration ratio (C_L/C_p) commonly used as an approximation of capillary filtrate-to-plasma concentration ratio.

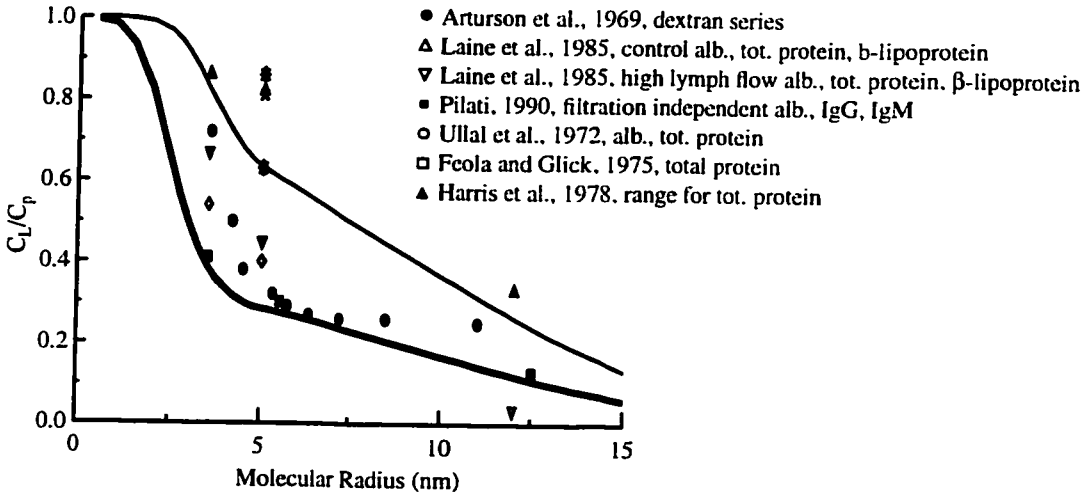

Figure 2-6 Steady-state C_L/C_p values predicted by the model for control conditions (thin line) and at filtration rate independence (thick line) compared to a compilation of experimental data in mammalian cardiac tissue. P, σ, and γ are functions of molecular size and diffusion coefficient given by Equation 2.32, 2.46, and 2.47; D was assumed proportional to $1/r_s$.

A model prediction of steady-state C_L/C_p as a function of molecular size (Figure 2-6) was generated for baseline conditions by matching fixed model parameters to the protocol of Laine and Granger (1985). However, C_L/C_p values are of little use unless they are obtained at high enough filtration rates to ensure the limit of 1-σ is reached, or lymph formation rates are measured simultaneously and used to correct for diffusive flux. The experimental record is particularly lacking in the heart, since multiple venous outlets into

the right ventricle limit experimental interventions to raise venous pressure, the usual mechanism of increasing lymph flows. Pilati (1990) is the only investigator to achieve filtration-rate independence for solutes as small as albumin, but he required infusion of adenosine in addition to coronary sinus occlusion to produce this effect. Pilati's data are well-fitted by the lower limit of C_L/C_p produced by the model by both increasing the venous pressure and lowering the lymph back-pressure until approximately constant values of C_L/C_p were obtained. Under normal control conditions, model C_L/C_p values are significantly higher, in rough agreement with most of the published observations. The series of Arturson et al. (1969) shows an unrealistic flattening out of C_L/C_p vs. r_p, probably because dextrans are long strands that reptate through narrow passages head-on, and additional molecular length does not significantly increase their resistance to transcapillary exchange.

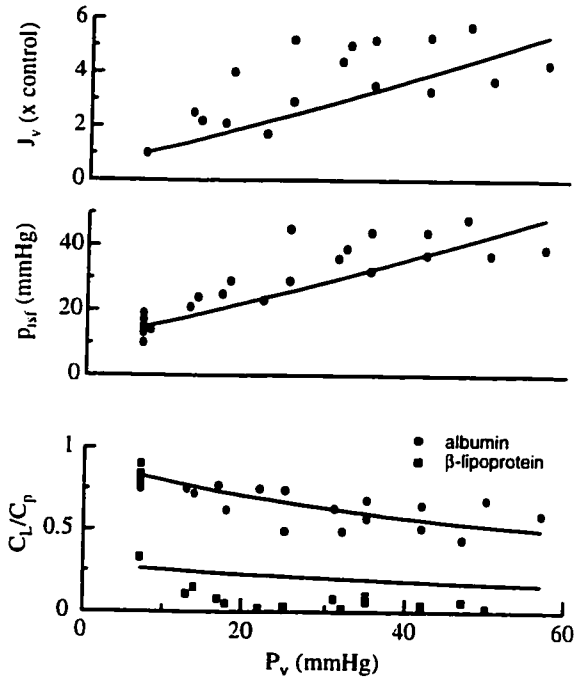

Figure 2-7 Simulated effect of changes in venous pressure (solid lines) at constant flow on the steady-state transcapillary filtration rate (J_V, top panel), interstitial pressure (p_{isf}, middle panel), and lymph to plasma concentration ratio of albumin and β-lipoprotein (C_L/C_p, lower panel) compared to data from dog heart (Laine and Granger, 1985).

The model fits can be greatly improved when model parameters including the venous outflow pressure and lymph conductance can be matched to the experimental conditions. The parameters for transcapillary exchange were optimized by comparing simulated lymph flow, interstitial pressure, and albumin and β-lipoprotein concentrations to data taken from Laine and Granger (1985) (Figure 2-7). In these experiments, the capillary filtration rate was elevated by raising venous pressure, which in turn increased the hydrostatic driving force for fluid filtration out of the capillaries. Under these conditions, the interstitium gained volume until increasing mechanical forces in the tissue raised interstitial pressure to balance capillary pressure resulting in a new steady-state at a higher filtration rate and lowered C_L/C_p for albumin and β-lipoprotein. Model steady-state filtration rates and interstitial pressures at a given venous pressures closely matched the experimental data, although some experimentally observed plateauing of interstitial pressures at high venous pressure is not shown by the model because a linear approximation to the interstitial pressure-volume relationship has been used.

2.3.4 Multiple indicator dilution studies

Solute permeability in whole organs can be measured by the multiple indicator dilution (MID) technique. In the simplest type of MID experiment, inflow and outflow concentration time courses are measured as a bolus containing two tracer solutes passes through an organ. One solute, for example albumin, is restricted to the vascular space and provides a measurement of the distribution of transit times through the organ; the other, e.g. L-glucose, is permeable and enters the interstitial space, resulting in a lower and broader peak relative to the vascular reference. Models ranging in complexity from the simple Crone (1963) expression to physiologically detailed models like MMID4 (Bassingthwaighte et al., 1989) can then be fit to extracellular tracer data to estimate a lumped solute conductance: the permeability surface area product PS. However, all previously described models assume purely diffusive solute exchange across the capillary wall.

L-glucose indicator dilution data (Figure 2-8) was fit using a concentration input function obtained by deconvolution of the albumin reference curve (Kuikka et al.. 1986), and optimized by varying only $A_{sf}/S\Delta r$. Under these conditions, $A_{sf}/S\Delta r$ is proportional to the PS product determined from the tracer flux. The optimized value of $A_{sf}/S\Delta r$ for the data set shown in Figure 2-8 translated into a PS of 1.1 ml s^{-1} g^{-1}, identical to value obtained by Kuikka et al., 1986 with a model specialized for tracer transient analysis (MMID4, described in Bassingthwaighte et al., 1989). Model predictions were also validated by direct comparison to the specialized model, and found to reproduce its concentration outflow waveforms to within 0.01% over a wide range of PS values.

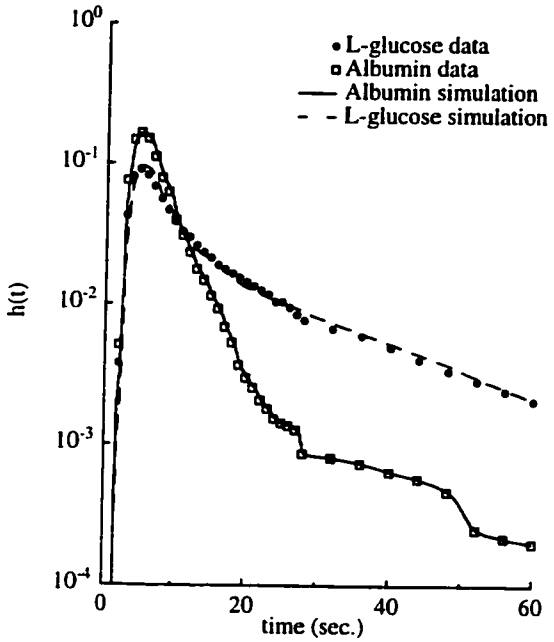

Figure 2-8 Model fit to multiple indicator dilution data (set 13078-1 (Kuikka et al., 1986). Data are normalized to give the transport function for passage through a BTEX unit ($h(t)$). Model parameters taken from the paper are F=1.7 ml min^{-1} g^{-1}, $\hat{V}_c$=0.035 ml/g, $\hat{V}_{isf}$=0.28 ml/g.

Extensive data summarized in Figure 2-9 shows solute permeabilities as measured by MID are roughly proportional to solute-free diffusion coefficients for hydrophilic solutes smaller than inulin, although charge effects may also play a role in ion exchange. This observation implies a lack of relative restriction among this group of solutes, so any

aqueous pores must be large compared to the solutes. Model predictions were generated for an ideal spherical solute obeying the Stokes-Einstein equation: $r_s = RT/N_A 6\pi\eta D$ in water at 37 °C. L-glucose and the other solutes shown in Figure 2-9 are markedly hydrophilic and therefore limited to the extracellular space. Note there is approximately a two-fold increase in solute permeability for Ringer-perfused hearts compared to blood-perfused preparations. We have used two values of $A_{sp}/S\Delta r$, 4.5 cm^{-1} and 2.5 cm^{-1}, to account for this disparity. For technical reasons, all reported C_L/C_p data in the heart has been obtained from blood-perfused preparations, while osmotic transient experiments have relied exclusively on the Ringer-perfused preparation. It was also necessary to vary the small pore radius from 7 to 5 nm in Ringer and blood perfused data sets to provide good fits to all data sets. The model parameterizations for the large pore and endothelial transcellular pathways remain constant in all simulations.

2.4 Discussion

The model presented in this chapter has a number of features that allow it to realistically simulate fluid and solute exchange under a variety of experimental conditions. The most significant advances are the use of an axially-distributed blood-tissue exchange region, inclusion of a lymphatic drain in the interstitium, and the independent computation of transcapillary solute and solvent fluxes through three different pathways.

2.4.1 Geometry of the blood-tissue exchange region

Accurate simulations of osmotic transient and multiple indicator dilution data can only be achieved by an axially-distributed BTEX region. Our results show that compartmental models, which by definition impose a uniform capillary solute concentration, always underestimate σ during an osmotic transient experiment because the influx of solute-free water into upstream capillary regions dilutes solute in downstream regions (Chapter 3). Well-mixed compartments, even in interstitial and parenchymal regions, are also inadequate for analyzing indicator dilution curves because they imply an infinite diffusion coefficient. Coupling a compartmental interstitium to an axially-distributed capillary model would lead to solute leaving upstream regions of the capillary

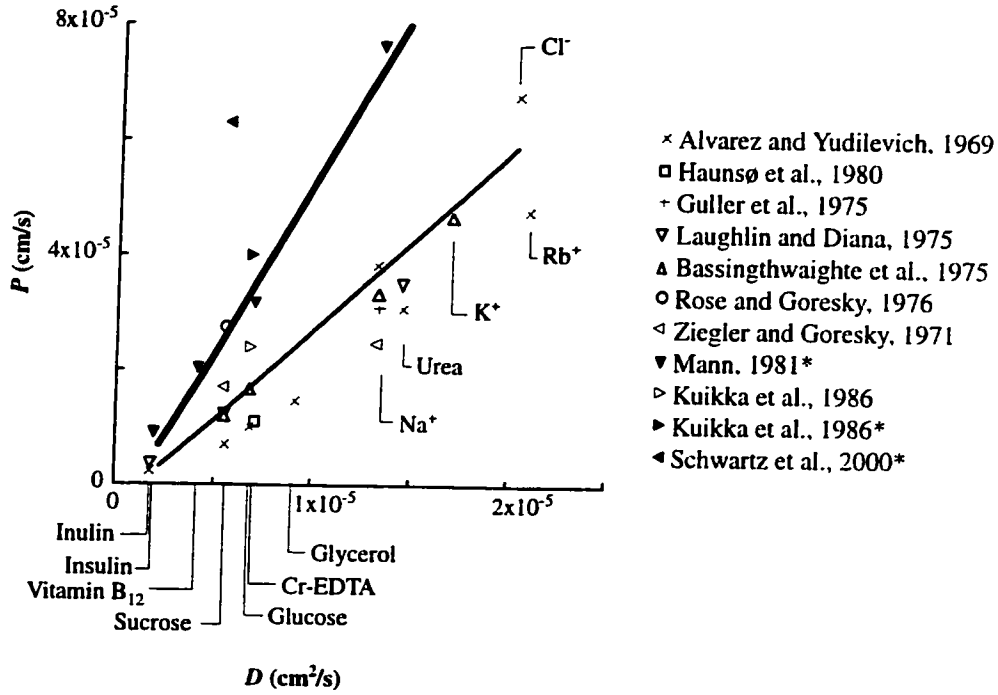

Figure 2-9 Comparison of model permeability predictions for blood (thin line) and Ringer-perfused (thick line) preparations to experimental results from multiple indicator dilution studies in mammalian cardiac tissue. Experimentally measured values of *PS* were converted to pure permeabilities assuming a capillary surface area of 500 cm^2/g for comparison to values calculated by the model. Data sets taken from Ringer perfused hearts are indicated by filled symbols and the references marked by *.

on one model time step, and then reentering downstream regions ahead of the convective front on the next time step, preventing an accurate reproduction of the postcapillary concentration waveform.

Neglecting axial diffusive and convective fluxes is an appropriate approximation in the long and narrow BTEX regions of cardiac tissue because radial exchange and axial convection in capillaries are rapid compared to axial transport in the interstitium. The intracapillary transient time (about 0.75 sec.) and the radial diffusive relaxation times are both several orders of magnitude faster than the axial diffusive relaxation time. The radial diffusional relaxation time for albumin, with an estimated interstitial diffusion coefficient of $1x10^{-7}$ cm^2/s, or 10% of its value in free solution (Aukland and Reed, 1993), based on a capillary-to-myocyte spacing of 2 μm is approximately 0.2 sec. for mixing in the region

adjacent to the capillary, and about 3.2 sec. for complete radial interstitial relaxation with a half-intercapillary distance of 8 μm. The axial diffusive relaxation time in a 639 μm BTEX region would be almost 6 hours. Axial gradients in the interstitium and cellular regions are therefore modest. Three-dimensional convective and diffusive fluxes of water and solutes in the interstitium have been modeled by Taylor et. al. (1990), and Levick (1994), but application of these models in practical settings has been limited because measurements of interstitial hydraulic resistances, diffusion coefficients, and sieving coefficients are technically difficult to obtain.

The use of uniform hexagonal Krogh cylinders to describe BTEX geometry is reasonable in cardiac tissue. The approach assumes solute entry into adjacent capillaries is synchronous and perfusate velocities are the same so that there is no net exchange among adjacent units. Although it is known that staggering of parallel capillaries and cross-connections between adjacent capillaries increases transport efficiency beyond that predicted by the Krogh model (Beard and Bassingthwaighte, 2000, Kassab et al., 1997), these anatomical features are most relevant for highly diffusible flow-limited solutes like O_2 and CO_2, which are not coupled to fluid exchange. We also assume that transport properties remain uniform along the length of the capillary, and that all exchange occurs in a well-defined bed of parallel capillaries. In reality there is no clear-cut distinct division between exchange and transport vessels, and the venular ends of capillaries may have higher permeabilities in some vascular beds (Wiederhielm, 1966). However, an alternative form of the model in which the large pores were localized to the downstream end of the capillary segment did not substantially affect the model fits to data presented in this paper.

Flow varies among exchange units in a whole organ, and flow heterogeneity within a vascular bed can influence transport, particularly for highly diffusible solutes like water, oxygen, and carbon dioxide (Beard and Bassingthwaighte, 2000, Kassab et al., 1997). Heterogeneity effects have been successfully modeled by splitting the capillary flow among a number of parallel pathways. For the data set given in Figure 2-8, a multi-capillary tracer model gave an estimated *PS* 21% greater than the value obtained by neglecting flow heterogeneity (Kuikka et al., 1986). We have ignored flow heterogeneity

because the time course of bulk fluid and hydrophilic solute exchange is much slower than tracer water and gas exchange, so the dispersion introduced by flow heterogeneity is less important for osmotic transient and lymph studies. Seale and Harris (2000) found that estimated parameter values varied by less than 10% between homogeneous and heterogeneous flow models in experiments on osmotically driven water exchange in the lung.

2.4.2 Lymph formation

Inclusion of a lymphatic drain is necessary to achieve the correct steady-state distribution of material across the capillary wall. A model by Grabowski and Bassingthwaighte (1976) that neglected the role of the lymphatics had a steady-state with no net fluid flux across the capillary wall. Consequently, all solutes eventually diffused to a uniform concentration in plasma and interstitial fluid, a model prediction incompatible with observed lymph to plasma concentration ratios. This assumption also led the authors to incorrectly predict that the mechanical elasticity of the tissue would eventually force the interstitium to return to its original volume following a plasma osmolarity change because it forced their model to a unique interstitial equilibrium volume, independent of plasma osmolarity. However, our model shows that an increased plasma osmolarity leads to a new steady-state at a lower J_v, V_{isf}, and p_{isf} after the transient transcapillary concentration difference dissipates.

The simple empirical model of lymph formation, represented by equations 2.35 and 2.36, approximates complex 3-dimensional flows of water and solutes from interstitium to terminal lymphatics by a distributed consumption of interstitial fluid driven by a single hydrostatic pressure difference across a uniform lumped hydraulic resistance. The actual mechanism of lymph formation is more complex, and most likely depends on rhythmic tissue motion to fill terminal lymphatics through junction strand free gaps between lymphatic endothelial cells, which act as one way valves (Schmid-Schöbein and Ikomi, 1995). Because lymphatic endothelial cells lack the surface glycocalyx and tight junctional strand proteins that could lead to restriction of solutes and development of an

osmotic pressure difference, our empirical formulation is consistent with this mechanism on time scales long compared to the heart rate. The approach presumes myocardial contractility and heart rate remain constant over the course of a simulation, since it is well established that cyclic muscular contraction augments lymph flow, which would change the effective K_L. Accounting for the relationships among fluid gain, myocardial force development, and lymph formation is beyond the scope of this study.

Large solutes are excluded from an appreciable fraction of the interstitial volume by components of the interstitial matrix, which raises their activity in the remainder of the solution. The extravascular volume available to albumin, for example, has been estimated at about 62% of interstitial fluid in cardiac tissue (Sunnergren, 1985), less than our prediction of $\gamma = 0.78$ from Equation 2.32, probably because negative charges on both albumin and matrix proteins cause a greater exclusion than would be expected based on size alone. Solute-free interstitial water is likely closely associated with components of the interstitial matrix, while lymph is likely composed primarily of more free-flowing fluid. Therefore true capillary filtrate concentrations rather than bulk interstitial concentrations were used to estimate lymph concentrations in the model.

2.4.3 Osmotic buffering

Dynamic model behavior is determined not only by the response to direct perturbations in Starling forces, but also to any additional changes in driving forces that develop due to induced water and solute movement. Since water moves across the capillary wall more rapidly than even highly permeable hydrophilic solutes, an increase in plasma osmolarity will transiently increase interstitial solute concentrations. The development of a secondary concentration gradient in solutes previously at steady-state which opposes the initial perturbation is known as osmotic buffering. The effect was first recognized by Keys (1937), who argued that perturbations to the water equilibrium caused by changes in posture, exercise, or ingestion of food would prove catastrophic if they were not buffered by retention of the small plasma solutes normally regarded to be at equilibrium.

The quantitative significance of this phenomenon during net bulk fluid exchange has been controversial, although osmotic buffering effects are clearly negligible during isogravimetric osmotic transients since they depend on sudden and large shifts of water across the capillary wall. Osmotic buffering was ignored by Vargas and Johnson (1964, 1967) in the original osmotic transient papers, and not quantitatively incorporated into a model until Farmer and Macy (1972) measured volume changes in red blood cells produced by osmotic perturbations of their bathing solution. Grabowski and Bassingthwaighte (1976) explicitly included osmotic buffering in their model of blood-tissue exchange in the heart, and concluded that it was quantitatively important for small electrolytes, while Bloom and Johnson (1981) reached the opposite conclusion with a different model.

We have found that this discrepancy arose because of an error in the implementation of the Grabowski model, which caused an overestimation of the formation of buffering concentration gradients in the interstitium. These predictions have been supported by simulations from the current model which duplicate Bloom and Johnson's (1981b) findings for buffering by NaCl. However, larger solutes like albumin, if present in osmotically significant quantities, would buffer capillary osmolarity changes. The importance of secondary solutes is dependent on the experimental conditions and the information one is trying to extract. In general, one must know something about all of the solutes present in order to predict the response to a systemic perturbation.

The significance of resident solutes in tissues is complicated by the fact that both the interstitium and the parenchymal cells must respond to perturbations in the circulation. Another point of confusion arose because Grabowski and Bassingthwaighte attempted to demonstrate the importance of solute buffering at the capillary wall by reducing the steady-state concentration of electrolyte throughout their system, causing a reduced weight loss from the organ during a capillary osmolarity increase. Although this result is correct, the conclusion drawn is not. Lowering resident electrolyte concentration reduces the buffering across the *parenchymal cell membrane*, not the capillary wall. Since the cell membranes are essentially impermeable to small electrolytes, an increase in plasma

osmolarity must cause a loss of nearly pure water from the parenchymal cells to restore osmotic balance. If the cell osmolarity is 280, a 50 mM sucrose transient will cause a reduction of cell volume to 280/330 = 85% of its original volume to restore osmotic balance. If the original cell osmolarity is 140, the same 50 mM sucrose transient will cause the cell volume to be reduced to 140/190 = 73% of the original volume. Including electrolytes is important in determining the time course of the weight transient, but not because of buffering at the capillary wall.

2.4.4 Multiple pathway models for transcapillary exchange

Model simulations suggest that the interplay among different pathways across the capillary wall is at least as important to understanding the transcapillary exchange processes as a detailed understanding of the mechanics of exchange through each pathway. Understanding how the proportions of J_v among the pathways change during an intervention is necessary to properly interpret experimental data, and is particularly important during osmotic weight transient studies because the equivalent single-path phenomenological model is dependent on the relative magnitudes of J_v in each pathway (Rippe and Haraldsson, 1994), and this quantity changes over the course of the experiment.

Unlike osmotic transient experiments, measurements of σ based on C_L/C_p are typically obtained by proportionally increasing J_v through all pathways by hydrostatic pressure changes. Because increases in capillary hydrostatic pressure would cause increased fluid filtration and convective solute exchange through even the largest pores, a lower estimate of σ will be obtained by lymph analysis than osmotic transient methods if a multipath model is not used. There is some evidence of higher reflection coefficients for large solutes measured with the osmotic transient technique compared to C_L/C_p analysis; $\sigma_{albumin}$ was only 0.59 by Pilati's (1990) measurement of filtration rate independent C_L/C_p. However, a more careful comparison of the two techniques in the same experimental system is needed to make definite conclusions.

2.4.5 Morphological basis for transcapillary exchange

Osmotic transient, lymphatic, and indicator dilution data sets are all consistent with a three-pathway description of capillary wall morphology. The small pore pathway likely corresponds to the periendothelial cleft. We have used the simple classical small and large pore approach in this paper for simplicity, which places the steric hindrance at the cleft walls. Although straight-walled cylindrical pores are only a crude approximation of capillary wall morphology, the areas and radii used in simplified pore theories provide a rough correspondence to observable anatomy. Our model requires a small pore radius of about 7 nm to provide some restriction to solutes the size of albumin (σ=0.45 for this path), but at the same time allow significant penetration of albumin into the interstitium by about 15 minutes into an osmotic transient in a Ringer-perfused preparation. This estimate of small pore width is larger than that obtained by other investigators using osmotic transient methods (Bloom and Johnson, 1981, Grabowski and Bassingthwaighte, 1976); but fits to a complete albumin transient have never been previously reported, and good fits to the initial slopes of the transients can be obtained with smaller pore sizes. Steady-state lymph to plasma concentration ratios, performed under blood perfusion suggest a more restrictive 5 nm radius pore. The fact that small solute permeabilities vary by over a factor of 2 between blood and Ringer perfused preparations suggests that this is likely a consequence of real differences in capillary function between the preparations.

Detailed three-dimensional models of the capillary glycocalyx and cleft junction provide a more complete description of pericellular transport (Hu and Weinbaum, 1999) , but do not eliminate the need for multiple pathways. With fibers of 0.6 nm radius spaced about 7 nm apart, these models suggest the capillary glycocalyx could provide restriction to solutes the size of albumin, but a transcellular pathway for water alone is still necessary to explain the large transient fluxes of solute-free water that leave the tissue in response to an acute increase in small solute plasma concentration. Tracer labeling of the interendothelial clefts (Fu et al., 1997), observations of the endothelial junction morphology (Adamson and Michel, 1993, Bundgaard, 1984), and increases in capillary permeability following pronase digestion of glycocalyx (Adamson, 1990, Huxley and

Williams, 2000) provide support for this view. Thinning of the glycocalyx under Ringer perfusion would also would also be interpreted as an increase in apparent small pore area and radius.

A large non-selective pore provides a transcapillary passage for even very large solutes, but its exact nature remains open to debate (Rippe and Haraldsson, 1994, Michel and Curry, 1999). Large pores could occur as junctions between three endothelial cells, vesicular transport, transport through fused vesicles, or infrequent gaps or thinning of the capillary glycocalyx. These are probably more frequent towards the venous end of capillaries as shown by the preferential escape of water-soluble dyes from the venous end of the microcirculation (Wiederhielm, 1966). However, an alternate form of our model in which the large pores were localized to the last axial segment of the BTEX unit gave model fits nearly identical to the distributed form. Developing a detailed mechanistic model of large pore structure is relatively unimportant, since these pores are large even compared to macromolecules.

The pathway for solute-free water exchange is likely through the endothelial plasmalemma, and at least partly mediated by the aquaporin-1 water channels present on cardiac endothelial cells (Hasegawa et al., 1994, Verkman et al., 1996). Recent experiments have shown that mercurials, known inhibitors of aquaporin-1, inhibit osmotically induced water exchange across the renal *vasa recta* and pulmonary capillaries (Carter et al., 1998, Effros et al., 1997, Pallone et al., 1997). The effect is most evident for small solutes like NaCl and sucrose, likely because small solutes exert significant osmotic pressure across only the water-exclusive aquaporin channels. Larger solutes like albumin induce fluid movements even in the presence of aquaporin blocking agents since they have a significant reflection coefficient for paracellular exchange. These results are qualitatively consistent with our three-pathway description of transcapillary fluid exchange, but quantitative comparisons of model and experiment are problematic because the toxicity of mercury makes well-controlled experiments under physiological normal conditions difficult.

2.4.6 Conclusions

Detailed models of tracer kinetics in whole organs are already in wide-spread use for the analysis of tracer-transient data. These models are computationally faster and a better choice for the practical analysis of MID experiments because they include phenomena like flow heterogeneity and the uptake and metabolism of substrates by cells that are ignored by our model. However, a fundamental assumption made by these sorts of models is that bulk fluid exchange is negligible, which clearly precludes their application to osmotic transient and lymph sampling techniques. Likewise, the steady-state sampling of lymph fluid does not require an elaborate kinetic model; current analysis techniques are adequate to explain most observations. However, analysis methods based on a steady-state assumption are fundamentally unsuited for application to understanding transient kinetic behaviors. The key contribution of the model presented in this chapter is its ability to integrate several distinct sets of experimental data into a single self-consistent theoretical framework. In fact, it is in the osmotic transient experiment, where a severe perturbation to system causes large and transient bulk fluid flows, where the model presented in this chapter has its greatest utility. The analysis of osmotic transient data sets, resulting in the estimation of parameters used in this chapter, is given Chapter 3.

3 Analysis of Osmotic Weight Transient Experiments in Isolated Rabbit Heart

The osmotic weight transient method is a well-established technique for the measurement of solute reflection coefficients in the vascular beds of intact organs, but overly simplified methods of analysis have limited the quality and quantity of information that has been extracted from these experiments. In this chapter, we use the physiologically realistic model of microcirculatory exchange developed in Chapter 2 to analyze novel osmotic weight transient experiments performed in the Ringer-perfused rabbit heart. By using this more sophisticated model, we are able to determine the values of key parameters that govern microcirculatory exchange. The transendothelial hydraulic conductivity is 1.8 ± 0.6 cm s^{-1} $mmHg^{-1}$, or 18% of the total transcapillary hydraulic conductivity; a small pore system exists with radius equal to 7.1 ± 1.7 nm and fractional pore area per unit path length equal to 4.3 ± 1.1 cm^{-1}. In conjunction with a unselective large pore system, these estimates are consistent with the other data sets described in Chapter 2. Thus, when analyzed by a sufficiently powerful model, osmotic weight transient experiments are a powerful way to examine the kinetics of microcirculatory exchange.

3.1 Introduction

The osmotic weight transient method is one of the few techniques available to measure the reflection coefficient (σ) of small hydrophilic solutes in the vascular beds of whole organs. Immediately following a step change in perfusate osmolarity, the volume flux across the capillary wall, J_v, is related to σ by a simple analytical expression developed by Vargas and Johnson (1964), $\sigma = J_v S / L_p S \Delta\Pi$. In a whole organ, the total fluid movement across the capillary wall, $J_v S$, is nearly equal to the rate of weight change of the organ; knowledge of the magnitude of the osmotic perturbation, $\Delta\Pi$, and the capillary hydraulic conductivity, L_p, is all that is needed to estimate σ. Estimates of σ using this analysis method and osmotic weight transient measurements have been obtained in many mammalian tissues including heart (Vargas and Johnson, 1964, Vargas and

Blackshear, 1981), skeletal muscle (Wolf and Watson, 1981, Wolf, 1996), and lung (Perl et al., 1975). For small solutes like sucrose, σ estimates range from 0.08 (Rippe and Haraldsson, 1986) to 0.41 (Wolf, 1996).

A few investigators (Vargas and Johnson, 1967, Grabowski and Bassingthwaighte 1976, Bloom and Johnson, 1981) have attempted to extract additional information from the complete time course of the weight transient using more sophisticated models. The intended use of these models was to provide estimates of the solute permeability (P), but it is not clear that any of these models have captured the underlying physiology in enough detail to provide meaningful parameter estimates. The standard methods for analyzing osmotic weight transient data have several shortcomings. First, although the necessity of viewing transport across the capillary wall as a process occurring simultaneously through several disparate pathways is now recognized (Rippe and Haraldsson, 1987), this information has not been built into any of the models that have built to analyze osmotic weight transient data. Therefore, the σ obtained from all previously developed methods of analysis is only a functional description of the behavior of the capillary wall as a whole; information on specific pathways cannot be obtained with any previously developed method of analysis. Second, estimates of σ obtained by compartmental models tend to increase with increasing flow through an organ, even there is no reason to suppose the capillary wall morphology is actually changing. Finally, previously described analytical models depend on the prior knowledge of the hydraulic conductivity (L_p) in order to obtain estimates of σ and/or P.

In Chapter 2, we developed a physiologically realistic model of the transcapillary exchange process, and showed that the model was consistent with data from multiple indicator dilution and lymph sampling experiments. In this chapter, we use this model to determine the key model parameters that govern water and solute exchange using osmotic weight transient experiments performed in isolated Ringer-perfused rabbit hearts. This new and more sophisticated model has allowed us to extract more complete and more accurate information from the weight transient record than previous methods of analysis. Solute and water exchange through the endothelial junction is best described by a small

pore system with a radius (r_{sp}) of 7 nm occupying 0.02% of the capillary wall surface area (A_{sp}/S). This pathway is supplemented by a transendothelial pathway for solute-free water exchange with a hydraulic conductivity ($L_{p,endo}$) equal to 1.8×10^{-8} cm s^{-1} $mmHg^{-1}$, or 18% of the total transcapillary L_p. A large pore system is also required to achieve the known distribution of large proteins in plasma and lymph, but the osmotic transient method is fundamentally unsuited for providing information about this pathway. The parameters obtained from this analysis do not require prior measurement of total L_p, and are independent of the flow. Thus, our approach marks a significant improvement over previous attempts to analyze osmotic weight transient experiments.

3.2 Experimental Methods

An osmotic weight transient experiment consists of the gravimetric measurement of the net transcapillary flow (J_v) induced by a step change in perfusate osmolarity. We based our experimental protocols on the basic experimental methodology developed by Vargas and Johnson (1964), but used a novel model for the analysis of the record of weight changes. We used sensitivity analysis on preliminary data and parameters obtained from one heart to determine the model parameters identifiable from the data. We then optimized the model parameters governing transcapillary exchange using a larger data set of 137 transients on 11 different hearts.

3.2.1 Experimental Methods

Our standard protocol was to induce weight transients in the isolated Ringer-perfused rabbit heart using as the osmotic agent one of a series of hydrophilic solutes with molecular weights ranging between 58 (NaCl) and 36,000 (albumin) daltons. The switch to a hyperosmotic solution lasted between 4 to 30 minutes, with the length of the transient increasing with the size of the osmotic agent. The perfusate was then switched back to control for a reequilibration period that lasted at least as long as the original transient. Typically, four to five test solutes were used as the osmotic agent in one experiment. For each solute, one to three transients were recorded; the total time for one experiment was three to four hours (Figure 3-1). In a second protocol, we conducted a set of transients

using sucrose as the osmotic agent while varying the flow through a range from 1.75 to 3.9 mL min^{-1} g^{-1}. Details of the experiment are given below regarding: 1. the standard and osmotically-active Ringer's solutions, 2. the perfusion system, 3. surgical procedures, and 4. the data recording devices.

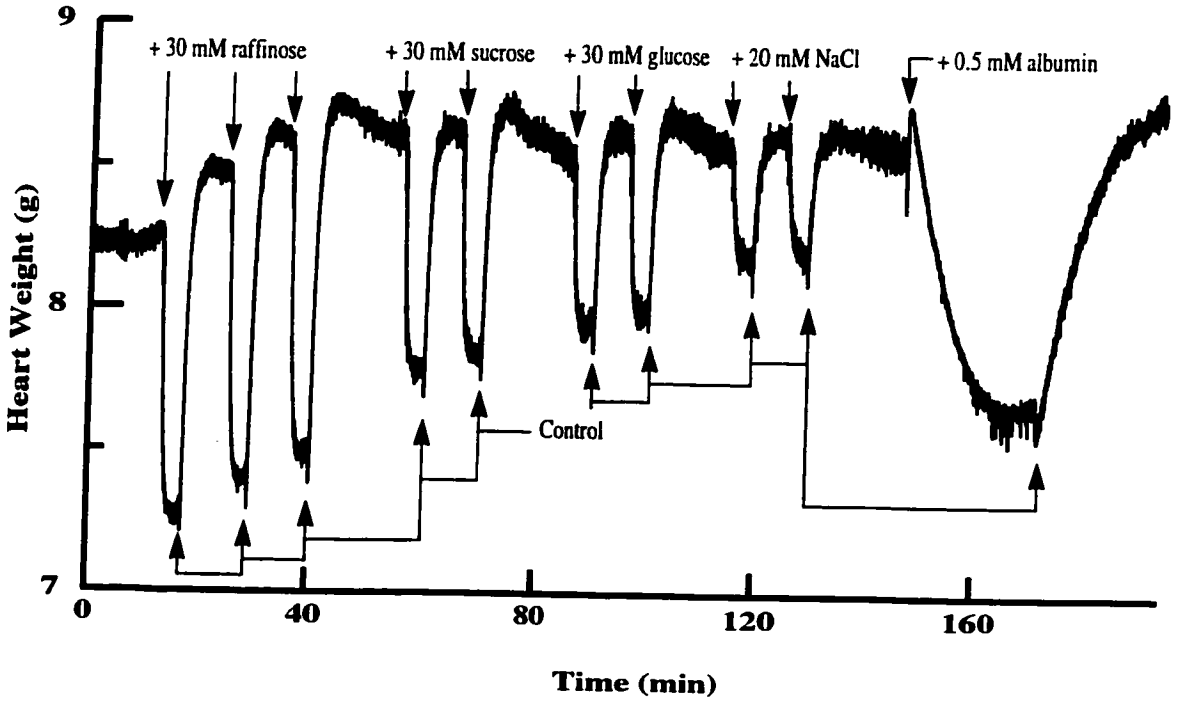

Figure 3-1 A representative osmotic transient experiment (#121202). The figure shows the weight record obtained over 3 hours of experimentation. The discontinuity in weight at the beginning of the albumin transient is an artifact arising from the increased perfusate viscosity of the albumin test solution. This causes an increased aortic volume due to an elevated aortic pressure. The initial equilibration phase where weight raises to a constant level is not shown.

3.2.1.1 Solutions

Krebs-Ringers solutions were prepared fresh each morning prior to the experiments. The control solution had the following composition: NaCl 118 mM, KCl 3.8 mM, KH_2PO_4 1.2 mM, $MgSO_4$ 0.7 mM, $CaCl_2$ 2.1 mM, $NaHCO_3$ 25 mM, EDTA 0.1 mM, dextrose 10 mM, pyruvate 5.5 mM, bovine serum albumin 1 g/L (all from Sigma Chemical Co.). Papaverine at 5 mg/L was also used in all solutions to ensure vasodilation of the preparation. Osmotic test solutions were identical to the control except for the

presence of one additional solute that served as the osmotic agent during the experiment. Test solute concentrations, unless otherwise noted, were: urea 30 mM, NaCl 20 mM, glucose 30 mM, sucrose 30 mM, raffinose 30 mM, inulin 5 mM, and albumin 0.5 mM. Solution osmolarity was validated using a freezing-point osmometer (Osmette A, Precision Systems, Inc.). All solutions were filtered through a 1.2 μm filter prior to use.

The albumin was purified by at least 72 hours of dialysis at 4 °C using a membrane with a molecular cut-off weight of 12,000-14,000 daltons (Spectra/Por, Spectrum Laboratories, Inc.) to remove small vasoactive compounds and control the ionic composition of the solution. The dialysis buffer was a physiological salt solution containing the same concentrations of NaCl, KCl, KH_2PO_4, $MgSO_4$, and $CaCl_2$ as in the standard Ringer's solution, and was changed at least 3 times during dialysis. The volume volume of the buffer was at least nine times that of the albumin solution. The final albumin concentration of the dialyzed protein solution was determined by refractometry and then diluted to the desired concentrations on the day of the experiment. Inulin was similarly purified by dialysis against deionized water using a membrane with a molecular cut-off weight of 2000 daltons (Spectra/Por, Spectrum Laboratories, Inc.).

3.2.1.2 Perfusion System

A perfusion system (Figure 3-2) was developed to allow rapid switching between control and test solutions. Solutions were circulated continually through membrane oxygenators (Medtronic Minimax Plus) using a 95% O_2 5% CO_2 gas mixture and a 10 μm in-line filter. A constant-flow perfusion pump (Gilson Minipuls II) was used to send fluid through a heat exchanger, consisting of a stainless steel tubing coil submersed in a temperature controlled water bath and a temperature controlled windkessel on its way to the heart. The temperature at the heart was approximately 33 °C. Two identical perfusion lines were kept running continuously, and a switching valve located about 0.1 mL before the heart ensured a sharp change between the lines.

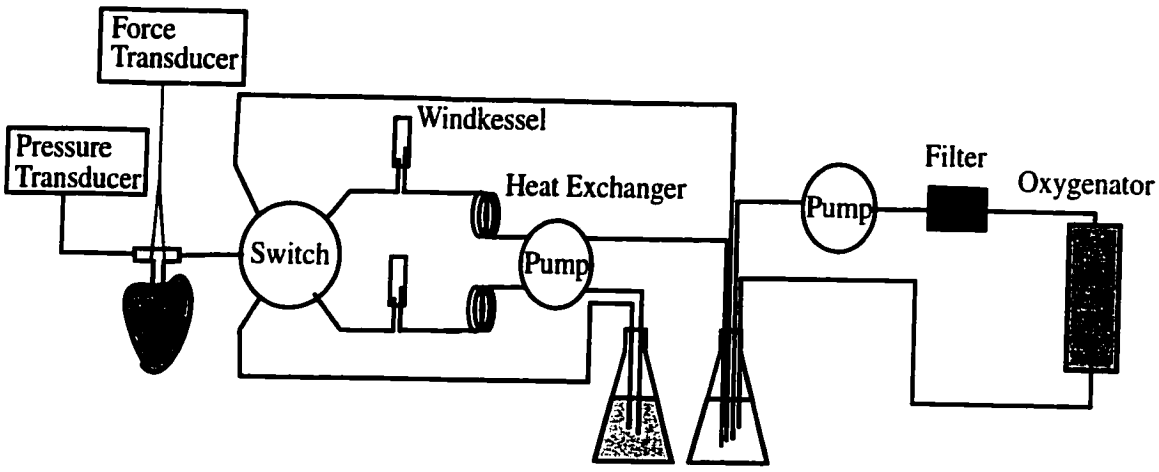

Figure 3-2 A dual perfusion system allows for rapid switching between many different solutions over the course of an experiment. For simplicity, the oxygenation circuit is only shown for one solution.

3.2.1.3 Animals and surgical procedure

Isolation of the hearts began by sedating adult female New Zealand White rabbits (2-3 kg) with acepromazine (1 mg/kg, subcutaneously) 20-30 minutes before surgery. (The protocols for animal use were developed in accordance with NIH guidelines and were reviewed and approved by the Institutional Animal Care and Use Committee of the University of Washington, IACUC protocol number 2027-09.) Surgical anesthesia was induced by intramuscular ketamine (40 mg/kg) and xylazine (5 mg/kg). Following a tracheotomy and switch to mechanical ventilation, the chest was opened with a midline incision through the sternum and a ligature was placed around the aorta. The rabbit was then given 300 U of heparin through the marginal ear vein. After 2 minutes, the aorta was occluded with the ligature to prevent air from entering the coronary arteries. The heart was removed immediately and temporarily immersed in iced Ringer's solution until contractions ceased. It was then perfused retrogradely through the aorta while suspended from a T-shaped cannula (Figure 3-3). The time from excision to reperfusion was typically less than a minute.

Prior to the onset of experiments, the perfused and isolated heart was trimmed of excess fat and other tissue. Cannulas were then inserted as drains into the left ventricle

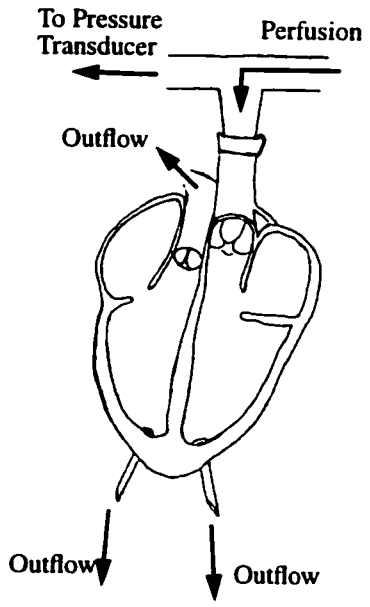

Figure 3-3 Retrograded perfusion of an isolated heart allows flow into the aorta through one arm of a T-shaped cannula and measurement of arterial perfusion pressure through the other. Fluid leaves the organ through drains placed in the ventricles or is ejected from the right ventricle.

through a pulmonary vein and into the right ventricle through the pulmonary artery. Preparations in which flow from the left ventricular drain comprised more than 5% of the total flow were discarded because they likely had a damaged aortic valve. The heart was paced with a stimulator (Harvard Apparatus Co.) a constant rate of about 150 bpm, and perfusion rate was set at approximately 20 mL/min (2-4 mL min^{-1} g^{-1}).

After isolation, the heart was equilibrated for at least 30 minutes. During this time the heart gained weight due to the low colloid osmotic pressure of the perfusate, but reached a steady baseline weight by the end of the equilibration period. At the end of the equilibration period, a series of switches was made between the two perfusion lines, both of which contained the control solution. By adjusting height and the gage of fine needles at the end of the return line, we were able to set the hydrostatic pressure in the at the switch equal in both perfusion lines, greatly reducing switching artifacts. One perfusion line was then changed to the test solution and the experimental protocol begun.

3.2.1.4 Data recording

Heart weight and aortic perfusion pressure were recorded from a force transducer (Transducer Techniques) and pressure transducer (Statham). The transducer outputs were amplified using a custom-built amplifier and the weight record was filtered by an analog RC filter with a time constant of 0.2 sec. to remove high frequency noise. Signals were digitized and acquired by a Macintosh Power Mac 7100 running LabVIEW4 (National Instruments) at 250 Hz. Both weight and pressure signals were recorded continuously from the beginning of perfusion to the completion of the experiment. At the conclusion of all experiments, the heart was quickly removed from the experimental equipment, blotted, weighed, and then dried at 100 °C to a constant dry weight.

3.2.2 Analytical techniques

The analysis of these experiments using sensitivity analysis and parameter optimization was based on a novel model of microcirculatory solute and water exchange (Chapter 2). All analysis was performed on a LINUX workstation using the XSIM modeling environment. The XSIM software package was developed by the National Simulation Resource for Circulatory Mass Transport, and is freely available for download from http://nsr.bioeng.washington.edu.

3.2.2.1 The model

The model used has been described in detail in the previous chapter. Briefly, it consists of an axially-distributed blood tissue exchange region in which fluid and solutes exchange between vascular, interstitial, and parenchymal cell volumes. Three separate pathways exist for the coupled exchange of water and solute across the capillary: one pathway for solute-free water exchange, and small pore and large pore pathways for coupled fluid and solute exchange. The pore equations of Curry (1974) were used to determine L_p, P, and σ through the large and small pore pathways.

We modified the standard parameter set given in Chapter 2 to more closely match the conditions of each experiment. The model's flow and aortic pressure were set to the values measured experimentally before the start of the experiment; venous outflow and lymph

back-pressure were assumed to be at atmospheric pressure. The initial value for the interstitial volume was adjusted in the model to match the estimated experimental value by increasing the model volume until the ratio of wet-to-dry weights of the simulated and experimental heats were equal. The interstitial volume was typically 2 to 3 times greater than the normal *in vivo* value because the low oncotic pressure of the perfusate caused the rapid formation of cardiac edema during the equilibration phase of the experiment. A more gradual gain throughout the experiment was also common as the preparation deteriorated.

3.2.2.2 Sensitivity analysis

Sensitivity analysis provides both insight into complex models and an aid to experimental design. The sensitivity functions, defined as the instantaneous fractional change in a model output (in this case organ weight, W) induced per fractional change in a model parameter, P, were approximated by comparing model solutions produced with a one-percent increase in the parameter values. Relative sensitivities ($(\delta W/W)/(\delta P/P)$ or $\delta \ln W/\delta \ln P$) rather than absolute sensitivities ($\delta W/\delta P$) were used to provide dimensionless sensitivity functions. Since the sensitivity functions are dependent on the parameter values, sensitivity analysis was performed after an initial manual fit to a small number of preliminary data sets. The sensitivity curves shown in the Results section were generated using the mean parameter values obtained from optimization against the full data set, but do not differ significantly from the preliminary results used for experimental design.

3.2.2.3 Parameter estimation

Optimization of model fits to data was used to determine three model parameters: 1. $L_{p,endo}$, the hydraulic conductivity through the transendothelial pathway, 2. $A_{sp}/(S\Delta r)$, the fractional pore area per unit path length through the intercellular junction, and 3. r_{sp}, the small pore radius. The complete weight record including both the switch to the test solution and the return to control were used in the optimization procedure. Optimization

was performed using the SENSOP program (REF), which uses sensitivity functions to optimize parameter sets and provide confidence ranges.

3.3 Results

Parameter estimates were obtained from a large set of high-quality osmotic weight transient data sets in Ringer-perfused rabbit hearts. A total of 139 transients in 11 different hearts were analyzed; the number of fits obtained to transients for each osmotic agent is listed in Table 3-2. Flows during the experiment ranged from 1.5 to 4 mL min^{-1} g^{-1}, and aortic pressures were typically between 20 and 30 mmHg. Heart weights at the conclusion of the experiments were 7.5 to 10 g, and 82-87% water, indicating significant edema as compared to the values measured *in vivo* (Gonzalez and Bassingthwaighte, 1990). However, most of this fluid gain occurred during the initial 20-30 minute equilibration period; the baseline weight was relatively stable over the experimental period.

3.3.1 Parameter estimates

Mean parameter estimates obtained from the complete set of osmotic weight transient data are presented in Table 3-1. According to these results, the endothelial pathway for water exchange constitutes about 18% of the total transcapillary hydraulic conductivity, the large pore pathway accounts for 3.5% of the hydraulic conductivity, and the remainder is assigned to the small pore. The small pore hydraulic conductivity of 7.9 cm s^{-1} $mmHg^{-1}$ occurred through a system with a relative area per unit path length of 4.3 cm^{-1}. The small pore has an effective radius of approximately 7.1 nm, while the large pore was assumed to be 24 nm in radius from prior model fits to lymph sampling data.

Table 3-1: Pathway Parameter Estimates

Pathway	$A_p/S\Delta r$ (cm^{-1})	r_p (nm)	L_p ($cm\ s^{-1}\ mmHg^{-1}$)
Endothelial	N/A	N/A	$1.83 \pm 0.57 \times 10^{-8}$‡
Small Pore	4.32 ± 1.05‡	7.1 ± 1.7‡	$7.9 \pm 2 \times 10^{-8}$†
Large Pore	0.02*	28*	3.8×10^{-9}†

* assumed from prior work
† calculated
‡ estimated from data

The coefficient of variation for individual parameter estimates was only around 1%, which is substantially smaller than the errors between different data sets. Table 3-1 therefore treats each transient as providing an independent parameter estimate, and presents means with an error equal to the standard deviation of parameter estimates.

The parameters obtained from this analysis can be used to calculate solute permeabilities and reflection coefficients for the solutes through each pathway (Table 3-2). Solute permeabilities for small solutes (NaCl through raffinose) are dominated by diffusion through the small pore, and are close to proportional to molecular free diffusion coefficient. However, there is a consistent decrease in the permeability to diffusion coefficient ratio (*P/D*) from about 3.8 to 3.0 cm^{-1}. Inulin and albumin are significantly hindered compared to the other solutes.

Table 3-2: Solute Phenomenological Transport Parameters

Solute	$D^{\dagger}$ (cm^2/sec)	r_s (nm)	σ_{sp}	P_{sp} (cm/s)	σ_{lp}	P_{lp} (cm/s)	n
NaCl	$1.72x10^{-5}$	2.5	0.0038	6.4×10^{-5}	0.0003	$3.3x10^{-7}$	31
Urea	$1.50x10^{-5}$	2.2	0.0029	$5.7x10^{-5}$	0.0002	$2.9x10^{-7}$	15
Glucose	$7.79x10^{-6}$	4.4	0.012	$2.6x10^{-5}$	0.0008	$1.5x10^{-7}$	16
Sucrose	$6.03x10^{-6}$	5.2	0.017	$1.9x10^{-5}$	0.0010	$1.1x10^{-7}$	38
Raffinose	$5.02x10^{-6}$	6.0	0.022	$1.5x10^{-5}$	0.0014	$9.2x10^{-8}$	20
Inulin	$1.85x10^{-6}$	16.6	0.17	$2.5x10^{-6}$	0.011	$2.8x10^{-8}$	6
Albumin	$7.87x10^{-7}$	36	0.62	$1.4x10^{-6}$	0.052	$8.8x10^{-9}$	13

† at 33 °C

3.3.2 Sample Results

Figure 3-4 shows a representative fit to an osmotic weight transient experiment on an isolated rabbit heart. Following a step change in perfusate osmolarity using 20 mM NaCl, there is an initial rapid loss of water from the interstitium and cells to the plasma as osmotic equilibrium is restored. This rapid shift of water diminishes the osmotic pressure gradient in the test solute, and also creates opposing concentration gradients in the resident solutes previously at equilibrium (osmotic buffering). Interstitial hydrostatic pressure falls as V_{isf} decreases. This is followed by a slower phase where the solute enters the interstitium to partially dissipate its transcapillary concentration gradient, and mechanical elastic and secondary osmotic forces act to partially restore interstitial volume. A steady-state interstitial-to-plasma concentration ratio is achieved when the rate of solute entry into the interstitium is equal to the rate of removal by lymph.

The time course of weight change is substantially different for larger solutes like albumin (Figure 3-5). Because only 0.5 mM albumin was used, the initial rate of weight loss is less than for NaCl, despite albumin's higher reflection coefficient. However, the duration of the weight transient is longer because transcapillary concentration gradients persist as the test solute penetrates the interstitium only very slowly. Osmotic buffering

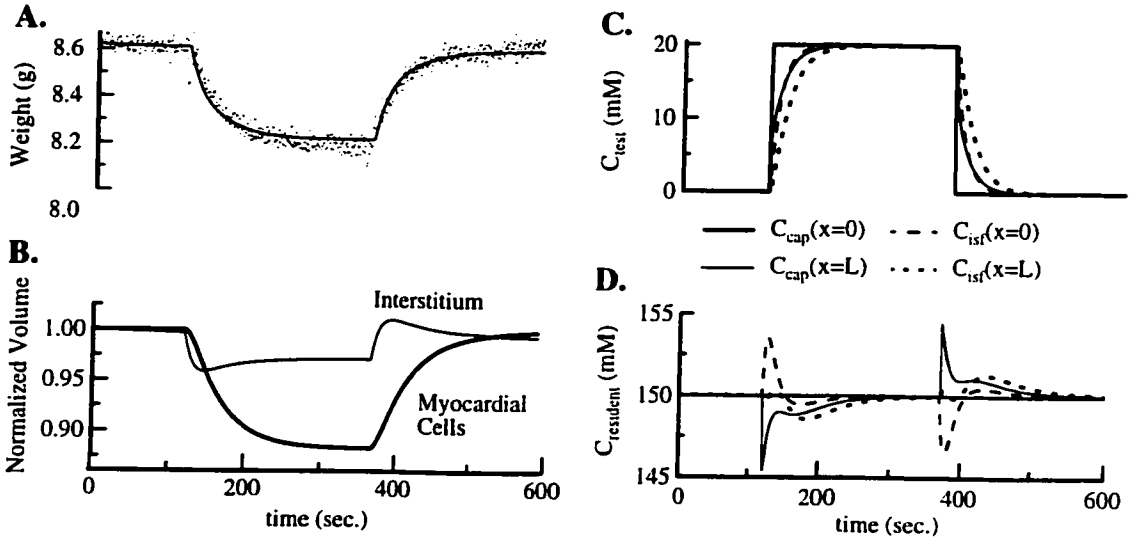

Figure 3-4 Model response with 20 mM NaCl as the osmotic agent. The basic parameter set was adjusted by increasing d_{myo} to 3 μm and decreasing Q_{col} and Q_{im} to 0.021 and 5.4×10^{-4} g/mL respectively to account for edema present in the experimental preparation. Flow was 13 mL/min, p_a was 24 mmHg, p_{isf} was 5.45 mmHg, and Ω_a was 1.33 mmHg min mL^{-1}. **A:** Fit of model (solid line) to organ weight data. **B:** Predicted volume loss from interstitial and parenchymal cells. **C:** Predicted time course of NaCl concentration. **D:** Time course of concentration of resident solutes at equilibrium prior to transient.

effects are minimal because the low J_v causes only a negligible transcapillary gradient in the resident solutes.

3.3.3 Sensitivity Analysis

Sensitivity analysis indicated that analysis of transients over a range of molecular weights for NaCl to albumin was needed to provide estimates of the small pore system parameters $A_{sp}/(S\Delta r)$ and r_{sp}, and the hydraulic conductivity ($L_{p,endo}$) of the transendothelial pathway. Data spanning a wide range of molecular sizes is crucial to getting reasonable estimates, as there is no solute size at which all three parameters have substantial and distinctly different sensitivity functions (Figure 3-6). Analysis of osmotic transients is unable to resolve the values of the large pore parameters because the sensitivity functions $\delta \ln W/\delta \ln r_{lp}$ and $\delta \ln W/\delta \ln A_{lp}$ with NaCl, sucrose, inulin, and

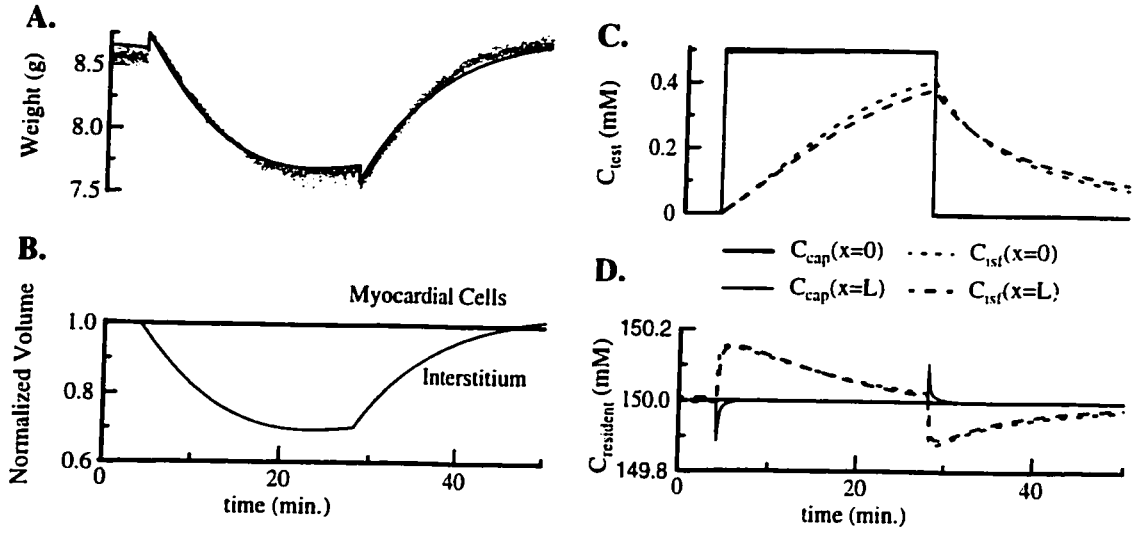

Figure 3-5 Osmotic response to 0.5 mM albumin in the same heart as in Figure 3-4. **A:** The rate of weight loss is lower, but longer-lasting than with smaller solutes. The small discontinuities in the weight record are experimental artifacts arising from the differences in control and test solution viscosity. **B:** Predicted volume loss from interstitial and parenchymal cells. **C:** Albumin penetration of the interstitium. **D:** The model predicts only a minimal rise in interstitial resident solute concentration.

albumin as the osmotic agent are all nearly 0 over the complete time course of an osmotic transient experiment.

3.3.4 Osmotic Transients at Variable Flows

We found that flow had no effect on the parameter estimates produced by our analysis. Osmotic transients with 30 mM sucrose as the osmotic agent produced weight responses with an increasing slope as flow increased from 1.75 to 3.9 mL min^{-1} g^{-1} (Figure 3-7). This trend was consistently observed over 22 transients in 2 different hearts. However, the parameters estimated from these data sets did not have a variability higher than that observed in the standard study, and showed no apparent correlation with flow.

3.4 Discussion

The use of a sophisticated model of the coronary microcirculation has enabled us to design effective osmotic weight transient protocols, and interpret the results more

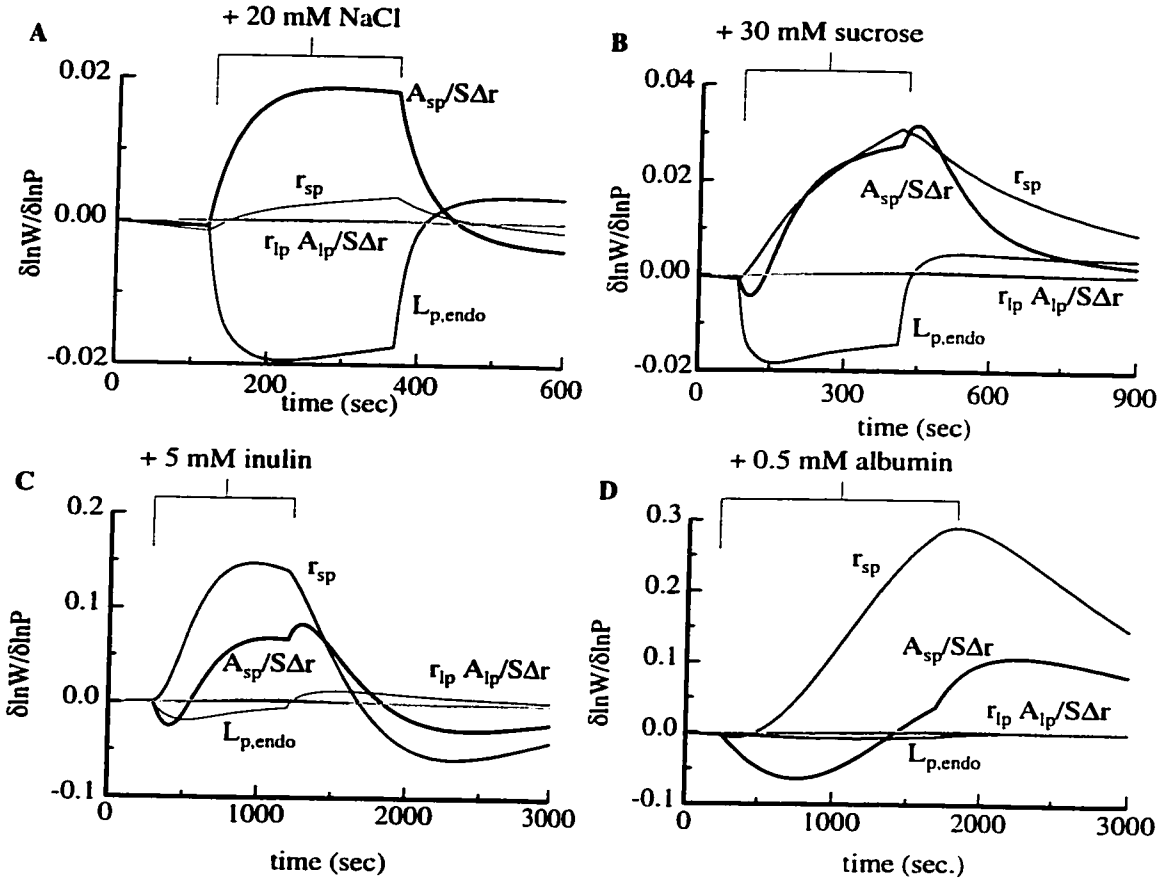

Figure 3-6 Sensitivity functions showing the fractional change in weight during an osmotic transient with respect to a fractional change in parameter values for osmotic transients induced by NaCl (A), sucrose (B), inulin (C), and albumin (D). The weight response to cases A and D are given in Figure 3-4 and Figure 3-5 respectively.

effectively than previous investigators. The osmotic transient methods provides a means of estimating the parameters governing exchange through the small pore and transendothelial pathways. The parameter estimates are in good agreement with results obtained from other studies, and provide for a more complete description of the exchange process than has previously been obtain in the heart.

3.4.1 Design of the Experiment

Sensitivity analysis provides a tool to develop strategies for parameter optimization. When applied to our osmotic transient protocol, sensitivity analysis suggested a means to

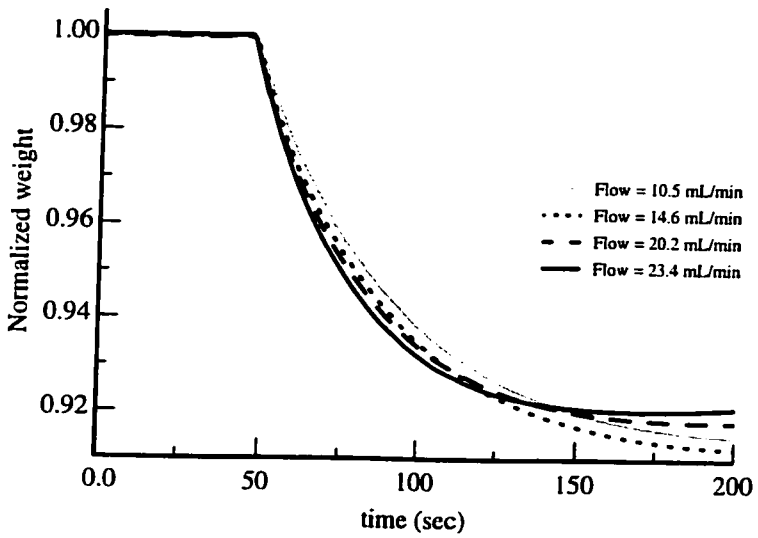

Figure 3-7 Sucrose induced osmotic transients at varying flows show an initial rate of weight loss that increases with increasing flow. For clarity, the figure shows model fits rather than the original data obtained at different flows in the same heart. Organ weight was around 7 g, and flows ranged from 1.75 to 3.9 mL min^{-1} g^{-1}. The tails of the curves do not equilibrate at the same total weight because the volume of the interstitium relative to the other compartments changes from transient to transient.

estimate the parameters $L_{p,endo}$, r_{sp}, and $A_{sp}/(S\Delta r)$. The parameters $A_{sp}/(S\Delta r)$ and r_{sp} can be determined from albumin transients since $\delta \ln W/\delta \ln A_{sp}$ and $\delta \ln W/\delta \ln r_{sp}$ are very different, and $\delta \ln W/\delta \ln L_{p,endo}$ is negligibly small. $L_{p,endo}$ can then be determined from NaCl transients, holding $A_{sp}/(S\Delta r)$ fixed. If the model is correct, midsized solutes provide redundant information, and fits to their transients should only require minor tweaking of parameter estimates.

This strategy makes sense given our understanding of the microcirculatory exchange model. Small hydrophilic solutes (MW < 1,000 daltons) only induce a significant J_v though the transendothelial pathway, where it can be assumed they have a σ equal to one because aquaporin channels and cell membranes exclude these solutes. The rate of the process is proportional to $L_{p,endo}$. The driving force for fluid exchange is dissipated by solute permeation into the interstitium, which is predominantly diffusive and proportional to $A_{sp}/(S\Delta r)$. As a first approximation, the magnitude of the weight transient is governed by the ratio of these processes, or $L_{p\,endo}$ to $A_{sp}/(S\Delta r)$. As solutes become larger, sensitivity

to $L_{p,endo}$ per unit osmolarity change stays the same and the absolute magnitude of the function decreases because lower concentrations are typically used experimentally for larger solutes due to their limited solubility and ability to induce water flux through the small pore pathway. $A_{sp}/(S\Delta r)$ begins to govern not only the rate of solute permeation into the interstitium, but also the magnitude of water flux out of the interstitium as σ for this pathway starts to increase. Thus, for larger solutes the sensitivity function starts out negative as increased small pore area results in an increased water efflux, and goes positive only later in the transient when osmotic equilibrium is achieved and solute permeation dominates the tail of the transient response. The sensitivity to r_{sp} also becomes increasingly greater as solute begins to be restricted by the small pore pathway; increased pore size leads to lower σ, increased water fluxes and reduced solute permeation.

Sensitivity analysis also implies that the parameters governing transport through the large pores cannot be determined from the experimental data. This is an intuitive finding because that even the largest solutes have a σ near 0 for this pathway, and consequently variations in solute concentration do not change $J_{v,lp}$ or alter organ weight. Although permeation of large solutes through the large pore path is a significant fraction of the total diffusive permeability, the tail of the weight transient response is also independent of the parameterization of the large pore pathway because the uptake of plasma proteins by the interstitium is too slow to affect the osmotic driving force, even late in the osmotic transient. Rather, weight loss ceases when falling interstitial hydrostatic pressure and increasing interstitial osmotic pressure (exerted by the permanent protein components of the interstitial matrix) balance the increased osmotic pressure in the capillaries. This result assumes that the large pore pathway is in fact in the neighborhood of $A_{lp}/S\Delta r = 0.05$ cm^{-1} and $r_{lp} = 24$ nm. Our model simulations show that a putative large pore pathway would not make a significant (>5%) contribution to the total osmotically induced water flux by albumin unless it was made both more restrictive and more prevalent; $A_{lp}/S\Delta r = 0.25$ cm^{-1} and $r_{lp} = 12$ nm is one such combination, but these values are well outside of the range compatible with the lymph to plasma concentration ratios of large plasma proteins (Laine and Granger, 1985, Pilati, 1990).

3.4.2 Interpretation of the weight transient curve

The initial interpretation of the osmotic weight transient experiment (Vargas and Johnson, 1964) was that the initial slope of the weight response, proportional to J_v, could be used to estimate a solute reflection coefficient from the relationship $J_v = \sigma L_p RT\Delta C$. This fundamental interpretation of the weight response has remained the same in all previously published models; the initial rate of weight loss is proportional to σL_p. Although this approach inherently assumes a single pathway for coupled fluid and solute exchange, it has been common practice to reinterpret the σ obtained from osmotic transient experiments as a single-path apparent σ. (More precisely, the technique provides the apparent osmotic reflection coefficient for the membrane as a whole, σ_d. Onsager reciprocity does not apply to heterogeneous membranes; σ_d is always less than the apparent solvent drag reflection coefficient for the membrane, σ_f.)

The high reflection coefficients obtained from osmotic transient experiments can then be understood as an averaging between a transendothelial pathway which excludes all solutes (giving them a σ of 1), and relatively unrestrictive aqueous pathways with σ close to 0 for at least the smaller hydrophilic solutes. By itself the apparent σ_d for a heterogeneous membrane is insufficient to provide a complete description of exchange kinetics. In conjunction with other data, Pappenheimer (1969) proposed that about 50% of transcapillary water exchange occurs through a water-exclusive pathway in order to explain early data on hydraulic conductivity and solute permeability in skeletal muscle measured by his isogravimetric technique (Pappenheimer et al., 1951) and the indicator-dilution work of Alverez and Yudilevich (1969). More recently, Watson (1995) and Wolf (1994, 1996) have proposed three pathway pore models for solute exchange in mammalian skeletal muscle, with 41% flow through a water exclusive pathway, a large-pore pathway of radius 28.5 nm allowing 17% of the hydraulic conductance, and a small-pore pathway of radius 4.57 nm permitting the remaining 42% of the transcapillary flow.

Using an apparent σ to describe a heterogeneous pathway hides the details of how the fluxes actually occur across the membrane. The total J_v at any time is actually the sum of the fluxes through each pathway, each with its own value of σ (Rippe and Haraldsson,

1994). Modeling these fluxes in detail provides a richer and more complete description of the events that actually occur during an osmotic transient experiment. An increased osmotic pressure in the capillaries induces water flux only through pathways that have a high σ for the test solute, so the distribution of fluxes changes during the course of an osmotic transient experiment (Figure 3-8). For small solutes like NaCl, the only pathway with a non-negligible σ is the transcellular pathway. Regardless of its fraction of total hydraulic conductivity, an increase in capillary NaCl concentration draws water out of the tissues predominately across the endothelial cells. Consequently the $\sigma_{apparent}$ at early times in an osmotic transient is larger than at steady state, because the fraction of J_v through the transendothelial cellular pathway is greater. In contrast, albumin can induce osmotically-driven fluid movements through the small pore system, as well as across the endothelial cells. The hydrostatic pressure changes employed in lymph sampling techniques cause the same change in driving force for each pathway, and thus $\sigma_{apparent}$ does not change. There is some evidence of higher reflection coefficients for large solutes measured with the osmotic transient technique compared to C_L/C_p analysis; $\sigma_{albumin}$ was only 0.59 by Pilati's (1990) measurement of filtration rate independent C_L/C_p. However, a more careful comparison of the two techniques in the same experimental system is needed to make definite conclusions.

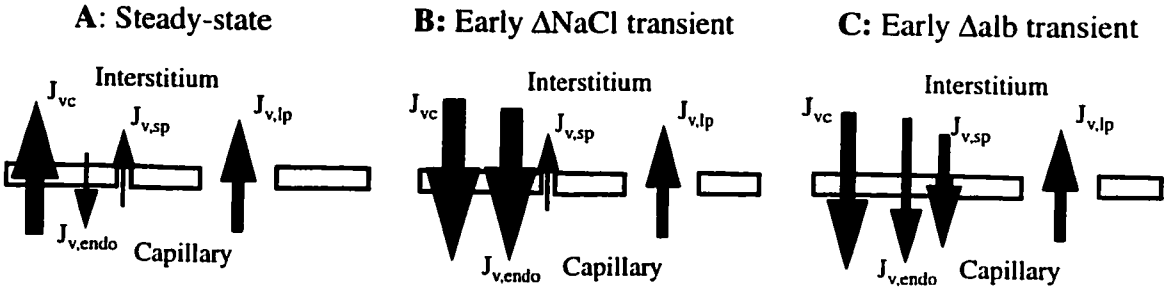

Figure 3-8 Distribution of transcapillary fluid fluxes across the endothelial cells ($J_{v,endo}$), small pores ($J_{v,sp}$) and large pores ($J_{v,lp}$), with a total transcapillary flux J_{vc}. (A) Steady-state condition. (B) Beginning of an osmotic transient with 20 mM NaCl as the osmotic agent. (C) Beginning of an osmotic transient with 0.5 mM albumin as the osmotic agent.

3.4.3 Parameter Values

Our estimates of the parameters governing exchange in the microvasculature of the heart are in good agreement with previous results. Our total estimated L_p of 1.1 cm s^{-1} $mmHg^{-1}$ is very close to the Vargas and Johnson (1964) estimate of 1.0 cm s^{-1} $mmHg^{-1}$ in isolated Ringer-perfused rabbit heart. A novel result is our estimation that 18% of the total L_p is contributed by the transendothelial pathway. This value is greater than the 5-10% estimated in frog mesentery (Curry et al., 1976), but less than the 40% predicted by Wolf (1994, 1996) in skeletal muscle.

The solute permeabilities obtained in this study are also consistent with estimates obtained from indicator dilution studies in Ringer-perfused heart preparations (Chapter 2). Solute permeability is proportional to $A_{sp}/(S\Delta r)$. A_{sp} is the cleft or pore surface area, S the capillary surface area, and Δr is the length of the pathway from capillary lumen to interstitium. These terms are kinetically inseparable. In anatomic studies, S is about 500 cm^2/g (Gonzalez and Bassingthwaighte, 1990) and in the geometry of our model is 487 cm^2/g. From electron microscopy studies the distance Δr is about 0.4 μm (REF); thus an estimate of $A_{sp}/(S\Delta r)$ of 4 cm^{-1} translates to A_{sp}/S of 0.32% and A_{sp} of 1.6 cm^2/g. This value is about one-quarter of the value obtained by indicator dilution methods in cardiac tissue by Guller et al. (1975), but the difference can be traced to those author's decision to use the diffusion coefficient for sodium in extracellular fluid rather than free solution in their calculations. Our model reduces the free diffusion coefficient only through frictional interactions with the capillary wall and steric exclusion effects, which cause a reduction of only 86% for NaCl in a 7 nm pore. If the lumenal glycocalyx hindered sodium diffusion rates, the effective area of the junction would need to be increased in order to compensate. As it stands, our model is roughly consistent with anatomical junction area, given that only 5% of the junctional may be free of junctional strand and effectively open to exchange (Bundgaard, 1984, Adamson and Michel, 1993).

We investigated significance of explicitly modeling fluxes through each pathway individually by fitting model results generated by the three-path model with a single-path model that lumped all transcapillary exchange into a single effective P and σ. The osmotic

transient results presented in Figure 3-4 are typical of small solutes, and can be closely matched using a parametrically reduced form of the model with a single lumped pathway for transcapillary exchange. The estimated NaCl permeability by the reduced model is $1x10^{-4}$ cm/s, significantly higher than the multipath model estimate (6.7×10^{-5} cm/s). Also, σ of the single-path model is 0.15, assuming the L_p of this single "effective" pathway is equal to the sums of the L_p's of the three-path description. The higher apparent solute permeability predicted by the single-path model at least partially explains the historic discrepancy between indicator dilution and osmotic transient measurements of small solute permeability. The actual permeability estimates obtained by Vargas and Johnson are higher than modern estimates even accounting for this error, presumably because they used no albumin in their perfusate. A single path reflection coefficient of 0.15 is incompatible with the observed lymph-to-plasma concentration ratio of unity for small solutes at even the highest filtration rates. It also implies a channel width of about 3 nm, incompatible with MID and electron microscopic observations.

Our use of a Ringer-perfused preparation has probably lead to an increase in the permeability and hydraulic conductivity of the small pore pathway as compared to the *in vivo* condition. The mechanism for this change is likely the degradation of the capillary glycocalyx, which contributes some of the resistance to exchange (Adamson, 1990, Huxley and Williams, 2000). As interpreted by our pore theory model, this degradation would be observed as both a increase in pore radius and pore area. Based on comparisons of multiple indicator dilution experiments in different heart preparations, we expect a roughly doubling of the pore area and increase in effective radius form 5 to 7 nm when comparing blood to Ringer-perfused preparations. Therefore, the transendothelial fraction of L_p in the *in vivo* heart is likely in the range of 40%.

3.4.4 Flow Effects

Investigators using the osmotic transient approach have long known that flow has an effect on the weight response. Our results confirmed the observation that the initial rate of weight loss during an osmotic response increases with increasing flow. Consequently,

when compartmental analysis techniques are used to obtain reflection coefficients, σ appears to increase with increasing flow rates (Wolf and Watson, 1989). This is because the Vargas and Johnson estimate of reflection coefficient is based on the prediction that the initial volume flux across the capillary wall is proportional to a step change in concentration. The presence of any axial concentration gradients in the capillaries will cause the osmotic driving force for fluid exchange to be overestimated by a compartmental model.

In their original papers, Vargas and Johnson (1964, 1967) handled the flow-limitation problem by performing experiments at increasing flows until constant estimates of phenomenological coefficients were obtained. A more extensive trans-capillary exchange model developed by Bloom and Johnson (1981) also neglected flow effects, which the authors argued were small for their experimental methods (Vargas and Blackshear 1981). At a flow of 1 mL/s, an extremely high flow for a rabbit heart of around 6 grams, Johnson and Bloom (1981) calculated that the reflection coefficient of NaCl, a solute with relatively high permeability, would be underestimated 16% by the basic Vargas and Johnson technique. The most complete set of flow vs. σ data available from Wolf and Watson show an apparently increasing σ without a plateau as flow increases.

However, axially distributed models produce sharper weight changes at higher flows because the capillary concentrations are more nearly uniform at higher flows (Figure 3-7). Similar parameter estimates, not correlated with flow rates, are obtained over the full range of flows. The only previous axially-distributed capillary model applied to the osmotic transient perturbation, developed by Grabowski and Bassingthwaighte (1976), should have accounted for axial concentration gradients in the capillaries but the authors did not examine the effect of flow on their model solutions.

However, the initial transcapillary volume flux predicted by the Vargas and Johnson method is never reached because the axial concentration gradient of the test solute in the capillary never completely dissipates, even at the highest flows. This can also be seen in the considerable time lag for the venous end of the capillary to respond to the step change at the capillary inlet (Figure 3-9). Model simulations show that concentration gradients

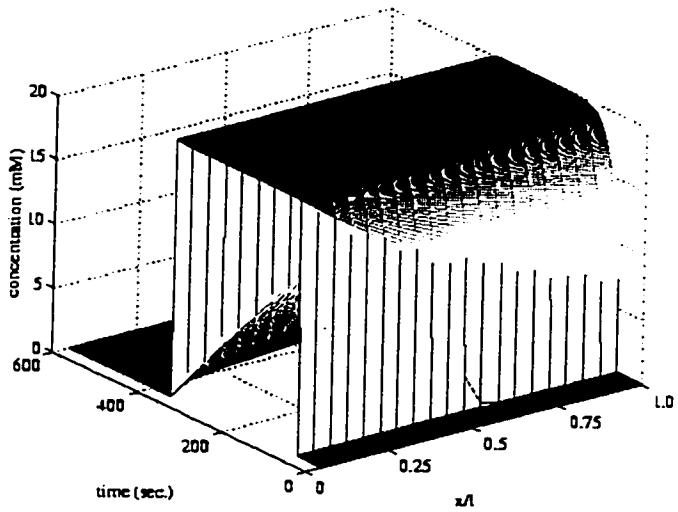

Figure 3-9 Capillary concentration of the osmotic agent (NaCl) as a function of time and location with a fractional capillary position (x/l) of 0 corresponding to the arterial end of the capillary.

develop not only because solute leaves the capillary as it moves downstream, but also because the influx of solute-free fluid into the capillary from the surrounding tissues dilutes test solute in the capillary as material moves downstream. This previously unrecognized mechanism for the establishment of axial concentration gradients is maximal during the initial phase of an osmotic transient experiments, independent of the solute's *PS/F*, when transcapillary water fluxes are the highest. Although our data mirror that of Wolf and Watson (1989), showing an increasing initial rate of weight loss at higher flows, the model lets us fit these results without altering the parameters governing transcapillary exchange.

3.4.5 The Osmotic Transient Experiment

3.4.5.1 Low oncotic pressure preparations

Although the osmotic transient approach is one of the few available techniques for quantifying fluid movements in a whole organ, there are limitations to the experimental approach. The isolated Ringer-perfused heart is a convenient preparation for osmotic transient studies, but it has important differences from the *in vivo* blood-perfused heart.

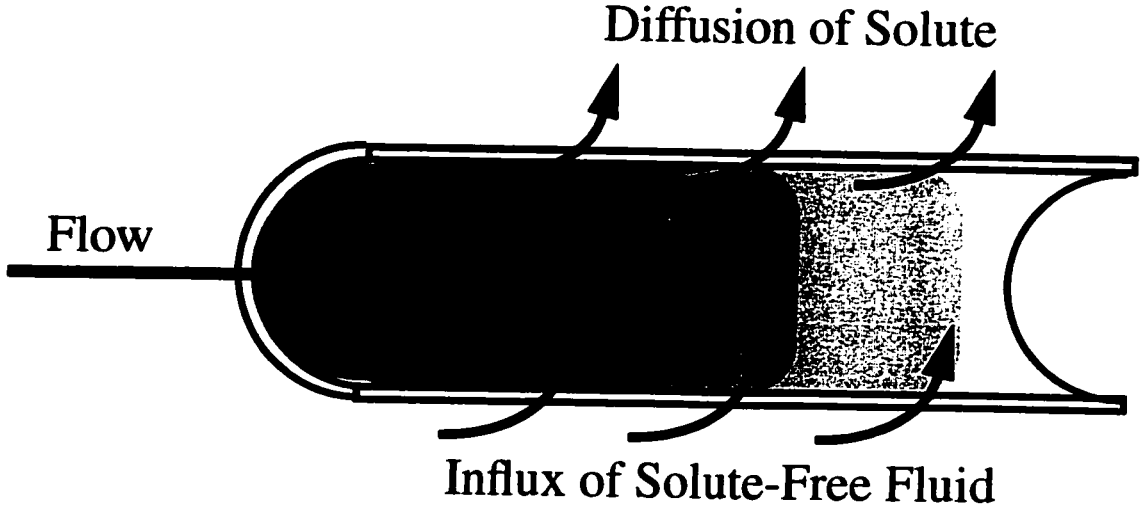

Figure 3-10 Mechanisms for the development of axial concentration gradients include both escape of solute from upstream regions of the capillary, and entrance of solute-free fluid into upstream regions, diluting the osmotic agent at the venous end of the capillary.

Ringer-perfused hearts are subject to substantial edema formation because of the lowered oncotic pressure of the perfusate. By the end of an experiment, hearts typically had water contents of over 85%, as measured by wet-to-dry weight ratio, compared to *in vivo* values of 79 ± 1% (Gonzalez and Bassingthwaighte, 1990). Since total perfusate osmolarity is kept at normal levels, it seems likely that much of this change is due to an increased interstitial volume. In our analysis, we have assumed that all weight gain during the baseline equilibration period is caused by expansion of the interstitial fluid volume; this typically required a doubling of interstitial volume.

Another problem with low protein preparations is that the lack of plasma proteins causes capillary permeability to become abnormally high (Huxley and Meyer, 1990, Huxley and Curry, 1991). While we used a background level of 1 g/L albumin in all solutions to help maintain normal permeability properties, it is likely that other serum proteins are necessary to maintain completely normal permeabilities. It must be kept in mind that parameters estimated for the Ringer-perfused heart are not necessarily representative of the *in vivo* values.

3.4.5.2 Pressure changes during the experiment

Drops in perfusion pressure are known to occur during osmotic transient experiments performed at constant flow (Vargas and Blackshear, 1981a,b, Grabowski and Bassingthwaighte, 1976). If these pressure changes propagated to the capillaries they would partially offset the increase in perfusate osmolarity, leading to a smaller than expected change in the Starling forces for a measured rate of fluid exchange. However, in a constant-flow preparation, only changes in post-capillary or capillary hydraulic resistances would cause this effect because the pressure at any given point in the vascular network is the product of the flow and the downstream resistances. Since coronary vascular smooth muscle is known to dilate in response to osmolarity changes (Avolio et al., 1980, Vlahakes et al., 1989), it seems likely that these pressure changes are not relevant to our analysis.

To test the hypothesis that the pressure changes are indeed caused by arteriolar coronary dilation, we infused increasing amounts of papaverine, a smooth muscle relaxant, causing a reduction in perfusion pressure. Although the majority of the perfusion pressure drop is seen with 5 mg/L, higher papaverine levels cause an additional small drop in arterial pressure (see Figure 3-11 A). Pressure decreases above 5 mg/L papaverine are likely due to decreased heart rate, which reduces vascular resistance by decreasing the time spent in systole, and not increasing coronary vasodilation because infusions of 5 mg/L papaverine followed by dipyridamole, which induces vasodilation of small arterioles by raising interstitial adenosine levels, show no further perfusion pressure changes (Figure 3-11 B).

A slow increase in baseline pressure accompanied by a tendency to develop edema was observed after injection of dipyridamole or dipyridamole and papaverine, but not after papaverine alone. This effect has also been observed to occur in isolated hearts perfused with adenosine (Rubboli et al., 1994). It is likely that increases in tissue water content, increases in venous resistance, and decreases in myocardial performance work together in a positive feedback cycle, particularly at constant flow where increased compression of veins during edema raises capillary pressures and increases capillary filtration rates. How

adenosine promotes this cycle is unknown, although it does increase venous resistance (Chilian et al., 1990, Pilati, 1990). We therefore chose to use papaverine as a vasodilator during our experiments, which kept capillary pressures low and partially offset the effect of the low oncotic pressure perfusate. Hydrostatic pressure changes at the aorta during a transient were typically about 2 mmHg.

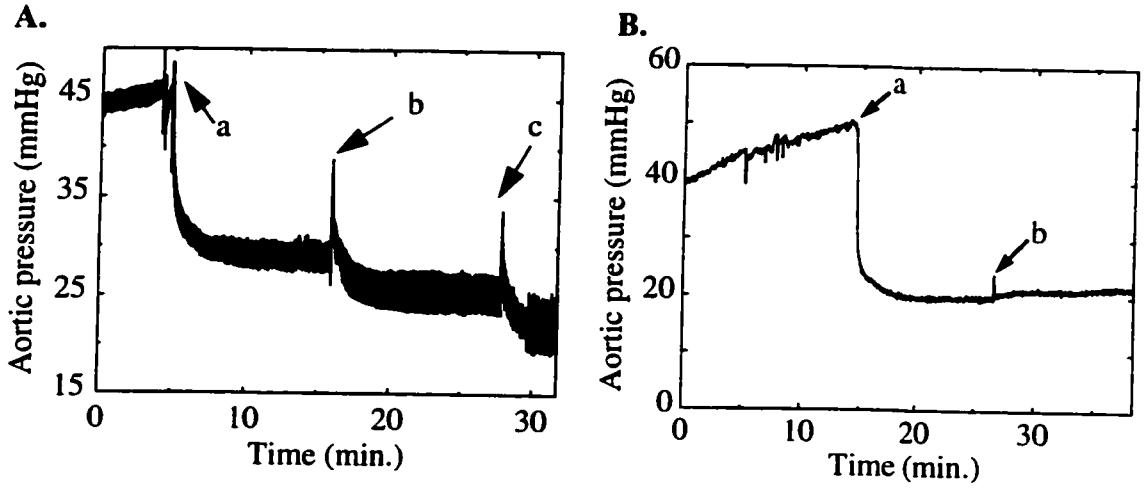

Figure 3-11 Response of isolated rabbit heart to papaverine at a constant flow of 2.5 ml min^{-1} g^{-1}. A: Increasing concentrations of papaverine (a) 5 mg/L, (b) 20 mg/L, (c) 50 mg/L caused perfusion pressure decreases at constant flow. Heart rate was 208 beats per minute in control, and decreased to 201, 180, and 108 with increasing papaverine concentrations. Myocardial contractility became severely impaired at highest papaverine levels, with irregular pacing and eventual cardiac failure. B: 10 μM dipyridamole added to the buffer (b) following 20 mg/L papaverine (a) produces no further drop in vascular resistance.

With vasodilation of the coronary arterioles, the pressure transient following an osmotic change is greatly diminished (Figure 3-12). Additionally, osmotic transients induced in the presence of glybenclamide, an ATP sensitive K^+ channel blocker, exhibit an initial drop in perfusion pressure followed by a rapid return toward the pre-transient pressure. Glybenclamide also attenuates osmolarity induced vasodilation in isolated coronary arterioles (Ishizaka and Kuo, 1997), which sometimes undergo a transient vasodilation before returning towards their initial diameters (Kuo, personal communication). If vascular resistance changes are restricted to pre-capillary vessels, the

capillary pressures at constant flow should remain unchanged and not impact osmotic transient experiments. Consequently, large arterial pressure changes seen in earlier osmotic weight transient studies should not have been greatly affected by changing capillary pressures. However, it is unknown whether venule smooth muscle responds to osmolarity changes in a similar manner to arterial smooth muscle. If it does, capillary hydrostatic pressures could be altered during a switch in perfusate osmolarity.

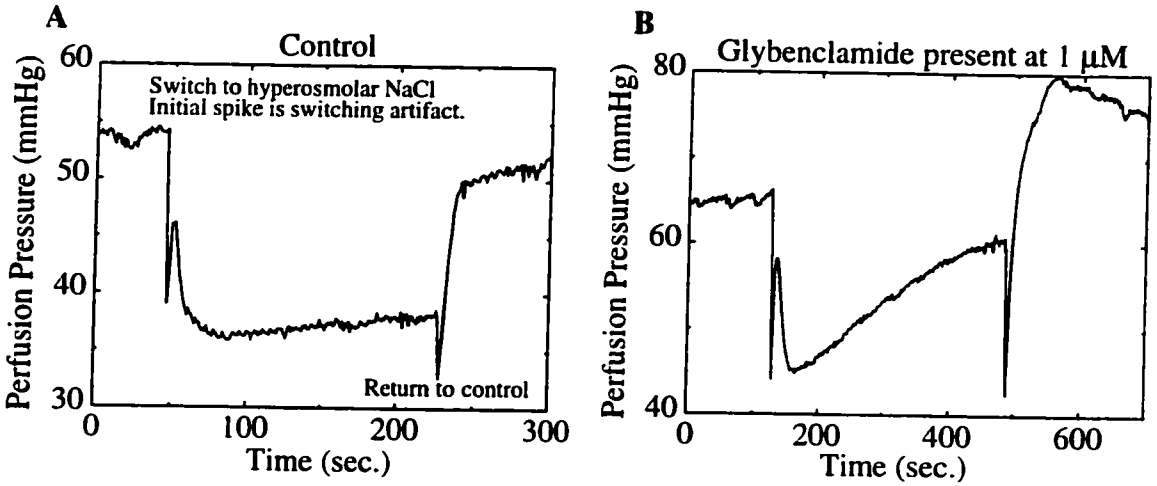

Figure 3-12 Coronary arteriole response to osmolarity A: An increase in osmolarity (20 mM NaCl added to perfusate) causes a rapid decrease in perfusion pressure as coronary arterioles dilate. B: Response to same osmotic perturbation in the presence of the K^+_{ATP} channel blocker glybenclamide.

3.4.5.3 Source of fluid loss

Gravimetric measurements can not distinguish whether the fluid lost from an organ originates from the cellular or interstitial spaces. Regardless of its original origin, the model predicts that this fluid is always hypotonic to interstitial fluid because at least a portion of the flux must be across the endothelial aquaporin pathway. As the osmotic agent becomes smaller, J_v becomes increasingly hypotonic as the flux is localized exclusively to the transcellular pathway, in agreement with the observations of Effros (1974). Our model predicts about 2/3 of the fluid loss during a small solute transient in the heart originates in the parenchymal cells. Wangensteen et al. (1981) used morphometric measurements in lungs to show that most of the water extracted during a shift in perfusate osmolarity

originated from cellular volumes. Lung endothelial and epithelial cells are in closer contact with the capillaries than much of the interstitium, which could shift the balance even more towards cellular water loss than in the heart. Morphometric or indicator dilution studies in heart to determine cellular and interstitial fluid volumes before and after an osmotic transient could provide additional validation of model predictions.

3.4.6 Conclusions

Despite the known limitations of osmotic transient experiments, we have made a significant advance over previous studies by using a more sophisticated method of analysis that allows the extraction of more information from the weight transient record than was previously possible. Our results suggest the small pore system is well-represented by a population of pores with radius of 7.1 ± 1.7 nm and $A_{sp}/S\Delta r$ of 4.3 ± 1.1 cm^{-1}. The size and density of the large pore pathway can not be determined by osmotic transient methods, but lymph sampling data suggests it is likely around 28 nm in radius with an $A_{lp}/S\Delta r$ of about 0.02. There is a significant pathway for solute-free water exchange in coronary microvessels, accounting for 18% of the total L_p in the Ringer-perfused heart.

4 Conclusion

4.1 Summary

Microcirculatory exchange can be a difficult process to model, not because the underlying physical processes are a mystery, but because it is hard to apply simple physical laws in complex biological contexts. Previous models of microcirculatory exchange have been tailored to fit data from only one of three types of experiments: osmotic transients, multiple indicator dilution, or lymph sampling. Although these analysis methods may have been sufficient for the immediate task at hand, their narrow focus makes these models unsuitable as tools for providing a unified understanding of the exchange process.

This thesis presents a model of coupled fluid and solute exchange that relates the fundamental processes occurring on the microvascular level to the organ-level responses that are the subject of experimental investigation. The model is a significant advance beyond previous efforts because it is the first to explicitly simulate the three major types of experimental data. Additionally, it provides the most complete and accurate representation of the events occurring during an osmotic weight transient experiment, one of the classical methods of measuring solute permeabilities and reflection coefficients, yet obtained. Several features of the model described in Chapter 2 have allowed these advances.

The most significant model advance is the independent calculation of fluxes through each of the pathways for exchange across the capillary wall. In continuous capillaries, these pathways include a transcellular pathway for solute-free water flux, likely mediated by aquaporin water channels, a small pore system likely corresponding to the endothelial junction, and a large pore system likely corresponding to infrequent breaks in the capillary wall structure. The behavior of the three-pathway model cannot be replicated by a single "equivalent pathway" representation, as changes in the Starling forces have disparate effects on fluid movements through the pathway. The single-path model is particularly inappropriate for the analysis of osmotic weight transient experiments because it fails to account for the fact that changes in plasma osmotic pressure cause fluid movements

through the pathways in proportion to σL_p for each pathway. This redistribution of fluid flux to high-σ pathways causes apparently high estimates of effective σ for small solutes like sucrose during an osmotic transient experiments, even though the steric hindrance to solute exchange is minimal for small solutes.

The use of an axially distributed blood-tissue exchange region allows the model to account for changes in the Starling forces along the length of the capillary. The most significant difference is the non-uniform concentration profile that develops immediately after a step change in concentration at the capillary inlet. Concentrations are lowered at the venous end of the capillaries for as long a minute after the step change due to solute escape from and water influx into upstream regions of the capillary. This approach is not only more accurate than a compartmental model because it provides the correct driving force for fluid exchange, but allows the model to account for changes in the weight transient response that occur as a function of flow.

Finally, the model includes a lymphatic drain in the interstitium, permitting net filtration across the capillary wall at steady-state. This addition is necessary to set the correct interstitial concentrations of chemical species, and correctly predict the third set of data, lymph to plasma concentration ratios. Its absence in the model of Grabowski and Bassingthwaighte (1976) was the key missing component that prevented that model from achieving accurate predictions of lymph to plasma concentration ratios.

Fits to osmotic weight transient experiments suggest the transcapillary exchange in the Ringer-perfused heart is well-described by a three pathway model, with an L_p across the endothelial cells of 1.8 ± 0.6 cm s^{-1} $mmHg^{-1}$, and small pore with radius of 7.1 ± 1.7 nm and $A_{sp}/S\Delta r$ of 4.3 ± 1.1 cm^{-1}. These parameters are reasonable in the context of multiple indicator dilution studies in the same preparation, and observations of endothelial junction widths of approximately 200 nm by serial section electron microscopy. Both multiple indicator dilution and lymph sampling studies in the blood-perfused heart suggest a slightly less prevalent small pore effective area and/or more restrictive pore dimensions. This most likely corresponds to a more prevalent capillary glycocalyx rather than actual changes in the dimensions of the endothelial junction. The size and density of the large

pore pathway can not be determined by osmotic transient methods, but lymph sampling data suggests it is likely around 28 nm in radius with an $A_{lp}/S\Delta r$ of about 0.02.

4.2 Future development

A key feature of the model is the presence of a paracellular pathway for solute-free water exchange across the coronary endothelial cells. Although accounting for only 20% of the total transcapillary hydraulic conductivity, the pathway accounts for the majority of osmotically-driven fluid fluxes, particularly when the osmotic agent is a small solute. Recent evidence suggests aquaporin water channels form the molecular basis for high transmembrane water permeabilities in a variety of tissues; this is likely to be the case in coronary capillaries because the magnitude of the solute-free water pathway is too high to to be explained by water diffusion through a lipid bilayer. The water channel protein aquaporin-1 is expressed by coronary endothelial cells although it is not known whether this is the only, or even the predominant route for water across the coronary endothelium. Future experimental work could confirm the functional significance of aquaporin water channels in the coronary microcirculation though the use of pharmacological block of the channels. However, this work will most likely require the development of more specific and less toxic agents than the mecurial-based compounds currently in use.

Multiple indicator dilution experiments have been analyzed under the assumption that small solute exchange across the capillary wall is purely diffusive. The validity of this assumption has been validated through simulations presented in Section 2.3.4. However, if fluid filtration rates are altered, as in the initial phase of an osmotic transient experiment, solvent drag may either augment or hinder the diffusive solute flux, resulting in an apparent permeability change as measured by indicator dilution. This will only be the case if the fluid and solute fluxes can interact, that is if they are occurring through the same pathway. Preliminary data obtained by Bassingthwaighte et al. (1979) show that the osmotically-driven efflux of water from cardiac tissue during an indicator-dilution experiment can result in an apparently lower permeability when inulin, but not sucrose, is

the osmotic agent. These results are in qualitative agreement with this model, but a more rigorous comparison of experiment and simulation are still required.

This thesis provides estimates of transport parameters in the whole heart, but it remains unclear how these parameters relate to measurements obtained in single capillaries. Although the whole organ response is simply the sum of the responses in each individual exchange unit, exchange properties are not necessarily uniform throughout the organ. Properties may vary with either with location in the vascular network, or in different anatomical regions of the heart. Therefore, a systematic study of exchange properties in coronary vessels from arterioles to venules, and from endocardium to epicardium may be required to relate the properties of individual microvessels to the behavior of the whole organ. If substantial heterogeneity is found, the organ-level model may have to be modified to account for exchange is distinct anatomical regions of the heart. This could most likely be achieved through the serial and/or parallel combination of parametrically varying versions of the basic exchange unit.

Glossary

Symbol	Definition	Values	Units
A_{sp}/S_c	Small pore fractional area	$2.25x10^{-5}$ (Ringer perfused) $1.05x10^{-5}$ (Blood perfused)	dimensionless
A_{lp}/S_c	Large pore fractional area	$2.5x10^{-7}$	dimensionless
C	Concentration	C^a_{NaCl} =150; C^a_{alb} =0.75 (perfusate)	mM
d_{ic}	distance between capillaries	d_{ic}= 18[2]	μm
d_{im}	distance between myocytes, or capillaries and myocytes	d_{im}=1.8[estimated from 5]	μm
D_j	Free diffusion coefficient of *j*th solute (at 37°C)	$D_{NaCl}=2.0x10^{-5}$ [11]; $D_{suc}= 7.0x10^{-6}$[11]; $D_{alb}=9.1x10^{-7}$ [11]	cm^2/s
E_n	*n*th elastance coefficient (interstitium, cell)	E_1=15 mmHg[1]; E_2=0; E_3=0	variable
F	Flow through organ	28.8	mL/min
$\hat{F}$	Specific flow through organ	4.8	mL min^{-1} g^{-1}
F_L	Flow through lymphatics	time dependent variable	mL min^{-1}
f(α)	Fractional reduction of D inside pore	$f(\alpha) = 1 - 2.104\alpha + 2.089\alpha^3 + \ldots$ [4]	dimensionless
g(α)	Ratio of solute velocity to solvent velocity on the pore axis	$g(\alpha) = 1 - 0.667\alpha^2 - 0.1628\alpha^5$ [4]	dimensionless
$J_{S,j}$	Total net transcapillary solute flux of *j*th solute	time dependent variable	mol s^{-1} cm^{-2}
$J_{V,k}$	Transcapillary volume flux through *k*th pathway	time dependent variable	cm/s
$J_{V,pc}$	Volume flux across parenchymal cell membrane	time dependent variable	cm/s
$J_{L,s}$	Mass loss through lymphatics	time dependent variable	mol/s
K_L	Lymphatic conductance	$1x10^{-4}$[6]	ml s^{-1} $mmHg^{-1}$ g^{-1}
l_c	capillary length	639[3]	μm

Symbol	Definition	Values	Units
$L_{p,sp}$	Small pore hydraulic conductivity	$1.3x10^{-8}$ (blood-perfused) $8.8x10^{-8}$ (Ringer-perfused)	cm s^{-1} $mmHg^{-1}$
$L_{p,lp}$	Large pore hydraulic conductivity	$6.8x10^{-9}$	cm s^{-1} $mmHg^{-1}$
$L_{p,endo}$	Trans-endothelial cell hydraulic conductivity	$1.4x10^{-8}$	cm s^{-1} $mmHg^{-1}$
$L_{p,pc}$	Hydraulic conductivity across parenchymal cell membrane	$1x10^{-9}$	cm s^{-1} $mmHg^{-1}$
n	quantity of solute	time dependent variable	moles
N_c	number of capillaries in whole organ	$2.8x10^{7}$	dimensionless
$\hat{N}_c$	Capillary density	$4.6x10^{6}$	g^{-1}
N_{seg}	Number of axial segments in BTEX unit	7	dimensionless
p	Pressure (arterial, capillary inlet, capillary outlet, venous, interstitial, lymphatic)	p_a=87; p_{ci}=16.9; p_{co}=13.3; p_v=7; p_{isf}=13 (steady-state) $p_L=p_v$	mmHg
P_j	Permeability of *j*th solute (blood-perfused or Ringer-perfused)	$P_{NaCl}=3.5x10^{-5}$ or $8.1x10^{-5}$ $P_{suc}=1.0x10^{-5}$ or $2.6x10^{-5}$ $P_{alb}=3.5x10^{-7}$ or $4.3x10^{-7}$	cm/s
Pe	Péclet number	$J_v(1-\sigma)/P$	dimensionless
Q	Quantity (interstitial matrix, collagen, parenchymal cell)	$Q_{im}=0.05^{(1)}$; $Q_{col}=0.0013^{(1)}$ $Q_{pc}=0.32$	g/mL
r_c	Capillary radius	$2.5^{(2)}$	μm
r_f	Fiber radius (interstitial matrix, collagen)	$r_{f,im}=0.3$ $r_{f,col}=4$	nm
r_{sp}	Small pore radius	9.0 (Ringer perfused) 5.0 (Blood perfused)	nm
r_{lp}	Large pore radius	23.5	nm
r_s	Solute radius	$r_{NaCl}=0.22$; $r_{albumin}=3.6$; $r_{sucrose}=0.45$	nm

Symbol	Definition	Values	Units
Δr	capillary wall thickness	0.5	μm
R	Gas constant	8.314	J mol^{-1} $°K^{-1}$
S	Surface area per BTEX unit (capillary, parenchymal cell)	S_c=1.00x10^4; S_{pc}=3.67x10^4	μm^2
$\hat{S}$	Specific surface area (capillary, parenchymal cell)	$\hat{S}_c$ =487; $\hat{S}_{pc}$ =1780	cm^2/g
t	Time	independent variable	s
T	Absolute temperature	310	°K
u	Perfusate velocity in capillary	time dependent variable	cm/s
v	Anatomical volume (BTEX unit, capillary, interstitial, parenchymal cell)	v_{btex}=1.77x10^5; v_c=1.25x10^4; v_{isf}=4.44x10^4; v_{pc}=1.20x10^5	μm^3
V_f	Fluid volume (capillary, interstitial, parenchymal cell)	$V_{f,c}$=1.25x10^4; $V_{f,isf}$ =4.30x10^4; $V_{f,pc}$=9.06x10^4	μm^3
V_s	Solid volume (capillary, interstitial, parenchymal cell)	$V_{s,c}$=0; $V_{s,isf}$ =1.78x10^3; $V_{s,pc}$=2.99x10^4	μm^3
$\widehat{V}$	Whole organ volume fraction (large vessels, capillaries, interstitium, parenchymal cells)	$\widehat{V}_{lv}$ =0.085; $\widehat{V}_c$ =0.064; $\widehat{V}_{f,isf}$ =0.226; $\widehat{V}_{f,pc}$ =0.462; $\widehat{V}_{s,isf}$ =0.009; $\widehat{V}_{s,pc}$ =0.154;	dimensionless
$\hat{V}$	Specific volume (large vessels, capillaries, interstitium, parenchymal cells)	$\hat{V}_{lv}$ =0.080[5]; $\hat{V}_c$ =0.060[5]; $\hat{V}_{f,isf}$ =0.213[5]; $\hat{V}_{f,pc}$ =0.436[5]; $\hat{V}_{s,isf}$ =0.008[5]; $\hat{V}_{s,pc}$ =0.146[5];	mL/g
W	Organ weight	W^o=6	g
x	Axial coordinate along capillary length	independent variable	cm
α	Ratio of solute radius to pore radius	calculated	dimensionless
γ	Fractional volume of distribution in interstitium (of a solute)	γ_{NaCl}=0.99; γ_{suc}=0.99; γ_{alb}=0.78	dimensionless

Symbol	Definition	Values	Units
ϕ_n	*n*th virial coefficient	NaCl: ϕ_1=1.87; ϕ_2=0; ϕ_3=0 [11] sucrose: ϕ_1=1.0; ϕ_2=0; ϕ_3=0 [11] alb: ϕ_1=0.92; ϕ_2=0.48; ϕ_3=0.30 [7]	variable
η	Perfusate viscosity (at 37°C)	0.007	g cm^{-1} s^{-1}
ρ	Density (solid, fluid, organ)	ρ_s=1.33 [2]; ρ_f=1.01 [11]; ρ_{org}=1.06 [2]	g/ml
Π	Osmotic pressure	time dependent variable	mmHg

σ	Reflection coefficient of *j*th solute through small pore (blood-perfused or Ringer-perfused), large pore, endothelial cell	NaCl: σ_{sp}=0.01 or 0.00;
		σ_{lp}=0.0; σ_{ec}=1.0
		sucrose: σ_{sp}=0.03 or 0.01;
		σ_{lp}=0.0; σ_{ec}=1.0
		albumin: σ_{sp}=0.89 or 0.44;
		σ_{lp}=0.07; σ_{ec}=1.0
			dimensionless

ψ	Matrix osmotic pressure coefficients	ψ_1=13.5; ψ_2=2320; ψ_3=1.54x10^5 [9]	variable
Ω	Vascular resistance (arterial, capillary, venous, total)	Ω_a=2.43; Ω_c=0.12; Ω_v=0.22; Ω_{tot}=2.77 [10]	mmHg min mL^{-1}

(1) Aukland and Reed (1993)
(2) Bassingthwaighte (1987)
(3) Batra and Rakusan (1990)
(4) Curry (1984)
(5) Gonzalez and Bassingthwaighte (1990)
(6) Laine and Grainger (1985)
(7) Levick (1994)
(8) Tanford (1961)
(9) Shaw (1971)
(10) Sipkema et al. (1998)
(11) Weast (1979)

References

Adamson RH. Permeability of frog mesenteric capillaries after partial pronase digestion of the endothelial glycocalyx. *J Physiol (Lond)* 428: 1-13, 1990.

Adamson RH and Clough G. Plasma proteins modify the endothelial cell glycocalyx of frog mesenteric microvessels. *J Physiol (Lond)* 445: 473-486, 1992.

Adamson RH and Michel CC. Pathways through the intercellular clefts of frog mesenteric capillaries. *J Physiol (Lond)* 466: 303-327, 1993.

Agre P, Preston GM, Smith BL, Jung JS, Raina S, Moon C, Guggino WB, and Nielsen S. Aquaporin CHIP: the archetypal molecular water channel. *Am J Physiol Ren Physiol* 265: F463-F476, 1993.

Alvarez OA and Yudilevich DL. Heart capillary permeability to lipid-insoluble molecules. *J Physiol (Lond)* 202: 45-58, 1969.

Anderson JL and Quinn JA. Restricted transport in small pores. A model for steric exclusion and hindered particle motion. *Biophys J* 14: 130-150, 1974.

Arturson G, Areskog NH, Arfors K, Grotte G, and Malmberg P. The transport of macromolecules across the blood-lymph barrier. Influence of capillary pressure on macromolecular composition of lymph. *Bibl Anat* 10: 228-233, 1969.

Asthagiri AR and Lauffenburger DA. Bioengineering models of cell signaling. *Annu Rev Biomed Eng* 2: 31-53, 2000.

Aukland K and Reed RK. Interstitial-lymphatic mechanisms in the control of extracellular fluid volume. *Physiol Rev* 73: 1-78, 1993.

Avolio AP, Spaan JA, and Laird JD. Plasma protein concentration and control of coronary vascular resistance in isolated rat heart. *Am J Physiol Heart Circ Physiol* 238: H471-H480, 1980.

Bains W. Genes to proteins in context. *Trend Biotech* 16: 2-4, 1998.

Bassingthwaighte JB, Knopp TJ, and Hazelrig JB. A concurrent flow model for capillary-tissue exchanges. In: *Capillary Permeability: The Transfer of Molecules and Ions from Capillary Blood and Tissue,* edited by Crone C and Lassen NA. Copenhagen: Munksgaard, 1970, p. 60-80.

Bassingthwaighte JB. A concurrent flow model for extraction during transcapillary passage. *Circ Res* 35: 483-503, 1974.

Bassingthwaighte JB, Yipintsoi T, and Grabowski EF. Myocardial capillary permeability: Hydrophilic solutes penetrate 100 Å clefts. *Bibl Anat* 13: 24-27, 1975.

Bassingthwaighte JB, Yipintsoi T, and Knopp TJ. Effect of transcapillary osmotic fluxes on tracer flux in rabbit hearts (abstract). *Microvasc Res* 17: S85, 1979.

Bassingthwaighte JB and Goresky CA. Modeling in the analysis of solute and water exchange in the microvasculature. In: *Handbook of Physiology, Section 2, The Cardiovascular System,* edited by Renkin EM and Michel CC. Bethesda: American Physiological Society, 1984, p. 549-626.

Bassingthwaighte JB. The Myocardial Cell. In: *Cardiology: Fundamentals and Practice,* edited by Brandenberg RO, Fuster V, Giuliani ER and Mcgoon DC. Chicago: Year Book Medical Publishers, 1987, p. 113-149.

Bassingthwaighte JB, Wang CY, and Chan IS. Blood-tissue exchange via transport and transformation by capillary endothelial cells. *Circ Res* 65: 997-1020, 1989.

Bassingthwaighte JB, King RB, and Roger SA. Fractal nature of regional myocardial blood flow heterogeneity. *Circ Res* 65: 578-590, 1989.

Bassingthwaighte JB. Toward modeling the human physionome. *Adv Exp Med Biol* 382: 331-339, 1995.

Bassingthwaighte JB. Design and strategy for the Cardionome Project. *Adv Exp Med Biol* 430: 325-339, 1997.

Bassingthwaighte JB, Li Z, and Qian H. Blood flows and metabolic components of the cardiome. *Prog Biophys Mol Biol* 69: 445-461, 1998.

Batra S and Rakusan K. Morphometric Analysis of Capillary Nets in Rat Myocardium. *Adv Exp Med Biol* 277: 261-270, 1990.

Baxter LT and Jain RK. Transport of fluid and macromolecules in tumors. I. Role of interstitial pressure and convection. *Microvasc Res* 37: 77-104, 1989.

Bean CP. The physics of porous membranes--neutral pores. In: *Membranes: Macroscopic Systems and Models,* edited by Einsenman G. New York: Dekker, 1972, p. 1-54.

Beard DA and Bassingthwaighte JB. Advection and diffusion of substances in biological tissues with complex vascular networks. *Ann Biomed Eng* 28: 253-268, 2000.

Bloom G and Johnson JA. A model for osmotically induced weight transient in the isolated rabbit heart. *Microvasc Res* 22: 64-79, 1981.

Brooks HL, Regan JW, and Yool AJ. Inhibition of aquaporin-1 water permeability by tetraethylammonium: involvement of the loop E pore region. *Mol Pharmacol* 57: 1021-1026, 2000.

Bundgaard M. The three-dimensional organization of tight junctions in a capillary endothelium revealed by serial-section electron microscopy. *J Ultrastruct Res* 88: 1-17, 1984.

Carter EP, Olveczky BP, Matthay MA, and Verkman AS. High microvascular endothelial water permeability in mouse lung measured by a pleural surface fluorescence method. *Biophys J* 74: 2121-2128, 1998.

Chambers R and Zwiefach BW. Intercellular cement and capillary permeability. *Physiol Rev* 27: 436-463, 1947.

Chilian WM, Layne SM, and Nellis SH. Microvascular pressure profiles in the left and right coronary circulations. In: *Coronary Circulation: Basic Mechanisms and Clinical Relevance,* edited by Kajiya F, Klassen GA, Spaan JAE and Hoffman JIE. Tokyo: Springer-Verlag, 1990.

Chinard FP, Vosburgh GJ, and Enns T. Transcapillary exchange of water and of other substances in certain organs of the dog. *Am J Physiol* 183: 221-234, 1955.

Crone C. The permeability of capillaries in various organs as determined by the use of the 'indicator diffusion' method. *Acta Physiol Scand* 58: 292-305, 1963.

Crone C and Levitt DG. Capillary Permeability to Small Solutes. In: *Handbook of Physiology, Section 2, The Cardiovascular System,* edited by Renkin EM and Michel CC. Bethesda: American Physiological Society, 1984.

Csete ME and Doyle JC. Reverse engineering of biological complexity. *Science* 295: 1664-1669, 2002.

Curry FE. A hydrodynamic description of the osmotic reflection coefficient with application to the pore theory of transcapillary exchange. *Microvasc Res* 8: 236-252, 1974.

Curry FE, Mason JC, and Michel CC. Osmotic reflexion coefficients of capillary walls to low molecular weight hydrophilic solutes measured in single perfused capillaries of the frog mesentery. *J Physiol (Lond)* 261: 319-336, 1976.

Curry FE and Michel CC. A fiber matrix model of capillary permeability. *Microvasc Res* 20: 96-99, 1980.

Curry FE. Mechanics and Thermodynamics of Transcapillary Exchange. In: *Handbook of Physiology, Section 2, The Cardiovascular System,* edited by Renkin EM and Michel CC. Bethesda: American Physiological Society, 1984, p. 309-374.

Diana JN, Long SC, and Yao H. Effect of histamine on equivalent pore radius in capillaries of isolated dog hindlimb. *Microvasc Res* 4: 413-437, 1972.

Diana JN and Laughlin MH. Effect of ischemia on capillary pressure and equivalent pore radius in capillaries of the isolated dog hind limb. *Circ Res* 35: 77-101, 1974.

Effros RM. Osmotic extraction of hypotonic fluid from the lungs. *J Clin Invest* 54: 935-947, 1974.

Effros RM, Darin C, Jacobs ER, Rogers RA, Krenz G, and Schneeberger EE. Water transport and the distribution of aquaporin-1 in pulmonary air spaces. *J Appl Physiol* 83: 1002-1016, 1997.

Eisenberg SR and Grodzinsky AJ. Electrokinetic micromodel of extracellular matrix and other polyelectrolyte networks. *Physiochem Hydrodyn* 10: 517-539, 1988.

Farmer RE and Macey RI. Perturbation of red cell volume: constancy of membrane transport parameters for certain slow penetrants. *Biochin Biophys Acta* 255: 502-516, 1972.

Feola M and Glick G. Cardiac lymph flow and composition in acute myocardial ischemia in dogs. *Am J Physiol* 229: 44-48, 1975.

Ferry JD. Statistical evaluation of sieve constants in ultrafiltration. *J Gen Physiol* 20: 95-104, 1936.

Fibich G, Lanir Y, Liron N, and Abovsky M. Modeling of coronary capillary flow. *Adv Exp Med Biol* 346: 137-150, 1993.

Fu B, Curry FR, Adamson RH, and Weinbaum S. A model for interpreting the tracer labeling of interendothelial clefts. *Ann Biomed Eng* 25: 375-397, 1997.

Fu BM, Weinbaum S, Tsay RY, and Curry FE. A junction-orifice-fiber entrance layer model for capillary permeability: application to frog mesenteric capillaries. *J Biomech Eng* 116: 502-513, 1994.

Giebisch GH, Granger JP, Greenleaf JE, Lydic RB, Mitchell RH, Nadel ER, Schultz SG, Wood JD, and Knobil E. What's past is prologue. *Physiologist* 33: 161-180, 1990.

Gonzalez F and Bassingthwaighte JB. Heterogeneities in regional volumes of distribution and flows in rabbit heart. *Am J Physiol Heart Circ Physiol* 258: H1012-H1024, 1990.

Grabowski EF and Bassingthwaighte JB. An osmotic weight transient model for estimation of capillary transport parameters in myocardium. In: *Microcirculation Vol. 2 (Proc. First World Cong. for the Microcirculation)*, edited by Grayson J and Zingg W. New York: Plenum, 1976, p. 29-50.

Granger DN and Taylor AE. Permeability of intestinal capillaries to endogenous macromolecules. *Am J Physiol* 238: H457-H464, 1980.

Grotte G. Passage of dextran molecules across the blood-lymph barrier. *Acta Chir Scand Suppl* 84: 1-84, 1956.

Guller G, Yipintsoi T, Orvis AL, and Bassingthwaighte JB. Myocardial sodium extraction at varied coronary flows in the dog. *Circ Res* 37: 359-378, 1975.

Guyton AC and Lindsey AW. Effect of elevated left atrial pressure and decreased plasma protein concentration on the development of pulmonary edema. *Circ Res* 7: 649-657, 1959.

Hairer E, Nørsett SP, and Wanner G. *Solving Ordinary Differential Equations I. Nonstiff Problems.* New York: Springer-Verlag, 1993.

Hairer E and Wanner G. *Solving Ordinary Differential Equations II. Stiff and Differential Algebraic Problems.* New York: Springer-Verlag, 1996.

Harris TR, Gervin CA, Burks D, and Custer P. Effects of coronary flow reduction on capillary-myocardial exchange in dogs. *Am J Physiol* 234: H679-H689, 1978.

Hasegawa H, Lian SC, Finkbeiner WE, and Verkman AS. Extrarenal tissue distribution of CHIP28 water channels by in situ hybridization and antibody staining. *Am J Physiol Cell Physiol* 266: C893-903, 1994.

Haunsø S, Paaske WP, Sejrsen P, and Amtorp O. Capillary permeability in canine myocardium as determined by bolus injection, residue detection. *Acta Physiol Scand* 108: 389-397, 1980.

Hedley W and Nelson M. *CellML Specification Recommendation.* URL: http:// www.cellml.org/public/specification/cellml_specification.html, 2001.

Hucka M, Finney A, Sauro H, and Bolouri H. *Systems Biology Markup Language (SBML) Level 1: Structures and Facilities for Basic Model Definitions.* URL: http:// www.cds.caltech.edu/erato/sbml/docs/papers/sbml-level-1/sbml-level-1.pdf, 2001.

Hu X and Weinbaum S. A new view of Starling's hypothesis at the microstructural level. *Microvasc Res* 58: 281-304, 1999.

Huxley VH and Meyer DJ Jr. Capillary permeability: an albumin component attenuates active changes in Lp. *Am J Physiol Heart Circ Physiol* 259: H1357-H1364, 1990.

Huxley VH and Curry FE. Differential actions of albumin and plasma on capillary solute permeability. *Am J Physiol Heart Circ Physiol* 260: H1645-H1654, 1991.

Huxley VH and Williams DA. Role of a glycocalyx on coronary arteriole permeability to proteins: evidence from enzyme treatments. *Am J Physiol Heart Circ Physiol* 278: H1177-1185, 2000.

Irvine LA, Jafri MS, and Winslow RL. Cardiac sodium channel Markov model with temperature dependence and recovery from inactivation. *Biophys J* 76: 1868-1885, 1999.

Ishizaka H and Kuo L. Endothelial ATP-sensitive potassium channels mediate coronary microvascular dilation to hyperosmolarity. *Am J Physiol Heart Circ Physiol* 273: H104-H112, 1997.

Johnson JA and Bloom G. Permeability and Reflection Coefficients from osmotic transients-extravascular factors. *Microvasc Res* 22: 80-92, 1981.

Kassab GS, Berkley J, and Fung YC. Analysis of pig's coronary arterial blood flow with detailed anatomical data. *Ann Biomed Eng* 25: 204-217, 1997.

Katchalsky A and Curran PF. *Nonequilibrium Thermodynamics in Biophysics.* Cambridge, MA: Harvard University Press, 1965.

Kedem O and Katchalsky A. Thermodynamic analysis of the permeability of biological membranes to non-electrolytes. *Biochin Biophys Acta*: 229-246, 1958.

Keys A. The apparent permeability of the capillary membrane in man. *Trans Farady Soc* 33: 930-939, 1937.

King RB, Raymond GM, and Bassingthwaighte JB. Modeling blood flow heterogeneity. *Ann Biomed Eng* 24: 352-372, 1996.

Kinsky MP, Guha SC, Button BM, and Kramer GC. The role of interstitial starling forces in the pathogenesis of burn edema. *J Burn Care Rehabil* 19: 1-9, 1998.

Kitano H. Systems biology: a brief overview. *Science* 295: 1662-1664, 2002.

Krogh AE, Landis EM, and Turner AH. The movement of fluid through the human capillary wall in relation to venous pressure and to the colloid osmotic pressure of the blood. *J Clin Invest* 11: 63-95, 1937.

Kuikka J, Levin M, and Bassingthwaighte JB. Multiple tracer dilution estimates of D- and 2-deoxy-D-glucose uptake by the heart. *Am J Physiol Heart Circ Physiol* 250: H29-H42, 1986.

Laine GA and Granger HJ. Microvascular, interstitial, and lymphatic interactions in normal heart. *Am J Physiol Heart Circ Physiol* 249: H834-H842, 1985.

Landis EM. Micro-injection studies of capillary permeability. II. The relation between capillary pressure and the rate at which fluid passes through the walls of single capillaries. *Am J Physiol* 82: 528-542, 1927.

Laughlin MH and Diana JN. Myocardial transcapillary exchange in the hypertrophied heart of the dog. *Am J Physiol Heart Circ Physiol* 229: H838-H846, 1975.

Levick JR. An analysis of the interaction between interstitial plasma protein, interstitial flow, and fenestral filtration and its application to synovium. *Microvasc Res* 47: 90-125, 1994.

Lewellen PC. *Hydrodynamic analysis of microporous mass transport.* Madison: University of Wisconsin, 1982.

Lightfoot EN, Bassingthwaighte JB, and Grabowski EF. Hydrodynamic models for diffusion in microporous membranes. *Ann Biomed Eng* 4: 78-90, 1976.

Macauley J, Wang H, and Goodman N. A model system for studying the integration of molecular biology databases. *Bioinformatics* 14: 575-582, 1998.

Mann GE. Alterations of myocardial capillary permeability by albumin in the isolated, perfused rabbit heart. *J Physiol (Lond)* 319: 311-323, 1981.

Ma T, Yang B, and Verkman AS. Cloning of a novel water and urea-permeable aquaporin from mouse expressed strongly in colon, placenta, liver, and heart. *Biochem Biophys Res Commun* 240: 324-328, 1997.

Mayerson HS, Wolfram CG, H.H. Shirley J, and Wasserman K. Regional differences in capillary permeability. *Am J Physiol* 198: 155-160, 1960.

Mellor JC, Yanai I, Clodfelter KH, Mintseris J, and Delisi C. Predictome: a database of putative functional links between proteins. *Nucleic Acids Res* 30: 306-309, 2002.

Michel CC. Fluid Movements through Capillary Walls. In: *Handbook of Physiology, Section 2, The Cardiovascular System,* edited by Renkin EM and Michel CC. Bethesda: American Physiological Society, 1984.

Michel CC and Curry FE. Microvascular permeability. *Physiol Rev* 79: 703-761, 1999.

Noble D. Modeling the Heart--from Genes to Cells to the Whole Organ. *Science* 295: 1678-1682, 2002.

Pallone TL, Kishore BK, Nielsen S, Agre P, and Knepper MA. Evidence that aquaporin-1 mediates NaCl-induced water flux across descending vasa recta. *Am J Physiol Ren Physiol* 272: F587-596, 1997.

Pappenheimer JR and Soto-Rivera A. Effective Osmotic Pressure of the Plasma Proteins and other Quantities Associated with the Capillary Circulation in the Hindlimbs of Cats and Dogs. *Am J Physiol* 152: 471-491, 1948.

Pappenheimer JR, Renkin EM, and Borrero LM. Filtration, diffusion, and molecular sieving through peripheral capillary membranes. *Am J Physiol* 167: 13-46, 1951.

Pappenheimer JR. Passage of Molecules through Capillary Walls. *Physiol Rev* 33: 387-423, 1953.

Pappenheimer JR. Osmotic reflection coefficients in capillary membranes. In: *Capillary Permeability,* edited by Crone C and Lawsen NA. New York: Academic, 1969, p. 278-286.

Patlak CS, Goldstein DA, and Hoffman JF. The Flow of Solute and Solvent Across a Two-Membrane System. *J Theor Biol* 5: 426-442, 1963.

Perl W, Chowdhury P, and Chinard FP. Reflection coefficients of dog lung endothelium to small hydrophilic solutes. *Am J Physiol* 228: 797-809, 1975.

Pilati CF. Macromolecular transport in canine coronary microvasculature. *Am J Physiol Heart Circ Physiol* 258: H748-H753, 1990.

Plante GE, Alfred J, and Chakir M. The blood vessel, linchpin of diabetic lesions. *Metabolism* 48: 406-409, 1999.

Popel AS, Greene AS, Ellis CG, Ley KF, Skalak TC, and Tonellato PJ. The Microcirculation Physiome Project. *Ann Biomed Eng* 26: 911-913, 1998.

Renkin EM. Capillary permeability to lipid-soluble molecules. *Am J Physiol* 168: 538-545, 1952.

Renkin EM. Filtration, diffusion, and molecular sieving through porous cellulose membrane. *J Gen Physiol* 38: 225-248, 1954.

Renkin EM. Transport of Large Molecules across Capillary Walls. *Physiologist* 7: 13-28, 1964.

Renkin EM, Watson PD, Sloop CH, Joyner WM, and Curry FE. Transport pathways for fluid and large molecules in microvascular endothelium of the dog's paw. *Microvasc Res* 14: 205-214, 1977.

Rippe B and Haraldsson B. Capillary permeability in rat hindquarters as determined by estimations of capillary reflection coefficients. *Acta Physiol Scand* 127: 289-303, 1986.

Rippe B and Haraldsson B. Transport of macromolecules across microvascular walls: the two-pore theory. *Physiol Rev* 74: 163-219, 1994.

Rose CP and Goresky CA. Vasomoter control of capillary transit time heterogeneity on the canine coronary circulation. *Circ Res* 39: 541-544, 1976.

Rubboli A, Sobotka PA, and Euler DE. Effect of acute edema on left ventricular function and coronary vascular resistance in the isolated rat heart. *Am J Physiol Heart Circ Physiol* 267: H1054-H1061, 1994.

Schmid-Schöbein GW and Ikomi F. Biomechanics of Lymph Transport. In: *Biological Flows,* edited by Jaffrin MY and Caro C. New York: Plenum Press, 1995, p. 353-360.

Schnitzer JE and Oh P. Aquaporin-1 in plasma membrane and caveolae provides mercury-sensitive water channels across lung endothelium. *Am J Physiol Heart Circ Physiol* 270: H416-H422, 1996.

Schwartz LM, Bukowski TR, Revkin JH, and Bassingthwaighte JB. Cardiac endothelial transport and metabolism of adenosine and inosine. *Am J Physiol Heart Circ Physiol* 277: H1241-H1251, 1999.

Schwartz LM, Bukowski TR, Ploger JD, and Bassingthwaighte JB. Endothelial adenosine transporter characterization in perfused guinea pig hearts. *Am J Physiol Heart Circ Physiol* 279: H1502-H1511, 2000.

Seale KT and Harris TR. A three-compartment model of osmotic water exchange in the lung microvasculature. *Ann Biomed Eng* 28: 1019-1027, 2000.

Shaw M. Exclusion in hyaluronate gels. *Biophys J* 17: 47-55, 1977.

Shepherd GM, Mirsky JS, Healy MD, Singer MS, Skoufos E, Hines MS, Nadkarni PM, and Miller PL. The Human Brain Project: neuroinformatics tools for integrating, searching and modeling multidisciplinary neuroscience data. *Trend Neurosci* 21: 460-468, 1998.

Simionescu M and Simionescu N. Ultrastructure of the Microvascular Wall: Functional Correlations. In: *Handbook of Physiology, Section 2, The Cardiovascular System,* edited by Renkin EM and Michel CC. Bethesda: American Physiological Society, 1984, p. 41-101.

Sipkema P, Takkenberg JJM, Zeeuwe PEM, and Westerhof N. Left coronary pressure-flow relations of the beating and arrested rabbit heart at different ventricular volumes. *Cardiovasc Res* 40: 88-95, 1998.

Starling EH. On the adsorbtion of fluid from interstitial spaces. *J Physiol (Lond)* 19: 667-677, 1896.

Staverman AJ. The theory of measurement of osmotic pressure. *Rec Trav Chim* 70: 344, 1951.

Stewart RH, Geissler HJ, Allen SJ, and Laine GA. Protein washdown as a defense mechanism against myocardial edema. *Am J Physiol Heart Circ Physiol* 279: H1864-1868, 2000.

Subramaniam S. The Biology Workbench--a seamless database and analysis environment for the biologist. *Proteins* 32: 1-2, 1998.

Suleymanian MA and Baumgarten CM. Osmotic gradient-induced water permeation across the sarcolemma of rabbit ventricular myocytes. *J Gen Physiol* 107: 503-514, 1996.

Sunnergren KP. The effects of hyaluronidase on interstitial hydration, plasma protein exclusion, and microvascular permeability in the isolated perfused rat heart. *Circ Res* 30: 286-297, 1985.

Tanford C. *Physical Chemistry of Macromolecules.* New York: John Wiley & Sons Inc., 1961.

Taylor AE and Granger DN. Exchange of macromolecules across the microcirculation. In: *Handbook of Physiology, Section 2, The Cardiovascular System,* edited by Renkin EM and Michel CC. Bethesda: American Physiological Society, 1984, p. 467-520.

Taylor DG, Bert JL, and Bowen BD. A mathematical model of interstitial transport. I. Theory. *Microvasc Res* 39: 253-278, 1990.

Ter Kuile BH and Westerhoff HV. Transcriptome meets metabolome: hierarchical and metabolic regulation of the glycolytic pathway. *FEBS Lett* 500: 169-171, 2001.

Ullal SR, Kluge TH, Kerth WJ, and Gerbode F. Flow and composition of cardiac lymph in dogs. *Ann Surg* 175: 299-304, 1972.

Vargas F and Johnson JA. An estimate of reflection coefficients for rabbit heart capillaries. *J Gen Physiol* 47: 667-677, 1964.

Vargas F and Johnson JA. Permeability of rabbit heart capillaries to nonelectrolytes. *Am J Physiol* 213: 87-93, 1967.

Vargas FF and Blackshear GL. Transcapillary osmotic flows in the in vitro perfused heart. *Am J Physiol Heart Circ Physiol* 240: H448-H456, 1981.

Vargas FF and Blackshear GL. Secondary driving forces affecting transcapillary osmotic flows in perfused heart. *Am J Physiol Heart Circ Physiol* 240: H457-H464, 1981.

Verkman AS, Van Hoek AN, Ma T, Frigeri A, Skach WR, Mitra A, Tamarappoo BK, and Farinas J. Water transport across mammalian cell membranes. *Am J Physiol Cell Physiol* 270: C12-30, 1996.

Verkman AS. Role of aquaporin water channels in kidney and lung. *Am J Med Sci* 316: 310-320, 1998.

Vlahakes GJ, Giamber SR, Rothaus KO, and Powell WJ Jr. Hyperosmotic mannitol and collateral blood flow to ischemic myocardium. *J Surg Res* 47: 438-446, 1989.

Wangensteen D, Bachofen H, and Weibel ER. Lung tissue volume changes induced by hypertonic NaCl: morphometric evaluation. *J Appl Physiol* 51: 1443-1450, 1981.

Watson PD. Permeability of cat skeletal muscle capillaries to small solutes. *Am J Physiol Heart Circ Physiol* 268: H184-H193, 1995.

Weast RC (Editor). *CRC Handbook of Chemistry and Physics.* Boca Raton, FL: CRC Press, Inc., 1979.

Weinbaum S, Tsay R, and Curry FE. A three-dimensional junction-pore-matrix model for capillary permeability. *Microvasc Res* 44: 85-111, 1992.

Wiederhielm CA. Transcapillary and interstitial transport phenomena in the mesentery. *Fed Proc* 25: 1789-1798, 1966.

Winslow RL, Scollan DF, Holmes A, Yung CK, Zhang J, and Jafri MS. Electrophysiological modeling of cardiac ventricular function: from cell to organ. *Annu Rev Biomed Eng* 2: 119-155, 2000.

Wolf MB and Watson PD. Measurement of osmotic reflection coefficient for small molecules in cat hindlimbs. *Am J Physiol Heart Circ Physiol* 256: H282-H290, 1989.

Wolf MB. Identification of microvascular transport pathways in skeletal muscle. *Am J Physiol Heart Circ Physiol* 267: H383-H399, 1994.

Wolf MB. Determination of the magnitude of the water-exclusive pathway in cat skeletal muscle microvasculature. *Microcirculation* 3: 59-73, 1996.

Ziegler WH and Goresky CA. Transcapillary exchange in the working left ventricle of the dog. *Circ Res* 29: 181-207, 1971.

Appendix A: Derivation of Kedem and Katchalsky Equations

For a more detailed review of irreversible thermodynamics and its application to coupled solute-solvent transmembrane transport see the texts by Katchalsky and Curran (1965) or Curry (1984). The theory of irreversible thermodynamics postulates that each flux, J_i, in a system tending to restore equilibrium is a function of each of the driving forces, X_i, present. If the forces are sufficiently small, this relationship is linear, and in general the system can be described by a system of equations:

$$\begin{aligned} J_1 &= L_{1,1}X_1 + L_{1,2}X_x + \ldots + L_{1,N}X_N \\ J_2 &= L_{2,1}X_1 + L_{2,2}X_x + \ldots + L_{2,N}X_N \\ J_N &= L_{N,1}X_1 + L_{N,2}X_x + \ldots + L_{N,N}X_N \end{aligned} \tag{A.1}$$

The L terms are called the phenomenological coefficients. The values of these parameters are constrained by Onsager's law of reciprocity which requires that:

$$L_{i,j} = L_{j,i} \tag{A.2}$$

For a system composed of two compartments separated by a thin membrane and containing a solution of a single solute, there are two possible flows: that of bulk solution, J_v, and the exchange flux, J_D, of solute relative to that of the bulk flow. The two driving forces for these fluxes are the hydrostatic pressure difference between the compartments, Δp, and the concentration difference of the solute, ΔC. Thus, the system can be described by the set of equations:

$$\begin{aligned} J_v &= L_p\Delta p + L_{pD}RT\Delta C \\ J_D &= L_{Dp}\Delta p + L_D RT\Delta C \\ L_{Dp} &= L_{pD} \end{aligned} \tag{A.3}$$

In non-selective membranes the volume and exchange flows are independent of each other, and L_{pD}=L_{Dp}=0. J_v is only dependent on the pressure gradient Δp, and J_D is only dependent on the concentration difference ΔC. The second law of thermodynamics requires that the coefficients L_p and L_D be positive. Physically, this means that passive flow of solution or solute occurs from regions of high to low hydrostatic pressure or solute concentration.

In more restrictive membranes, $L_{pD} \neq 0$ and coupling exists between the fluxes. While L_{pD} can be either positive or negative, it is restricted by the condition:

$$L_p L_D - L_{pD}^2 > 0 \tag{A.4}$$

which ensures that the total entropy production is always positive. The volume flux induced by a concentration gradient is known as osmotic flow, while a pressure difference that causes a difference in the relative velocity in the solute-solvent flow is known as ultrafiltration.

In practical use, it is convenient to rewrite these equations in terms of a different set of phenomenological coefficients and fluxes. The concept of the reflection coefficient, σ, was introduced by Staverman (1951), with the definition:

$$\sigma = -\frac{L_{pD}}{L_p} \tag{A.5}$$

Thus, the condition $\sigma = 0$ applies to a non-selective membrane, while $\sigma = 1$ applies to an impermeable membrane. This definition of the solute reflection coefficient is known as the osmotic reflection coefficient, and is sometimes denoted σ_d. The corresponding definition using L_{Dp} instead of L_{pD} is knows as the solvent drag reflection coefficient, denoted σ_f. If Onsager reciprocity condition holds, these two definitions are equivalent, so we will simply refer to the reflection coefficient as σ. Substitution into the expression for volume flow gives:

$$J_v = L_p(\Delta p - \sigma RT\Delta C) \tag{A.6}$$

Since the total solute flow, J_s, is more experimentally assessable than the exchange flux, J_D, it is convenient to write the solute flux in terms of J_s. These two fluxes are related by

$$J_s = (J_v + J_D)\overline{C}. \tag{A.7}$$

where J_s is the solute flux across a membrane per unit surface area. The average concentration, $\overline{C}$ in the membrane is given by

$$\overline{C} = \frac{C_1 - C_2}{\ln(C_1/C_2)}. \tag{A.8}$$

The solute mobility, ω, is defined by

$$\omega = \frac{L_pL_D - L_{pD}^2}{L_p}\overline{C} = (L_D - L_p\sigma^2)\overline{C} \ . \tag{A.9}$$

Therefore, the solute flux equations can be re-written in terms of J_s, σ, and ω:

$$J_s = \overline{C}L_p(1-\sigma)\Delta p + (\omega - \overline{C}L_p(1-\sigma)\sigma)RT\Delta C \tag{A.10}$$

or

$$J_s = \omega RT\Delta C + (1-\sigma)J_v\overline{C}. \tag{A.11}$$

The solute permeability coefficient is

$$P = RT\omega, \tag{A.12}$$

so the Kedem and Katchalsky solute flux equation is

$$J_s = P\Delta C + (1-\sigma)J_V\bar{C} \qquad \text{(A.13)}$$

Appendix B: Derivation of Patlak Equations

The starting point for this derivation is the Kedem and Katchalsky (1958) expressions for volume flux (J_v) and solute flux (J_s) across a thin membrane separating two well-stirred compartments, and it follows the development in Patlak (1963). If fluxes are defined as positive from the compartment 1 to compartment 2, these expressions are:

$$J_v = L_p[(p_1 - p_2) - \sigma RT(C_1 - C_2)] \tag{B.1}$$

$$J_s = \omega RT(C_1 - C_2) + (1 - \sigma)\bar{C}J_v \tag{B.2}$$

These equations are applicable to thin membranes, or to any infinitesimally thin lamina of a thick membrane. In the later case, we can write the Kedem and Katchalsky equations in a differential form:

$$J_v = L_p'\left(\frac{dp}{dx} - \sigma RT\frac{dC}{dx}\right) \tag{B.3}$$

$$J_s = \omega' RT\frac{dC}{dx} + (1 - \sigma)CJ_v \tag{B.4}$$

with $L'_p = L_p/\delta$ and $\omega' = \omega/\delta$ where δ is the thickness of the membrane. $\bar{C}$ is now replaced by the actual concentration, C, at each infinitely thin slice of the membrane. The solute flux equation for a thick membrane can be found by integrating these equations across the membrane from side 1 to side 2. The volume flux equation can be expressed as:

$$J_v dx = L_p' dp - L_p'\sigma RT dC \tag{B.5}$$

and integrated across the membrane:

$$J_v\int_0^{\delta} dx = L'_p\int_{p_1}^{p_2} dp - L'_p\sigma RT\int_{C_1}^{C_2} dC \tag{B.6}$$

$$J_v\delta = -L_p'[(p_1 - p_2) - \sigma RT(C_1 - C_2)] \tag{B.7}$$

or

$$J_v = L_p[\Delta p - \sigma RT\Delta C]. \tag{B.8}$$

The he volume flux equation for a thick membrane is of the same form as the solute flux equation for an infinitesimally thin membrane.

For the solute flux equation:

$$\frac{dx}{\omega' RT} = \frac{dC}{J_s - (1-\sigma)J_v C} \tag{B.9}$$

Integrating across the membrane:

$$\int_0^{\delta}\frac{dx}{\omega' RT} = \int_{C_1}^{C_2}\frac{dC}{J_s - (1-\sigma)J_v C} \tag{B.10}$$

$$\frac{\delta}{\omega' RT} = \frac{-1}{J_v(1-\sigma)}\ln(J_s - J_v(1-\sigma)C)\Big|_{C_1}^{C_2} \tag{B.11}$$

With the substitution for permeability:

$$P = \frac{\omega' RT}{\delta} \tag{B.12}$$

and the definition of the Péclet number as the ratio of convective to diffusive fluxes:

$$Pe = \frac{J_v(1-\sigma)}{P} \tag{B.13}$$

this expression can be evaluated as:

$$Pe = \ln(J_s - J_v(1-\sigma)C_2) - \ln(J_s - J_v(1-\sigma)C_1) \tag{B.14}$$

$$Pe = \ln\left(\frac{J_s - J_v(1-\sigma)C_2}{J_s - J_v(1-\sigma)C_1}\right) \tag{B.15}$$

$$e^{Pe} = \frac{J_s - J_v(1-\sigma)C_2}{J_s - J_v(1-\sigma)C_1} \tag{B.16}$$

$$e^{Pe}(J_s - J_v(1-\sigma)C_1) = J_s - J_v(1-\sigma)C_2 \tag{B.17}$$

$$J_s(e^{Pe} - 1) = J_v(1-\sigma)(C_1 e^{Pe} - C_2) \tag{B.18}$$

With the substitution

$$C_2 = C_1 - (C_1 - C_2) = C_1 - \Delta C \tag{B.19}$$

this becomes:

$$J_s = \frac{J_v(1-\sigma)}{(e^{Pe} - 1)}(C_1 e^{Pe} - C_1 + \Delta C) \tag{B.20}$$

$$J_s = \frac{J_v(1-\sigma)}{(e^{Pe} - 1)}[\Delta C + C_1(e^{Pe} - 1)] \tag{B.21}$$

$$J_s = \frac{J_v(1-\sigma)}{(e^{Pe}-1)}\Delta C + J_v(1-\sigma)C_l \qquad \text{(B.22)}$$

Substituting from Equation B.13 gives

$$J_s = P\Delta C\left(\frac{Pe}{e^{Pe}-1}\right) + J_v(1-\sigma)C_l\,. \qquad \text{(B.23)}$$

This is the Patlak non-linear solute flux equation. The two terms on the right-hand side of the equation are the diffusive and solvent-drag components to the total solute flux at the left hand membrane-solution interface, respectively. It is crucial to note that this is the only location where this interpretation can be made. At other locations in the membrane the concentration profile will be different, and the ratio of convective to diffusive transport will consequently change. However, if the total amount of solute in the membrane is presumed to be constant, conservation of mass requires that the total flux be the same throughout the membrane.

Compared to the linear flux equation, the nonlinear equation has a term modifying P involving the Péclet number, that accounts for the alteration of the steady-state concentration profile in the membrane in the presence of convection. With increasing convection in the same direction as diffusion, the concentration profile at the entrance to the membrane becomes flatter. Thus diffusion is reduced in the presence of convection not because the molecular mobility of the solutes changes, but because the concentration gradient driving net diffusive flux is reduced. Also, the solvent-drag component of transport is defined more precisely at the left hand interface by the concentration of solute in solution on the left hand side of the membrane, as compared to the averaging across the whole membrane inherent in the Kedem and Katchalsky solute flux equation. As noted by Curry (1984), these two errors have opposite signs, so the sum of terms in the Kedem and Katchalsky is a better approximation to the total transmembrane solute flux than either term is to a specific component of that flux.

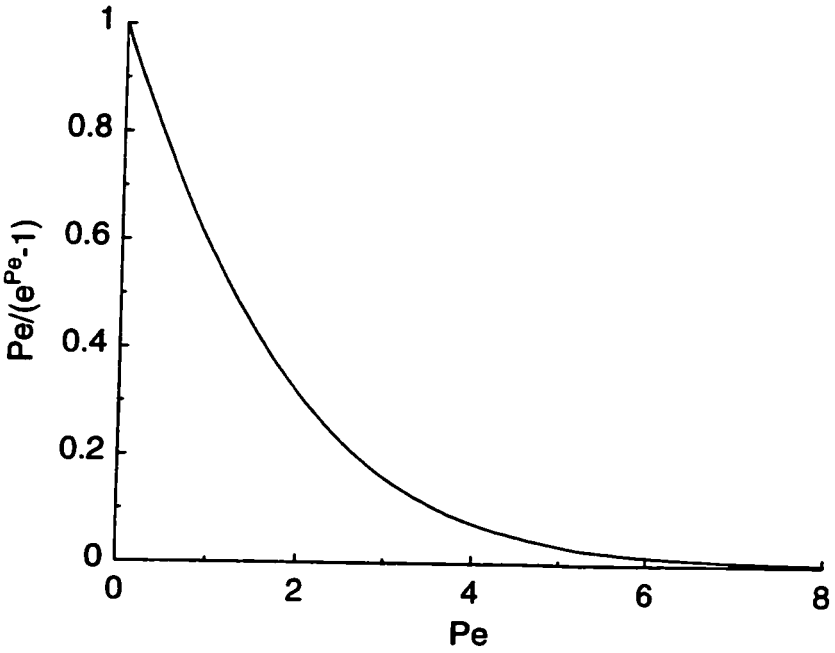

Figure B-1 Fractional reduction in diffusion rate with increasing convection as predicted by Eqn. B.23.

Appendix C: Pore Theory

Pappenheimer et al. (1951) first applied Poiseuille's law of flow through tubes to predict capillary hydraulic conductivity assuming that the capillary wall was penetrated by a population of uniform cylindrical pores. Obviously, as a pore approaches molecular dimensions the relevance of this macro-scale law will diminish. On very small scales, structuring of water molecules could raise the effective viscosity, and the no-slip boundary condition may not be appropriate. Experimentally, a close correspondence is observed between pore radius determined by bulk flow and by other experimental methods down to at least 6 nm, while for smaller pores the experimental evidence is inconsistent. The other experimental methods used to determine the pore radius include the pressure necessary to balance the surface tension of fluid in the pores, the radius of the largest solute that penetrates the membrane, and pore dimensions determined by electron microscopy. These issues are more fully explained by Curry (1984), who also gives the derivation of hydraulic conductivity for flow through a population of uniform cylindrical pores

$$L_p = \frac{A_p r_p^2}{8\eta S \Delta x} \tag{C.1}$$

where A_p is the total pore area available for water transport, S is the total capillary surface area, η is the solvent viscosity, r_p is the pore radius, and Δx is the pore length. L_p can be interpreted in terms of two characteristic pore parameters, r_p, and the lumped parameter $A_p/S\Delta x$, the fractional pore area per path length. For a long, parallel-walled slit the equivalent equation is

$$L_p = \frac{A_p w^2}{12\eta S \Delta x} \tag{C.2}$$

where the pore radius is replaced by the slit width, w. Pappenheimer et al. (1951) used these equations to predict uniform cylindrical pore radii of 3 nm or slits of 3.7 nm width based on experimental measurements of hydraulic conductivity in the hindlimbs of cats.

The process of molecular diffusion is slowed when the mobility of the solute decreases, so a solute in a pore would be expected to have a diffusion coefficient, D_p, less than that in free solution. This restriction becomes more significant as the solute's molecular dimensions approaches those of the pore. Additionally, solute may be sterically restricted from entering some regions of the pore (Figure C-1). A solute's partition coefficient, ϕ, is the ratio of the area available to the solute to the total pore surface area.

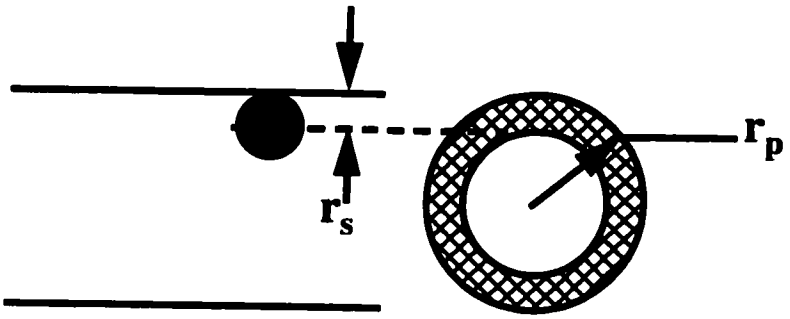

Figure C-1 A spherical solute in a cylindrical pore is restricted from occupying any position with in r_s of the cylinder wall, thus it is excluded from the cross-hatched region of the pore's area.

The permeability coefficient is related to these parameters by (Curry, 1984)

$$P = \frac{A_p}{S\Delta x}\phi D_p \tag{C.3}$$

A spherical solute is restricted from occupying any position in a pore within one solute radius from the pore's edge, so for a cylindrical pore the solute partition coefficient can be calculated from the expression

$$\phi = \frac{\pi(r_p - r_s)^2}{\pi r_p^2} = (1-\alpha)^2 \tag{C.4}$$

with α the ratio of solute radius to pore radius.

The ratio of D_p to D_{fr} is defined by the hydrodynamic function $F(\alpha)$, so

$$P = \frac{A_p}{S\Delta x}(1-\alpha)^2 F(\alpha) D_{fr} \tag{C.5}$$

The function $F(\alpha)$ (shown in Figure C-2) can be approximated by several functions given by Curry (1984). For a parallel walled slit, the equivalent equation is (Curry, 1974):

$$P = \frac{A_p D_{fr}}{S\Delta x}(1-\alpha) F_{slit}(\alpha) \tag{C.6}$$

In this context, α becomes the ratio of solute radius to one-half the slit width, with

$$F_{slit}(\alpha) = 1.0 - 1.004\alpha + 0.418\alpha^3 + 2.10\alpha^4 - 0.1696\alpha^5 \tag{C.7}$$

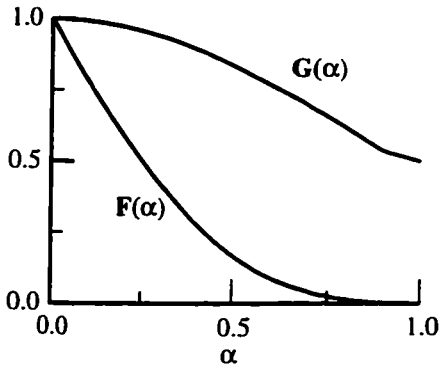

Figure C-2 Hydrodynamic functions F(α) and G(α)

From the Kedem and Katchalsky or the Patlak solute flux equations (Section 1.3.3), the reflection coefficient can be defined as

$$\sigma = 1 - \left(\frac{J_s}{J_v C}\right)_{\Delta C = 0} \tag{C.8}$$

Since J_s is the solute flow, and $J_v C$ is the total amount of solute carried up to the entrance of the pore, their ratio is the solute partition coefficient, and this equation can also be written

$$\sigma = 1 - \phi = 1 - (1 - \alpha)^2 \tag{C.9}$$

This derivation of the solute reflection coefficient ignores the frictional interaction of solute and water within the pore, and the nonuniform solvent velocity within the pore. Early estimates of solute reflection coefficients were made by Ferry (1936), who accounted for the presence of a parabolic velocity profile while calculating a filtration coefficient for an artificial membrane by assuming that the solute in the pore moved at the local water velocity. Renkin (1954) predicted the reflection coefficient for a spherical solute traveling through a cylindrical pore and attempted to include the effects of the frictional interaction with the water. Bean (1972), first realized that the term $F(\alpha)$ should be replaced by the hydrodynamic function $G(\alpha)$, which accounts for the difference between solute velocity and water velocity (Figure C-2). Additionally, Bean accounted for the effects of pressure on the solute velocity and derived the expression

$$\sigma = 1 - (2(1 - \alpha)^2 - (1 - \alpha)^4)G(\alpha) - \frac{16}{9}\alpha^2(1 - \alpha)^2 F(\alpha) \tag{C.10}$$

Other investigators using more complex theories have developed numerically similar or identical expressions including Anderson and Quinn (1974), Curry (1974), Lightfoot et al. (1976), and Lewellen (1982). The equivalent expression derived for a rectangular slit is (Curry, 1974)

$$\sigma = \frac{2\alpha^2}{3}(1 - \alpha)F_{slit}(\alpha) + \frac{3}{2}(1 - \alpha)\left(\frac{2}{3} + \frac{2}{3}\alpha - \frac{7}{12}\alpha^2\right) \tag{C.11}$$

Appendix D: Computer Code

The following FORTRAN code is archived in the NSR source code . The model consists of subroutines which run under the XSIM interface.

```
FILE osmotic.f
**********************************************************************
SUBROUTINE OSMOT
c
c Axial distributed model of water and solute exchange.
c
c.....
c
c From:  National Simulation Resource
c       Center for Bioengineering
c       University of Washington
c       Box 357962
c       Seattle, WA 98195-7962
c
c       Dr. J. B. Bassingthwaighte, Director
c
c.....
c
c Copyright (C) 1998, 1999 by National Simulation Resource, Univ of WA.
c All Rights Reserved.
c
c Software may be copied so long as this copyright notice is included.
c This software was developed with support from NIH grant RR-01243.
c Please cite this grant in any publication for which this software
c is used and send one reprint to the address given above.
c
c.....
c
c SYNOPSIS
c     SUBROUTINE   osmotic(p)
c     ENTRY        simic(p)
c     ENTRY        simlop(p)
c     ENTRY        simend(p)
c
c     REAL p(*)
c
c.....
c
c DESCRIPTION
c
c Osmotic is a three region, multiple solute model for water and
c solute exchange in an organ.  The model includes transcapillary
c exchanges of solutes and water, lymph drainage from the interstitial
c space, pressure profiles in the vascular tree and tissue, parenchymal
```

```
c cell permeability to water, and the mechanical compliance of the
c tissue. The model is axially distributed, and solved using either the
c DOPRI5 (a 4-5th order Runga Kuta method) or RADAU (a stiff solver)
c ODE solvers. Transcapillary exchange occurs through inter-endothelial
c clefts and a transcellular pathway.
c
c.....
c
c P ARRAY USAGE
c
c ODE SOLVER PARAMETERS:
c
c Basic ODE control parameters:
c p-array Name    Description                          Typical Values
c p( 1) rlevel   INPUT: The level of user's control        1,2
c             the ODE solvers.
c             1=BASIC
c             2=ADVANCED
c p( 2) rmode    INPUT: Integrator selector:              1,2
c             1=DOPRI5
c             2=RADAU
c p( 4) rtol     INPUT: Relative error tolerance for the     0.00001
c             local error test.
c p( 5) atol     INPUT: Absolute error tolerance for the     0.000001
c             local error test.
c p( 7) rfcn     OUTPUT: # of function evaluations
c p( 8) rstep    OUTPUT: # of computed steps
c p( 9) raccpt   OUTPUT: # of accepted steps
c p( 10) rrejct   OUTPUT: # of rejected steps
c
c Advanced ODE solver parameters: (not currently implemented)
c p-array Name    Description                          Typical Values
c p( 11) nJeval   OUTPUT: # of Jacobian evaluations
c p( 12) nLUdecom OUTPUT: # of LU decompositions
c p( 13) nforback OUTPUT: # of forward-backward substitutions
c p( 21) tolcontr switch for tolerance control
c p( 22) inidelh  initial step size (H) guess
c p( 25) rounduni rounding unit
c p( 26) saftyfct safety factor in step prediction
c p( 27) lob_schg lower bound for step size selection
c p( 28) upb_schg upper bound for step size selection
c p( 29) betafct  beta factor for stabilized step size control
c p( 30) maxStapS maximal step size
c p( 31) maxNstep maximal # of allowed steps
c p( 32) sw_coef  switch for the schoce of the RK coefficients
c p( 33) errunit  unit # for printing error messages
c p( 34) sw_stfts switch for testing stiffness
c p( 36) sw_jac   switch for internal/external Jacobian computations
c p( 37) sw_lobaJ switch for lower bandwidth of Jacobian
c p( 38) sw_upbaJ switch for upper bandwidth of Jacobian
c p( 40) J_recomp decides whether the Jacobian should be recomputed
```

```
c p( 41) min_Nosc minimum for no step size change
c p( 42) max_Nosc maximum for no step size change
c p( 43)- bounds for contractivity factor
c p( 46)
c p( 51) sw_J2H  decides whether to transform Jacobian to Hessenberg form
c p( 52) maxNnew  maximan # of Newton iterations in implic calculation
c p( 53) sw_extco switch for extrapolated collocation
c p( 54)- dimIn1v- dimension of hte index i (i=1,2,3) variables
c p( 56) dimIn3v
c p( 57) sw_sss  switch for the step size strategy
c p( 58) valm1   value of m1
c p( 59) valm2   value of m2
c p( 60)- min_,max_,ini_NS   minimum, maximum, and initial values for
c p( 62)                number of stages Ns
c
c General Parametersc
c
c p-array Name   Description                          Typical Values
c p( 91) Raout   OUTPUT: vascular resistance of artery       450
c                ((mmHg min)/mL)
c p( 92) Rvout   OUTPUT: vascular resistance of veins  150
c                ((mmHg min)/mL)
c p( 93) xrsel   INPUT: Arterial fractional hydraulic        0-1
c                resistence, if pfs=5
c p( 94) Rtub   INPUT: cannula hydraulic resistence (mmHg min/mL)
c p( 95) Pmout   OUTPUT: Measured upstream pressure (mmHg)
c p( 97) extyp   INPUT: Type of solute exchange equation      1,2,3
c            1 = Kedem & Katchalsky equation with
c              arithmetic mean
c            2 = Kedem and Katchalsky equation with
c              logrithmic mean
c            3 = Patlack equation
c p( 99) sread   INPUT: Switch for reading from initialization  1,2
c  file
c  1 = Normal run
c  2 = Read from file 'osmotic.in'
c p(100) swrite  INPUT: Switch for saving run into          1,2
c                initialization file.
c            1 = Don't write file
c            2 = Write file
c p(101) temp    INPUT: Temperature (K)                 300
c p(102) denw    INPUT: Water density (g/cm^3)           1.0
c p(108) denp    INPUT: Protein density (g/cm^3)  1.38
c p(103) rLpm    INPUT: Hydraulic conductivity though cell     1e-9
c            membrane (mL/(s mmHg cm^2))
c p(104) segN    INPUT: Number of axial segments            1 to MAXSEG
c p(105) rmu     OUTPUT: Solute viscosity (g/cm s)          0.008
c p(106) rLk     INPUT: Lymph conductance (mL/(min g mmHg))    0.01
c p(107) pL  INPUT: pressure in lymphatics (mmHg)        0
c
c Mechanical Elastance parameters:
```

```
c p(111)- Ei(i)   INPUT: Elastance parameters for ISF (mmHg)
c p(113)          P = Pi + E(1)*(delV/Vi) + E(2)*(delV/Vi)^2 + E(3)*delV/Vi)^3
c p(114)- Em(i)   INPUT: Elastance parameters for ISF (mmHg)
c p(116)          P = Pi + E(1)*(delV/Vi) + E(2)*(delV/Vi)^2 + E(3)*delV/Vi)^3
c p(117)  pisfin  INPUT: Initial interstitial pressure (mmHg)   10
c p(118)  pmyoin  INPUT: Initial cellular pressure (mmHg)       10
c
c Pressure-flow parameters:
c p(119)  pfs     INPUT: Switch for pressure or flow as input   1-5
c                 function
c              1 = Flow is the computed output
c              2 = Pressure is the computed output
c              3 = Arterial resistance is computed
c              4 = Venous resistance is computed
c              5 = Both arterial and venous resistence computed
c
c p(120)  ptype   INPUT: Selection for pressure-flow model      1
c              1 = Three constant resistances model
c p(121)  omegaV  INPUT: Venous hydraulic resistance           150
c                 ((mmHg min)/mL)
c p(122)  omegaA  INPUT: Arteriole hydraulic resistance        450
c                 ((mmHg min)/mL))
c p(123)  omegaC  OUTPUT: Capillary hydraulic resistance       100
c                 ((mmHg min)/mL)
c p(124)  Pm      INPUT: arterial input pressure (mmHg)        50
c p(125)  Pv      INPUT: venout outflow pressure (mmHg)        0
c p(126)  Paout   OUTPUT: arterial pressure (mmHg)             50
c p(127)  Pvout   OUTPUT: venous pressure (mmHg)               0
c p(134)  pcapin  OUTPUT: pressure at capillary input (mmHg)   30
c p(135)  pcapou  OUTPUT: pressure at capillary output (mmHg)  15
c p(136)  Fout    OUTPUT: Capillary outflow (mL/s/g)           0.029
c p(138)  flowin  INPUT: Capillary inlet flow (mL/min)         0.03
c p(139)  flowo   OUTPUT: Capillary inlet flow (mL/min)        0.03
c
c Time parameters:
c p(130)  xstime  INPUT: current time (s)                      0-100
c p(131)  xsdt    INPUT: XSIM time increment (s)               1
c p(132)  time    OUTPUT: model time (s)                       0-100
c p(133)  dt      OUTPUT: model time increment(s)              0.1
c
c Pore parameters:
c p(140)- Permin(i,j) INPUT: Permeability for ith solute through  1E-5
c p(154)              jth pathway if specified directly.  (cm/s)
c p(155)- sigin(i,j)  INPUT: Reflection coefficient for ith
c p(169)              solute through jth pathway          0-1
c p(170)- rLpin(j)    INPUT: Hydraulic conductivity through jth   1E-7
c p(172)              pathway, cm/s/mmHg/g
c p(173)- rLpout(j)   OUTPUT: Hydraulic conductivity through jth  1E-7
c p(175)              pathway, cm/s/mmHg/g
c p(176)  rLptot      OUTPUT: Total Hydraulic conductivity        1E-7
c p(177)- rp(j)       INPUT: Pore radius through jth pathway, A.  50
```

```
c p(179)
c p(180)- ApSdx(j)   INPUT: Relative pore area per unit       4
c p(182)              path length, cm^-1
c p(183)- slitw(j)   INPUT: Slit width, A.                   50
c p(185)
c p(186)- AsSdx(j)   INPUT: Relative pore area per unit path  5
c p(188)              length for a slit, cm^-1
c p(189)- rf(j)      INPUT: Fiber radius, fiber matrix, A. for 5
c p(191)              jth pathway
c p(192)- eps(j)     INPUT: Fiber matrix fractional void for   0.98
c p(194)              jth pathway
c p(195)- pathch(j)  INPUT: Model selection for jth pathway    1-6
c p(197)              1 = Not Used
c                     2 = Pure Phenomenological
c                     3 = Renkin Cylinder
c                     4 = Bean Cylinder
c                     5 = Curry Slit
c                     6 = Curry Fiber Matrix
c p(198)- ASdx(j)    INPUT: Fractional pore area per unit path
c p(200)              lenght, cm
c State variables:
c p-array Name   Description
c p(201)- Vcap(i)  OUTPUT: Capillary volume of segment i (mL/g)
c p(220)
c p(221)- Visf(i)  OUTPUT: ISF water volume of segment i (mL/g)
c p(240)
c p(241)- Vmyo(i)  OUTPUT: parenchymal cell water volume of segment i (mL/g)
c p(260)
c p(261)- pcap(i)  OUTPUT: pressure in capillary segment i (mmHg)
c p(280)
c p(281)- pisf(i)  OUTPUT: pressure in ISF segment i (mmHg)
c p(300)
c p(301)- pmyo(i)  OUTPUT: pressure in parenchymal segment i (mmHg)
c p(320)
c p(321)- rncap(i,j) OUTPUT: moles of solute i in capillary segment j
c p(420)          i ranges from 1 to MAXSOL, j from 1 to MAXSEG
c p(421)- rnisf(i,j) OUTPUT: moles of solute i in ISF segment j
c p(520)          i ranges from 1 to MAXSOL, j from 1 to MAXSEG
c
c Additional variables, (combinations of State variables):
c p(521)- Ccap(i,j) OUTPUT: activity of solute i in cap segment j
c p(620)          i ranges from 1 to MAXSOL, j from 1 to MAXSEG
c p(621)- Cisf(i,j) OUTPUT: activity of solute i in ISF segment j
c p(720)          i ranges from 1 to MAXSOL, j from 1 to MAXSEG
c p(75n)  Cout[n]  OUTPUT: Outflow activity of species n (mM)   0-300
c p(76n)  Cin[n]   OUTPUT: Inflow activity of species n  (mM)   0-300
c p(771)  Vcapt    OUTPUT: Total capillary volume (mL/unit cell)
c p(772)  Vwisf    OUTPUT: Total ISF water volume (mL/unit cell)
c p(773)  Vwmyo    OUTPUT: Total cell water volume (mL/unit cell)
c p(774)  Vcapg    OUTPUT: Total capillary volume (mL/g tissue)
c p(775)  Visfg    OUTPUT: Total interstitial volume (mL/g tissue)
```

```
c p(776) Vmyog    OUTPUT: Total cell volume (mL/g tissue)
c p(777) Vlvg     OUTPUT: Total large vessel volume (mL/g tissue)
c p(778) Vsisf    OUTPUT: Total interstitial solid volume (mL/unit cell)
c p(779) Vsmyo    OUTPUT: Total myocardial solid volume (mL/unit cell)
c p(780) velin    OUTPUT: Inflow velocity (cm/s)
c p(78n) vel(n)   OUTPUT: Velocity at capillary segment n (cm/s)
c
c
c Geometrical Parameters
c Inputs:
c
c p-array Name      Description                          Typical Values
c Input parameters used for Hex geometry:
c p(802) dic       INPUT: Inter capillary distance (um)      19
c p(803) Rcap      INPUT: Capillary radius (um)              2.5
c p(804) dmyo      INPUT: Inter myocyte distance (um)        1.9
c p(805) rlen      INPUT: Capillary length (um)              1000
c p(806) fVti      INPUT: Initial tissue fractional volume   0.9
c
c Output parameters for all geometry models:
c p(821) Dheart    OUTPUT: Heart density (g/ml)              1.06
c p(822) capD      OUTPUT: Number of caps per g              3000
c p(826) SAc       OUTPUT: Capillary surface area (cm^2/unit cell)
c p(827) SAm       OUTPUT: Myocyte surface area (cm^2/unit cell)
c p(828) SAcg      OUTPUT: Capillary surface area (cm^2/g)
c p(829) SAmg      OUTPUT: Cell surface area (cm^2/g)
c
c
c Solute Parameters
c
c INPUTS:
c
c p(87n) solact[N,1] 1st solute activity coefficient         1
c p(88n) solact[N,2] 2nd solute activity coefficient
c p(89n) solact[N,3] 3rd solute activity coefficient
c p(90n) soltyp[N]  Solute type, solutes 1-5                 1,2,3
c              1 = Test solute
c              2 = Resident solute
c              3 = Not used
c p(91n) solcap[N]  Solute initial capillary concentration for  0-300 mM
c              a resident solute.
c p(92n) solisf[N]  Solute initial ISF concentration for     0-300 mM
c              a resident solute.
c p(93n) solrad[N]  Solute radius 5 A.
c p(94n) Dfr[N]     Solute free diffusion coefficient  1E-5
c p(95n) solVd[N]   Output: fractional volume of distrbution  0-1
c              for solute in ISF
c p(96n) solf[n]    Inflow test solute concentration, feed (mM) 50
c
c OUTPUTS:
c p(970)- permout(i,j) permeability of ith solute through jth   1E-5
```

```
c p(984)            path, cm/s
c p(985)- sigout(i,j)  reflection coefficient of ith solute      0-1
c p(999)            through jth path, dimensionless
c p(1000)- permt(i)   total permeability of ith solute, cm/s    1E-5
c p(1004)
c p(1005)- sigt(i)    total reflection coefficient of ith solute 0-1
c p(1009)
c
c Interstitial matrix parameters
c p(1050) Ccoli      INPUT: Collagin fiber concentration (g/mL) 0.05
c p(1051) Cgagi      INPUT: GAG concentration (g/mL)          0.003
c p(1052) actisf(1)  INPUT: 1st ISF matrix virial coefficient  1
c p(1053) actisf(2)  INPUT: 2nd ISF matrix virial coefficient  0
c p(1054) actisf(3)  INPUT: 3rd ISF matrix virial coefficient  0
c p(1055) rfgag      INPUT: GAG fiber radius (A)               4
c p(1056) wfisf      OUTPUT: isf water fraction
c p(1057) rfcol      INPUT: collagen fiber radius (A)          40
c p(1058) Ccol       OUTPUT: collen fiber concentration (g/mL) 0.05
c p(1059) Cgag       OUTPUT: GAG fiber concentration (g/mL)    0.003
c
c Cellular matrix parameteres:
c p(1060) Csolm      OUTPUT: cell solid phase concentration (g/mL)
c p(1061) Csolmi     INPUT: cell solid phase concentration (g/ml).25
c p(1062) actmyo(1)  INPUT: 1st cell matrix virial coefficient  1
c p(1063) actmyo(2)  INPUT: 2nd cell matrix virial coefficient  0
c p(1064) actmyo(3)  INPUT: 3rd cell matrix virial coefficient  0
c p(1065) rfmyo      INPUT: Myocyte matrix fiber radius
c p(1066) wfmyo      OUTPUT: Myocyte water fraction
c
c
c Global Behavior Outputs:
c p(1099) Wti        INPUT: Initial weight of organ (g)
c p(1100) Wt         OUTPUT: Weight of organ (g)
c p(1110) rJwmt      OUTPUT: Total water flux across parenchymal
c                    cell membrane (ml/min/g)
c p(111j) rJwm(j)    OUTPUT: Water flux across parenchymal cell
c                    membrane at segment j
c                    (ml/min/g)
c p(120j) rJwc1(j)   OUTPUT: Water flux across capillary wall
c                    through 1st path at jth segment
c                    (ml/min/g)
c p(122j) rJwc2(j)   OUTPUT: Water flux across capillary wall
c                    through 2nd path at jth segment
c                    (ml/min/g)
c p(124j) rJwc3(j)   OUTPUT: Water flux across capillary wall
c                    through 3rd path at jth segment
c                    (ml/min/g)
c p(1260) rJwct      OUTPUT: Total water flux across capillary wall
c                    (ml/min/g)
c p(1261) rJwc1t     OUTPUT: Total water flux across capillary
c                    wall through 1st pathway (ml/min/g)
```

```
c p(1262) rJwc2t    OUTPUT: Total water flux across capillary
c                  wall through 2nd pathway (ml/min/g)
c p(1263) rJwc3t    OUTPUT: Total water flux across capillary
c                  wall through 3rd pathway (ml/min/g)
c
c Osmolarities:
c p(172n)  osmolc(j) OUTPUT: osmolarity of capillary at segment j (mmHg)
c p(174n)  osmoli(j) OUTPUT: osmolarity of ISF at segment j (mmHg)
c p(176n)  osmolm(j) OUTPUT: osmolarity of cells at segment j (mmHg)
c
c Pore locations along capillary length
c p(199n) ploc(j) INPUT: location of path with axial position in capillary
c       1 = even distribution
c       2 = lumped in last axial segmentc
c
c.....
c
c LIMITATIONS/WARNINGS
c
c    NONE
c
c.....
c
c DIAGNOSTICS
c
c    NONE
c
c.....
c
c REFERENCES
c
c
c.....
c
c SUBROUTINES/FUNCTIONS CALLED
c    vslideModified Lagrangian sliding fluid algorythm with linear
c          interpolation.
c    viscos  Viscosisity calculation.
c    reng2p  Renkin model for pore geometry to phenomenological
c          coefficient calculation.
c    beag2p  Bean model for pore geometry to phenomenological
c          coefficient calculation.
c    dopri5  4/5th order Runga-Kutta ODE solver
c    radau   stiff ODE solver
c    dlogm   logrythmic mean
c    presf   pressure-flow module
c    hexti   tissue initialization routine
c    hext    tissue update module
c
c.....
c
```

```
c AUTHOR
c
c     National Simulation Resource
c     Center for Bioengineering
c     University of Washington
c     Box 357962
c     Seattle, WA 98195-7962
c
c.....
c
c FOR ASSISTANCE
c     Questions regarding this software can be sent by electronic
c     mail to: librarian@nsr.bioeng.washington.edu
c
c.....
c
c HISTORY
c
c Written: 01/14/99 - M.R. Kellen
c
c----------DECLARATION SECTION
c
c I.  Declaration section
c
c     A. Declare the p-array common block and osmotic parameters.
c
      REAL*4    p(32000)
      COMMON    p
c
c     B. Declare local parameters.
c
      REAL R,PI,CONV
      INTEGER MAXSEG,MAXSOL,NRPAR,ND,LJ,LM,LE,NRDENS,LW,LIWORK,LIPAR
      INTEGER MAXPATH
      PARAMETER (R=0.0623656,PI=3.141593,CONV=1333.22)
      PARAMETER (MAXSEG=20, MAXSOL=5, MAXPATH=3)
      PARAMETER (NRPAR=MAXSOL*MAXPATH*2+4*MAXSOL+26+MAXPATH)
      PARAMETER (ND=2*MAXSOL+3)
      PARAMETER (LJ=ND,LM=0,LE=ND,NRDENS=0)
      PARAMETER (LW=ND*(LJ+LM+7*LE+24)+20+8*ND+5*NRDENS+20)
      PARAMETER (LIWORK=NRDENS+20+5*ND+20)
      PARAMETER (LIPAR=2)
      EXTERNAL DFDYDT, VSLIDE, RADAU, DUMJAC, DUMOUT, DUMMAS, DOPRI5,
     +       RENG2P, BEAG2P, SLTG2P, DLOGM, SCFMSG, PRESF,
     +       HEXTi, HEXT, F7OPEN, F7CLOS, SCWMSG
      DOUBLE PRECISION  rpar(NRPAR),y(ND),dtime,drtol,datol,work(LW),
     + xend,h, DLOGM
c
      REAL rlevel, rmode, rtol, atol, rfcn, rstep, raccpt, rrejct
      REAL Vcap(MAXSEG), Visf(MAXSEG), Vmyo(MAXSEG)
      REAL pcap(MAXSEG), pisf(MAXSEG), pmyo(MAXSEG)
```

```
      REAL rncap(MAXSOL,MAXSEG), rnisf(MAXSOL,MAXSEG), Cout(MAXSOL)
      REAL Ccap(MAXSOL,MAXSEG), Cisf(MAXSOL,MAXSEG), Cin(MAXSOL)
      REAL soltyp(MAXSOL), solcap(MAXSOL), solisf(MAXSOL)
      REAL solrad(MAXSOL), Dfr(MAXSOL), permin(MAXSOL,MAXPATH)
      REAL solact(10,3), solVd(MAXSOL), sigin(MAXSOL, MAXPATH)
      REAL actmyo(3), actisf(3), rfgag, rfmyo, denp
      REAL extyp, sread, swrite, temp, denw, rLpm, segN, rmu, pL, Csolmi
      REAL Ei(3), Em(3), ptype, omegaV, Cmyos, Cgagi, Ccoli, Csolm
      REAL omegaA, flowin, rlk, omegaC, pcapin, xstime,time, dt
      REAL xsdt, pcapou, Fout, pathch(MAXPATH), rp(MAXPATH)
      REAL ApSdx(MAXPATH), slitw(MAXPATH), AsSdx(MAXPATH), rLptot
      REAL ASdx(MAXPATH), ploc(MAXPATH)
      REAL rf(MAXPATH), eps(MAXPATH), rLpin(MAXPATH), rLpout(MAXPATH)
      REAL Vcapt, Visft, Vmyot, SAcs, SAms, vseg, visfsi, wfisf, wfmyo
      REAL dic, Rcap, dmyo, rlen, Sac, SAm, vmyosi, SAcg, SAmg
      REAL Dheart, capD, Vcapg, Visfg, Vmyog, Vlvg, rfcol
      REAL Wt, wfmP, wfL, sfsd(MAXSOL), sfcd(MAXSOL)
      REAL sfl(MAXSOL), solfin(MAXSOL), solfou(MAXSOL), rnmyo, rnisfm
      REAL osmolc(MAXSEG), osmoli(MAXSEG), osmolm(MAXSEG), flowo
      REAL permout(MAXSOL, MAXPATH), sigout(MAXSOL, MAXPATH), velin
      REAL permt(MAXSOL), sigt(MAXSOL), vel(MAXSEG+1), dum, Raout, Rvout
      REAL Wti, pisfin, pmyoin, Omyom(MAXSEG), Rvci, Rvcm, pfs, Pmin
      REAL tempR, Pm, Pv, Paout, Pvout, tempP(MAXSOL), temps(MAXSOL)
      REAL als(MAXSOL), xrsel, dtiss, WtLV, Ncaps, fVti, Vsisf, Vsmyo
      REAL Vout, Oisfm(MAXSEG), solf(MAXSOL), Adx(MAXPATH)
      REAL wk1(0:MAXSEG),wk2(MAXSEG+1),wk3(MAXSOL,0:MAXSEG), wkg(4)
      REAL wk4(MAXSOL,MAXSEG+1), VISCOS, sft(MAXSOL)
      REAL cmean(MAXSOL), sdrag(MAXSOL), dif(MAXSOL), deln(MAXSOL)
      REAL Ocap(MAXSOL,MAXSEG), Oisf(MAXSOL,MAXSEG)
      REAL rJwm(MAXSEG), rJwmt, rJwc1(MAXSEG), rJwc2(MAXSEG)
      REAL rJwc3(MAXSEG), rJwct, rJwc1t, rJwc2t, rJwc3t
      REAL summ(MAXSEG), sumc1(MAXSEG), sumc2(MAXSEG), sumc3(MAXSEG)
      INTEGER i,j,Nseg, ijac, mljac, mujac, imas, iout, itol
      INTEGER iwork(liwork), nfcn, nstep, naccpt, nrejct, nloop
      INTEGER ipar(lipar), idid, mlmas, mumas, lu
      LOGICAL eflag, lex
      CHARACTER*16 readfile, writefile
      SAVE
c
c     C. Rename P array variables
c
      EQUIVALENCE (p(1), rlevel), (p(2), rmode ), (p(4),  rtol ),
     +          (p(5), atol  ), (p(7), rfcn  ), (p(8),  rstep),
     +          (p(9), raccpt), (p(10),rrejct), (p(91), Raout),
     +          (p(92), Rvout), (p(93), xrsel), (p(99), sread),
     +          (p(94), Rtub ), (p(95), Pmout)
      EQUIVALENCE (p( 97), extyp), (p(100),swrite), (p(106), rlk  ),
     +          (p(101), temp ), (p(102), denw ), (p(103), rLpm ),
     +          (p(104), segN ), (p(105), rmu  ), (p(111), Ei   ),
     +          (p(114), Em   ), (p(117),pisfin), (p(118),pmyoin),
     +          (p(119), pfs  ), (p(107), pL   ), (p(108), denp )
```

```
      EQUIVALENCE (p(120), ptype), (p(121),omegaV), (p(122),omegaA),
     +        (p(123),omegaC), (p(124), Pm  ), (p(125), Pv  ),
     +        (p(126), Paout), (p(127), Pvout), (p(130),xstime),
     +        (p(131), xsdt ), (p(132), time ), (p(133), dt  ),
     +        (p(134),pcapin), (p(135),pcapou), (p(136), Fout ),
     +        (p(138),flowin), (p(139), flowo)
      EQUIVALENCE (p(140),permin), (p(155), sigin), (p(170), rLpin),
     +        (p(173),rLpout), (p(176),rLptot), (p(177), rp  ),
     +        (p(180), ApSdx), (p(183), slitw), (p(186), AsSdx),
     +        (p(189), rf  ), (p(192), eps ), (p(195),pathch),
     +        (p(198), ASdx )
      EQUIVALENCE (p(201), Vcap ), (p(221), Visf ), (p(241), Vmyo ),
     +        (p(261), pcap ), (p(281), pisf ), (p(301), pmyo ),
     +        (p(321), rncap), (p(421), rnisf), (p(521), Ccap ),
     +        (p(621), Cisf ), (p(751), Cout ), (p(761), Cin  ),
     +        (p(771), Vcapt), (p(772), Vwisf), (p(773), Vwmyo),
     +        (p(774), Vcapg), (p(775), Visfg), (p(776), Vmyog),
     +        (p(777), Vlvg ), (p(780), velin), (p(781), vel  ),
     +        (p(778), Vsisf), (p(779), Vsmyo)
      EQUIVALENCE
     +        (p(802), dic  ), (p(803), Rcap ), (p(804), dmyo ),
     +        (p(805), rlen ), (p(806), fVti ),
     +        (p(821),Dheart), (p(822), capD ),
     +        (p(826), SAc  ), (p(827), SAm  ), (p(828), SAcg ),
     +        (p(829), SAmg ), (p(871),solact)
      EQUIVALENCE (p(901), soltyp), (p(911), solcap), (p(921), solisf),
     +        (p(931), solrad), (p(941), Dfr  ), (p(951), solVd ),
     +        (p(961), solf  ), (p(970),permout), (p(985), sigout),
     +        (p(1000), permt), (p(1005), sigt ), (p(1057), rfcol),
     +        (p(1050), Ccoli), (p(1051), Cgagi), (p(1052),actisf),
     +        (p(1055), rfgag), (p(1060), Csolm), (p(1099), Wti  ),
     +        (p(1061),Csolmi), (p(1062),actmyo), (p(1065), rfmyo),
     +        (p(1058), Ccol ), (p(1059), Cgag ), (p(1056), wfisf),
     +        (p(1066), wfmyo), (p(1991), ploc )
      EQUIVALENCE (p(1100), Wt  ), (p(1101), wfmP ), (p(1102), wfL  ),
     +        (p(1110), rJwmt), (p(1111), rJwm ), (p(1201), rJwc1),
     +        (p(1221), rJwc2), (p(1241), rJwc3), (p(1270), rJwct),
     +        (p(1261),rJwc1t), (p(1262),rJwc2t), (p(1263),rJwc3t),
     +        (p(1721),osmolc), (p(1741),osmoli), (p(1761),osmolm)
      EQUIVALENCE (nfcn,  iwork(17)), (nstep, iwork(18)),
     +        (naccpt,iwork(19)), (nrejct,iwork(20))
c
c-----------------------------------------------INITIALIZATION SECTION
c
c This portion of the code in entered one time for each
c simulation run (i.e. each time option 1 is selected from the SIMCON
c main menu).
c
      ENTRY simic
c Initial conditions
c
```

```
c Model initial conditions:
c
      IF (swrite.EQ.2.0) THEN
        lu2=-1
        ier=0
        istat1 = iscgts(2, writefile)
        CALL F7OPEN(lu2,writefile(1:LNBLNK(writefile)),
     +            'NEW','WO','FOR',ier)
        IF (ier.EQ.-1) THEN
          CALL SCWMSG('File '//writefile(1:LNBLNK(writefile))//
     +              ' already exists.')
          CALL SCFMSG('Failed to save simulation.')
          RETURN
        ENDIF
      ENDIF
      IF (sread.NE.2.0) THEN
        nseg  = NINT(segN)
        tempR = R*temp
        rmu   = VISCOS(temp)
        CALL HEXTi(Rcap, dmyo, dic, rlen, Vcapt, Visft, Vmyot, Vwisf,
     +           Vwmyo, Vtiss, dtiss, SAc, SAm, Csolmi, Cgagi+Ccoli,
     +           denw, denp, wkg, eflag)
        IF (eflag) THEN
          CALL SCFMSG('Error in geometry initialization')
          RETURN
        ENDIF
        Vsisf = Visft-Vwisf
        Vsmyo = Vmyot-Vwmyo
c
c Solid component concentrations and weights
c
        Csolm  = Csolmi
        rWsolm = Csolm*Vmyot
        rWgag  = Cgagi*Visft
        rWcol  = Ccoli*Visft
        Ccol   = Ccoli
        Cgag   = Cgagi
c
c Tissue parameters
c
        Dheart = dtiss*fVti + denw*(1.0-fVti)
        capD   = fVti/(Vtiss*2.0)/Dheart
        Ncaps  = capD*Wti
        omegaC = (8*rmu*(rlen*1E-4)/PI/(Rcap*1E-4)**4)/Ncaps/CONV/60.0
        Wt = Wti
        Vlvg = (1.0-fVti)/Dheart
        WtLV = Wt*Vlvg*denw
        IF (flowin.LT.1) THEN
          CALL SCFMSG('Flow too low!!!')
          RETURN
        ENDIF
```

```
      dt = (Ncaps*Vcapt*2.0)/(flowin/60.0)/segN
      velin = rlen/10000.0/dt/segN
      DO 2 j=1,Nseg
        vel(j)=velin
    2 CONTINUE
c
c Fractional volumes of distribution for solutes
c
      DO 1 i=1,MAXSOL
        solVd(i) = VDIST(Cgag,Ccol,rfgag,rfcol,solrad(i))
    1 CONTINUE
c
c Setting concentration arrays. Cell concentration is set to osmotically
c balance ISF osmolarity. ISF osmolarity is determined from resident
c solutes plus contributions from GAG component of solid phase.
c
      DO 10 j=1,Nseg
        Oisfm(j) = (Cgagi*actisf(1) + Cgagi**2*actisf(2) +
     +            Cgagi**3*actisf(3))*tempR
        Omyom(j) = Oisfm(j)
        DO 15 i=1,MAXSOL
          IF (soltyp(i).EQ.(2.0)) THEN
            Ccap(i,j) = solcap(i)
            Ocap(i,j) = (Ccap(i,j)*solact(i,1) +
     +                  Ccap(i,j)**2*solact(i,2) +
     +                  Ccap(i,j)**3*solact(i,3))*tempR
            Cisf(i,j) = solisf(i)/solVd(i)
            Oisf(i,j) = (Cisf(i,j)*solact(i,1) +
     +                  Cisf(i,j)**2*solact(i,2) +
     +                  Cisf(i,j)**3*solact(i,3))*tempR
            Omyom(j)  = Omyom(j)+Oisf(i,j)
          ELSE
            Ccap(i,j) = 0.0
            Cisf(i,j) = 0.0
            Ocap(i,j) = 0.0
            Oisf(i,j) = 0.0
          ENDIF
   15   CONTINUE
   10 CONTINUE
      Cmyo = CUBIC(actmyo(3),actmyo(2),actmyo(1),Omyom(1))
c
c Setting pressure, mole, and volume arrays
c
      DO 20 j=1,Nseg
        pisf(j) = pisfin
        pmyo(j) = pmyoin
        Vcap(j) = Vcapt/segN
        Visf(j) = Vwisf/segN
        Vmyo(j) = Vwmyo/segN
        DO 25 i=1,MAXSOL
          rncap(i,j) = Ccap(i,j)*Vcap(j)
```

```
            rnisf(i,j) = Cisf(i,j)*Visf(j)*solVd(i)
 25       CONTINUE
 20     CONTINUE
        rnisfm  = Cgagi*Visf(1)
        rnmyo   = Cmyo*Vmyo(1)
        vseg    = Vcap(1)
        Visfsi  = Visf(1)
        Vmyosi  = Vmyo(1)
      ELSE
        lu=-1
        ier=0
        istat1 = iscgts(1, readfile)
        CALL F7OPEN(lu,readfile(1:LNBLNK(readfile)),
     +          'OLD','RO','FOR',ier)
        IF (ier.EQ.-1) THEN
          CALL SCWMSG('File '//readfile(1:LNBLNK(readfile))
     +            //' does not exist.')
          CALL SCFMSG('Error in run initialization')
          RETURN
        ENDIF
        READ (lu,901) Nseg, segN, tempR, WtLV, Vsisf, Vsmyo
 901    FORMAT (I4,5(E14.8,1X))
        READ (lu,905) vseg, Visfsi, Vmyosi, actisf(3), actmyo(3)
        READ (lu,905) actisf(1), actisf(2), rwgag, rwcol, rnisfm
 905    FORMAT (5(E14.8,1X))
        READ (lu,905) actmyo(1), actmyo(2), rnmyo, SAc, SAm
        READ (lu,905) velin, Ncaps, rmu, Dheart, Wt
 904    FORMAT (4(E14.8,1X))
        READ (lu,902) Fout, omegaC
        DO 30 j=1,NSEG
          READ (lu,904) Vcap(j),Visf(j),Vmyo(j),Omyom(j)
          READ (lu,904) pcap(j),pisf(j),pmyo(j), vel(j)
          DO 35 i=1,MAXSOL
            READ (lu,902) Ccap(i,j),Cisf(i,j)
 902          FORMAT (2(E14.8,1X))
            READ (lu,902) rncap(i,j),rnisf(i,j)
 35       CONTINUE
 30     CONTINUE
        DO 40 i=1,MAXSOL
          READ(lu,906) solcap(i)
 906      FORMAT (E14.5)
 40     CONTINUE
        DO 41 k=1,4
          READ(lu,904) wkg(1), wkg(2), wkg(3), wkg(4)
 41     CONTINUE
        CALL F7CLOS(lu,'KEE',ier)
        IF (ier.EQ.-1) THEN
          CALL SCFMSG('Error closing file '//
     +            readfile(1:LNBLNK(readfile))//'.')
          RETURN
        ENDIF
```

```
          Vcapt = 0.0
          Vwisf = 0.0
          Vwmyo = 0.0
          DO 50 j=1,Nseg
            Vcapt = Vcapt+Vcap(j)
            Vwisf = Vwisf+Visf(j)
            Vwmyo = Vwmyo+Vmyo(j)
   50     CONTINUE
          Visft = Vwisf + Vsisf
          Vmyot = Vwmyo + Vsmyo
          Cgag = rwgag/Visft
          Ccol = rwgag/Visft
          DO 55 i=1,MAXSOL
            solVd(i)=VDIST(Cgag,Ccol,rfgag,rfcol,solrad(i))
   55     CONTINUE
        ENDIF
        SAcs = SAc/segN
        SAms = SAm/segN
c
c Volumes and surface areas on a per gram tissue basis
        CapD  = Ncaps/Wt
        SAcg  = 2*SAc*capD
        SAmg  = 2*SAm*capD
        Visfg = 2*Vwisf*capD
        Vmyog = 2*Vwmyo*capD
        Vcapg = 2*Vcapt*capD
c
c ODE solver initialization:
c
      IF (rlevel.EQ.(1.0)) THEN
c compute the jacobian analytically
        ijac=0
c jacobian is a banded matrix (LOWER AND UPPER BAND-WIDTHS ARE 1, 2)
        mljac=ND
        mujac=ND
c differential equation is in implicit form
        imas=0
c output routine is not used during integration
        iout=0
c required tolerance
        drtol=DBLE(rtol)
        datol=DBLE(atol)
        itol=0
c set default values
        DO 60 i=1,20
          iwork(i)=0
          work(i)=0.D0
   60   CONTINUE
c initial step size
        h=DBLE(dt)*1.0D-1
      ENDIF
```

```
c
      DO 70 i=1,MAXSOL
        solfin(i) = 0.0
        solfou(i) = 0.0
        Cin(i) = Ccap(i,1)
        Cout(i) = Ccap(i,Nseg)
   70 CONTINUE
c
c Calculate total osmolarities
c
      DO 80 j=1,Nseg
        osmolc(j) = 0.0
        osmoli(j) = Oisfm(j)
        osmolm(j) = Omyom(j)
        DO 85 i=1,MAXSOL
          osmolc(j) = osmolc(j) + Ocap(i,j)
          osmoli(j) = osmoli(j) + Oisf(i,j)
   85   CONTINUE
   80 CONTINUE
c
c Calculation of phenomenological coefficients
c
      DO 100 j=1,MAXPATH
        IF (pathch(j).LT.(1.1)) THEN
          rLpout(j)=0.0
          DO 101 i=1,MAXSOL
            permout(i,j)=0.0
            sigout(i,j)=1.0
  101       CONTINUE
        ELSEIF (pathch(j).LT.(2.1)) THEN
          rLpout(j)=rLpin(j)
          DO 102 i=1,MAXSOL
            permout(i,j)=permin(i,j)
            sigout(i,j)=sigin(i,j)
  102       CONTINUE
        ELSEIF (pathch(j).LT.(3.1)) THEN
          DO 103 i=1,MAXSOL
            als(i) = solrad(i)/rp(j)
  103       CONTINUE
          CALL RENG2P (MAXSOL,rp(j),ApSdx(j),0.0,als,Dfr,rmu,
     +                 tempP,temps,dum,rLpout(j),eflag)
          IF (eflag) THEN
            CALL SCFMSG('Error detected in RENG2P.')
            RETURN
          ENDIF
          DO 104 i=1,MAXSOL
            permout(i,j) = tempP(i)
            sigout(i,j)  = temps(i)
  104       CONTINUE
        ELSEIF (pathch(j).LT.(4.1)) THEN
          DO 105 i=1,MAXSOL
```

```
            als(i) = solrad(i)/rp(j)
  105       CONTINUE
            CALL BEAG2P(MAXSOL,rp(j),ApSdx(j),0.0,als,Dfr,rmu,
     +              tempP,temps,dum,rLpout(j),eflag)
            IF (eflag) THEN
              CALL SCFMSG('Error detected in BEAG2P.')
              RETURN
            ENDIF
            DO 106 i=1,MAXSOL
              permout(i,j) = tempP(i)
              sigout(i,j)  = temps(i)
  106       CONTINUE
          ELSEIF (pathch(j).LT.(5.1)) THEN
            DO 107 i=1,MAXSOL
              als(i) = solrad(i)*2.0/rp(j)
  107       CONTINUE
            CALL SLTG2P (MAXSOL,slitw(j),AsSdx(j),0.0,als,Dfr,rmu,
     +              tempP,temps,dum,rLpout(j),eflag)
            IF (eflag) THEN
              CALL SCFMSG('Error detected in SLTG2P.')
              RETURN
            ENDIF
            DO 108 i=1,MAXSOL
              permout(i,j) = tempP(i)
              sigout(i,j)  = temps(i)
  108       CONTINUE
          ELSEIF (pathch(j).LT.(6.1)) THEN
c           CALL FMG2P(MAXSOL,rf(j),ASdx(j),eps(j),solrad,Dfr,rmu,
c    +              tempP,temps,rLpout(j),eflag)
            DO 109 i=1,MAXSOL
              permout(i,j)=tempP(i)
              sigout(i,j)=temps(i)
  109       CONTINUE
          ELSE
            CALL SCFMSG('Invalid path selection')
            RETURN
          ENDIF
  100 CONTINUE
      rLptot = 0.0
      DO 92 i=1,MAXSOL
        sigt(i)  = 0.0
        permt(i) = 0.0
   92 CONTINUE
      DO 90 j=1,MAXPATH
        rLptot = rLptot + rLpout(j)
        DO 91 i=1,MAXSOL
          sigt(i)  = sigt(i) + sigout(i,j)*rLpout(j)
          permt(i) = permt(i) + permout(i,j)
   91   CONTINUE
   90 CONTINUE
      DO 93 i=1,MAXSOL
```

```
          sigt(i) = sigt(i)/rLptot
   93 CONTINUE
c
c rpar array initialization (for passing through the ODE solvers)
      DO 110 i=1,MAXSOL
        DO 111 j=1,MAXPATH
          rpar((i-1)*MAXPATH+j) = DBLE(permout(i,j))
          rpar(MAXSOL*MAXPATH+(i-1)*MAXPATH+j) = DBLE(sigout(i,j))
  111   CONTINUE
        rpar(i+MAXSOL*MAXPATH*2) = DBLE(solVd(i))
        rpar(i+MAXSOL*MAXPATH*2+1*MAXSOL) = DBLE(solact(i,1))
        rpar(i+MAXSOL*MAXPATH*2+2*MAXSOL) = DBLE(solact(i,2))
        rpar(i+MAXSOL*MAXPATH*2+3*MAXSOL) = DBLE(solact(i,3))
  110 CONTINUE
      rpar(MAXSOL*MAXPATH*2+4*MAXSOL+1)  = DBLE(rLpm)
      rpar(MAXSOL*MAXPATH*2+4*MAXSOL+2)  = DBLE(tempR)
      rpar(MAXSOL*MAXPATH*2+4*MAXSOL+3)  = DBLE(SAcs)
      rpar(MAXSOL*MAXPATH*2+4*MAXSOL+4)  = DBLE(SAms)
      rpar(MAXSOL*MAXPATH*2+4*MAXSOL+5)  = DBLE(rLk/segN/(Ncaps*2)/60.0)
      rpar(MAXSOL*MAXPATH*2+4*MAXSOL+6)  = DBLE(pL)
      rpar(MAXSOL*MAXPATH*2+4*MAXSOL+7)  = DBLE(rnmyo)
      rpar(MAXSOL*MAXPATH*2+4*MAXSOL+8)  = DBLE(rnisfm)
      rpar(MAXSOL*MAXPATH*2+4*MAXSOL+9)  = DBLE(Pisfin)
      rpar(MAXSOL*MAXPATH*2+4*MAXSOL+10) = DBLE(Pmyoin)
      rpar(MAXSOL*MAXPATH*2+4*MAXSOL+11) = DBLE(Visfsi)
      rpar(MAXSOL*MAXPATH*2+4*MAXSOL+12) = DBLE(Vmyosi)
      DO 115 k=1,3
        rpar(MAXSOL*MAXPATH*2+4*MAXSOL+13+k)  = DBLE(Ei(k))
        rpar(MAXSOL*MAXPATH*2+4*MAXSOL+16+k)  = DBLE(Em(k))
        rpar(MAXSOL*MAXPATH*2+4*MAXSOL+19+k)  = DBLE(actmyo(k))
  115 CONTINUE
      rpar(MAXSOL*MAXPATH*2+4*MAXSOL+13) = DBLE(extyp)
      DO 118 j=1,MAXPATH
        rpar(MAXSOL*MAXPATH*2+4*MAXSOL+22+k)  = DBLE(actisf(k))
  118 CONTINUE
      rpar(MAXSOL*MAXPATH*2+4*MAXSOL+25+j) = DBLE(rLpout(j))
      IPAR(1) = MAXSOL
      IPAR(2) = MAXPATH
      time=0.0
c
c Return to the XSIM mainline following initialization.
c
c-----------------------------------------------------SOLUTION SECTION
c
c The mandatory name of the solution section is "simlop". This section
c of the code is entered once for each increment of the independent
c variable, xstime.
c
c Matching of xsim time to model time. At each XSIM time step, the model
c recieves as input the time to which it must integrate. The model will
c take as many steps of size dt as it can without going beyond the XSIM
```

```
c time.
c
      ENTRY simlop
      nloop=0
      Fout = 0.0
c
c Pressure drops
      IF (ptype.LT.(1.1)) THEN
        flowo=flowin
        CALL PRESF(flowo,Pm,Paout,pcapin,pcapou,Pv,omegaA,omegaC,
     +           omegaV,Rtub,INT(pfs),xrsel,eflag)
        IF (eflag) THEN
          CALL SCFMSG('Error in pressure-flow module')
          RETURN
        ENDIF
    Pvout=Pv
        Pmout=Pm
        Raout=omegaA
        Rvout=omegaV
      ENDIF
      dt   = (Ncaps*Vcapt*2.0)/(flowo/60.0)/segN
      velin = rlen/10000.0/dt/segN
      DO 125 j=1,Nseg
        pcap(j) = Pcapou+omegaC*flowo*(segN-REAL(j)+0.5)/segN
  125 CONTINUE
c
c
 1000 CONTINUE
     IF (xstime.GE.time+dt) THEN
c
c CALCULATIONS HERE DONE ONCE EACH MODEL TIME STEP
c Radial transfer calculations, loop for each axial segment:
        DO 2000 j=1,nseg
c
c Set up dependent variable:
          dtime = DBLE(time)
          xend  = DBLE(time+dt)
c Independent variables in the solution array Y:
          DO 2010 i=1,MAXSOL
            y(i)      = DBLE(rncap(i,j))
            y(i+MAXSOL) = DBLE(rnisf(i,j))
 2010       CONTINUE
          y(1+2*MAXSOL)=DBLE(Vcap(j))
          y(2+2*MAXSOL)=DBLE(Visf(j))
          y(3+2*MAXSOL)=DBLE(Vmyo(j))
c
c Transfer of variables into rpar array:
c
          DO 2011 i=1,MAXSOL
            solVd(i)=VDIST(Cgag,Ccol,rfgag,rfcol,solrad(i))
            rpar(i+MAXSOL*MAXPATH*2) = DBLE(solVd(i))
```

```
 2011      CONTINUE
           rpar(MAXSOL*MAXPATH*2+4*MAXSOL+26+MAXPATH) = DBLE(pcap(j))
c
c Check if paths should be lumped at end of capillary or left
c evenly distributed:
          DO 2015 k=1,MAXPATH
        IF ( ploc(k) .GT. (1.0) ) THEN
      DO 2016 i=1,MAXSOL
        IF (j.EQ.Nseg) THEN
      rpar((i-1)*MAXPATH+k) =
     +    DBLE(permout(i,k))*Nseg
        ELSE
          rpar((i-1)*MAXPATH+k) = 0.0D0
        ENDIF
 2016     CONTINUE
     IF (j.EQ.Nseg) THEN
       rpar(MAXSOL*MAXPATH*2+4*MAXSOL+25+k) =
     +      DBLE(rLpout(j))*Nseg
         ELSE
       rpar(MAXSOL*MAXPATH*2+4*MAXSOL+25+k) = 0.0D0
     ENDIF
   ENDIF
 2015     CONTINUE

c
c Call of the ODE solver:
         IF (rmode.EQ.(2.0)) THEN
           CALL RADAU(ND,DFDYDT,dtime,y,xend,h,
     +              drtol,datol,itol,
     +              DUMJAC,ijac,mljac,mujac,
     +              DUMMAS,imas,mlmas,mumas,
     +              DUMOUT,iout,
     +              work,LW,iwork,LIWORK,rpar,ipar,idid)
           IF (idid.NE.1) THEN
             CALL SCFMSG('Error detected in RADAU subroutine')
             RETURN
           ENDIF
         ELSE
           CALL DOPRI5(ND,DFDYDT,dtime,y,xend,
     +              drtol,datol,itol,
     +              DUMOUT,iout,
     +              work,LW,iwork,LIWORK,rpar,ipar,idid)
           IF (idid.EQ.-4) THEN
             CALL SCFMSG('Problem appears to become stiff,
     + try RADAU ODE solver.')
             RETURN
           ENDIF
           IF (idid.LT.1) THEN
             CALL SCFMSG('Error detected in DOPRI subroutine')
             RETURN
           ENDIF
```

```
          ENDIF
c
c Return the results of the time integration to the model parameters:
          DO 2020 i=1,MAXSOL
            rncap(i,j) = SNGL(Y(i))
            rnisf(i,j) = SNGL(Y(i+MAXSOL))
2020        CONTINUE
          Vcap(j) = SNGL(Y(1+2*MAXSOL))
          Visf(j) = SNGL(Y(2+2*MAXSOL))
          Vmyo(j) = SNGL(Y(3+2*MAXSOL))
          Rvci = (Visf(j)-Visfsi)/Visfsi
          Rvcm = (Vmyo(j)-Vmyosi)/Vmyosi
      IF (Rvci. GE. 0.0) THEN
            pisf(j)=Pisfin+Ei(1)*Rvci+Ei(2)*Rvci**2+Ei(3)*Rvci**3
      ELSE
        pisf(j)=Pisfin+Ei(1)*Rvci-Ei(2)*Rvci**2+Ei(3)*Rvci**3
      ENDIF
      IF (Rvcm. GE. 0.0) THEN
            pmyo(j)=Pmyoin+Em(1)*Rvcm+Em(2)*Rvcm**2+Em(3)*Rvcm**3
      ELSE
        pmyo(j)=Pmyoin+Em(1)*Rvcm-Em(2)*Rvcm**2+Em(3)*Rvcm**3
      ENDIF
c
c Now calculate new concentrations in each compartment:
          DO 2040 i=1,MAXSOL
            Cisf(i,j) = rnisf(i,j)/(Visf(j)*SolVd(i))
            Oisf(i,j) = (Cisf(i,j)*solact(i,1)
     +              + Cisf(i,j)**2*solact(i,2)
     +              + Cisf(i,j)**3*solact(i,3))*tempR
2040        CONTINUE
          Omyom(j) = (rnmyo/Vmyo(j))*actmyo(1) +
     +              (rnmyo/Vmyo(j))**2*actmyo(2) +
     +              (rnmyo/Vmyo(j))**3*actmyo(3)
          Oisfm(j) = ((rnisfm/Visf(j))*actisf(1) +
     +              (rnisfm/Visf(j))**2*actisf(2) +
     +              (rnisfm/Visf(j))**3*actisf(3))*tempR
c
c Calculate new velocity profile:
          vel(j+1) = vel(j)+(Vcap(j)-vseg)/(0.5*PI*rcap**2*capD*dt)
2000      CONTINUE
        vel(1) = rlen/10000.0/dt/segN
c
c Axial convection: Slide the fluid elements one step.
c There is only convection now, but any acial stuff would go here
c
        DO 1010 i=1,MAXSOL
          IF (soltyp(i).LT.(1.1)) THEN
            Cin(i) = solf(i)
            solfin(i) = solf(i)*vseg
          ELSEIF (soltyp(i).LT.(2.1)) THEN
            Cin(i) = solcap(i)
```

```
            solfin(i) = solcap(i)*vseg
          ELSE
            Cin(i) = 0.0
            solfin(i) = 0.0
          ENDIF
 1010   CONTINUE
        CALL vslide(MAXSOL,Nseg,Vseg,solfin,rncap,Vcap,solfou,Vout,
     +          wk1,wk2,wk3,wk4,eflag)
        IF (eflag) THEN
          CALL SCFMSG('Problem occurs in vslide subroutine.')
          RETURN
        ENDIF
        Fout = Fout+Vout
        DO 1020 i=1,MAXSOL
          Cout(i) = solfou(i)/Vout
          DO 1025 j=1,Nseg
            Ccap(i,j) = rncap(i,j)/Vcap(j)
            Ocap(i,j) = (Ccap(i,j)*solact(i,1) +
     +                  Ccap(i,j)**2*solact(i,2) +
     +                  Ccap(i,j)**3*solact(i,3))*tempR
 1025     CONTINUE
 1020   CONTINUE
        nloop=nloop+1
        time=time+dt
        GOTO 1000
      ENDIF
c
c CALCULATIONS HERE DONE ONCE EACH XSIM TIME STEP:
c Calcuate total ISF and myocardial volumes:
      DO 3005 i=1,MAXSOL
        solfin(i)=solfin(i)/dt
        solfou(i)=solfou(i)/dt
 3005 CONTINUE
      Vcapt = 0.0
      Vwisf = 0.0
      Vwmyo = 0.0
      DO 3010 j=1,nseg
        Vcapt = Vcapt + Vcap(j)
        Vwisf = Vwisf + Visf(j)
        Vwmyo = Vwmyo + Vmyo(j)
 3010 CONTINUE
c
c Calculate weight
c
      CALL HEXT(Vwisf, Vwmyo, Vcapt, Visft,Vmyot,Vtiss,denw, dtiss, wkg)
      Wt    = 2.0*Vtiss*dtiss*Ncaps + WtLV
      Dheart = Wt/(2.0*Vtiss*Ncaps + WtLV/denw)
      Vlvg  = WtLV/Wt/denw
      capD  = Ncaps/Wt
      Cgag  = rWgag/Visft
      Ccol  = rWcol/Visft
```

```
      Csolm  = rWsolm/Vmyot
      wfisf  = 1.0-(Cgag+Ccol)/denp
      wfmyo  = 1.0-Csolm/denp
c
c Volumes and surface areas on a per gram tissue basis
      SAcg  = 2.0*SAc*capD
      SAmg  = 2.0*SAm*capD
      Visfg = 2.0*Vwisf*capD
      Vmyog = 2.0*Vwmyo*capD
      Vcapg = 2.0*Vcapt*capD
c
c Calculate osmolarities
c
      wfL = 0.0
      DO 3020 j=1,Nseg
        osmolc(j) = 0.0
        osmoli(j) = Oisfm(j)
        osmolm(j) = Omyom(j)
        DO 3025 i=1,MAXSOL
          osmolc(j) = osmolc(j) + Ocap(i,j)
          osmoli(j) = osmoli(j) + Oisf(i,j)
 3025   CONTINUE
c
c Lymph outflow
c
        IF (pisf(j).GT.pL) THEN
          wfL = wfL + rLk*(pisf(j)-pL)/segN
        ENDIF
 3020 CONTINUE
c
c Current Water fluxes:
c
      DO 4000 j=1,Nseg
        rJwm(j)  = 0.0
        summ(j) = Oisfm(j) - Omyom(j)
        sumc1(j) = Oisfm(j)
        sumc2(j) = Oisfm(j)
        sumc3(j) = Oisfm(j)
        rJwc1(j) = 0.0
        rJwc2(j) = 0.0
        rJwc3(j) = 0.0
        DO 4030 i=1,MAXSOL
          sumc1(j) = sumc1(j) + sigout(i,1)*(Oisf(i,j)-Ocap(i,j))
          sumc2(j) = sumc2(j) + sigout(i,2)*(Oisf(i,j)-Ocap(i,j))
          sumc3(j) = sumc3(j) + sigout(i,3)*(Oisf(i,j)-Ocap(i,j))
          summ(j) = summ(j) + Oisf(i,j)
4030    CONTINUE
      rJwc1(j) = rJwc1(j) + rLpout(k)*SAcs*
     +           ( (pisf(j)-pcap(j)) - sumc1(j) )
      rJwc2(j) = rJwc2(j) + rLpout(k)*SAcs*
     +           ( (pisf(j)-pcap(j)) - sumc2(j) )
```

```
          rJwc3(j) = rJwc3(j) + rLpout(k)*SAcs*
     +               ( (pisf(j)-pcap(j)) - sumc3(j) )
          rJwm(j) = rJwm(j) + rLpm*SAms*((pisf(j)-pmyo(j)) - summ(j))
 4000 CONTINUE
c
c Convert to ml/min/g
      DO 4002 j=1,Nseg
         rJwm(j)  = rJwm(j)*60.0*capD
         rJwc1(j) = rJwc1(j)*60.0*capD
         rJwc2(j) = rJwc2(j)*60.0*capD
         rJwc3(j) = rJwc3(j)*60.0*capD
 4002 CONTINUE
c
c Integrate over cap length
      rJwmt = 0.0
      rJwct = 0.0
      rJwc1t = 0.0
      rJwc2t = 0.0
      rJwc3t = 0.0
      DO 4005 j=1,Nseg
         rJwmt  = rJwmt + rJwm(j)
         rJwc1t = rJwc1t + rJwc1(j)
         rJwc2t = rJwc2t + rJwc2(j)
         rJwc3t = rJwc3t + rJwc3(j)
 4005 CONTINUE
      rJwct = rJwc1t + rJwc2t + rJwc3t
c
c Transfer of ODE output to p array:
      rfcn=REAL(nfcn)
      rstep=REAL(nstep)
      raccpt=REAL(naccpt)
      rrejct=REAL(nrejct)
c
c Return to the SIMCON interface for plotting, etc.:
      RETURN
c-----------------------------------------------------COMPLETION SECTION
c
c The mandatory name of the optional completion section is "simend".
c This section of code is entered once after each simulation run (i.e.
c before returning to the main SIMCON menu).
c
      ENTRY simend
c
      IF (swrite.EQ.2.0) THEN
         WRITE(lu2,901) Nseg, segN, tempR, WtLV, Vsisf, Vsmyo
         WRITE(lu2,905) vseg, Visfsi, Vmyosi, actisf(3), actmyo(3)
         WRITE(lu2,905) actisf(1), actisf(2), rwgag, rwcol, rnisfm
         WRITE(lu2,905) actmyo(1), actmyo(2), rnmyo, SAc, SAm
         WRITE(lu2,905) velin, Ncaps, rmu, Dheart, Wt
         WRITE(lu2,902) Fout, omegaC
         DO 10030 j=1,NSEG
```

```
            WRITE(lu2,904) Vcap(j),Visf(j),Vmyo(j),Omyom(j)
            WRITE(lu2,904) pcap(j),pisf(j),pmyo(j), vel(j)
            DO 10035 i=1,MAXSOL
              WRITE(lu2,902) Ccap(i,j),Cisf(i,j)
              WRITE(lu2,902) rncap(i,j),rnisf(i,j)
10035       CONTINUE
10030     CONTINUE
          DO 10040 i=1,MAXSOL
            WRITE(lu2,906) solcap(i)
10040     CONTINUE
          DO 10041 k=1,4
            WRITE(lu2,904) wkg(1), wkg(2), wkg(3), wkg(4)
10041     CONTINUE
          CALL F7CLOS(lu2,'KEE',ier)
          IF (ier.EQ.-1) THEN
            CALL SCFMSG('Error closing file '//
     +              writefile(1:LNBLNK(writefile))//'.')
            RETURN
          ENDIF
        ENDIF
        RETURN
        END
c
c-------------------------------------------------ADDITIONAL SUBROUTINES
c
c RIGHT-HAND SIDE OF CHARACTERISTIC EQUATIONS FOR ODE SOLVERS
c
      SUBROUTINE DFDYDT(N,x,y,ydot,rpar,ipar)
      INTEGER i,MAXSOL,MAXPATH
      PARAMETER(MAXSOL=10, MAXPATH=3)
      DOUBLE PRECISION x,y(*),ydot(*)
      DOUBLE PRECISION rpar(MAXSOL*MAXPATH*2+4*MAXSOL+26+MAXPATH)
      INTEGER ipar(*),N,Nsol, Npath
      DOUBLE PRECISION perm(MAXSOL,MAXPATH),Ccap(MAXSOL),Cisf(MAXSOL),
     +          Omyom,dnmyom,actmyo(3),solact(MAXSOL,3),
     +          solVd(MAXSOL),cmean(MAXSOL),
     +          deln(MAXSOL,MAXPATH), sigma(MAXSOL,MAXPATH),
     +          dif(MAXSOL,MAXPATH), sdrag(MAXSOL,MAXPATH),
     +          dnisfm, Oisfm, actisf(3),iPi,iPm,iVi,iVm, pL,
     +          Ei(3), Em(3), Rvci, Rvcm, pisf, pmyo,
     +          dlogm, dLpm, dLp(MAXPATH), dLk, extyp, pcap,
     +          sacs, sams, sumc(MAXPATH), summ, tempR, vcap,
     +          visf, vmyo, dJwc(MAXPATH), dncap(MAXSOL),
     +          dnisf(MAXSOL), dJwm, dJwL, dJwct, delnt(MAXSOL),
     +          Oisf(MAXSOL), Ocap(MAXSOL)
      EXTERNAL DLOGM, PATLAK
c
c Unpack ipar and rpar arrays
c
      Nsol=ipar(1)
      Npath=ipar(2)
```

```
c
      DO 5110 i=1,NSOL
        DO 5111 j=1,NPATH
          perm(i,j) = rpar((i-1)*NPATH+j)
          sigma(i,j)  = rpar(NSOL*NPATH+(i-1)*NPATH+j)
 5111   CONTINUE
        solVd(i)   = rpar(i+NSOL*NPATH*2)
        solact(i,1) = rpar(i+NSOL*NPATH*2+1*NSOL)
        solact(i,2) = rpar(i+NSOL*NPATH*2+2*NSOL)
        solact(i,3) = rpar(i+NSOL*NPATH*2+3*NSOL)
 5110 CONTINUE
      dLpm   = rpar(NSOL*NPATH*2+4*NSOL+1)
      tempR  = rpar(NSOL*NPATH*2+4*NSOL+2)
      SAcs   = rpar(NSOL*NPATH*2+4*NSOL+3)
      SAms   = rpar(NSOL*NPATH*2+4*NSOL+4)
      dLk    = rpar(NSOL*NPATH*2+4*NSOL+5)
      pL     = rpar(NSOL*NPATH*2+4*NSOL+6)
      dnmyom = rpar(NSOL*NPATH*2+4*NSOL+7)
      dnisfm = rpar(NSOL*NPATH*2+4*NSOL+8)
      iPi    = rpar(NSOL*NPATH*2+4*NSOL+9)
      iPm    = rpar(NSOL*NPATH*2+4*NSOL+10)
      iVi    = rpar(NSOL*NPATH*2+4*NSOL+11)
      iVm    = rpar(NSOL*NPATH*2+4*NSOL+12)
      extyp  = rpar(NSOL*NPATH*2+4*NSOL+13)
      DO 5115 k=1,3
        Ei(k) = rpar(NSOL*NPATH*2+4*NSOL+13+k)
        Em(k) = rpar(NSOL*NPATH*2+4*NSOL+16+k)
        actmyo(k) = rpar(NSOL*NPATH*2+4*NSOL+19+k)
        actisf(k) = rpar(NSOL*NPATH*2+4*NSOL+22+k)
 5115 CONTINUE
      DO 5118 j=1,MAXPATH
        dLp(j)= rpar(NSOL*NPATH*2+4*NSOL+25+j)
 5118 CONTINUE
      pcap= rpar(NSOL*NPATH*2+4*NSOL+26+NPATH)
c
c Test for error conditions
c
      IF (Y(1+2*Nsol).GE.0.0D0) THEN
        Vcap = y(1+2*Nsol)
      ELSE
        CALL SCFMSG('Error: Capillary volume segment goes to 0')
        RETURN
      ENDIF
      IF (Y(2+2*Nsol).GE.0.0D0) THEN
        Visf = y(2+2*Nsol)
      ELSE
        CALL SCFMSG('Error: Interstitial volume segment goes to 0')
        RETURN
      ENDIF
      IF (Y(3+2*Nsol).GE.0.0D0) THEN
        Vmyo = y(3+2*Nsol)
```

```
      ELSE
        CALL SCFMSG('Error: Cell volume segment goes to 0')
        RETURN
      ENDIF
      DO 5020 i=1,Nsol
        IF (Y(i).GE.0.0D0) THEN
          dncap(i)=Y(i)
        ELSE
          dncap(i)=0.0D0
        ENDIF
        IF (Y(i+Nsol).GE.0.0D0) THEN
          dnisf(i)=Y(i+Nsol)
        ELSE
          dnisf(i)=0.0D0
        ENDIF
c
c Set osmolarities
c
        Ccap(i) = dncap(i)/Vcap
        IF (Ccap(i).LT.0.0D0) THEN
          Ccap(i)=0.0D0
        ENDIF
        Ocap(i) = (Ccap(i)*solact(i,1) + Ccap(i)**2*solact(i,2) +
     +            Ccap(i)**3*solact(i,3))*tempR
        Cisf(i) = dnisf(i)/(Visf*solVd(i))
        IF (Cisf(i).LT.0.0D0) THEN
          Cisf(i)=0.0D0
        ENDIF
        Oisf(i) = (Cisf(i)*solact(i,1) + Cisf(i)**2*solact(i,2) +
     +            Cisf(i)**3*solact(i,3))*tempR
 5020 CONTINUE
      Oisfm = ((dnisfm/Visf)*actisf(1) + (dnisfm/Visf)**2*actisf(2) +
     +        (dnisfm/Visf)**3*actisf(3))*tempR
      Omyom = (dnmyom/Vmyo)*actmyo(1) + (dnmyom/Vmyo)**2*actmyo(2) +
     +        (dnmyom/Vmyo)**3*actmyo(3)
      Rvci = (Visf-iVi)/iVi
      Rvcm = (Vmyo-iVm)/iVm
      IF (Rvci .GE. 0.0) THEN
        pisf = ipi + Ei(1)*Rvci + Ei(2)*Rvci**2 + Ei(3)*Rvci**3
      ELSE
 pisf = ipi + Ei(1)*Rvci - Ei(2)*Rvci**2 + Ei(3)*Rvci**3
      ENDIF
      IF (Rvcm .GE. 0.0) THEN
        pmyo = ipm + Em(1)*Rvcm + Em(2)*Rvcm**2 + Em(3)*Rvcm**3
      ELSE
 pmyo = ipm + Em(1)*Rvcm - Em(2)*Rvcm**2 + Em(3)*Rvcm**3
      ENDIF
c
c First, volume flux across capillary and cells:
c
      DO 5029 j=1,NPATH
```

```
          sumc(j)=Oisfm
 5029 CONTINUE
        summ=Oisfm-Omyom
        DO 5030 i=1,Nsol
          DO 5033 k=1,NPATH
            sumc(k) = sumc(k) + sigma(i,k)*(Oisf(i)-Ocap(i))
 5033     CONTINUE
          summ = summ + Oisf(i)
 5030 CONTINUE
      dJwct = 0.0D0
      DO 5035 k=1,NPATH
        dJwc(k) = dLp(k)*SAcs*((pisf-pcap) - sumc(k))
        dJwct = dJwct + dJwc(k)
 5035 CONTINUE
      dJwm = dLpm*SAms*((pisf-pmyo) - summ)
c
c Solute fluxes. If extyp=1 then the Kedem and Katchalsky equations
c are used with an arithemetic mean. If extyp=2 then the Kedem
c and Katchalsky equaitons are used with a logrithmic mean. If
c extyp=3 then the Patlak equation is used:
c
      IF (extyp.LE.2.1) THEN
        DO 5040 i=1,Nsol
          IF (extyp.GE.1.1) THEN
            cmean(i) = DLOGM(Ccap(i),Cisf(i))
          ELSE
            cmean(i) = (Ccap(i)+Cisf(i))/2.0D0
          ENDIF
          DO 5045 j=1,NPATH
            sdrag(i,j) = dJwc(j)*(1-sigma(i,j))*cmean(i)
            dif(i,j)   = perm(i,j)*(Cisf(i)-Ccap(i))*SAcs
            deln(i,j)  = sdrag(i,j)+dif(i,j)
 5045       CONTINUE
 5040     CONTINUE
      ELSE
        DO 5050 i=1,Nsol
          DO 5055 j=1,NPATH
            CALL PATLAK(perm(i,j)*SAcs, sigma(i,j), Cisf(i), Ccap(i),
     +                  dJwc(j), dif(i,j), sdrag(i,j), deln(i,j))
 5055     CONTINUE
 5050   CONTINUE
      ENDIF
      DO 5060 i=1,NSOL
        delnt(i)=0.0D0
        DO 5070 j=1,NPATH
          delnt(i) = delnt(i) + deln(i,j)
 5070   CONTINUE
 5060 CONTINUE
c
      IF (pisf.GT.pL) THEN
        dJwL = dlK*(pisf-pL)
```

```
      ELSE
        dJwL = 0.0D0
      ENDIF
c
c Final definition of right-hand side of characteristic equations:
c
      DO 5080 i=1,Nsol
        ydot(i)     = delnt(i)
        ydot(i+Nsol) = delnt(i)*(-1.D0)-Cisf(i)*dJwL
 5080 CONTINUE
      ydot(1+Nsol*2)=dJwct
      ydot(2+Nsol*2)=dJwct*(-1.D0)-dJwm-dJwL
      ydot(3+Nsol*2)=dJwm
      RETURN
      END
c
      SUBROUTINE DUMJAC (N,X,Y,DFY,LDFY,rpar,ipar)
      RETURN
      END
c
      SUBROUTINE DUMMAS (N,B,LB,rpar,ipar)
      RETURN
      END
c
      SUBROUTINE DUMOUT (NR,XOLD,X,Y,CONT,LRC,N,rpar,ipar,IRTRN)
      RETURN
      END
c
      REAL FUNCTION VISCOS(temp)
c
c temperature must not be negative.  config file should be set up to prevent
c temperatures less than 273K. Function will return a value of zero for
c temperatures out of range 273-313 (K).
c
      REAL temp,tstd(273:313)
      INTEGER t
      DATA tstd/0.017870,0.017280,0.016710,0.016180,0.015670,0.015190,
     + 0.014720,0.014280,0.013860,0.013460,0.013070,0.012710,0.012350,
     + 0.012020,0.011690,0.011390,0.011090,0.010810,0.010530,0.010270,
     + 0.010020,0.009779,0.009548,0.009325,0.009111,0.008904,0.008705,
     + 0.008513,0.008327,0.008148,0.007975,0.007808,0.007647,0.007491,
     + 0.007340,0.007194,0.007052,0.006915,0.006783,0.006654,0.006529/
      DO 10 t=273,313
      IF ((REAL(t).LE.temp).AND.(REAL(t+1).GT.temp)) THEN
        VISCOS = tstd(t) + (tstd(t+1)-tstd(t))*(temp-REAL(t))
        RETURN
      ENDIF
 10 CONTINUE
      VISCOS = 0.0
      RETURN
      END
```

```
c
      REAL FUNCTION CUBIC(a,b,c,d)
c
c solves the equation ax^3 + bx^2 + c^x = d
c returns one real root (it dosen't really matter which root coresponds
c to the actual number of moles, since this number is only used
c internally in the program to get back to concentrations.
c
      REAL a,b,c,d
      REAL f,g,h,aa,bb,r,t
      IF ((a.EQ.0.0).AND.(b.EQ.0.0)) THEN
        CUBIC=d/c
        RETURN
      ELSEIF (a.NE.0) THEN
        f=((3.0*c/a)-(b/a)**2)/3.0
        g=(2.0*(b/a)**3 - 9.0*b*c/a**2 - 27.0*d/a)/27.0
        h=g**2/4.0 + f**3/27.0
        IF (h.GE.0) THEN
          aa=-0.5*g+SQRT(h)
          IF (aa.GE.0.0) THEN
            aa=aa**0.333333
          ELSE
            aa=((aa*(-1.0))**0.333333)*(-1.0)
          ENDIF
          bb=-0.5*g-SQRT(h)
          IF (bb.GE.0.0) THEN
            bb=bb**0.333333
          ELSE
            bb=((bb*(-1.0))**0.333333)*(-1.0)
          ENDIF
          CUBIC=aa+bb-b/a/3.0
          RETURN
        ELSE
          r=SQRT(g**2/4.0 - h)
          t=ACOS(-0.5*g/r)
          CUBIC=2*r**0.333333*COS(t/3)-b/a/3.0
          RETURN
        ENDIF
      ELSE
        CUBIC=(SQRT(c**2+4.0*b*d)-c)/2.0/b
        RETURN
      ENDIF
      END
c
c-----------------------------------------------------------------------
c
      REAL FUNCTION VDIST(C1,C2,r1,r2,s)
c
c Calculates the volume of distribution based on exclusion of
c two populations of cylindrical fibers and spherical solutes
c
```

```
      REAL RHOGAG
      PARAMETER (RHOGAG=1.39)
      REAL C1,C2,r1,r2,s
      VDIST =  EXP(-1*C1/RHOGAG*(2*s/r1 + (s/r1)**2))*
     +       EXP(-1*C2/RHOGAG*(2*s/r2 + (s/r2)**2))
      RETURN
      END
*****************************************************************************
FILE dlogm.f
*****************************************************************************
DOUBLE PRECISION FUNCTION DLOGM (X,Y)
c
c This function calculates the logarithmic mean of two numbers.
c
c File %M% (Version %I%).  Last modified at %U% on %G%.
c
c.....
c
c From:  National Simulation Resource
c       Center for Bioengineering
c       University of Washington
c       Box 357962
c       Seattle, WA 98195-7962
c
c       Dr. J. B. Bassingthwaighte, Director
c
c.....
c
c Copyright (C) 1998 by National Simulation Resource, Univ of WA.
c All Rights Reserved.
c
c Software may be copied so long as this copyright notice is included.
c This software was developed with support from NIH grant RR-01243.
c Please cite this grant in any publication for which this software
c is used and send one reprint to the address given above.
c
c.....
c
c SYNOPSIS:
c
c     DOUBLE PRECISION FUNCTION dlogm(X,Y)
c     DOUBLE PRECISION X,Y
c
c.....
c
c DESCRIPTION:
c
c     This function calculates the logarithmic mean of two double-
c     precision numbers.
c
c.....
```

```
c
c RETURN VALUE:
c
c     The logarithmic mean is given by DLOGM=(x-y)/ln(x/y)
c     For X=Y then the function returns X
c     For X or Y less than or equal to 0 the function returns 0.
c
c.....
c
c FORMAL PARAMETERS:
c
c INPUTS:
c   Name  Description                          Typical values
c   ------ ------------------------------------ --------------
c   X     First number                         positive
c   Y     Second number                          positive
c
c.....
c
c LIMITATIONS/WARNINGS:
c
c   The logarithmic mean is undefined for negative numbers, or when X=Y.
c   See return value for these cases.
c.....
c
c DIAGNOSTICS:
c
c    NONE
c.....
c
c KNOWN BUGS:
c
c    NONE
c
c.....
c
c SUBROUTINES/FUNCTIONS CALLED:
c
c    NONE
c
c.....
c
c FILES:
c
c /usr/local/lib/libnsr.a              - library archive
c ~libnsr/lib/libmath/dlogm - source files
c
c.....
c
c AUTHOR:
c
```

```
c National Simulation Resource
c Center for Bioengineering
c University of Washington
c Box 357962
c Seattle, WA 98195-7962
c
c.....
c
c FOR ASSISTANCE:
c
c Questions regarding this software can be sent by electronic mail to:
c  librarian@nsr.bioeng.washington.edu
c
c.....
c
c HISTORY:
c
c Written:  Michael Kellen (1-1998)
c
c Modified:
c Ver. {1.0}: Formal development and archiving of code
c         (Michael Kellen - 12-1998)
c
c-----------------------------------------------------------------------
c
      DOUBLE PRECISION X,Y
      CHARACTER*64  sid1, sid2
c
      DATA       sid1
     + /'%W% created on %G% at %U%.\n'/
      DATA       sid2
     + /'%Z% Retrieved on %H% at %T%.\n'/
c
c Main routine
c
      IF ((X.NE.Y).AND.(X.GT.0.0D0).AND.(Y.GT.0.0D0)) THEN
        DLOGM = (X-Y)/(LOG(X/Y))
      ELSEIF ((X.EQ.Y).AND.(X.GT.0.0D0)) THEN
        DLOGM = X
      ELSE
        DLOGM = 0.0D0
      ENDIF
      RETURN
      END
*************************************************************************
FILE hext.f
*************************************************************************
c hext.f
c
c Model of capillary whole organ tissue archeteture
c
```

```
c.....
c
c From:  National Simulation Resource
c        Center for Bioengineering
c        University of Washington
c        Box 357962
c        Seattle, WA 98195-7962
c
c        Dr. J. B. Bassingthwaighte, Director
c
c.....
c
c Copyright (C) 2000 by National Simulation Resource, Univ of WA.
c All Rights Reserved.
c
c Software may be copied so long as this copyright notice is included.
c This software was developed with support from NIH grant RR-01243.
c Please cite this grant in any publication for which this software
c is used and send one reprint to the address given above.
c
c.....
c
c SYNOPSIS
c    SUBROUTINE HEXTi(Rcap, dm, dic, len, Vcap, Visf, Vcell, Vwisf,
c                     Vwcell, Vtiss, dtiss, SAc, SAm, Cmyo, Cisf,
c                     fWisf, fWcell, eflag)
c
c REAL Rcap, dm, dic, len, Vcap, Visf, Vcell, Vwisf
c      REAL Vwcell, Vtiss, dtiss, SAc, SAm, Cmyo, Cisf,
c      REAL fWisf, fWcell
c LOGICAL eflag
c
c    ENTRY HEXT(Vwisf, Vwcell, Vcap, Visf, Vcell, Vtiss, dtiss)
c
c      REAL Vwisf, Vwcell, Vcap, Visf, Vcell, Vtiss, dtiss
c
c.....
c
c DESCRIPTION
c
c hext.f contains subroutines for calculating tissue arctecture
c
c.....c
c LIMITATIONS/WARNINGS:
c
c.....
c
c DIAGNOSTICS:
c
c    NONE.
c
```

```
c.....
c
c EXAMPLES:
c
c.....
c
c REFERENCES:
c
c NONE
c
c.....
c
c SUBROUTINES/FUNCTIONS CALLED:
c
c NONE
c
c.....
c
c FILES:
c
c /usr/local/lib/libnsr.a          - library archive
c ~libnsr/lib/libmath/geom         - source files
c
c.....
c
c AUTHOR:
c
c National Simulation Resource
c Center for Bioengineering
c University of Washington
c Box 357962
c Seattle, WA 98195-7962
c
c.....
c
c FOR ASSISTANCE:
c
c Questions regarding this software can be sent by electronic mail to:
c librarian@nsr.bioeng.washington.edu
c
c.....
c
c HISTORY
c
c Written 7/25/00 by M. Kellen
c
c-----------------------------------------------------------------
      SUBROUTINE HEXTi(Rcap, dm, dic, len, Vcap, Visf, Vcell, Vwisf,
     +           Vwcell, Vtiss, dtiss, SAc, SAm, Cmyo, Cisf,
     +           denw, denp, wk, eflag)
c
```

```
c Model Inputs
c
c parameterdescriptionunits
c -------------------------------------------------
c Rcapcapillary radiusum
c dmintermyocyte distanceum
c dicintercapillary distanceum
c lencapillary lengthum
c Cisfisf solid concentration       g/mL
c Cmyocell solid concentration      g/mL
c denw        fluid phase density         g/mL
c denp  solid phase density         g/mL
c
c Model Outputs
c
c parameterdescriptionunits
c -------------------------------------------------
c Vcapcapillary volumemL
c Visfinterstitial anatomical volume  mL
c Vcell cellular anatomical volume    mL
c Vwisfinterstitial water volumemL
c Vwcellcell water volume    mL
c Vtisstotal unit cell volumemL
c dtissunit cell density  g/mL
c SAccapillary surface areacm^2
c SAmcell surface areacm^2
c eflag       set to .TRUE. for bad parameters
c
c******************** Declaration Section ******************************
c
      REAL Rcap,dm,dic,len,Cisf,Cmyo,Vcap,Visf,Vcell,Vtiss,Acap,Aisf,
     +    Acell,Atiss,Vwisf,Vwcell,dtiss,Risf,Wwcap,Wwisf,
     +    Wwcell,Wtiss,denw,denp,wk(4)
      LOGICAL eflag
      PARAMETER (PI=3.141593)
      SAVE
c
c******************** Initialization Section ***************************
c
c II. Error Checking
c
      eflag=.FALSE.
      IF ((Rcap.LT.0.0) .OR. (dm.LT.0.0) .OR. (dic.LT.0.0) .OR.
     +  (len.LT.0.0) .OR. (Cisf.LT.0.0) .OR. (Cmyo.LT.0.0).OR.
     +  (denp.LE.0.0) .OR. (denw.LE.0.0)) THEN
         eflag=.TRUE.
        RETURN
      ENDIF
c
c III. Calculations
c
```

```
c Calculate volumes from dimensions
c
      Acap  = 0.5*PI*Rcap**2
      Risf  = Rcap+dm
      Aisf  = 0.5*PI*(Risf**2-Rcap**2) + (dic-2*Risf)*dm
      Atiss = SQRT(3.0)/4.0*dic**2
      Acell = Atiss-Aisf-Acap
      Vcap  = Acap*len*1E-12
      Visf  = Aisf*len*1E-12
      Vcell = Acell*len*1E-12
      Vtiss = Atiss*len*1E-12
      SAc   = (PI*Rcap)*len*1E-8
      SAm   = (PI*Risf - 2.0*dm + 2.0*(dic-2.0*Risf))*len*1E-8
      Wsisf = Cisf*Visf
      Wscell= Cmyo*Vcell
      Vsisf = Wsisf/denp
      Vscell= Wscell/denp
      Vwisf = Visf-Vsisf
      Vwcell= Vcell-Vscell
      Wwcap = Vcap*denw
      Wwisf = Vwisf*denw
      Wwcell= Vwcell*denw
      Wtiss = Wsisf+Wscell+Wwcap+Wwisf+Wwcell
      dtiss = Wtiss/Vtiss
      wk(1) = Vsisf
      wk(2) = Vscell
      wk(3) = Wsisf
      wk(4) = Wscell
      RETURN
c
c******************** Solution Section *********************************
c
      ENTRY HEXT(Vwisf, Vwcell, Vcap, Visf, Vcell, Vtiss, denw,dtiss,wk)
c
c Model Inputs
c
c paramterdesctiptionunits
c-------------------------------------------------
c Vwisfinterstitial water volumemL
c Vwcellcell water volumemL
c Vcapcapillary water volumemL
c denwwater densitymL/g
c
c Model Outputs
c
c parameterdescriptionunits
c-------------------------------------------------
c Visfinterstitial anatomical volume  mL
c Vcell       cellular anatomical volume     mL
c Vtisstotal tissue volumemL
c dtisstotal tissue densitymL/g
```

```
c
c
      Vsisf = wk(1)
      Vscell= wk(2)
      Wsisf = wk(3)
      Wscell= wk(4)
      Wwcap = Vcap*denw
      Wwisf = Vwisf*denw
      Wwcell= Vwcell*denw
      Wtiss = Wsisf+Wscell+Wwcap+Wwisf+Wwcell
      Vtiss = Vwisf+Vwcell+Vcap+Vsisf+Vscell
      dtiss = Wtiss/Vtiss
      Visf  = Vsisf + Vwisf
      Vcell = Vscell + Vwcell
      RETURN
      END
*************************************************************************
File patlak.f
*************************************************************************
c    patlak.f
c
c This subroutine calculates the solute flux and the diffusive and convective
c components of flux of a solute across a membrane using the Patlak equation
c
c File %M% (Version %I%).  Last modified at %U% on %G%.
c
c.....
c
c From:  National Simulation Resource
c       Center for Bioengineering
c       University of Washington
c       Box 357962
c       Seattle, WA 98195-7962
c
c       Dr. J. B. Bassingthwaighte, Director
c
c.....
c
c Copyright (C) 2000 by National Simulation Resource, Univ of WA.
c All Rights Reserved.
c
c Software may be copied so long as this copyright notice is included.
c This software was developed with support from NIH grant RR-01243.
c Please cite this grant in any publication for which this software
c is used and send one reprint to the address given above.
c
c.....
c
c SYNOPSIS:
c
c     SUBROUTINE PATLAK(PS,sigma,C1,C2,Jv,Jsdif,Jscon,Jstot)
```

```
c     DOUBLE PRECISION PS,sigma,LpS,C1,C2,Jv,Jsdif,Jscon,Jstot
c
c.....
c
c DESCRIPTION:
c
c     This subroutine calculates the diffusive and convective solute
c     fluxes across a membrane using the nonlinear Patlak equation.
c
c.....
c
c RETURN VALUE:
c
c     The Patlak equation is given by:
c     Js = PS*(C1-C2)*Pe/(EXP(Pe)-1) + Jv(1-sigma)*C1
c     The first term of this equation is the diffusive flux and the
c     second term is the convective flux.
c
c.....
c
c FORMAL PARAMETERS:
c
c INPUTS:
c    Name   Description                          Units
c    ------ ---------------------------------- ----------
c    PS     Permeability-Surface area product of solute  cm^3/s
c    sigma  Reflection coefficient of solute          0-1
c    Jv     Volume flux from 1 to 2                cm^3/s
c    C1     Concentration on side 1 mol/cm^3
c    C2     Concentration on side 2                 mol/cm^3
c
c OUTPUTS:
c    Name   Description                          Units
c    ------ ---------------------------------- ----------
c    Jstot  Total solute flux from 1 to 2           mol/s
c    Jsdif  Diffusive solute flux from 1 to 2 mol/s
c    Jscon  Convective solute flux from 1 to 2        mol/s
c
c.....
c
c LIMITATIONS/WARNINGS:
c
c    None
c
c.....
c
c DIAGNOSTICS:
c
c    NONE
c.....
c
```

```
c KNOWN BUGS:
c
c    NONE
c
c.....
c
c SUBROUTINES/FUNCTIONS CALLED:
c
c    NONE
c
c.....
c
c FILES:
c
c /usr/local/lib/libnsr.a              - library archive
c ~libnsr/lib/libmath/dlogm - source files
c
c.....
c
c AUTHOR:
c
c National Simulation Resource
c Center for Bioengineering
c University of Washington
c Box 357962
c Seattle, WA 98195-7962
c
c.....
c
c FOR ASSISTANCE:
c
c Questions regarding this software can be sent by electronic mail to:
c  librarian@nsr.bioeng.washington.edu
c
c.....
c
c HISTORY:
c
c Written:  Michael Kellen (2-2000)
c
c-----------------------------------------------------------------------
c
      SUBROUTINE PATLAK (PS,sigma,C1,C2,Jv,Jsdif,Jscon,Jstot)
      DOUBLE PRECISION PS,sigma,Jv,C1,C2,Jstot,Jscon,Jsdif
      DOUBLE PRECISION Pe
      CHARACTER*64  sid1, sid2
c
      DATA       sid1
     + /'%W% created on %G% at %U%.\n'/
      DATA       sid2
     + /'%Z% Retrieved on %H% at %T%.\n'/
```

```
c
c Main routine
c
      IF (PS.EQ.0.0D0) THEN
        JSdif = 0.0D0
      ELSE
        Pe = Jv*(1.0D0-sigma)/PS
        IF ( (EXP(Pe)-1.0D0).NE.0.0D0 ) THEN
          Jsdif = PS*(C1-C2)*Pe/(Exp(Pe)-1.0D0)
        ELSE
          Jsdif = PS*(C1-C2)
        ENDIF
      ENDIF
      Jscon = C1*(1.0D0-sigma)*Jv
      Jstot = Jscon + Jsdif
      RETURN
      END
*************************************************************************
FILE pore.f
*************************************************************************
c pore.f
c
c The pore subroutines are used for converting between the phenomenological
c coefficients Lp, P, and sigma and the geometrical parameters of several
c different pore models.
c
c File %M% (Version %I%).  Last modified at %U% on %G%.
c
c.....................................................................
c
c From:  National Simulation Resource
c        Center for Bioengineering  WD-12
c        University of Washington
c        Seattle, WA 98195
c
c        Dr. J. B. Bassingthwaighte, Director
c
c.....................................................................
c
c Copyright (C) 1998 by
c National Simulation Resource, Center for Bioengineering,
c University of Washington, Seattle, WA 98195.
c All rights reserved.
c
c This software was developed with support from NIH grant RR-01243.
c Please cite this grant in publications for which the software or
c derivatives from it were used.  Please send one reprint to the address
c given above.
c
c.....................................................................
c
```

```
c SYNOPSIS:
c
c     SUBROUTINE RENG2P(Nsol,radp,ApSdx,eLp,als,solDfr,nu,
c                perm,sigma,tLp,pLp,eflag)
c       INTEGER Nsol
c       REAL radp,ApSdx,eLp,solrad,solDfr,nu,perm,sigma,tLp,pLp
c       LOGICAL eflag
c
c
c     SUBROUTINE BEAG2P(Nsol,radp,ApSdx,eLp,als,solDfr,nu,
c                perm,sigma,tLp,pLp,eflag)
c       INTEGER Nsol
c       REAL radp,ApSdx,eLp,solrad,solDfr,nu,perm,sigma,tLp,pLp
c       LOGICAL eflag
c
c
c     SUBROUTINE SLTG2P(Nsol,slitw,ApSdx,eLp,als,solDfr,nu,
c                perm,sigma,tLp,pLp,eflag)
c       INTEGER Nsol
c       REAL slitw,ApSdx,eLp,solrad,solDfr,nu,perm,sigma,tLp,pLp
c       LOGICAL eflag
c
c
c     SUBROUTINE RENP2G(Nsol,radp,ApSdx,eLp,rads,solDfr,nu,
c                perm,sigma,tLp,pLp,isol,eflag)
c       INTEGER Nsol, isol
c       REAL radp,ApSdx,eLp,rads,solDfr,nu,perm,sigma,tLp,pLp
c       LOGICAL eflag
c
c
c     SUBROUTINE BEAP2G(Nsol,radp,ApSdx,eLp,rads,solDfr,nu,
c                perm,sigma,tLp,pLp,isol,eflag)
c       INTEGER Nsol, isol
c       REAL radp,ApSdx,eLp,rads,solDfr,nu,perm,sigma,tLp,pLp
c       LOGICAL eflag
c
c
c     SUBROUTINE SLTP2G(Nsol,slitw,ApSdx,eLp,rads,solDfr,nu,
c                perm,sigma,tLp,pLp,isol,eflag)
c       INTEGER Nsol, isol
c       REAL slitw,ApSdx/eLp,rads,solDfr,nu,perm,sigma,tLp,pLp
c       LOGICAL eflag
c
c
c     REAL FUNCTION PD(a)
c       REAL a
c
c
c     REAL FUNCTION RENF(a)
c       REAL a
c
```

```
c
c     REAL FUNCTION BEANG(a)
c       REAL a
c
c
c     REAL FUNCTION RENC(a)
c       REAL a
c
c
c     REAL FUNCTION ASAP(a)
c       REAL a
c
c
c     REAL FUNCTION POREF(a)
c       REAL a
c
c
c     REAL FUNCTION GSLIT(a)
c       REAL a
c
c.....
c
c DESCRIPTION:
c
c     The set of pore subroutines are used to convert between
c     phenomenological and geometrical descriptions of solute transport
c     across the capillary membrane. The relevant phenomenological
c     transport coefficients are the water hydraulic conductance, Lp,
c     the solute permeability, P, and the solute reflection coefficient,
c     sigma. The geometrical description of transport depends on the
c     model being used. For the Renkin and Bean pore models, the relevant
c     geometrical parameters are the pore radius, rp, the pore area
c     per unit path length, Ap/deltaX, and the hydraulic conductance through
c     the endothelial cells, Lpe. A description of each pore model in the
c     set is included at the beginning of the specific model code. All
c     subroutines ending in G2P convert from geometry to phenomenological
c     coefficients, those ending in P2G convert from phenomenological to
c     geometric parameters. The other functions included in this package
c     are specific hydrodynamic functions called by the pore sub-models.
c
c.....
c
c FORMAL PARAMETERS:
c
c     Listed in each submodel.
c
c.....
c
c LIMITATIONS/WARNINGS:
c
c     In general, parameter values are not checked for realistic values.
```

```
c     The calling program is responsible for insuring that non-physical
c     parameter values (such as non-positive viscosities) are not used.
c
c.....
c
c DIAGNOSTICS:
c
c     NONE.
c
c.....
c
c EXAMPLES:
c
c.....
c
c REFERENCES:
c
c 1. Curry, F.E. "Mechanics and thermodynamids of transcapillary
c    exchange". Handbook of Physiology, 2nd ed., E.M. Renkin and
c    C.C. Michel ed. Section 2, Volume IV, Part 1, Chapter 8.
c    pp 309-374.
c
c.....
c
c SUBROUTINES/FUNCTIONS CALLED:
c
c    NONE
c
c.....
c
c FILES:
c
c /usr/local/lib/libnsr.a              - library archive
c ~libnsr/lib/libmath/pore               - source files
c
c.....
c
c AUTHOR:
c
c National Simulation Resource
c Center for Bioengineering
c University of Washington
c Box 357962
c Seattle, WA 98195-7962
c
c.....
c
c FOR ASSISTANCE:
c
c Questions regarding this software can be sent by electronic mail to:
c librarian@nsr.bioeng.washington.edu
```

```
c
c.....
c
c HISTORY:
c
c Written:  Michael Kellen (12-1998)
c
c-----------------------------------------------------------------
      SUBROUTINE RENG2P(Nsol,radp,ApSdx,eLp,als,solDfr,nu,
     +                  perm,sigma,tLp,pLp,eflag)
c
c.....
c
c DESCRIPTION
c
c     RENG2P calculates Lp, P, and sigma, for a dual pathway model.
c     The model consists of Renkin's description of solute transport
c     through a cylindrical pore assuming spherical solutes.  All solute
c     transport occurs through the porous pathway.  A water exclusive
c     pathway (transendothelial) pathway occurs in parallel with the
c     porous pathway.  The total hydraulic conductivity, Lpt, is given
c     by the sum of the calculated Lpp for the pore, and the user
c     specified Lpe for the trans-endothelial cell pathway.
c
c.....
c
c FORMAL PARAMETERS:
c
c    Inputs:
c
c    Name   I Description
c    ---------------------------------------------------------
c    Nsol   I Number of solutes.
c    radp   I pore radius (A).
c    ApSdx  I Lumped geometrical parameter. Total pore surface
c           I area devided by the total capillary surface area
c           I and the mean path length, deltaX (cm^-1).
c    eLp    I Water hydraulic conductance through trans-endothelial
c           I pathway (ml s^-1 cm^-2 mmHg^-1).
c    als    I ratio of solute radius to pore radius.
c    solDfr I solute free diffusion coefficient (cm^2/s).
c    nu     I viscosity (g cm^-1 s^-1).
c    als    I ratio of solute
c
c    Outputs:
c
c    Name   I Description
c    ---------------------------------------------------------
c    perm   I solute permeability (cm/s)
c    sigma  I solute reflection coefficient (dimensionless)
c    pLp    I water hydraulic conductance through porous
```

```
c          ! pathway (ml s^-1 cm^-2 mmHg^-1).
c     tLp  ! total water hydraulic conductance (ml s^-1 cm^-2 mmHg^-1).
c     eflag ! error flag
c
c.....
c
c LIMITATIONS/WARNINGS
c
c     Renkin's model is not the most modern development, and other models
c     in this package are probabally more correct.  See the handbook
c     chapter by Curry.
c
c     If the solute size is less than the size of a water molecule, the
c     reflection coefficient through the pore will be negative.
c
c.....
c
c I.  Declaration Section
c
c     A. Formal Parameters
c
      INTEGER Nsol
      REAL radp, ApSdx, eLp, als(Nsol), solDfr(Nsol), nu
      REAL perm(Nsol), sigma(Nsol), tLp, pLp
      LOGICAL eflag
c
c     B. Local variables
c
      PARAMETER (CONV=1333.224)
      PARAMETER (radw=1.0)
      REAL alw
c
c     C. Source Control Data strings
c
      CHARACTER*64 sid1, sid2
      DATA       sid1
     +/'%W% created on %G% at %U%.\n'/
      DATA       sid2
     +/'%Z% Retrieved on %H% at %T%.\n'/
c
c II. Error checking
c
      alw=radw/radp
      eflag=.FALSE.
      IF (ApSdx.LT.0) THEN
        eflag=.TRUE.
      ELSEIF (Nsol.LE.0) THEN
        eflag=.TRUE.
      ELSEIF (radp.LE.RADW) THEN
        eflag=.TRUE.
      ELSEIF (eLp.LT.0) THEN
```

```
          eflag=.TRUE.
        ELSEIF (nu.LE.0) THEN
          eflag=.TRUE.
        ENDIF
        DO 50 i=1,Nsol
          IF ((als(i).LT.0).OR.(solDfr(i).LT.0)) THEN
            eflag=.TRUE.
          ENDIF
     50 CONTINUE
        IF (eflag) THEN
          RETURN
        ENDIF
c
cIII. Phenomenological coefficient calculations.
c
c    A. Lp calculations.
c
      pLp=ApSdx*(radp*1.0E-8)**2/8.0/nu*CONV
      tLp=pLp+eLp
c
c    B. Solute perm and sigma calculations:
c
      DO 10 i=1,Nsol
        IF (als(i).LT.(1.0)) THEN
      Perm(i)=ApSdx*ASAP(als(i))*solDfr(i)
           sigma(i)=1-(pLp/tLp)*((RENC(als(i))*RENF(als(i)))/
     +                    (RENC(alw)*RENF(alw)))
        ELSE
          Perm(i)=0.0
          sigma(i)=1.0
        ENDIF
     10 CONTINUE
      RETURN
      END
c
c-----------------------------------------------------------------------
      SUBROUTINE BEAG2P(Nsol,radp,ApSdx,eLp,als,solDfr,nu,
     +           perm,sigma,tLp,pLp,eflag)
c
c.....
c
c DESCRIPTION
c
c    BEAG2P calculates Lp, P, and sigma, for a dual pathway model.
c    The model consists of Bean's description of solute transport
c    through a cylindrical pore assuming spherical solutes. All solute
c    transport occurs through the porous pathway. A water exclusive
c    pathway (transendothelial) pathway occurs in parallel with the
c    porous pathway. The total hydraulic conductivity, Lpt, is given
c    by the sum of the calculated Lpp for the pore, and the user
c    specified Lpe for the trans-endothelial cell pathway. Permeability
```

```
c     and Lp are the same as the Renkin model. The reflection coefficient
c     calculation is more correct than the Renkin model.
c
c.....
c
c FORMAL PARAMETERS:
c
c    Inputs:
c
c    Name   | Description
c    ---------------------------------------------------------
c    Nsol   | Number of solutes.
c    radp   | pore radius (A).
c    ApSdx  | Lumped geometrical parameter. Total pore surface
c           | area devided by the total capillary surface area
c           | and the mean path length, deltaX (cm^-1).
c    eLp    | Water hydraulic conductance through trans-endothelial
c           | pathway (ml s^-1 cm^-2 mmHg^-1).
c    als    | ratio of solute radius to pore radius.
c    solDfr | solute free diffusion coefficient (cm^2/s).
c    nu     | viscosity (g cm^-1 s^-1).
c    als    | ratio of solute
c
c    Outputs:
c
c    Name   | Description
c    ---------------------------------------------------------
c    perm   | solute permeability (cm/s)
c    sigma  | solute reflection coefficient (dimensionless)
c    pLp    | water hydraulic conductance through porous
c           | pathway (ml s^-1 cm^-2 mmHg^-1).
c    tLp    | total water hydraulic conductance (ml s^-1 cm^-2 mmHg^-1).
c    eflag  | error flag
c
c.....
c
c LIMITATIONS/WARNINGS
c
c    Bean's model is the most recent based on cylindrical pores. However,
c    parallel-plate or fiber matrix models may be more physically
c    meaningful.
c
c.....
c
c I. Declaration Section
c
c    A. Fc.mal Parameters
c
      INTEGER Nsol
      REAL ApSdx, eLp, als(Nsol), solDfr(Nsol), nu
      REAL perm(Nsol), sigma(Nsol), tLp, pLp
```

```
      LOGICAL eflag
c
c    B. Local variables
c
      PARAMETER (CONV=1333.224)
c
c    C. Source Control Data strings
c
      CHARACTER*64 sid1, sid2
      DATA       sid1
     + /'%W% created on %G% at %U%.\n'/
      DATA       sid2
     + /'%Z% Retrieved on %H% at %T%.\n'/
c
c II. Error checking
c
      eflag=.FALSE.
      IF (ApSdx.LT.0) THEN
        eflag=.TRUE.
      ELSEIF (Nsol.LE.0) THEN
        eflag=.TRUE.
      ELSEIF (radp.LT.0) THEN
        eflag=.TRUE.
      ELSEIF (eLp.LT.0) THEN
        eflag=.TRUE.
      ELSEIF (nu.LE.0) THEN
        eflag=.TRUE.
      ENDIF
      DO 50 i=1,Nsol
        IF ((als(i).LT.0).OR.(solDfr(i).LT.0)) THEN
          eflag=.TRUE.
        ENDIF
   50 CONTINUE
      IF (eflag) THEN
        RETURN
      ENDIF
c
cIII. Phenomenological coefficient calculations.
c
c    A. Lp calculations.
c
      pLp=ApSdx*(radp*1.0E-8)**2/8.0/nu*CONV
      tLp=pLp+eLp
c
c    B. Solute perm and sigma calculations:
c
      DO 10 i=1.Nsol
        IF (als(i).LT.(1.0)) THEN
          Perm(i)=ApSdx*ASAP(als(i))*solDfr(i)
          sigma(i)=1-(pLp/tLp)*(RENC(als(i))*BEANG(als(i)) +
     +                    PD(als(i)))
```

```
        ELSE
          Perm(i)=0.0
          sigma(i)=1.0
        ENDIF
   10 CONTINUE
      RETURN
      END
c
c-----------------------------------------------------------------
      SUBROUTINE SLTG2P (Nsol,slitw,ApSdx,eLp,als,solDfr,nu,
     +                   perm,sigma,tLp,pLp,eflag)
c
c.................................................................
c
c DESCRIPTION
c
c     SLTG2P calculates Lp, P, and sigma, for a dual pathway model.
c     The model consists of Curry's description of solute transport
c     through a parallel-walled rectangular slit assuming spherical
c     solutes.  All solute transport occurs through the porous pathway.
c     A water exclusive (transendothelial) pathway occurs in
c     parallel with the porous pathway.  The total hydraulic conductivity,
c     tLp, is given by the sum of the calculated Lp for the pore, and the
c     user specified Lp for the trans-endothelial cell pathway. Reflection
c     coefficents are for solute transport across the complete capillary
c     wall.  Thus they are a hydraulic conductivity weighted average of the
c     reflection coefficent through the slit and the reflection coefficent
c     through the endothelial cells (equal to 1 by definition).
c
c.................................................................
c
c FORMAL PARAMETERS:
c
c    Inputs:
c
c    Name   I Description
c    ------------------------------------------------------------
c    Nsol   I Number of solutes.
c    slitw  I slit width (A).
c    ApSdx  I Lumped geometrical parameter. Total pore surface
c           I area devided by the total capillary surface area
c           I and the mean path length, deltaX (cm^-1).
c    eLp    I Water hydraulic conductance through trans-endothelial
c           I pathway (ml s^-1 cm^-2 mmHg^-1).
c    als    I ratio of solute radius to half slit width.
c    solDfr I solute free diffusion coefficient (cm^2/s).
c    nu     I viscosity (g cm^-1 s^-1).
c
c    Outputs:
c
c    Name   I Description
```

```
c   ------------------------------------------------------------
c   perm   I solute permeability (cm/s)
c   sigma  I solute reflection coefficient (dimensionless)
c   pLp    I water hydraulic conductance through porous
c          I pathway (ml s^-1 cm^-2 mmHg^-1).
c   tLp    I total water hydraulic conductance (ml s^-1 cm^-2 mmHg^-1).
c   eflag  I error flag
c
c.....
c
c LIMITATIONS/WARNINGS
c
c   The equations used in this calculation are different than those
c   given in Curry's Handbook chapter and paper, which contain errors.
c   The equation for hydraulic conductivity is Lp=(Ap*w^2)/(12*S*deltaX*nu).
c   The equation for solute permeability is P=Ap*Dfr/(S*deltaX)*(1-a)*F(a).
c   The equation for solute reflection coefficent is
c   sigma=2/3*a^2*(1-a)*F(a) + 3/2*(1-a)*(2/3 + 2/3*a - 7/12*a^2)
c
c.....
c
c I. Declaration Section
c
c   A. Formal Parameters
c
      INTEGER Nsol
      REAL slitw, ApSdx, eLp, als(Nsol), solDfr(Nsol), nu
      REAL perm(Nsol), sigma(Nsol), tLp, pLp
      LOGICAL eflag
c
c   B. Local variables
c
      PARAMETER (CONV=1333.224)
c
c   C. Source Control Data strings
c
      CHARACTER*64 sid1, sid2
      DATA       sid1
     + /'%W% created on %G% at %U%.\n'/
      DATA       sid2
     + /'%Z% Retrieved on %H% at %T%.\n'/
c
c II. Error checking
c
      eflag=.FALSE.
      IF (ApSdx.LT.0) THEN
        eflag=.TRUE.
      ELSEIF (Nsol.LE.0) THEN
        eflag=.TRUE.
      ELSEIF (slitw.LT.0) THEN
        eflag=.TRUE.
```

```
      ELSEIF (eLp.LT.0) THEN
        eflag=.TRUE.
      ELSEIF (nu.LE.0) THEN
        eflag=.TRUE.
      ENDIF
      DO 50 i=1,Nsol
        IF ((als(i).LT.0).OR.(solDfr(i).LT.0)) THEN
          eflag=.TRUE.
        ENDIF
   50 CONTINUE
      IF (eflag) THEN
        RETURN
      ENDIF
c
cIII. Phenomenological coefficient calculations.
c
c    A. Lp calculations.
c
      pLp=ApSdx*(slitw*1.0E-8)**2/12.0/nu*CONV
      tLp=pLp+eLp
c
c    B. Solute perm and sigma calculations:
c
      DO 10 i=1,Nsol
        IF (als(i).LT.(1.0)) THEN
      Perm(i)=ApSdx*POREF(als(i))*solDfr(i)
      sigma(i)=1.0-2.0/3.0*als(i)**2*POREF(als(i))-GSLIT(als(i))
          sigma(i)=(sigma(i)*pLp + eLp)/tLp
        ELSE
          Perm(i)=0.0
          sigma(i)=1.0
        ENDIF
   10 CONTINUE
      RETURN
      END
c
c-----------------------------------------------------------------------
      SUBROUTINE RENP2G(Nsol,radp,ApSdx,eLp,rads,solDfr,nu,
     +                  perm,sigma,tLp,pLp,isol,eflag)
c
c.....
c
c DESCRIPTION
c
c    RENP2G calculates pore geometry for Renkin's cylindrical pores
c    and the magnitudes of porous and endotheilial water conductivities
c    given Lpt, and P and sigma for one of the solutes (isol). The
c    subroutine will then calculate the remaining solutes' P and sigma from
c    the geometry so that the set of phenomological coefficients are self-
c    consistent.
c
```

```
c.....
c
c FORMAL PARAMETERS:
c
c   Inputs:
c
c   Name       | Description
c   ----------------------------------------------------------
c   Nsol       | Number of solutes.
c   isol       | The solue used to calculate pore geometry
c   perm(isol) | solute permeability of solute isol (cm/s)
c   sigma(isol) | solute reflection coefficient of solute isol (dimensionless)
c   tLp        | total water hydraulic conductance (ml s^-1 cm^-2 mmHg^-1).
c   rads       | solute radius (A).
c   solDfr     | solute free diffusion coefficient (cm^2/s).
c   nu         | viscosity (g cm^-1 s^-1).
c
c   Outputs:
c
c   Name  | Description
c   ----------------------------------------------------------
c   radp  | pore radius (A).
c   ApSdx | Lumped geometrical parameter. Total pore surface
c         | area devided by the total capillary surface area
c         | and the mean path length, deltaX (cm^-1).
c   pLp   | water hydraulic conductance through porous
c         | pathway (ml s^-1 cm^-2 mmHg^-1).
c   eLp   | Water hydraulic conductance through trans-endothelial
c         | pathway (ml s^-1 cm^-2 mmHg^-1).
c   perm  | solute permeability of solutes other than isol (cm/s)
c   sigma | solute reflection coefficient of solutes other than
c         | isol (dimensionless)
c
c.....
c
c I. Declaration Section
c
c   A. Formal Parameters
c
      INTEGER Nsol, isol
      REAL radp, ApSdx, eLp, rads(Nsol), solDfr(Nsol)
      REAL perm(Nsol), sigma(Nsol), tLp, pLp, nu
      LOGICAL eflag
c
c   B. Local variables
      PARAMETER (TOL=2.0E-6)
      PARAMETER (radw=1.0)
      PARAMETER (CONV=1333.224)
      REAL alw, dum, als, alsmax, alsmin, check, testLpp, testsig
c
c   C. Source Control Data strings
```

```
c
      CHARACTER*64 sid1, sid2
      DATA       sid1
     +/'%W% created on %G% at %U%.\n'/
      DATA       sid2
     +/'%Z% Retrieved on %H% at %T%.\n'/
c
c II. Error condition checking
c
      eflag=.FALSE.
      IF (isol.LE.0) THEN
        eflag=.TRUE.
      ELSEIF (nu.LE.0) THEN
        eflag=.TRUE.
      ELSEIF (tLp.LE.0) THEN
        eflag=.TRUE.
      ELSEIF (perm(isol).LE.0) THEN
        eflag=.TRUE.
      ELSEIF ((sigma(isol).LE.0).OR.(sigma(isol).GE.1)) THEN
        eflag=.TRUE.
      ELSEIF (rads(isol).LE.radw) THEN
        eflag=.TRUE.
      ENDIF
      DO 50 i=1,Nsol
        IF ((rads(i).LT.0).OR.(solDfr(i).LE.0)) THEN
          eflag=.TRUE.
        ENDIF
   50 CONTINUE
      IF (eflag) THEN
        RETURN
      ENDIF
c
cIII. Calculation of pore radius useing the bracketing and bisection
c     method.  (Adapted from Numerical Recipies, Chapter 9.1)
c
c     A. Initial guess and limits on alpha for solute isol.
c
      als = 0.5
      alsmax = 1.0
      alsmin = 0.0
c
c     B. Bracketing and Bisection
c
c        1. Loop until you find the value of alpha that gives right sigma
c
   99 CONTINUE
      radp = rads(isol)/als
      alw = radw/radp
      testLpp=((Perm(isol)*(radp*1.0E-8)**2)/
     +        (8*nu*solDfr(isol)*ASAP(als))) * CONV
      testsig=1-(testLpp/tLp)*((RENC(als)*RENF(als))/
```

```
     +                  (RENC(alw)*RENF(alw)))
      check=sigma(isol)-testsig
      IF (check.LT.(-1.0*TOL)) THEN
        dum = als
   als = (als+alsmin)/2
   alsmax = dum
        GOTO 99
      ELSEIF (check.GT.TOL) THEN
        dum = als
        als = (als+alsmax)/2
        alsmin = dum
        GOTO 99
      ENDIF
c
c     2. Check to see if this give a reasonable value of pLp
c
      IF (testLpp.GT.tLp) THEN
        eflag=.TRUE.
        RETURN
      ENDIF
c
c   C. Final values of geometrical parameters.
c
      radp = rads(isol)/als
      ApSdx = Perm(isol)/(ASAP(als)*solDfr(isol))
c
c   D. Distribution of tLp between pLp and eLp
c
      pLp=ApSdx*((radp*1.0E-8)**2)/(8*nu)*CONV
      eLp = tLp - pLp
c
c III. Calculation of P and sigma for all solutes except isol.
c
      DO 360 i=1,Nsol
        IF (i.NE.isol) THEN
          als=rads(i)/radp
          IF ((als.LT.(1.0)).AND.(als.GE.(0.0))) THEN
            Perm(i)=ApSdx*ASAP(als)*solDfr(i)
            sigma(i)=1-(pLp/tLp)*((RENC(als)*RENF(als))/
     +                  (RENC(alw)*RENF(alw)))
          ELSE
          Perm(i)=0.0
          sigma(i) = 1.0
          ENDIF
        ENDIF
  360 CONTINUE
      RETURN
      END
c
c-----------------------------------------------------------------
      SUBROUTINE BEAP2G(Nsol,radp,ApSdx,eLp,rads,solDfr,nu,
```

```
     +              perm,sigma,tLp,pLp,isol,eflag)
c
c.....
c
c DESCRIPTION
c
c     BEAP2G calculates pore geometry for Bean's cylindrical pores
c     and the magnitudes of porous and endotheilial water conductivities
c     given Lpt, and P and sigma for one of the solutes (isol). The
c     subroutine will then calculate the remaining solutes' P and sigma from
c     the geometry so that the set of phenomological coefficients are self-
c     consistent.
c
c.....
c
c FORMAL PARAMETERS:
c
c    Inputs:
c
c    Name       | Description
c    ----------------------------------------------------------
c    Nsol       | Number of solutes.
c    isol       | The solue used to calculate pore geometry
c    perm(isol) | solute permeability of solute isol (cm/s)
c    sigma(isol) | solute reflection coefficient of solute isol (dimensionless)
c    tLp        | total water hydraulic conductance (ml s^-1 cm^-2 mmHg^-1).
c    rads       | solute radius (A).
c    solDfr     | solute free diffusion coefficient (cm^2/s).
c    nu         | viscosity (g cm^-1 s^-1).
c
c    Outputs:
c
c    Name  | Description
c    ----------------------------------------------------------
c    radp  | pore radius (A).
c    ApSdx | Lumped geometrical parameter. Total pore surface
c          | area devided by the total capillary surface area
c          | and the mean path length, deltaX (cm^-1).
c    pLp   | water hydraulic conductance through porous
c          | pathway (ml s^-1 cm^-2 mmHg^-1).
c    eLp   | Water hydraulic conductance through trans-endothelial
c          | pathway (ml s^-1 cm^-2 mmHg^-1).
c    perm  | solute permeability of solutes other than isol (cm/s)
c    sigma | solute reflection coefficient of solutes other than
c          | isol (dimensionless)
c
c.....
c
c I. Declaration Section
c
c    A. Formal Parameters
```

```
c
      INTEGER Nsol, isol
      REAL radp, ApSdx, eLp, rads(Nsol), solDfr(Nsol)
      REAL perm(Nsol), sigma(Nsol), tLp, pLp, nu
      LOGICAL eflag
c
c     B. Local variables
c
      PARAMETER (TOL=2.0E-6)
      PARAMETER (CONV=1333.224)
      REAL dum, als, alsmax, alsmin, check, testLpp, testsig
c
c     C. Source Control Data strings
c
      CHARACTER*64 sid1, sid2
      DATA       sid1
     + /'%W% created on %G% at %U%.\n'/
      DATA       sid2
     + /'%Z% Retrieved on %H% at %T%.\n'/
c
c II. Initial error condition checking
c
      eflag=.FALSE.
      IF (isol.LE.0) THEN
        eflag=.TRUE.
      ELSEIF (nu.LE.0) THEN
        eflag=.TRUE.
      ELSEIF (tLp.LE.0) THEN
        eflag=.TRUE.
      ELSEIF (perm(isol).LE.0) THEN
        eflag=.TRUE.
      ELSEIF ((sigma(isol).LE.0).OR.(sigma(isol).GE.1)) THEN
        eflag=.TRUE.
      ENDIF
      DO 50 i=1,Nsol
        IF ((rads(i).LT.0).OR.(solDfr(i).LE.0)) THEN
          eflag=.TRUE.
        ENDIF
   50 CONTINUE
      IF (eflag) THEN
        RETURN
      ENDIF
c
cIII. Calculation of pore radius useing the bracketing and bisection
c     method. (Adapted from Numerical Recipies, Chapter 9.1)
c
c     A. Initial guess and limits on alpha for solute isol.
c
      als = 0.5
      alsmax = 1.0
      alsmin = 0.0
```

```
c
c    B. Bracketing and Bisection
c
c       1. Loop until you find the value of alpha that gives right sigma
c
  89 CONTINUE
     radp = rads(isol)/als
     testLpp=((Perm(isol)*(radp*1.0E-8)**2)/
    +       (8*nu*solDfr(isol)*ASAP(als)))*CONV
     testsig=1-(testLpp/tLp)*(RENC(als)*BEANG(als)+PD(als))
     check=sigma(isol)-testsig
     IF (check.LT.(-1.0*tol)) THEN
      dum = als
      als = (als+alsmin)/2
      alsmax = dum
      GOTO 89
     ELSEIF (check.GT.tol) THEN
      dum = als
      als = (als+alsmax)/2
      alsmin = dum
      GOTO 89
     ENDIF
c
c       2. Check to see if this give a reasonable value of pLp
c
    IF (testLpp.GT.tLp) THEN
      eflag=.TRUE.
      RETURN
    ENDIF
c
c    C. Final values of geometrical parameters.
c
    radp = rads(isol)/als
    ApSdx = Perm(isol)/(ASAP(als)*solDfr(isol))
c
c    D. Distribution of tLp between pLp and eLp
c
    pLp=ApSdx*((radp*1.0E-8)**2)/(8*nu)*CONV
    eLp = tLp - pLp
c
c III. Calculation of P and sigma for all solutes except isol.
c
    DO 361 i=1,Nsol
      IF (i.NE.isol) THEN
        als=rads(i)/radp
        IF ((als.LT.(1.0)).AND.(als.GE.(0.0))) THEN
          Perm(i)=ApSdx*ASAP(als)*solDfr(i)
          sigma(i)=1-(pLp/tLp)*(RENC(als)*BEANG(als)+PD(als))
        ELSE
          Perm(i)=0.0
          sigma(i) = 1.0
```

```
          ENDIF
        ENDIF
  361 CONTINUE
      RETURN
      END
c
c-----------------------------------------------------------------------
      SUBROUTINE SLTP2G(Nsol,slitw,ApSdx,eLp,rads,Dfr,nu,
     +                  perm,sigma,tLp,pLp,isol,eflag)
c
c.....
c
c DESCRIPTION
c
c     SLTP2G calculates pore geometry for Curry's parallel walled slit
c     and the magnitudes of porous and endotheilial water conductivities
c     given Lpt, and P and sigma for one of the solutes (isol). The
c     subroutine will then calculate the remaining solutes' P and sigma from
c     the geometry so that the set of phenomological coefficients are self-
c     consistent.
c
c.....
c
c FORMAL PARAMETERS:
c
c    Inputs:
c
c    Name        | Description
c    ----------------------------------------------------------
c    Nsol        | Number of solutes.
c    isol        | The solue used to calculate pore geometry
c    perm(isol)  | solute permeability of solute isol (cm/s)
c    sigma(isol) | solute reflection coefficient of solute isol (dimensionless)
c    tLp         | total water hydraulic conductance (ml s^-1 cm^-2 mmHg^-1).
c    rads        | solute radius (A).
c    Dfr         | solute free diffusion coefficient (cm^2/s).
c    nu          | viscosity (g cm^-1 s^-1).
c
c    Outputs:
c
c    Name   | Description
c    ----------------------------------------------------------
c    slitw  | slit width (A).
c    ApSdx  | Lumped geometrical parameter. Total pore surface
c           | area devided by the total capillary surface area
c           | and the mean path length, deltaX (cm^-1).
c    pLp    | water hydraulic conductance through porous
c           | pathway (ml s^-1 cm^-2 mmHg^-1).
c    eLp    | Water hydraulic conductance through trans-endothelial
c           | pathway (ml s^-1 cm^-2 mmHg^-1).
c    perm   | solute permeability of solutes other than isol (cm/s)
```

```
c    sigma  I solute reflection coefficient of solutes other than
c           isol (dimensionless)
c
c.....
c
c I.  Declaration Section
c
c    A. Formal Parameters
c
      INTEGER Nsol, isol
      REAL slitw, ApSdx, eLp, rads(Nsol), Dfr(Nsol)
      REAL perm(Nsol), sigma(Nsol), tLp, pLp, nu
      LOGICAL eflag
c
c    B. Local variables
c
      PARAMETER (TOL=2.0E-6)
      PARAMETER (CONV=1333.224)
      REAL dum, als, alsmax, alsmin, check, testLpp, testsig
c
c    C. Source Control Data strings
c
      CHARACTER*64 sid1, sid2
      DATA       sid1
     + /'%W% created on %G% at %U%.\n'/
      DATA       sid2
     + /'%Z% Retrieved on %H% at %T%.\n'/
c
c II. Initial error condition checking
c
      eflag=.FALSE.
      IF (isol.LE.0) THEN
        eflag=.TRUE.
      ELSEIF (nu.LE.0) THEN
        eflag=.TRUE.
      ELSEIF (tLp.LE.0) THEN
        eflag=.TRUE.
      ELSEIF (perm(isol).LE.0) THEN
        eflag=.TRUE.
      ELSEIF ((sigma(isol).LE.0).OR.(sigma(isol).GE.1)) THEN
        eflag=.TRUE.
      ENDIF
      DO 50 i=1,Nsol
        IF ((rads(i).LT.0).OR.(Dfr(i).LE.0)) THEN
          eflag=.TRUE.
        ENDIF
   50 CONTINUE
      IF (eflag) THEN
        RETURN
      ENDIF
c
```

```
cIII. Calculation of pore radius useing the bracketing and bisection
c    method.  (Adapted from Numerical Recipies, Chapter 9.1)
c
c    A. Initial guess and limits on alpha for solute isol.
c
      als = 0.5
      alsmax = 1.0
      alsmin = 0.0
c
c    B. Bracketing and Bisection
c
c       1. Loop until you find the value of alpha that gives right sigma
c
   79 CONTINUE
      slitw = rads(isol)/als*2.0
      testLpp=Perm(isol)/Dfr(isol)/POREF(als)*(slitw*1.0E-8)**2/12.0/nu*
     +      CONV
      testsig=1.0-2.0/3.0*als**2*POREF(als)-GSLIT(als)
      testsig=(testsig*testLpp + tLp-testLpp)/tLp
      check=sigma(isol)-testsig
      IF (check.LT.(-1.0*tol)) THEN
       dum = als
       als = (als+alsmin)/2
       alsmax = dum
       GOTO 79
      ELSEIF (check.GT.tol) THEN
       dum = als
       als = (als+alsmax)/2
       alsmin = dum
       GOTO 79
      ENDIF
c
c      2. Check to see if this give a reasonable value of pLp
c
     IF (testLpp.GT.tLp) THEN
       eflag=.TRUE.
       RETURN
     ENDIF
c
c    C. Final values of geometrical parameters.
c
     slitw = rads(isol)/als*2.0
     ApSdx = Perm(isol)/Dfr(isol)/POREF(als)
c
c    D. Distribution of tLp between pLp and eLp
c
     pLp=ApSdx*((slitw*1.0E-8)**2)/(12*nu)*CONV
     eLp = tLp - pLp
c
c III. Calculation of P and sigma for all solutes except isol.
c
```

```
      DO 370 i=1,Nsol
        IF (i.NE.isol) THEN
          als=rads(i)/slitw*2.0
          IF ((als.LT.(1.0)).AND.(als.GE.(0.0))) THEN
            Perm(i)=ApSdx*POREF(als)*Dfr(i)
            sigma(i)=1.0-2.0/3.0*als**2*POREF(als)-GSLIT(als)
            sigma(i)=(sigma(i)*pLp + eLp)/tLp
          ELSE
          Perm(i)=0.0
          sigma(i) = 1.0
          ENDIF
        ENDIF
  370 CONTINUE
      RETURN
      END
c
c-----------------------------------------------------------------
c PD
c
c Computes the pressure-diffusion term in Bean's expression for the
c solute reflection coefficient.
c
      REAL FUNCTION PD(a)
      REAL a
      PD = 16.0/9.0*(a**2)*((1-a)**2)*RENF(a)
      RETURN
      END
c-----------------------------------------------------------------
c RENF
c
c Computes the hydrodynamic function F useing values tabulated in
c Curry (1984). The argument a is the ratio of solute size to pore
c size. It is undefined for negative values. The function returns
c a value of 1 and prints and error message for this case.
c
      REAL FUNCTION RENF(a)
      REAL a
      REAL val(47), ac(47)
      LOGICAL ldone
      DATA val/1.00000,0.95791,0.91593,0.87415,0.83266,
     +   0.79158,0.75098,0.71096,0.67162,0.63305,0.59530,0.55849,
     +   0.52266,0.48789,0.45433,0.42174,0.39047,0.36045,0.33171,
     +   0.30428,0.27819,0.25343,0.23002,0.20795,0.18721,0.16780,
     +   0.14969,0.13285,0.11727,0.10291,0.08972,0.07767,0.06672,
     +   0.05681,0.04791,0.03998,0.03294,0.02674,0.02135,0.01670,
     +   0.01273,0.00940,0.00665,0.00443,0.00268,0.00135,0.00000/
      DATA ac/0.00,0.02,0.04,0.06,0.08,0.10,0.12,0.14,
     +   0.16,0.18,0.20,0.22,0.24,0.26,0.28,0.30,0.32,0.34,0.36,
     +   0.38,0.40,0.42,0.44,0.46,0.48,0.50,0.52,0.54,0.56,0.58,
     +   0.60,0.62,0.64,0.66,0.68,0.70,0.72,0.74,0.76,0.78,0.80,
     +   0.82,0.84,0.86,0.88,0.90,1.00/
```

```
c
      ldone=.FALSE.
      i = 1
   11 CONTINUE
      IF ((i.LT.47).AND.(.NOT.ldone)) THEN
        IF ((a.GE.ac(i)).AND.(a.LT.ac(i+1))) THEN
          ldone=.TRUE.
          renf=Val(i)-(a-ac(i))*(Val(i)-Val(i+1))/(ac(i+1)-ac(i))
        ENDIF
        i=i+1
        GOTO 11
      ELSE
        IF (a.LT.0) THEN
          RENF =1.0
        ELSEIF (a.GT.1.0) THEN
          RENF =0.0
        ENDIF
      ENDIF
      RETURN
      END
c
c-----------------------------------------------------------------------
c BEANG
c
c Computes the hydrodynamic function G useing values tabulated in
c Curry (1984). he argument a is the ratio of solute size to pore
c size. It is undefined for negative values. The function returns
c a value of 1 and prints and error message for this case.
c
      REAL FUNCTION BEANG(a)
      REAL a
      REAL val(47), ac(47)
      LOGICAL ldone
      DATA (val(i),i=1,47)/1.00000,0.99973,0.99894,0.99756,0.99573,
     +    0.99333,0.99040,0.98693,0.98293,0.97840,0.97333,0.96773,
     +    0.96160,0.95494,0.94776,0.94006,0.93184,0.92312,0.91389,
     +    0.90417,0.89397,0.88330,0.87218,0.86062,0.84863,0.83626,
     +    0.82347,0.81033,0.79684,0.78303,0.76892,0.75452,0.73986,
     +    0.72492,0.70985,0.69454,0.67904,0.66338,0.64751,0.63164,
     +    0.61558,0.59942,0.58316,0.56680,0.55036,0.53382,0.50000/
      DATA (ac(i),i=1,47)/0.00,0.02,0.04,0.06,0.08,0.10,0.12,0.14,
     +    0.16,0.18,0.20,0.22,0.24,0.26,0.28,0.30,0.32,0.34,0.36,
     +    0.38,0.40,0.42,0.44,0.46,0.48,0.50,0.52,0.54,0.56,0.58,
     +    0.60,0.62,0.64,0.66,0.68,0.70,0.72,0.74,0.76,0.78,0.80,
     +    0.82,0.84,0.86,0.88,0.90,1.00/
      ldone=.FALSE.
      i = 1
   11 CONTINUE
      IF ((i.LT.47).AND.(.NOT.ldone)) THEN
        IF ((a.GE.ac(i)).AND.(a.LT.ac(i+1))) THEN
          ldone=.TRUE.
```

```
            beang=Val(i)-(a-ac(i))*(Val(i)-Val(i+1))/(ac(i+1)-ac(i))
          ENDIF
          i=i+1
          GOTO 11
        ELSE
          IF (a.LT.0) THEN
            beang=1.0
          ELSEIF (a.GT.1.0) THEN
            beang=0.50
          ENDIF
        ENDIF
        RETURN
        END
c
c-------------------------------------------------------------
c RENC
c
c Computes the term 2(1-a)^2 - (1-a)^4
c
      REAL FUNCTION RENC(a)
      REAL a
      RENC = (2*(1-a)**2)-((1-a)**4)
      RETURN
      END
c
c-------------------------------------------------------------
c ASAP
c
c Computes the quantity As/Ap useing the centerline approximation.
c
      REAL FUNCTION ASAP(a)
      REAL a
      ASAP = ((1-a)**2)*(1 - 2.104*a + 2.09*a**3 - 0.95*a**5)
      RETURN
      END
c
c-------------------------------------------------------------
c POREF
c
c Calulates the hydrodynamic function F for slit geometry.
c
      REAL FUNCTION POREF(a)
      REAL a
      IF ((a.LT.(1.0)).AND.(a.GE.(0.0))) THEN
        POREF = (1-a)*(1.0 - 1.004*a + 0.418*a**3 + 0.21*a**4 -
     +           0.1696*a**5)
      ELSE
        POREF = 0.0
      ENDIF
      RETURN
      END
```

```
c
c-----------------------------------------------------------------
c GSLIT
c
c Calulates the second term (G intergral term) in the expression for
c sigma in parallel walled slits.
c
      REAL FUNCTION GSLIT(a)
      REAL a
      IF ((a.LT.(1.0)).AND.(a.GE.(0.0))) THEN
        GSLIT = 3.0/2.0*(1-a)*(2.0/3.0+2.0/3.0*a-7.0/12.0*a**2)
      ELSEIF (a.GE.(1.0)) THEN
        GSLIT = 0.0
      ELSE
        GSLIT = 1.0
      ENDIF
      RETURN
      END
c-----------------------------------------------------------------
*************************************************************************
FILE presf.f
*************************************************************************
      SUBROUTINE PRESF(F,Pm,Pa,Pcin,Pcout,Pv,Ra,Rc,Rv,Rcan,
     +                 icase,x,eflag)
c
c Model of pressure-flow relationships for a whole organ
c
c.....
c
c From:  National Simulation Resource
c        Center for Bioengineering
c        University of Washington
c        Box 357962
c        Seattle, WA 98195-7962
c
c        Dr. J. B. Bassingthwaighte, Director
c
c.....
c
c Copyright (C) 2000 by National Simulation Resource, Univ of WA.
c All Rights Reserved.
c
c Software may be copied so long as this copyright notice is included.
c This software was developed with support from NIH grant RR-01243.
c Please cite this grant in any publication for which this software
c is used and send one reprint to the address given above.
c
c.....
c
c SYNOPSIS
c     SUBROUTINE presf()
```

```
c
c REAL F, Pa, Pcin, Pcout, Pv, Ra, Rc, Rv, x
c  INTEGER icase
c LOGICAL eflag
c
c.....
c
c DESCRIPTION
c
c Presf is a three-resistence model of the pressure-flow relationship
c in a whole organ.  Simple Poisuille flow is assumed, so Ohm's law is
c applied to arterial, capillary, and venous resisters in series.
c In experimental systems, the cannula acts as a fourth series
c resistence prior to the organ vasculature, so the true arterial
c pressure is less than the measured pressure.
c
c  Pm   Pa   Pcin  Pcout   Pv
c  |    |    |     |      |
c F--//--//--//--//-
c    Rcan   Ra    Rc    Rv
c
c The system is goverened by the following equations:
c
c Pa = Pm - F*Rcan(1)
c (Pa-Pv) = F*(Ra + Rc + Rv)(2)
c Pcout  = F*Rv + Pv(3)
c Pcin   = F*(Rv+Rc) + Pv(4)
c
c This model can be used to relate measureable whole-organ quantities
c like F, Pa, and Pv to capillary level parameters important for determining
c blood-tissue exchange, Pcin and Pcout.  The following cases are supported:
c
c Case I: F is unknown and calculated from equation (1) from known
c       Pa, Ra, and Rv. Pcin and Pcout calculated from (2) and (3).
c
c Case II: Pa is unknown and calculated from equation (1) from known
c       F, Ra, and Rv. Pcin and Pcout calculated from (2) and (3).
c
c Case III: Ra is unknown and calculated from equation (1) from known
c       Pa, F, and Rv. Pcin and Pcout calculated from (2) and (3).
c
c Case IV: Rv is unknown and calculated from equation (1) from known
c       Pa, F, and Ra. Pcin and Pcout calculated from (2) and (3).
c
c Case V: Rv and Ra are unknown, their sum is calculated from equation (1)
c       from known Pa and F.  The fraction of this sum that belongs to
c       Ra is given by x.  Pcin and Pcout calculated form (2) and (3).
c
c Successful completion of the subroutine is indicated by a return of
c eflag as FALSE.
c.....
```

```
c
c MODEL PARAMETERS
c
c NameDescriptionUnitsType
c ----- ---------------------------  ----------------------
c FFlowmL/minInput/Output
c PaArterial pressuremmHgOutput
c Pm    Measured arterial pressure     mmHgInput/Output
c PcinPressure at capillary inletmmHgOutput
c Pcout Pressure at capillary outletmmHgOutput
c Pv Venous pressuremmHgInput
c RaArterial segment resistance(mmHg min)/mLInput/Output
c Rc    Capillary segment resistance   (mmHg min)/mL   Input
c RvVenous segment resistance(mmHg min)/mL   Input/Output
c Rcan  Cannula resistance(mmHg min)/mL   Input
c x     Fraction of RadimensionlessInput
c icase Case switchN/AInput
c eflagError flagN/AOutput
c
c.....
c
c LIMITATIONS/WARNINGS
c
c     NONE
c
c.....
c
c DIAGNOSTICS
c
c     NONE
c
c.....
c
c REFERENCES
c
c
c.....
c
c SUBROUTINES/FUNCTIONS CALLED
c
c.....
c
c AUTHOR
c
c     National Simulation Resource
c     Center for Bioengineering
c     University of Washington
c     Box 357962
c     Seattle, WA 98195-7962
c
c.....
```

```
c
c FOR ASSISTANCE
c     Questions regarding this software can be sent by electronic
c     mail to: librarian@nsr.bioeng.washington.edu
c
c.....
c
c HISTORY
c
c-----------------------------------------------DECLARATION SECTION
c
c I.  Declaration section
c
      REAL F, Pa, Pcin, Pcout, Pv, Ra, Rv, Rc, x, Rcan, Pm
      INTEGER icase
      LOGICAL eflag
c
c II. Error Checking
c
      eflag=.FALSE.
      IF ((F.LE.0.0).AND.(icase.NE.1)) THEN
        eflag=.TRUE.
        RETURN
      ENDIF
      IF ((Pv.GE.Pm).AND.(icase.NE.2)) THEN
        eflag=.TRUE.
        RETURN
      ENDIF
      IF ((Ra.LT.0.0).AND.((icase.NE.3).AND.(icase.NE.5))) THEN
        eflag=.TRUE.
        RETURN
      ENDIF
      IF ((Rv.LT.0.0).AND.((icase.NE.4).AND.(icase.NE.5))) THEN
        eflag=.TRUE.
        RETURN
      ENDIF
      IF ((icase.EQ.5).AND.((x.LT.0.0).OR.(x.GT.1.0))) THEN
        eflag=.TRUE.
        RETURN
      ENDIF
      IF (Rcan.LT.0.0) THEN
        eflag=.TRUE.
        RETURN
      ENDIF
c
c III. Calculations
c
      IF (icase.EQ.1) THEN
        F = (Pm-Pv)/(Ra+Rv+Rc+Rcan)
      ELSEIF (icase.EQ.2) THEN
        Pm = F*(Ra+Rv+Rc+Rcan) + Pv
```

```
      ELSEIF (icase.EQ.3) THEN
        Ra = (Pm-Pv)/F - Rv - Rc - Rcan
      ELSEIF (icase.EQ.4) THEN
        Rv = (Pm-Pv)/F -Ra - Rc - Rcan
      ELSEIF (icase.EQ.5) THEN
        Ra = x*((Pm-Pv)/F - Rc - Rcan)
        Rv = (1-x)*((Pm-Pv)/F - Rc - Rcan)
      ELSE
        eflag=.TRUE.
        RETURN
      ENDIF
      Pa   = F*(Rv+Rc+Ra) + Pv
      Pcin = F*(Rv+Rc) + Pv
      Pcout= F*Rv + Pv
      RETURN
      END
*****************************************************************************
FILE vslide.f
*****************************************************************************
      SUBROUTINE vslide(Nsol,Nseg,Vseg,rnin,rn,V,rnout,Vout,Vold,Vnew,
     +                  rnold,rnnew,eflag)
c
c VSLIDE handles convective transport by sliding elements.  It differs
c from the standard slide in that variable volumes are permitted.
c
c File %M% (Version %I%).  Last modified at %U% on %G%.
c
c.....
c
c From:  National Simulation Resource
c        Center for Bioengineering  WD-12
c        University of Washington
c        Seattle, WA 98195
c
c        Dr. J. B. Bassingthwaighte, Director
c
c.....
c
c Copyright (C) 1999 by
c National Simulation Resource, Center for Bioengineering,
c University of Washington, Seattle, WA 98195.
c All rights reserved.
c
c This software was developed with support from NIH grant RR-01243.
c Please cite this grant in publications for which the software or
c derivatives from it were used.  Please send one reprint to the address
c given above.
c
c.....
c
c SYNOPSIS:
```

```
c
c SUBROUTINE   slidemk(Nsol,Nseg,Vseg,rnin,rn,V,rnout,Vout,Vold,Vnew
c                rnold,rnnew,eflag)
c INTEGER      Nsol,Nseg
c REAL         Vseg,rnin(Nsol),rn(Nsol,Nseg),V(Nseg),rnout(Nseg),Vout
c REAL         rnold(Nsol,0:Nseg), rnnew(Nsol,Nseg+1)
c REAL         Vold(0:Nseg), Vnew(Nseg+1)
c LOGICAL      eflag
c
c.....
c
c DESCRIPTION:
c
c   This subroutine accounts for axial convection in blood-tissue
c   exchange models with constant capillary volumes and radial volume
c   transfers. In these sorts of models, the capillary consists of a
c   rigid cylinder devided into Nseg segments of volume Vseg. After the
c   radial exchange is computed, the capillary volume array will be
c   be described by the array volume array V and mole array rn,
c   at each position the volume may be less than, equal to, or greater than
c   Vseg.
c
c   vslide takes this volume array and simultaneously slides the fluid
c   elements down stream to account for convection and introduces mixing
c   between segments to restore the capillary volume array to constant
c   values of Vseg. Thus the model calling the routine should have a
c   time step of dt = V/(F*Nseg) so that the convection is appropiate.
c   Any "left-over" volume pushed out the end of the capillary is returned
c   In the arrays Vout and nout.
c
c.....
c
c FORMAL PARAMETERS:
c
c INPUTS:
c   Name   Description
c   ------ -----------------------------------------------------------
c   rn     Mole array. Used both as input and output. The shifted
c          output will be returned in the same array.
c   Nseg   Number of axial segments.
c   Nsol   Number of solutes.
c   Vseg   Final volume of segment.
c   V      Volume array. Used both as input and output. THe shifted output
c          will be returned in the same array.
c   rnin   inflow moles.
c
c Internal variables passed as inputs so arrays can be dimensioned in model.
c These should be working arrays in model:
c
c   Vold   Volume working array dimensioned from 0 to Nseg
c   Vnew   Volume working array dimensioned from 1 to Nseg+1
```

```
c   rnold  Mole working array 1st dimension 1 to Nsol, 2nd dimension 0 to Nseg
c   rnnew  Mole working array 1st dimension 1 to Nsol, 2nd dimension 1 to Nseg+1
c
c OUTPUTS:
c   Name   Description
c   ------ -----------------------------------------------------
c   rn     Concentration array
c   V      Volume array
c   Vout   outflow volume
c   rnout  outflow concentration
c   Eflag  Error flag, .FALSE. when no errors, .TRUE. when errors present.
c
c.....
c
c LIMITATIONS/WARNINGS:
c
c   For large transfers of volume the routine may not be accurate.  If
c   Vseg is not large enough to replace lost volume, the error condition
c   is set to .TRUE.  This occurs when the sum of the initial values of V
c   plus Vseg is less than Nseg*Vseg
c
c.....
c
c DIAGNOSTICS:
c
c   None.
c
c.....
c
c EXAMPLES:
c
c This example is for a situation with only one solute.
c
c Initial conditions
c -----------------
c   Nseg = 4
c   Vseg = 0.2
c   Cin  = 20
c   V  = [0.198,0.195,0.202,0.207]
c   rn = [20.1,20.2,19.7,19.6]
c
c Output conditions
c ----------------
c   V = 0.200,0.200,0.200,0.200
c   Vout = 0.202
c   rn = 20.0,20.101,20.1825,19.6975
c   rnout = 19.6
c
c.....
c
c SUBROUTINES/FUNCTIONS CALLED:
```

```
c
c   NONE
c
c.....
c
c SEE ALSO
c
c   slide.f
c
c.....
c
c FILES:
c
c /usr/local/lib/libnsr.a              - library archive
c ~libnsr/lib/libmath/vslide             - source files
c
c.....
c
c AUTHOR:
c
c National Simulation Resource
c Center for Bioengineering
c University of Washington
c Box 357962
c Seattle, WA 98195-7962
c
c.....
c
c FOR ASSISTANCE:
c
c Questions regarding this software can be sent by electronic mail to:
c librarian@nsr.bioeng.washington.edu
c
c.....
c
c HISTORY:
c
c Written:  Michael Kellen (12-1998)
c
c Modified: Michael Kellen (5-9-99) Rewrote subroutine in terms of
c         number of moles of solute instead of concentrations.
c         This change is necessary when concentration is not a linear
c         function of moles.
c
c-----------------------------------------------------------------------
c
c    Arguments of the subroutine
c    ---------------------------
      INTEGER Nseg,Nsol
      REAL rn(Nsol,Nseg), V(Nseg), rnin(Nsol), rnout(Nsol), Vseg
      REAL rnold(Nsol,0:Nseg), rnnew(Nsol,Nseg+1)
```

```
      REAL Vold(0:Nseg), Vnew(Nseg+1)
      LOGICAL eflag
c
c     Local variables
c     ---------------
      INTEGER n,m
c
c n indexes old array, m indexes new array
c
      CHARACTER*64  sid1, sid2
c
      DATA       sid1
     + /'%W% created on %G% at %U%.\n'/
      DATA       sid2
     + /'%Z% Retrieved on %H% at %T%.\n'/
c
c I.  Initial Conditions
c
      eflag  = .FALSE.
      Vold(0) = Vseg
      DO 10 i = 1,Nsol
        rnold(i,0)  = rmin(i)
        DO 20 j = 1,Nseg
          rnnew(i,j)  = 0.0
          rnold(i,j)  = rn(i,j)
          Vold(j)    = V(j)
          Vnew(j)    = 0.0
 20     CONTINUE
        rnnew(i,Nseg+1) = 0.0
 10   CONTINUE
      Vnew(Nseg+1) = 0.0
      n = 0
      m = 1
c
c II. Slide algorythm
c
 100  IF (n.GT.Nseg) THEN
c
c ERROR CONDITION
c
        eflag = .TRUE.
        RETURN
      ELSEIF (m.LE.Nseg) THEN
        IF (Vold(n).GT.(Vseg-Vnew(m))) THEN
          DO 30 i=1,Nsol
            rnnew(i,m)=rnnew(i,m)+rnold(i,n)*(Vseg-Vnew(m))/Vold(n)
            rnold(i,n)=rnold(i,n)-rnold(i,n)*(Vseg-Vnew(m))/Vold(n)
 30         CONTINUE
          Vold(n) = Vold(n)-(Vseg-Vnew(m))
          Vnew(m) = Vseg
          m = m+1
```

```
          ELSE
            DO 40 i=1,Nsol
              rnnew(i,m) = rnnew(i,m) + rnold(i,n)
              rnold(i,n) = 0.0
   40       CONTINUE
            Vnew(m) = Vnew(m) + Vold(n)
            Vold(n) = 0.0
            n = n+1
          ENDIF
          GOTO 100
        ELSE
 c
 c III.Now we are filling up the last segment of the new array.
 c    Unlike the previous segments, it is volume variable.
 c
  200   CONTINUE
        DO 50 n = n, Nseg
          Vnew(Nseg+1) = Vnew(Nseg+1) + Vold(n)
          DO 70 i=1,Nsol
            rnnew(i,Nseg+1) = rnnew(i,Nseg+1) +
     +                  rnold(i,n)
   70     CONTINUE
   50   CONTINUE
 c
 c IV. Reseting the concentration and volume arrays
 c
       DO 99 j = 1,Nseg
         DO 80 i=1,Nsol
           rn(i,j) = rnnew(i,j)
   80    CONTINUE
         V(j) = Vnew(j)
   99  CONTINUE
       DO 90 i=1,Nsol
         rnout(i) = rnnew(i,Nseg+1)
   90  CONTINUE
       Vout = Vnew(Nseg+1)
     ENDIF
     RETURN
     END
*************************************************************************
```

Vita

Michael R. Kellen was born in Chicago, IL in 1975. He received a Bachelor of Science in General Engineering with a college option in Bioengineering from the University of Illinois (Champaign) in December of 1996. In June of 2002, he earned a Doctor of Philosophy in Bioengineering from the University of Washington in Seattle.